

FRONTIERS IN LIFE SCIENCES AND RELATED TECHNOLOGIES



AGRICULTURAL SCIENCES BIOLOGY BIOCHEMISTRY
BIOINFORMATICS BIOTECHNOLOGY BIOCONTROL
BIOMECHANICS BIOCOMPUTERS BIOENGINEERING
BIOELECTRONICS BIOPHYSICS BIOMATERIALS
BIOMEDICAL SCIENCES BIOMONITORING BIOPOLYMERS
CELL BIOLOGY CONSERVATION BIOLOGY CRYOBIOLOGY
ECOLOGY ENVIRONMENTAL SCIENCES FOOD SCIENCES
GENETICS GENOMICS IMMUNOTHERAPY MARINE SCIENCES
MEDICAL SCIENCES MICROBIOLOGY MOLECULAR BIOLOGY
METABOLOMICS NANOTECHNOLOGY NEUROSCIENCES
PHYSIOLOGY PHARMACOGENOMICS PHARMACOLOGY
POPULATION DYNAMICS PROTEOMICS REMEDIATION
SYNTHETIC BIOLOGY SYSTEMATICS TOXICOLOGY

APRIL, 2024, VOLUME 5, ISSUE 1

Contents

Research Articles

- **Impacts of PM10 exposure on hospitalization for acute bronchitis in Ankara, Türkiye**

Hilal Arslan, Adnan Agir, Goksel Demir

Pages: 1-5

- **Growth and organotypic branching of lung-specific microvascular cells on 2D and in 3D lung-derived matrices**

Sena Nur Ozkan, Ece Ozturk

Pages: 6-14

- **The most relevant drought-tolerant indices for selecting barley drought-tolerant genotypes**

Mbarek Ben Naceur, Hatem Cheikh-Mhamed

Pages: 15-23

- **Investigation of the effect of superabsorbent polymer application on soil moisture and plant growth**

Senem Avaz Seven, Yesim Menciloglu, Kemal Unlu, Kadriye Kahraman, Ogeday Rodop, Ipek Bilge, Mustafa Atilla Yazici, Yusuf Ziya Menciloglu

Pages: 24-30

- **Effects of cold stress on protein metabolism of certain walnut cultivars**

Sergul Ergin, Firat Altintas

Pages: 31-37

- ***In silico* analysis of sirtuin-type histone deacetylase genes in sugar beet (*Beta vulgaris* L.)**

Seher Yolcu

Pages: 38-47

- **The effect of epetraborole on the transcriptome and proteome profiles of an *Escherichia coli* strain overexpressing *leuS*, Leucyl-tRNA Synthetase**

Anara Babayeva, Esra Dibek, Deniz Sunnetci Akkoyunlu, Naci Cine, Murat Kasap, Gurler Akpinar, Bekir Col

Pages: 48-58

- **Impact of the COVID-19 pandemic on pharmacy students: A comprehensive survey**

Ahmet Canbaz, Harika Oyku Dinc, Aysenur Kilic, Bekir Kocazeybek, Gulactı Topcu

Pages: 59-64

- **Effects of keratin6/16 heterodimer on diabetic wound healing treatment with topical metformin**

Fatma Kubra Tombulturk

Pages: 65-73

- **Identification of potential hub genes as biomarkers for breast, ovarian, and endometrial cancers**

Sema Atasever

Pages: 74-82

Issue Editorial Board

Prof. Dr. Kasim BAJROVIC
Institution: University of Sarajevo

Asst. Prof. Dr. Onur INAM
Institution: Gazi University

Prof. Dr. Memet Vezir KAHRAMAN
Institution: Marmara University

Assoc. Prof. Dr. Roswanira AB. WAHAB
Institution: Universiti Teknologi Malaysia

Editor

Prof. Dr. Ibrahim Ilker OZYIGIT

Co-Editors

Asst. Prof. Dr. Ibrahim Ertugrul YALCIN

Assoc. Prof. Dr. Aysegul YILDIZ



Research article

Impacts of PM₁₀ exposure on hospitalization for acute bronchitis in Ankara, Türkiye

Hilal Arslan^{*1} , Adnan Agir² , Goksel Demir¹ 

¹ University of Health Sciences Türkiye, Hamidiye Faculty of Health Sciences, Department of Occupational Health and Safety, 34668, Istanbul, Türkiye

² Andes Construction Inc., Department of Occupational Health and Safety, 48500, Ankara, Türkiye

Abstract

The purpose of this study is to investigate the relationship between PM₁₀ exposure and acute bronchitis admissions in Ankara, Türkiye. PM₁₀ data and daily acute bronchitis admissions were obtained in Ankara for 2020-2021. A generalized additive model was applied to estimate the effects of daily PM₁₀ concentration on hospital admissions for acute bronchitis. The Distributed Lag Non-linear Model was utilized to evaluate the lagged effects of PM₁₀ concentration. Additionally, the model was adjusted for stratified analyses according to gender and age groups. Relative risks with corresponding 95% confidence intervals (CIs) were obtained for each 10 µg/m³ increment in PM₁₀ values. A rise of 10 µg/m³ in PM₁₀ concentrations was significantly linked with an elevated risk of acute bronchitis with relative risks observed at lag3 (RR: 1.010, 95% CI: 1.001-1.019) and lag4 (RR: 1.010, 95% CI: 1.002-1.019). There were associations for middle-aged individuals (45 to 64 years), with a 0.5% increase in risk at lag3 (RR: 1.005; 95% CI: 1.001-1.009) and lag4 (RR: 1.005; 95% CI: 1.001-1.010). PM₁₀ exposure could increase the risk of acute bronchitis and better air quality would be beneficial to human health.

Keywords: Acute bronchitis; Ankara; generalized additive model; PM₁₀; Türkiye

1. Introduction

Air pollution refers to the presence of various chemical, physical, or biological substances that lead to contamination of both outdoor and indoor atmosphere (WHO, 2021). Air pollution originates from a range of sources, both anthropogenic and naturally occurring. Natural sources of air pollution include desert dust, wildfires, and volcanic emissions (Baltaci et al., 2022; Arslan, 2023), whereas anthropogenic sources of air pollution include industrial sites, power plants, transportation, agriculture, residential and commercial heating, cooking, waste disposal, construction, mining, and oil and gas production (Castagna et al., 2021; Zhou et al., 2021; Lestari et al., 2022; Arslan and Toltar, 2023). Air pollution can also be transported over long distances by winds, which can make it difficult to

identify the sources of certain pollutants in a specific location (National Oceanic and Atmospheric Administration, 2021). This has numerous adverse impacts on human health and harms the environment by reducing visibility, causing acid rain, and damaging forests (Mohajan, 2018; Saxena and Sonwani, 2019; Shammass et al., 2020; Savita, 2021).

Particulate matter (PM) is one of the criteria for air pollutants that can pose risks to human health (Arslan et al., 2022; Baltaci et al., 2022; Chung et al., 2023; He et al., 2023; Zhang et al., 2023). Different sizes and types of PM can have varying health impacts, and the duration and level of exposure can also affect the severity of health problems. For instance, PM₁₀ is identified as inhalable particles which can cause health issues. Epidemiological studies have revealed that being exposed to PM₁₀ may result in increased incidence of hospital

* Corresponding author.

E-mail address: hilal.arslan@sbu.edu.tr (H. Arslan).

<https://doi.org/10.51753/flsrt.1322260> Author contributions

Received 03 July 2023; Accepted 03 March 2024

Available online 30 April 2024

2718-062X © 2024 This is an open access article published by Dergipark under the [CC BY](https://creativecommons.org/licenses/by/4.0/) license.

admissions for respiratory disease (Leung et al., 2021; WHO, 2021; Arslan et al., 2022; Baltaci et al., 2022; Shams et al., 2023). Guo et al. (2014) found that every $10 \mu\text{g}/\text{m}^3$ increment in PM_{10} values corresponded to a rise of 0.94% (95% CI: 0.83%-1.05%) in hospitalizations for acute bronchitis at lag6 in Shanghai, China. Similarly, in southwestern China, Zhang and Zhou (2022) found that $\text{PM}_{2.5}$ and PM_{10} exposure was found to contribute to increased hospital admissions for acute bronchitis. In another study, Capraz and Deniz (2021) found that a $10 \mu\text{g}/\text{m}^3$ increment in $\text{PM}_{2.5}$ values led to an 8.06% rise (95 % CI: 3.36-19.4 %) in admission rates for acute bronchitis at lag9 in Istanbul, Türkiye.

Ankara is among the largest cities in Türkiye and is reported to experience high levels of PM_{10} due to vehicular emissions and industrial activities. High levels of particulate matter concentration pose significant threats to both the environment and public health. This research aims to examine the correlation between PM_{10} exposure and hospitalizations due to acute bronchitis in Ankara from 2020 to 2021.

2. Materials and methods

2.1. Study area

Due to the low preference for public transportation and the use of fossil fuel-consuming public vehicles, high pollutant concentrations are found in Ankara. Almost 50% of public vehicles use fossil fuels, which significantly contributes to the problem. Furthermore, compared to larger cities such as Istanbul and Izmir, Ankara has a high rate of vehicle ownership per 100 people, exacerbating the issue. As a result, the city's air quality is significantly compromised (Dark Report, 2019).

Ankara has a semi-arid central Anatolian climate characterized by hot and arid summers and cold, snowy winters. The mean temperature during summer is around 23°C , while in winter, the mean temperature drops to around 2.1°C . The hottest month is July-August, and the coldest is January. Most precipitation falls during the spring and fall months, with relatively low rainfall during the summer and winter (Akkose et al., 2021).

2.2. Hospital admissions and air quality data

Hourly PM_{10} concentrations data were provided by the National Air Quality and Monitoring database for 2020-2021.

Additionally, hourly temperature and relative humidity data were obtained from the Turkish State Meteorological Service (TSMS). Hospital admission numbers for acute bronchitis, based on the International Classification of Diseases-Tenth Revision, were obtained from the Etimesgut State Hospital database for 2020-2021. The daily respiratory hospital admission numbers (ICD-10: J20 for acute bronchitis) were derived by each patient's age (18-44, 45-64, and >64 years) and gender. The relationship between PM_{10} values and hospital admissions for acute bronchitis was investigated using data from the Etimesgut air quality station (Fig. 1), as it is the nearest station to the hospital.

2.3. Statistical analysis

A generalized additive model was constructed using a quasi-Poisson link to estimate the effects of daily PM_{10} concentration on hospital admissions related to acute bronchitis. The lagged effects of PM_{10} concentration were assessed with the Distributed Lag Non-linear Model.

The following model is fitted:

$$\begin{aligned} \text{Log } E(Y_t) = & \alpha + \beta X_{t,l} + ns(\text{time}_t, df) + ns(\text{temperature}_t, \\ & df) + ns(\text{humidity}_t, df) \\ & + \text{factor}(\text{DOW}) + \text{factor}(\text{holiday}), \end{aligned} \quad (1)$$

$\text{Log } E(Y_t)$ is the expected number of hospitalized patients due to acute bronchitis on day t , α is the intercept, β is the vector of regression coefficients, X_t is the cross-basis matrix of PM_{10} concentration on day t , and l is lag days. A single-day lag between lag 0 (day of occurrence) and lag 7 (which indicated the value on the 7th day succeeding the occurrence) was used. The model is controlled for the meteorological elements, i.e., temperature and humidity, by using the natural spline (ns) function with 3 degrees of freedom (df). Time represents the date variable, which was defined with ns with 7 df per year to check for long-term trends and seasonality (Liu and Zhai, 2022). Day of the week (DOW) (1, 2, ..., 7) and an indicator of public holiday (0/1) were used in the model as factor variables. The model was also fitted for stratified analyses according to gender and age groups. The adjusted relative risks (RRs) were calculated along with their 95% CIs per $10 \mu\text{g}/\text{m}^3$ increase in the PM_{10} value. The statistical analyses were performed utilizing the *dlm* package in the R 4.2.1 edition (Gasparrini et al., 2011).

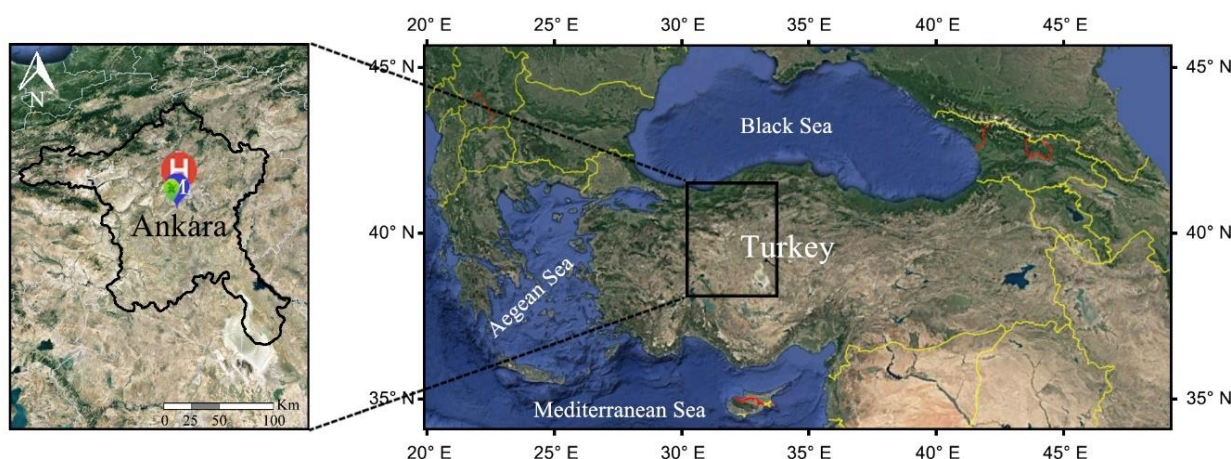


Fig. 1. The distribution of air quality monitoring station (green circle), meteorological station (blue circle) and hospital in Ankara (red circle) (Google Maps, 2024).

3. Results and discussion

This research aimed to examine the association between PM₁₀ exposure and the risk of being hospitalized with acute bronchitis in Ankara from 2020 to 2021. Table 1 and Figure 2 show the relative risks (RRs), along with their corresponding 95% CIs, for hospital admissions due to acute bronchitis associated with a 10 µg/m³ increment in PM₁₀ values.

The significant effects of PM₁₀ on hospital admission were found at lag3, lag4 and lag5. Although RRs are not much different than the other lag days, the RR peak of PM₁₀ is lag5, which was associated with a 1.1% (RR:1.011, 95% CI: 1.001-1.021) increase in the risk of hospitalization for acute bronchitis. An increase of 10 µg/m³ in PM₁₀ value increased the risk of acute bronchitis related hospital admission by 1.0% at lag3 (RR:1.010, 95% CI: 1.001-1.019) and lag4 (RR:1.010, 95% CI: 1.002-1.019).

Table 1

Relative risk and 95% CIs of hospitalizations due to acute bronchitis with an increment of 10 µg/m³ in PM₁₀ value.

| Lag Days | RR | 95% CI |
|----------|--------------|----------------------|
| lag0 | 1.009 | (0.992-1.027) |
| lag1 | 1.010 | (0.996-1.023) |
| lag2 | 1.010 | (0.999-1.021) |
| lag3 | 1.010 | (1.001-1.019) |
| lag4 | 1.010 | (1.002-1.019) |
| lag5 | 1.011 | (1.001-1.021) |
| lag6 | 1.011 | (0.997-1.025) |
| lag7 | 1.011 | (0.994-1.029) |

In a similar study, a connection between increased exposure to PM_{2.5} and heightened risk of bronchitis-related hospitalizations was established (Hertz-Picciotto et al., 2007). Additionally, a positive correlation between NO₂, PM₁₀, PM_{2.5}, and SO₂ levels and hospital admissions linked to acute bronchitis and COPD was identified (Muñoz and Carvalho, 2009). Furthermore, evidence supporting an increased risk of hospitalization due to bronchitis in association with PM_{2.5} exposure was provided (Ostro et al., 2009). Studies also showed that 10 µg/m³ rise in PM₁₀ led to 4% increase in hospitalizations due to acute bronchitis/bronchiolitis (Meszaros et al., 2015) and 10 µg/m³ increment in PM_{2.5} resulted in 25% and 1% increase in the rates of hospitalization due to acute bronchitis and asthma, respectively (Jo et al., 2017). Additionally, hospitalizations for childhood acute bronchitis were reported to be significantly increased by an interquartile range rise in the NO₂, PM_{2.5}, and CO concentrations, with 4-day cumulative effect estimates (RR: 1.03, 95% CI: 1.01-1.05; 1.09, 95% CI: 1.07-1.11; 1.07, 95% CI: 1.05- 1.09) (Bai et al., 2018) and 10 µg/m³ rise in PM_{2.5} values resulted in 8.06 % increment (95% CI: 3.36–19.4%) in admission rates for acute bronchitis at lag 9 (Capraz and Deniz, 2021). Moreover, particulate matter concentrations were associated with increased number of hospitalizations as 10 µg/m³ increase in PM_{2.5} was reported to cause 25% increment in acute bronchitis, 14% in allergic rhinitis, and 1% in asthma (Jo et al., 2017). Relationship between PM₁₀ exposure and the prevalence of the chronic bronchitis was also observed (Hooper et al., 2018).

The stratified analysis for gender revealed that, females were significantly at higher risk of acute bronchitis related hospital admissions from an increment in PM₁₀ at lag3 (RR: 1.009; 95% CI:1.001-1.017), lag4 (RR: 1.010; 95% CI:1.002-

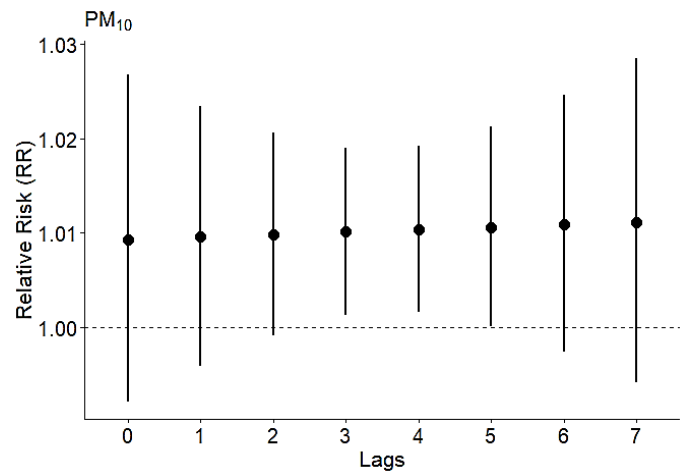


Fig. 2. Relative risk and 95% CIs of hospitalizations due to acute bronchitis for 10 µg/m³ increment in PM₁₀ concentration across the different time periods.

1.017), and lag5 (RR: 1.010; 95% CI:1.001-1.020) as shown in Table 2 and Fig. 3. In a similar study, 10 µg/m³ increment in PM₁₀, SO₂ and NO₂ values were found to correspond to 0.94% (95% CI: 0.83% to 1.05%), 11.12% (95% CI: 10.76% to 11.48%), and 4.84% (95% CI: 4.49% to 5.18%) rise in hospital admissions attributed to acute bronchitis at lag6, respectively and these correlations were significantly higher for females than males (Guo et al., 2014). Correlation between particulate matter and increased risk of respiratory hospitalizations attributed to conditions such as asthma, chronic bronchitis, and COPD was also reported in another study and their findings similarly indicated that females faced 1.5 times greater risk than males when exposed to both PM₁₀ and PM_{2.5} (Shakerkhatibi et al., 2021).

Table 2

Relative risk and 95% CIs of hospitalizations due to acute bronchitis for 10 µg/m³ increment in PM₁₀ concentration across genders.

| PM ₁₀ Lag Days | Male | | Female | |
|------------------------------|-------|---------------|--------------|----------------------|
| | RR | 95% CI | RR | 95% CI |
| lag0 | 1.012 | (0.989-1.035) | 1.007 | (0.991-1.023) |
| lag1 | 1.012 | (0.994-1.030) | 1.008 | (0.995-1.020) |
| lag2 | 1.011 | (0.997-1.026) | 1.008 | (0.999-1.018) |
| lag3 | 1.011 | (1.000-1.023) | 1.009 | (1.001-1.017) |
| lag4 | 1.011 | (0.999-1.023) | 1.010 | (1.002-1.017) |
| lag5 | 1.011 | (0.997-1.025) | 1.010 | (1.001-1.020) |
| lag6 | 1.011 | (0.993-1.029) | 1.011 | (0.999-1.023) |
| lag7 | 1.011 | (0.988-1.034) | 1.011 | (0.996-1.027) |

On the other hand, there are also studies that show no significant gender difference in the correlation between PM₁₀ exposure and acute bronchitis related hospitalizations (He et al., 2022).

While epidemiological research has primarily concentrated on the health impacts of PM exposure on children (Muñoz and Carvalho, 2009; Zhang and Zhou, 2021; He et al., 2022), effects of PM₁₀ on chronic bronchitis, asthma, emphysema, and COPD were reported to show no significant difference between age groups, however, there was a significant increase in health problems among the 18-60 and >60 age groups associated with PM_{2.5} exposure (Shakerkhatibi et al., 2021). This study reveals negative impacts on the middle-aged group. Stratified analysis based on age groups at various lags was presented in Table 3 and Fig. 4. In the middle-aged group (45 to 64 years), 10 µg/m³

Table 3

Relative risk and 95% CIs of hospitalizations due to acute bronchitis for 10 µg/m³ increment in PM₁₀ concentration across age groups.

| PM ₁₀ Lag Days | 18-44 years | | 45-64 years | | >64 years | |
|------------------------------|-------------|---------------|--------------|----------------------|-----------|---------------|
| | RR | 95% CI | RR | 95% CI | RR | 95% CI |
| lag0 | 1.003 | (0.991-1.015) | 1.002 | (0.993-1.012) | 1.005 | (0.990-1.021) |
| lag1 | 1.003 | (0.994-1.013) | 1.003 | (0.996-1.010) | 1.005 | (0.993-1.017) |
| lag2 | 1.004 | (0.996-1.011) | 1.003 | (0.998-1.009) | 1.005 | (0.995-1.014) |
| lag3 | 1.004 | (0.998-1.010) | 1.004 | (1.000-1.009) | 1.004 | (0.996-1.013) |
| lag4 | 1.005 | (0.999-1.010) | 1.005 | (1.001-1.009) | 1.004 | (0.995-1.013) |
| lag5 | 1.005 | (0.998-1.012) | 1.005 | (1.001-1.010) | 1.004 | (0.993-1.016) |
| lag6 | 1.005 | (0.996-1.014) | 1.006 | (0.999-1.013) | 1.004 | (0.989-1.019) |
| lag7 | 1.006 | (0.994-1.017) | 1.006 | (0.998-1.015) | 1.004 | (0.985-1.022) |

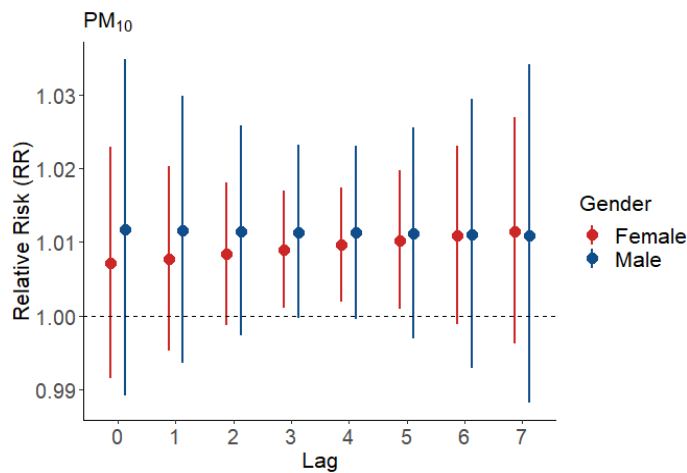


Fig. 3. Relative risk and 95% CIs of hospitalizations due to acute bronchitis for 10 µg/m³ increment in PM₁₀ concentration across genders at the different time periods.

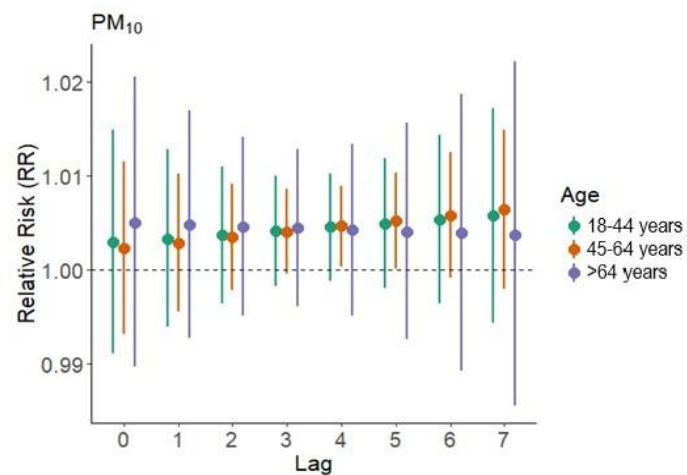


Fig. 4. Estimated relative risk (RR) and 95% CIs of hospitalizations due to acute bronchitis for a 10 µg/m³ increment in PM₁₀ concentration across age groups at the different time periods.

increment in PM₁₀ significantly raised the risk of acute bronchitis-related hospital admission by 0.5% at lag3 (RR: 1.005; 95% CI:1.001-1.009) and lag4 (RR: 1.005; 95% CI: 1.001-1.010). However, no significant correlation was found between PM₁₀ and acute bronchitis admissions in the age group

References

Akkose, G., Akgul, C. M., & Dino, I. G. (2021). Educational building retrofit under climate change and urban heat island effect. *Journal of Building Engineering*, 40, 102294.

of 18 to 45 years or over 64 years.

4. Conclusion

The findings of this study indicate a substantial correlation between PM₁₀ exposure and hospitalizations due to acute bronchitis. The significant impacts of PM₁₀ on hospital admission were observed at lag3, lag4, and lag5. At lag3 (RR:1.010, 95% CI: 1.001-1.019) and lag4 (RR:1.010, 95% CI: 1.002-1.019), a 10 µg/m³ rise in PM₁₀ concentration increased the risk of acute bronchitis-related hospital admission by 1.0%. Also, a 10% increase in PM₁₀ concentration in the middle-aged (45 to 64 years) group substantially increased the risk of acute bronchitis-related hospital admission by 0.5% on lag 3 (RR: 1.005; 95% CI:1.001- 1.009) and lag4 (RR: 1.005; 95% CI: 1.001-1.010).

Air pollution is a significant environmental risk, posing a substantial threat to human health. The WHO Air Quality Guidelines serve as a cornerstone in setting objectives to safeguard human health against the harmful effects of air pollution. These objectives involve reducing activities such as incineration of agricultural waste and forest fires, which are prominent contributors to air pollution. Furthermore, these objectives entail enhancing the handling of household, industrial, and municipal waste, investing in power generation methods that prioritize energy efficiency, constructing environmentally conscious, energy-efficient, and compact urban areas, and establishing secure and affordable public transportation systems along with pedestrian and cyclist-friendly networks.

The findings of this study are anticipated to offer valuable insights into the health impacts of air pollution, providing policymakers with guidance for improving both health outcomes and air quality. Reducing air pollution levels has the potential to decrease the incidence of various serious health conditions, including acute bronchitis, asthma, pneumonia, lung cancer, stroke, and COPD.

Conflict of interest: The authors declare that they have no conflict of interests.

Informed consent: The authors declare that this manuscript did not involve human or animal participants and informed consent was not collected.

Arslan H. (2023). Impacts of Meteorological Parameters on Tropospheric Ozone Concentrations in Çanakkale, *International Journal of Advances in Engineering and Pure Sciences*, 35 (1). 10-17.

- Arslan, H., & Toltar, A. (2023). The influence of meteorological parameters on PM_{2.5} and PM₁₀ values in Ümraniye and Silivri districts of İstanbul. *Environmental Research and Technology*, 6(4), 288-301.
- Arslan, H., Baltacı, H., Sahin, U. A., & Onat, B. (2022). The relationship between air pollutants and respiratory diseases for the western Turkey. *Atmospheric Pollution Research*, 13(2), 101322.
- Bai, L., Su, X., Zhao, D., Zhang, Y., Cheng, Q., Zhang, H., ... & Su, H. (2018). Exposure to traffic-related air pollution and acute bronchitis in children: season and age as modifiers. *Journal of Epidemiology and Community Health*, 72(5), 426-433.
- Baltacı, H., Arslan, H., & Akkoyunlu, B. O. (2022). High PM₁₀ source regions and their influence on respiratory diseases in Canakkale, Turkey. *International Journal of Environmental Science and Technology*, 1-10.
- Capraz, O., & Deniz, A. (2021). Assessment of hospitalizations from asthma, chronic obstructive pulmonary disease and acute bronchitis in relation to air pollution in İstanbul, Turkey. *Sustainable Cities and Society*, 72, 103040.
- Castagna, J., Senatore, A., Bencardino, M., & Mendicino, G. (2021). Concurrent influence of different natural sources on the particulate matter in the central mediterranean region during a wildfire season. *Atmosphere*, 12(2), 144.
- Chung, H. W., Hsieh, H. M., Lee, C. H., Lin, Y. C., Tsao, Y. H., Feng, M. C., & Hung, C. H. (2023). Air pollution after acute bronchiolitis is a risk factor for preschool asthma: a nested case-control study. *Environmental Health*, 22(1), 83.
- Dark Report, (2019). Air Pollution and Health Impacts, <https://www.temizhavahakki.org/wp-content/uploads/2019/08/Hava-Kirlilig%C4%B1k-Etkileri-Kara-Rapor-2019.pdf>, Last Accessed on March 18, 2024.
- Gasparini A. (2011). Distributed lag linear and non-linear models in R: The package dlnm. *Journal of Statistical Software*, 43(8):1-20.
- Guo, L. J., Zhao, A., Chen, R. J., Kan, H. D., & Kuang X. Y. (2014). Association between ambient air pollution and outpatient visits for acute bronchitis in a Chinese City. *Biomedical and Environmental Sciences*, 27(11), 833-840.
- He, Y., Jiang, W., Liao, J. Q., Jing, L., Li, J., & Yang, L. (2022). Short-term effects of air pollutants on hospital admissions for acute bronchitis in children: a multi-city time-series study in Southwest China. *World Journal of Pediatrics*, 18(6), 426-434.
- He, Y., Jiang, W., Gao, X., Lin, C., Li, J., & Yang, L. (2023). Short-term effects and economic burden of air pollutants on acute lower respiratory tract infections in children in Southwest China: a time-series study. *Environmental Health*, 22(1), 6.
- Hertz-Picciotto, I., Baker, R. J., Yap, P. S., Dostál, M., Joad, J. P., Lipsett, M., ... & Šrám, R. (2007). Early childhood lower respiratory illness and air pollution. *Environmental Health Perspectives*, 115(10), 1510-1518.
- Hooper, L. G., Young, M. T., Keller, J. P., Szpiro, A. A., O'Brien, K. M., Sandler, D. P., ... & London, S. J. (2018). Ambient air pollution and chronic bronchitis in a cohort of US women. *Environmental Health Perspectives*, 126(2), 027005.
- Jo, E. J., Lee, W. S., Jo, H. Y., Kim, C. H., Eom, J. S., Mok, J. H., ... & Park, H. K. (2017). Effects of particulate matter on respiratory disease and the impact of meteorological factors in Busan, Korea. *Respiratory Medicine*, 124, 79-87.
- Lestari, P., Arrohman, M. K., Damayanti, S., & Klimont, Z. (2022). Emissions and spatial distribution of air pollutants from anthropogenic sources in Jakarta, *Atmospheric Pollution Research*, 13, 9.
- Leung, S. Y., Lau, S. Y. F., Kwok, K. L., Mohammad, K. N., Chan, P. K. S., & Chong, K. C. (2021). Short-term association among meteorological variation, outdoor air pollution and acute bronchiolitis in children in a subtropical setting. *Thorax*, 76 (4): 360-369.
- Liu D. J., & Zhai G. (2022). Association between air pollution and hospital admissions for hypertension in Lanzhou, China. *Environmental Science and Pollution Research*, 29, 11976-1198.
- Mészáros, D., Markos, J., FitzGerald, D. G., Walters, E. H., & Wood-Baker, R. (2015). An observational study of PM₁₀ and hospital admissions for acute exacerbations of chronic respiratory disease in Tasmania, Australia 1992-2002. *BMJ Open Respiratory Research*, 2(1), e000063.
- Mohajan, H. (2018). Acid rain is a local environment pollution but global concern. published in: *Open Science Journal of Analytical Chemistry*, 3, 5, 47-55.
- Muñoz, F., & Carvalho, M. S. (2009). Effect of exposure time to PM₁₀ on emergency admissions for acute bronchitis. *Cadernos de Saúde Pública*, 25(3), 529-539.
- National Oceanic and Atmospheric Administration. (2021). What is Air Pollution?, Retrieved from <https://www.noaa.gov/education/resource-collections/air-quality/>, Last Accessed on March 18, 2024.
- Ostro, B., Roth, L., Malig, B., & Marty, M. (2009). The effects of fine particle components on respiratory hospital admissions in children. *Environmental Health Perspectives*, 117(3), 475-480.
- Savita, (2021). Impacts of air pollutants on forest ecosystem and role in ecological imbalance. In: Tiwari S., Saxena P. (eds) *Air Pollution and Its Complications* (pp. 129-142). Springer, Cham.
- Saxena, P., Sonwani, S., Saxena, P., & Sonwani, S. (2019). Primary criteria air pollutants: environmental health effects. *Criteria Air Pollutants and Their Impact on Environmental Health*, 49-82.
- Shakerkhatibi, M., Seifipour, H., Sabeti, Z., Kahe, D., Asghari Jafarabadi, M., Zoroufchi Benis, K., & Hajaghadadeh, M. (2021). Correlation of ambient particulate matters (PM₁₀, PM_{2.5}) with respiratory hospital admissions: a case-crossover study in Urmia, Iran. In: *Human and Ecological Risk Assessment: An International Journal*, 27(8), 2184-2201.
- Shammas, N. K., Wang L. K., & Wang M. H. S. (2020). Sources, chemistry and control of acid rain in the environment. In: Hung, Y. T., Wang L. K. (eds) *Handbook of Environment and Waste Management* (pp. 1-26). World Scientific.
- Shams, S. R., Kalantary, S., Jahani, A., Shams, S. M. P., Kalantari, B., Singh, D., ... & Choi, Y. (2023). Assessing the effectiveness of artificial neural networks (ANN) and multiple linear regressions (MLR) in forecasting AQI and PM₁₀ and evaluating health impacts through AirQ+ (case study: Tehran). *Environmental Pollution*, 338, 122623.
- WHO, (2021). Official Website of World Health Organization, Air Pollution, Retrieved from https://www.who.int/health-topics/air-pollution#tab=tab_1, Last Accessed on March 18, 2024.
- Zhang, P., & Zhou, X. (2022). Pricing air pollution: evidence from short-term exposure to air pollution on hospitalization of acute bronchitis and chronic obstructive pulmonary disease in southwestern China. *International Health*, 14(6), 572-579.
- Zhang, W., Ling, J., Zhang, R. Dong J., Zhang, L., Chen, R., & Ruan, Y. (2023). Short-term effects of air pollution on hospitalization for acute lower respiratory infections in children: a time-series analysis study from Lanzhou, China. *BMC Public Health*, 23(1629), 1-11.
- Zhou, M., Jiang, W., Gao, W., Gao, X., Ma, M., & Ma, X. (2021). Anthropogenic emission inventory of multiple air pollutants and their spatiotemporal variations in 2017 for the Shandong Province, China. *Environmental Pollution*, 288, 117666.

Cite as: Arslan, H., Agir, A., & Demir, G. (2024). Impacts of PM₁₀ exposure on hospitalization for acute bronchitis in Ankara, Türkiye. *Front Life Sci RT*, 5(1), 1-5.



Research article

Growth and organotypic branching of lung-specific microvascular cells on 2D and in 3D lung-derived matrices

Sena Nur Ozkan^{1,2} , Ece Ozturk^{*1,2,3} ¹ Koc University, Engineered Cancer and Organ Models Laboratory, 34450, Istanbul, Türkiye² Koc University, Research Center for Translational Medicine (KUTTAM), 34450, Istanbul, Türkiye³ Koc University, Department of Medical Biology, School of Medicine, 34450, Istanbul, Türkiye

Abstract

Tissue-specific endothelial cells have vital roles in maintenance and functioning of native tissues with constant reciprocal crosstalk with resident cells. Three-dimensional (3D) physio-mimetic *in vitro* models which incorporate lung-specific microvasculature are needed to model lung-related diseases which involve modulation of endothelial cell behavior like cancer. In this study, we investigated the growth kinetics, morphological changes and responses to biological cues of lung microvasculature on two-dimensional (2D) and in lung matrix-derived 3D hydrogels. HUVEC and HULEC-5a cells were cultured on 2D and compared for their growth, morphologies, and responses to varying growth medium formulations. Brightfield and immunofluorescence imaging was performed to assess differences in morphology. For 3D cultures, native bovine lungs were decellularized, lyophilized, solubilized, and reconstituted into hydrogel form in which endothelial cells were embedded. Cell growth and organotypic branching was monitored in 3D hydrogels in the presence of varying biological cues including lung cancer cell secretome. HUVEC and HULEC-5a cells demonstrated comparable growth and morphology on 2D. However, in 3D lung-derived ECM hydrogels, tissue-specific HULEC-5a cells exhibited much better adaptation to their microenvironment, characterized by enhanced organotypic branching and longer branches. HULEC-5a growth was responsive to lung cancer cell-conditioned medium in both 2D and 3D conditions. In 3D, the concentration of ECM ligand significantly affected cell growth in long-term culture where molecular crowding had an inhibitory role. Our data reveals that HULEC-5a cells offer a reliable alternative to frequently pursued HUVECs with comparable growth and morphology. Due to their intrinsic program for cellular crosstalk with resident cells, the use of tissue-specific endothelium constitutes a vital aspect for modeling physiological and pathological processes. Furthermore, our study is the first demonstration of the synergy between lung-specific microvasculature with lung-specific ECM within a 3D *in vitro* model.

Keywords: Cancer; endothelial cells; extracellular matrix; lung microenvironment; tissue engineering

1. Introduction

Endothelial cells form an intact and continuous lining which constitute veins, capillaries, arterioles, heart, and lymphatic vessels (Bloom, 2023). They demonstrate high levels of cellular plasticity as they adopt distinct functions within different tissues and organs of the body. The endothelium acts

an integral active machinery which supports tissues via enabling nutrient and oxygen flow, mediates the fluidity of the blood, and serves as an immune regulator (Hennigs, 2021). On the other hand, tissue-specific endothelium has the ability to secrete specialized factors which regulate developmental processes, regeneration, physiological homeostasis, and stem-cell activation. Moreover, resident non-endothelial cells in tissues

* Corresponding author.

E-mail address: ozturkece@ku.edu.tr (E. Ozturk).

<https://doi.org/10.51753/flsrt.1351292> Author contributions

Received 28 August 2023; Accepted 21 January 2024

Available online 30 April 2024

2718-062X © 2024 This is an open access article published by Dergipark under the [CC BY](https://creativecommons.org/licenses/by/4.0/) license.

similarly secrete factors to stimulate endothelial cells which supports the formation of tissue-specific micro-vasculature (Barabutis et al., 2016; Rafii et al., 2016). Therefore, this reciprocal crosstalk is crucial for the proper functioning of distinct tissues and organs. Human umbilical vein endothelial cells (HUVECs) are one of the most prominent and highly demanded primary endothelial cell source in the field due to their expression of generic endothelial markers, easy isolation, and culturing processes. HUVECs have been widely used in literature to reveal key information regarding the biology of endothelium including colony-stimulating activity, vessel permeability, and established as a model system to study angiogenesis as well as pathological phenomena including atherosclerosis, and inflammation (Han and Geng, 2011; Jang et al., 2017; Medina-Leyte et al., 2020; Tatla et al., 2021). Although non-specific endothelial cells such as HUVECs have dominated the field, they are limited by the lack of representing the high variety of tissue-specific endothelial phenotypes which support tissue and organ functioning (Jourde-Chiche et al., 2019; Rosen et al., 2023). Thus, implementation of tissue-specific endothelium is needed for increasing the validity and accuracy of experimental models (Urbanczyk et al., 2022; Wakabayashi and Naito, 2023).

Lung-specific endothelium is more than just a simple barrier and holds vital importance in the proper functioning of the lung. It resides within lung-specific extracellular matrix (ECM), undergoes continuous stretch and encounters foreign materials during respiration. Under these external stresses, lung endothelial cells form a tightly regulated dynamic sheet. Any interference with this microenvironmental regulation contributes to pathological conditions such as chronic obstructive pulmonary disease (COPD), pneumonia, and hypertension (Goncharova et al., 2020). In cancer, endothelial cells are a vital part of the tumor microenvironment which through neo-angiogenesis, support tumor growth and dissemination. Cancer cells modulate the behavior of tissue-specific endothelium and promote their chaperoning of malignant progress (Hida et al., 2018; Klein, 2018). Therefore, cellular crosstalk between endothelial and tumor cells is a critical regulator of disease.

Extracellular tissue microenvironment is another essential impact on the heterogeneity and specification of endothelium. Biochemical content of ECM as well as mechanical cues act as key regulators of endothelial cell fate and behavior (Nguyen, 2021). Three-dimensional culture models which enable interaction of cells with ECM cues offer biomimetic approaches for studying cellular behavior. Decellularization of native organs is a promising strategy which supports preservation of tissue-specific ECM and reconstitution into hydrogels that can be used as 3D scaffolds (Kusoglu et al., 2023).

Physiologically relevant lung tissue models which employ tissue-specific endothelium are needed for a better understanding of the role of endothelium in homeostatic and pathological conditions. HULEC-5a, as a lung microvascular cell line, contains various features of the primary vascular cells, yet studies on the characterization of this cell line are very limited. Unlike HUVECs, these cells are insufficiently characterized in terms of culture conditions, growth medium requirements, and 3D microenvironmental adaptability. In this study, we aimed to thoroughly characterize lung-specific endothelium in conventional 2D as well as in 3D hydrogels derived from decellularization of native lung tissues. Our results

demonstrate the potential use of lung-specific endothelium in vascularized lung tissue models and provide a promising tool for developing therapeutic approaches in lung-related vascular diseases.

2. Materials and methods

2.1. 2D cell culture

The human primary umbilical vein endothelial cells, HUVEC (PCS-100-010TM), immortalized human lung microvascular endothelial cells, HULEC-5a (CRL-3244TM) were purchased from American Type Culture Collection (ATCC). In all experiments, endothelial cells were used between passage (p) 1 and 4 and were incubated in an environment of 37°C and 5% CO₂. Cells were either cultured in Endothelial Cell Growth Basal Medium-2 (EBMTM-2 CC-3156) supplemented with EGMTM-2 SingleQuotsTM supplement kit (Lonza, CC-4176), endothelial culture medium (EC)-1, EC-2, EC-3, PneumaCultTM ExPlus Medium (StemCell Technologies), Wnt-conditioned medium (Wnt-CM) or A549-CM. Serum-free generic EC medium recipe is formulated with DMEM/F12 as basal medium supplemented with 0.25 mg/ml BSA, 10 ng/ml VEGF and FGF, 0.1% ITS, 2% L-glutamine, 2% Pen-strep, 0.2 µg/ml hydrocortisone, 100 µg/ml ascorbic acid. Then, specific EC-1, EC-2, and EC-3 mediums were prepared by adding 50 µg/ml bovine pituitary extract (BPE), insulin-like growth factor (IGF-1), and T3 (3,3',5-triiodo-L-thyronine sodium salt) respectively to the generic serum-free EC medium. For the Wnt-CM, 1 × 10⁶ L-Wnt3A cells were cultured in DMEM/F12 basal medium supplemented with 10% fetal bovine serum (FBS) and 0.4 mg/ml geneticin for 4 days. First batch of media was collected and filter-sterilized. 12 ml fresh culture media was added, and cells were cultured until they were confluent. Second batch of media was collected, filter-sterilized, and the two batches were mixed with 1:1 ratio. Next, this conditioned medium is mixed with EGM-2 at a proportion of 1:1 to formulate Wnt-CM. For A549-CM, 1 × 10⁶ A549 cells were cultured for 4 days, and their media was collected and filter-sterilized. Similarly, collected media was mixed with EGM-2 at a proportion of 1:1.

2.2. MTT assay

5 mg MTT (InvitrogenTM, M6494) was dissolved in 1 ml of Phosphate Buffered Saline (PBS) and filter-sterilized. Old culture media was aspirated, and a fresh medium-MTT mixture (100 µl medium and 10 µl MTT) was added to the wells of a 96-well plate containing various cell concentrations. 4 hours of incubation at 37°C was implemented. The precipitate was dissolved in 100 µl DMSO, incubated at 37°C for 10 minutes which was followed by 5 minutes of shaking. Absorbance values were read at 570 nm with a plate reader. Three replicates were used.

2.3. CTG (Cell Titer Glo) 2D assay

HUVEC and HULEC-5a cells were cultured in a 96-well plate with EGM-2. 10 µl CTG reagent (Promega) was added into 100 µl medium (1:10). The lysis procedure was implemented via 2 minutes of orbital shaking. Luminescence values for three replicates were recorded upon 10 min room temperature

stabilization of the plate.

2.4. Decellularization of lung tissue

Fresh bovine lungs were obtained from a local slaughterhouse. Bovine lung tissue was washed thoroughly with ultrapure water supplemented with penicillin/streptomycin (P/S) and immersed in a 2% iodine solution. Then, tissues were subjected to 5 consecutive freeze-thaw cycles of 2 min freezing in liquid nitrogen and 10 min thawing in a 37°C water bath. Next, 10U/ml DNase (in 10 mM MgCl₂ buffer, pH:7.5) treatment was performed which was followed by a sterile dH₂O wash for 3 days.

2.5. Pepsin digestion

Decellularized tissue pieces were lyophilized and then cryo-milled into a fine powder for further digestion procedures. Digestion was performed with incubation of samples within 1 mg/ml pepsin in 0.01M HCl solution at room temperature under constant stirring for 48 hours. ECM concentration of 15 mg/ml and 20 mg/ml was used for digestion. Digested ECM samples were then neutralized to physiological conditions (pH 7, 1X PBS) by adding NaOH and 10X PBS. These pre-gel forms were stored at -20°C for further studies.

2.6. 3D cell culture

For encapsulation into 3D hydrogels, cell suspensions were gently mixed with cold pre-gel dECM solutions at a concentration of 2×10^6 cells/ml. The mixture was then cast onto well plates, and incubated at 37°C for 45 minutes until proper gelation after which culture medium was carefully added. Hydrogels were incubated under 37°C and 5% CO₂ conditions and the culture medium was changed every other day until the end of the experiment.

2.7. 3D CTG assay

HUVEC and HULEC-5a cells that were embedded in decellularized ECM (dECM) gels in a 24-well plate were cultured and monitored for 4 weeks. CellTiter-Glo 3D (Promega) assay was utilized on days 1, 14, 21 and 28. After 1 hour of CTG incubation, culture media was collected and transferred into a 96-well plate where luminescence was measured with a microplate reader. A growth curve was generated for each condition tested.

2.8. Phalloidin/DAPI staining

Cells which were seeded on glass-bottom 24-well plates were first fixed with 4% PFA for 15 min and then washed three times with PBS. Wells were incubated with a blocking solution containing PBS and 5% normal goat serum for 1 hour. Cells were incubated with phalloidin solution (Phalloidin-iFluor 647 Reagent, ab176759) for 45 min and then incubated with DAPI for 5 min in the dark at room temperature. Imaging was performed using a Leica SP8 confocal microscope.

2.9. Statistics

Statistical analyses were performed using Prism 9 (GraphPad). Data were analyzed using an unpaired t-test when

two independent groups were compared (minimum n=3). The results are expressed as mean and error with a 95% confidence interval. A p-value<0.05 was considered statistically significant.

3. Results and discussion

This study aimed to implement a thorough characterization of lung-specific endothelial cells in terms of growth kinetics, morphological features, response to biochemical stimuli as well as their interaction with 3D native lung-derived matrices (Fig. 1). The first part of the study focused on the assessment of cell growth and behavior on 2D conventional cultures to compare tissue-specific HULEC-5a cells to the widely adopted HUVEC cells. Our results demonstrate that both cell types revealed similar actin cytoskeletal structure and elongated cellular morphology (Fig. 2A). On the other hand, HULEC-5a cells exhibited significantly smaller cell size (Fig. 2B). Differences in cell size could be attributed to the fact that HULEC-5a is a microvascular endothelial cell type whereas HUVEC is vein-derived. Cells lining larger vessels like veins have been reported to have relatively larger size (Kruger-Genge et al., 2019). We then assessed the growth kinetics of HUVEC and HULEC-5a cells. Both cell types were seeded at a constant density of 20×10^3 cells per each well of a 96-well plate and growth was monitored over 3 days in culture (Fig. 2C). The results indicated that lung-specific and generic endothelial cells did not reveal any significant difference in proliferation rate. Then we investigated the effect of initial cell seeding density on the growth dynamics of HULEC-5a cells up to a week (Fig. 2D). The growth curves demonstrated that seeding cells at a density of 500×10^3 cells per well of a 96-well plate caused an immediate drop in cell growth which then was stabilized. A density of 100×10^3 cells/well on the other hand did not promote further cell growth but maintained the initial conditions. The optimal cell seeding density for obtaining a proper growth curve from HULEC-5a cells was in the range of $10\text{-}50 \times 10^3$ cells per well.

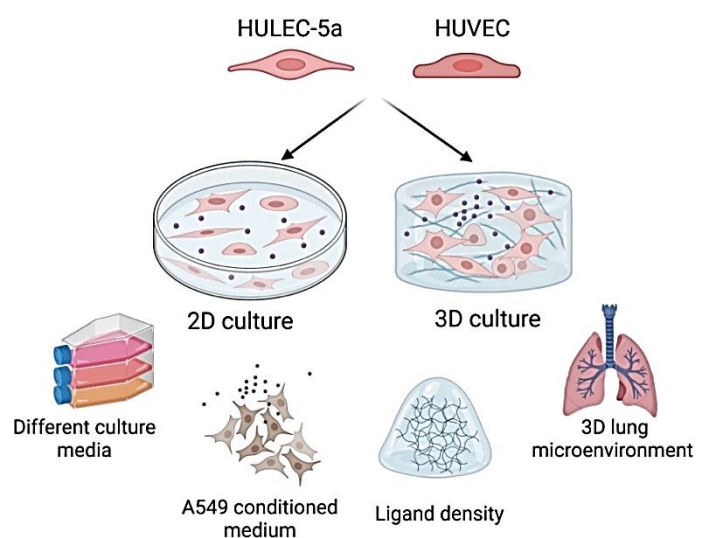


Fig. 1. Schematic description of the study (Created with BioRender).

Next, we assessed the effects of different growth medium formulations on lung-specific endothelial cells in terms of cellular morphology and growth dynamics (Fig. 3). We used a commercially available culture medium optimized for endo-

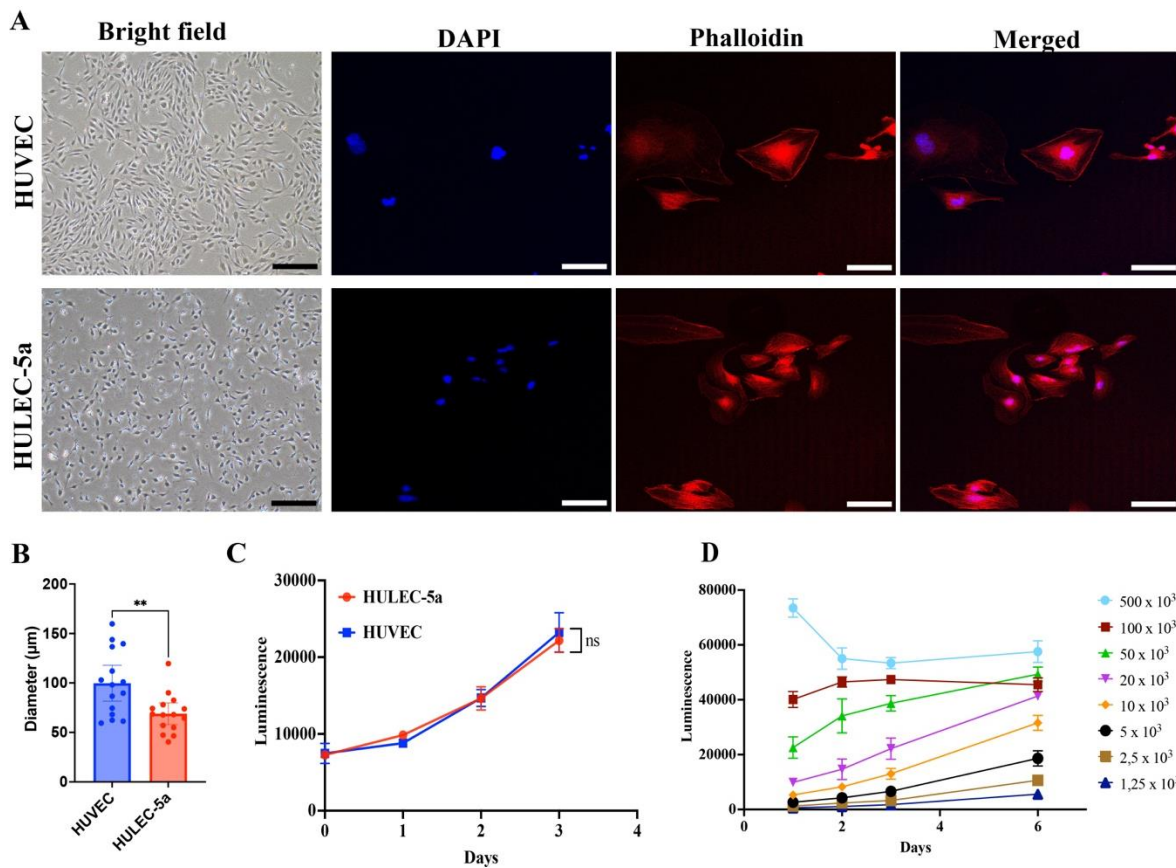


Fig. 2. Comparison of HUVEC and HULEC-5a growth and morphology on 2D cultures. (A) Phenotypic characterizations of endothelial cells: Bright field images (Scale bars: 150 μm) and confocal microscopy images for phalloidin-DAPI staining (Scale bars: 30 μm). (B) Diameter size differences of HUVEC and HULEC-5a under 20X magnification. (C) Growth curves of HUVEC and HULEC-5a for 3 days on 2D culture. (D) Growth curves of HULEC-5a with differing initial cell seeding density on 2D culture.

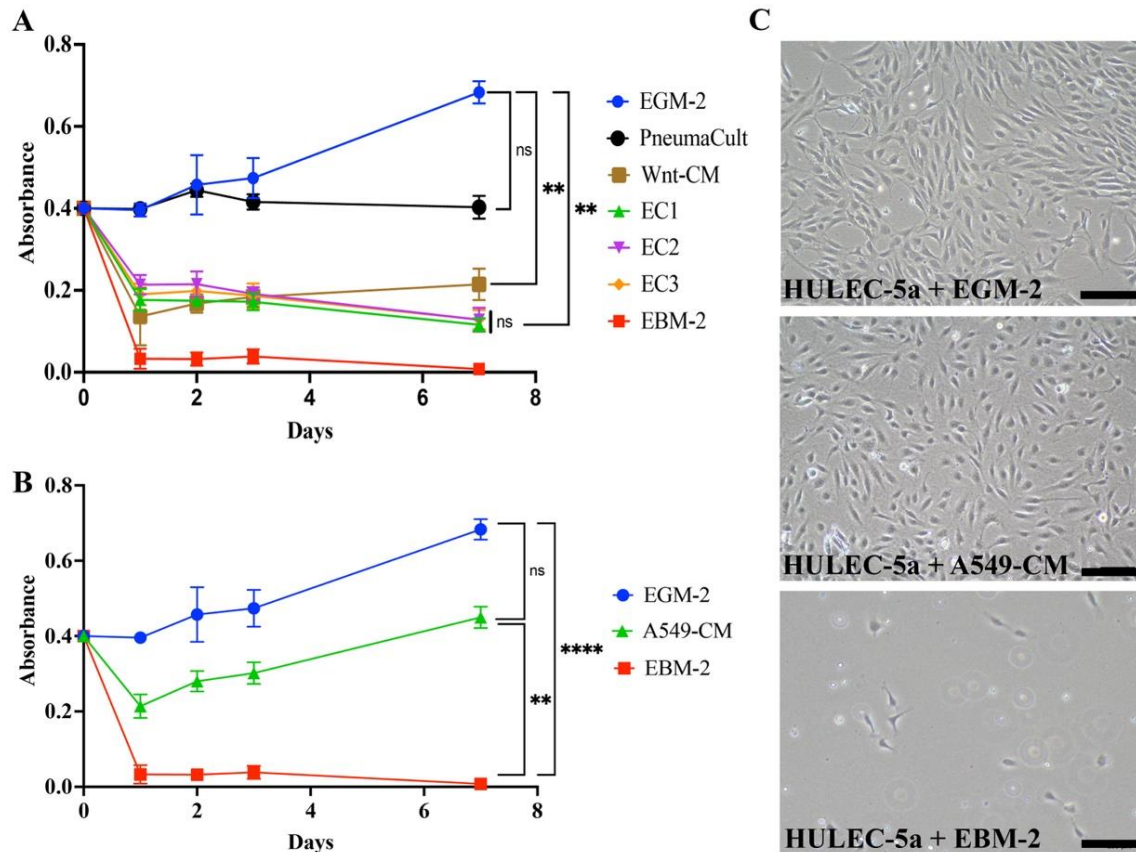


Fig. 3. HULEC-5a growth on 2D. (A) Growth of HULEC-5a cells within different medium conditions and (B) in A549-conditioned medium assessed by MTT assay. (C) Bright field images of HULEC-5a cells cultured in EGM-2, A549-CM and EBM-2 media. (Scale bars: 100 μm).

thelial cells, EGM-2, as a positive control, whereas basal medium without endothelium-supporting supplements was used as a negative control (EBM-2). Moreover, we monitored HULEC-5a cells in different media formulations to find out lung-specific endothelial cell synergy with media content. Culture media compositions with the ability to support different cell types within engineered tissues are a critical challenge in the field. Vascularized, engineered tissue models combine endothelial cells with tissue-resident epithelial and stromal cells, and all those cell types have different requirements of biological cues for growth and functioning. Therefore, it is crucial to find formulations that provide an optimal media to support collective cell growth in such co-culture models. Accordingly, to assess the potential use of HULEC-5a cells in vascularized *in vitro* lung tissue models, we tested their growth in media optimized for pulmonary epithelium such as PneumaCult™ (Rayner et al., 2019). HULEC-5a growth in PneumaCult™ was comparable to EGM-2 for the first three days of culture, however, after 7 days, cell growth in EGM-2 was significantly higher whereas cells ceased to grow in PneumaCult™ (Fig. 3A). This indicates that using growth media formulated for pulmonary epithelium could only serve as an approach for short-term co-cultures whereas lack of endothelium-specific cues hinders their use for long-term cultures of vascularized *in vitro* lung models. Next, we wanted to examine the effect of several serum-free media formulations on lung-specific endothelial cell growth. Undefined composition and batch-to-batch variations in sera have motivated the development of more defined, serum-free formulations for endothelial cell culture (Andrée et al., 2019). We have adapted a serum-free formulation (EC) which has been reported to support the growth of HUVEC cells in the literature. However, the majority of studies that employed this serum-free approach demonstrated complementary techniques such as cultivating endothelial cells with stromal cells to induce growth with the aid of paracrine factors (Huttala et al., 2015). Since the use of stromal cells may also lead to experimental variability, we aimed to avoid their use and opted to enrich the EC formulation with additional supplements. EC medium was supplemented with BPE (EC-1), IGF-1 (EC-2) and T3 (EC-3) to generate three distinct defined media formulations. BPE, IGF-1, and T3 have been shown to have additional and dose-dependent growth-stimulating effects on endothelial cells which was specifically established for microvascular endothelium (Balzan et al., 2013; Lin et al., 2017). Similarly, we assessed HULEC-5a growth in all three formulations for 7 days (Fig. 3A). However, none of the three media supported the growth of lung-specific endothelium. Next, we examined the effect of Wnt-CM, derived from the culture of L-Wnt3A cells, on the growth of HULEC-5a cells. Wnt signaling has been established as an important regulator of endothelial cell growth and functioning. Being an evolutionarily conserved pathway with crucial roles in embryonic development, Wnt signaling has been shown to have a key importance in cell fate determination. It has been reported to have a role in survival, proliferation as well as plasticity and specification of endothelium (Dejana and Kuhl, 2010). Therefore, we tested Wnt-CM as a means to promote the growth of lung-specific endothelial cells. Contrarily, Wnt-CM had an adverse effect on both proliferation and morphology of HULEC-5a cells (Fig. 3A). Cancer cell secretome is another crucial regulator of endothelial cell growth and heterogeneity (McHenry and Prospero, 2023). Cancer progression and metastasis heavily depend on the angiogenic switch which involves neo-vascularization. Therefore, cancer cells and

endothelial cells affect each other with continuous reciprocal communication. Cancer cells specifically activate the proliferation of endothelial cells that are present in neighboring tissues and promote their specialization. As a result, a unique tumor-associated endothelium is created by the cancer cells, constitutively promoting their growth and dissemination (Ritchie et al., 2021; Zahari et al., 2023). Thus, we next aimed to inspect the effect of cancer cell secretome on the growth kinetics of HULEC-5a cells. Conditioned medium was collected from the cultures of a non-small cell lung adenocarcinoma cell line (A549-CM). As anticipated, A549-CM strongly promoted the growth of HULEC-5a cells (Fig. 3B). Even though the stimulation of cell growth was not to the extent achieved with EGM-2, the growth curves of both media formulations demonstrated a similar trend in which endothelial cells still preserved their proliferative abilities after a week of culturing. As opposed to other media formulations (EBM-2, Pneumacult™, EC-1, EC-2, EC-3, Wnt-CM), A549-CM supported the maintenance of growth and distinct endothelial cell morphology (Fig. 3C). Therefore, our data confirms that lung cancer secretome has growth-stimulatory effects on lung-specific microvasculature. Such synergy between lung cancer cells and lung endothelium supports the development of *in vitro* vascularized tumor tissue models which allow investigation of the role of cellular interactions in disease progression.

After characterizing the growth kinetics of HULEC-5a in comparison to HUVEC cells and response to different media formulations with distinct biological cues, we assessed the use of HULEC-5a cells within a more physiologically relevant, 3D tissue model (Fig. 4). Conventional 2D cultures lack a faithful representation of the intricate architecture of native tissue microenvironments where cell-cell and cell-matrix interactions play a vital role in regulation of biological processes in both homeostasis and disease conditions. 3D cultures on the other hand, offer physiological relevance through mimicking the key biochemical and physical aspects of the ECM (Mierke, 2023). 3D culturing has been shown to have an effect on the growth, differentiation and phenotypic stability of endothelial cells as well as vascular network formation (Paek et al., 2019). Native ECM-derived hydrogels are frequently pursued in tissue engineering for their ability to present tissue-specific extracellular cues. They are comprised of decellularization of native organs and reconstitution into hydrogels within which cell types of interest can be embedded for modeling a plethora of cellular processes. This allows the preservation of tissue-specific ECM cues and the investigation of cell-matrix interactions. We fabricated bovine lung-derived ECM hydrogels (dLung) to assess the growth and behavior of lung-specific microvasculature within a native-like microenvironment (Fig. 4A). HULEC-5a and HUVEC cells were encapsulated in dLung gels and cultured for 10 days to compare their growth and organotypic branching ability in 3D. Both cell types exhibited adaptation and branching patterns in dLung hydrogels (Fig. 4B). Further morphological assessment was done with quantification of branch number and branch length. Interestingly, lung-specific microvasculature in lung ECM-derived hydrogels demonstrated a significantly higher number of branches with increased length compared to non-specific HUVEC cells (Fig. 4C). This indicates a synergy between tissue-specific endothelium with tissue-specific ECM. Such synergy and microenvironmental adaptation are critical for promoting endothelial cells' ability to curve the surrounding matrix for further sprouting and angiogenic events in different physiological processes.

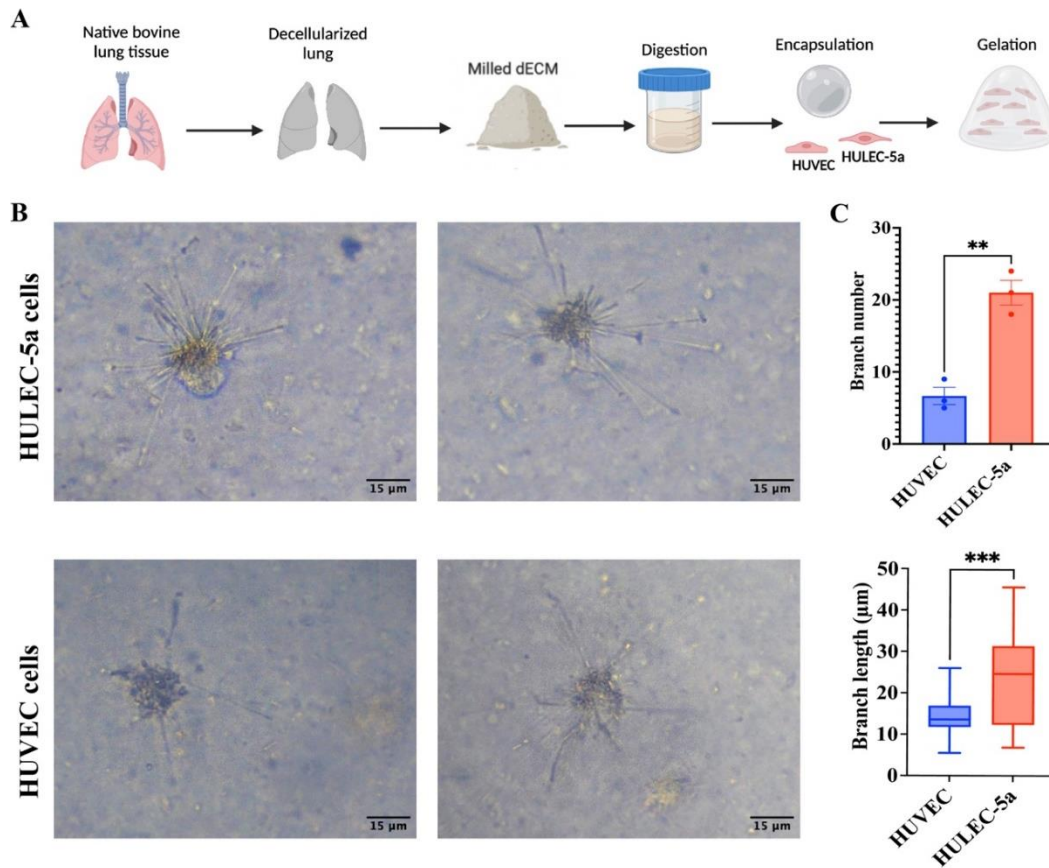


Fig. 4. 3D culturing of endothelial cells within decellularized lung-derived ECM hydrogels. (A) Scheme depicting the decellularization procedure for bovine lungs. (B) Encapsulation of HULEC-5a and HUVEC into dLung (15 mg/ml) hydrogels (Scale bar: 15 µm). (C) Quantification of branch number and length of HULEC-5a and HUVEC in dLung hydrogels.

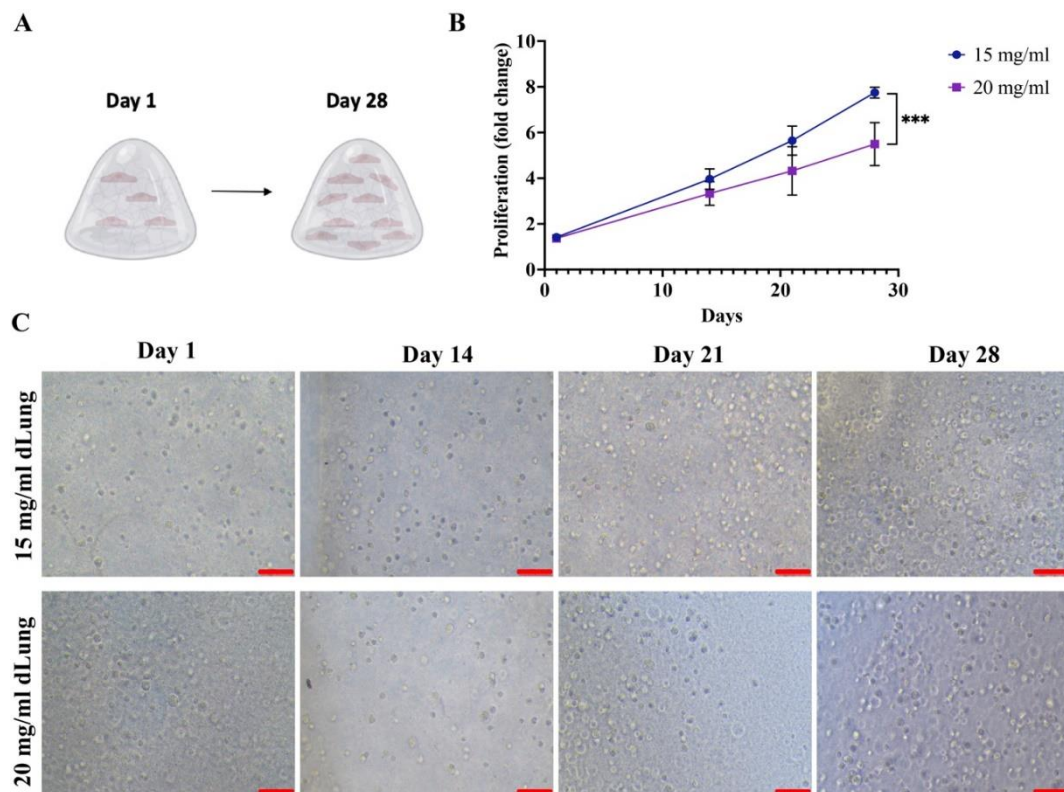


Fig. 5. Encapsulation and long-term growth monitoring of HULEC-5a in dLung hydrogels with changing ligand density. (A) Scheme representing encapsulation and 3D culturing of endothelium. (B) Cellular proliferation of HULEC-5a within dLung hydrogels with 15 mg/ml or 20 mg/ml ECM ligand density up to 28 days assessed with CTG assay and normalized to day 0. (C) Bright field images of HULEC-5a cells in dLung gels on days 1, 14, 21 and 28 (Scale bar: 70 µm).

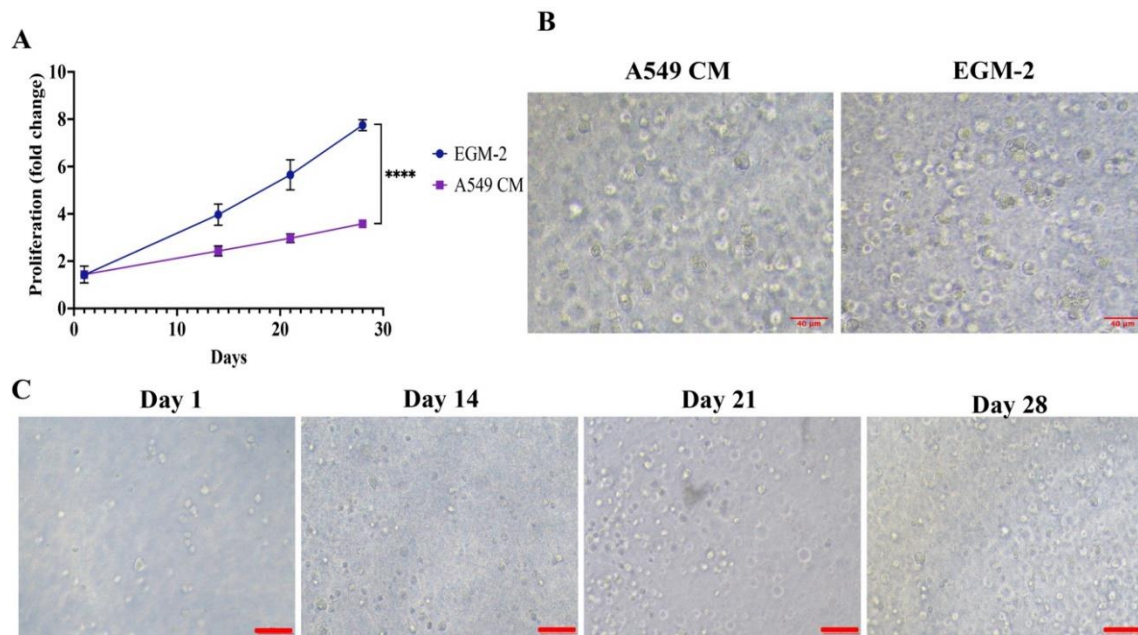


Fig. 6. The effect of lung cancer cell secretome on the growth of HULEC-5a in dLung hydrogels. (A) Cellular proliferation of HULEC-5a within dLung hydrogels in the presence of EGM-2 or A549-CM up to 28 days. (B) Brightfield images of HULEC-5a cells in dLung hydrogels within EGM-2 or A549-CM. (Scale bar: 40 μ m). (C) Brightfield images of HULEC-5a cells in dLung gels within A549-CM on days 1, 14, 21 and 28. (Scale bar: 70 μ m).

We then evaluated the growth kinetics of HULEC-5a cells within dLung hydrogels over 4 weeks (Fig. 5A). Additionally, we assessed the effect of ECM ligands via modulating the native matrix concentration in the hydrogels. dLung hydrogels supported the long-term culturing of HULEC-5a cells and stimulated their growth at both 15 mg/ml and 20 mg/ml ECM concentrations (Fig. 5B and 5C). Cellular growth was comparable in both hydrogels for 3 weeks, however, 15 mg/ml hydrogels yielded a significantly higher number of cells at the end of 4 weeks (Fig. 5B). This reveals that ECM crowding had a particularly adverse effect on the growth of endothelium. Furthermore, an increase in ligand content alters the mechanical properties of the hydrogels and correlates with increased stiffness. Tissue stiffness is a known regulator of endothelial cell growth and behavior which could account for the differences observed within the two hydrogel fields (Gordon et al., 2020).

We next looked into the effect of A549-CM on HULEC-5a cells within 3D, native ECM-derived, dLung hydrogels (Fig. 6). As opposed to 2D, dLung hydrogels provide a more representative model for the lung tissue microenvironment. It has been established in the literature that cellular behavior on 2D marked by adherent morphology is quite different than in the 3D (Jensen and Teng, 2020). Nonetheless, cancer research has heavily relied on conventional 2D cultures and the intersection of tissue engineering and cancer fields has been rather recent. Various important oncogenic signaling routes are altered in 3D, as key molecular players get either inactive or hyperactive in 3D, such as YAP (Lee et al., 2019) and ROCK (Matsubara and Bissell, 2016). Similarly, the expression pattern of pro-angiogenic factors on both transcriptional and translational levels is altered within the 3D context (Fontana et al., 2020). Therefore, we aimed to investigate the growth and morphological changes in lung-specific endothelium in response to biological cues presented by the cancer cells within a physio-mimetic, 3D context. A549-CM promoted the growth of HULEC-5a in dLung hydrogels although to a lesser extent when compared with EGM-2 (Fig. 6A). Different media formulations

did not have an observable effect on cellular morphology (Fig. 6B). On the other hand, long-term culturing of HULEC-5a up to 28 days in dLung hydrogels within A549-CM conditions (Fig. 6C) and maintenance of cellular growth provides a promising *in vitro* model which enables the use of lung-specific endothelium within native lung matrix and allows investigation of the molecular effects of cancer cell secretome on microvasculature.

4. Conclusion

In conclusion, our experimental data demonstrates that HULEC-5a cells provide a lung tissue-specific endothelial cell source with growth kinetics and morphological characteristics comparable to the widely used HUVEC cells. The study also denotes the proliferative impact of the lung cancer secretome on microvascular lung endothelial cells that can preserve the proper morphology of HULEC-5a cells. Furthermore, native lung-derived ECM hydrogels provide a physio-mimetic microenvironment for endothelium and support their organotypic branching, a phenomenon not observed in conventional 2D culturing. To our knowledge, this is the first study that investigated endothelial cell behavior in native lung-derived 3D hydrogels. The better adaptation of HULEC-5a cells to dLung hydrogels in terms of the number of branches and branch length compared to HUVECs emphasizes the importance of models that enable investigation of tissue-specific cell types within relevant matrices. Furthermore, such models allow investigation of particular molecular effects, such as paracrine signaling in the tumor microenvironment, and have the potential to shed light on the complex cellular crosstalk between cancer cells and endothelium.

Acknowledgements: This work was funded by the Scientific and Technological Research Council of Turkey (TÜBİTAK) (Grant No. 118C238). The entire responsibility of the publication/paper belongs to the owner of the publication. The financial support received from TÜBİTAK does not mean that

the content of the publication is approved in a scientific sense by TÜBİTAK. The authors gratefully acknowledge the use of services and facilities of Koç University Research Center for Translational Medicine (KUTTAM). The authors declare no competing interests. Figure 1, Figure 4A and Figure 5A were created with BioRender.com.

References

- Andrée, B., Ichanti, H., Kalies, S., Heisterkamp, A., Strauß, S., Vogt, P.-M., Haverich, A., & Hilfiker, A. (2019). Formation of three-dimensional tubular endothelial cell networks under defined serum-free cell culture conditions in human collagen hydrogels. *Scientific Reports*, 9(1), 5437.
- Balzan, S., Del Carratore, R., Nardulli, C., Sabatino, L., Lubrano, V., & Iervasi, G. (2013). The stimulative effect of T3 and T4 on human myocardial endothelial cell proliferation, migration and angiogenesis. *Journal of Clinical & Experimental Cardiology*, 4(280), 2.
- Barabutis, N., Verin, A., & Catravas, J. D. (2016). Regulation of pulmonary endothelial barrier function by kinases. *American Journal of Physiology Lung Cellular and Molecular Physiology*, 311(5), L832-L845.
- Bloom, S. I., Islam, M. T., Lesniewski, L. A., & Donato, A. J. (2023). Mechanisms and consequences of endothelial cell senescence. *Nature Reviews Cardiology*, 20(1), 38-51.
- Dejana, E., & Kuhl, M. (2010). The role of wnt signaling in physiological and pathological angiogenesis. *Circulation Research*, 107(8), 943-952.
- Fontana, F., Raimondi, M., Marzagalli, M., Sommariva, M., Gagliano, N., & Limonta, P. (2020). Three-dimensional cell cultures as an in vitro tool for prostate cancer modeling and drug discovery. *International Journal of Molecular Sciences*, 21(18), 6806.
- Goncharova, E. A., Chan, S. Y., Ventetuolo, C. E., Weissmann, N., Schermuly, R. T., Mullin, C. J., & Gladwin, M. T. (2020). Update in pulmonary vascular diseases and right ventricular dysfunction 2019. *American Journal of Respiratory and Critical Care Medicine*, 202(1), 22-28.
- Gordon, E., Schimmel, L., & Frye, M. (2020). The importance of mechanical forces for *in vitro* endothelial cell biology. *Frontiers in Physiology*, 11, 684.
- Han, H. X., & Geng, J. G. (2011). Over-expression of Slit2 induces vessel formation and changes blood vessel permeability in mouse brain. *Acta Pharmacologica Sinica*, 32(11), 1327-1336.
- Hennigs, J. K., Matuszcak, C., Trepel, M., & Körbelin, J. (2021). Vascular endothelial cells: Heterogeneity and targeting approaches. *Cells*, 10(10), 2712.
- Hida, K., Maishi, N., Annan, D. A., & Hida, Y. (2018). Contribution of tumor endothelial cells in cancer progression. *International Journal of Molecular Sciences*, 19(5), 1272.
- Huttala, O., Vuorenpää, H., Toimela, T., Uotila, J., Kuokkanen, H., Ylikomi, T., Sarkanen, J. R., & Heinonen, T. (2015). Human vascular model with defined stimulation medium - a characterization study. *Altex*, 32(2), 125-136.
- Jang, J., Jung, Y., Kim, Y., Jho, E.-h., & Yoon, Y. (2017). LPS-induced inflammatory response is suppressed by Wnt inhibitors, Dickkopf-1 and LGK974. *Scientific Reports*, 7(1), 41612.
- Jensen, C., & Teng, Y. (2020). Is it time to start transitioning from 2D to 3D cell culture? *Frontiers in Molecular Biosciences*, 7, 33.
- Jourde-Chiche, N., Fakhouri, F., Dou, L., Bellien, J., Burtey, S., Frimat, M., ... & Roumenina, L. T. (2019). Endothelium structure and function in kidney health and disease. *Nature Reviews Nephrology*, 15(2), 87-108.
- Klein, D. (2018). The tumor vascular endothelium as decision maker in cancer therapy. *Frontiers on Oncology*, 8, 367.
- Kruger-Genge, A., Blocki, A., Franke, R. P., & Jung, F. (2019). Vascular endothelial cell biology: An update. *International Journal of Molecular Sciences*, 20(18), 4411.
- Kusoglu, A., Yangin, K., Ozkan, S. N., Sarica, S., Ornek, D., Solcan, N., ... & Ozturk, E. (2023). Different decellularization methods in bovine lung tissue reveals distinct biochemical composition, stiffness, and viscoelasticity in reconstituted hydrogels. *ACS Applied Bio Materials*, 6(2), 793-805.
- Lee, J. Y., Chang, J. K., Dominguez, A. A., Lee, H. P., Nam, S., Chang, J., ... & Chaudhuri, O. (2019). YAP-independent mechanotransduction drives breast cancer progression. *Nature Communications*, 10(1), 1848.
- Lin, S., Zhang, Q., Shao, X., Zhang, T., Xue, C., Shi, S., Zhao, D., & Lin, Y. (2017). IGF-1 promotes angiogenesis in endothelial cells/adipose-derived stem cells co-culture system with activation of PI3K/Akt signal pathway. *Cell Proliferation*, 50(6), e12390.
- Matsubara, M., & Bissell, M. J. (2016). Inhibitors of Rho kinase (ROCK) signaling revert the malignant phenotype of breast cancer cells in 3D context. *Oncotarget*, 7(22), 31602-31622.
- McHenry, P. R., & Prosperi, J. R. (2023). Proteins found in the triple-negative breast cancer secretome and their therapeutic potential. *International Journal of Molecular Sciences*, 24(3), 2100.
- Medina-Leyte, D. J., Domínguez-Pérez, M., Mercado, I., Villarreal-Molina, M. T., & Jacobo-Albavera, L. (2020). Use of human umbilical vein endothelial cells (HUVEC) as a model to study cardiovascular disease: A review. *Applied Sciences*, 10(3), 938.
- Mierke, C. T. (2023). Physical and biological advances in endothelial cell-based engineered co-culture model systems. *Seminars in Cell & Developmental Biology*, 147, 58-69.
- Nguyen, J., Lin, Y. Y., & Gerecht, S. (2021). The next generation of endothelial differentiation: Tissue-specific ECs. *Cell Stem Cell*, 28(7), 1188-1204.
- Paek, J., Park, S. E., Lu, Q., Park, K. T., Cho, M., Oh, J. M., ... & Huh, D. (2019). Microphysiological engineering of self-assembled and perfusable microvascular beds for the production of vascularized three-dimensional human microtissues. *ACS Nano*, 13(7), 7627-7643.
- Rafii, S., Butler, J. M., & Ding, B. S. (2016). Angiocrine functions of organ-specific endothelial cells. *Nature*, 529(7586), 316-325.
- Rayner, R. E., Makena, P., Prasad, G. L., & Cormet-Boyaka, E. (2019). Optimization of normal human bronchial epithelial (NHBE) cell 3D cultures for *in vitro* lung model studies. *Scientific Reports*, 9(1), 500.
- Ritchie, S., Reed, D. A., Pereira, B. A., & Timpson, P. (2021). The cancer cell secretome drives cooperative manipulation of the tumour microenvironment to accelerate tumourigenesis. *Faculty Reviews*, 10, 4.
- Rosen, R. S., Yang, J. H., Peña, J. S., Schloss, R., & Yarmush, M. L. (2023). An in vitro model of the macrophage-endothelial interface to characterize CAR T-cell induced cytokine storm. *Scientific Reports*, 13(1), 18835.
- Tatla, A. S., Justin, A. W., Watts, C., & Markaki, A. E. (2021). A vascularized tumoroid model for human glioblastoma angiogenesis. *Scientific Reports*, 11(1), 19550.
- Urbanczyk, M., Zbinden, A., & Schenke-Layland, K. (2022). Organ-specific endothelial cell heterogeneity and its impact on regenerative medicine and biomedical engineering applications. *Advanced Drug Delivery Reviews*, 186, 114323.
- Wakabayashi, T., & Naito, H. (2023). Cellular heterogeneity and stem cells of vascular endothelial cells in blood vessel formation and homeostasis: Insights from single-cell RNA sequencing. *Frontiers in Cell and Developmental Biology*, 11, 285.
- Zahari, S., Syafruddin, S. E., & Mohtar, M. A. (2023). Impact of the cancer cell secretome in driving breast cancer progression. *Cancers*, 15(9), 2653.

Cite as: Ozkan, S. N., & Ozturk, E. (2024). Growth and organotypic branching of lung-specific microvascular cells on 2D and in 3D lung-derived matrices. *Front Life Sci RT*, 5(1), 6-14.



Research article

The most relevant drought-tolerant indices for selecting barley drought-tolerant genotypes

Mbarek Ben Naceur^{*1} , Hatem Cheikh-Mhamed² 

¹ Carthage University, National Gene Bank of Tunisia, 1080, Cherguia-1, Tunisia

² Carthage University, National Agronomic Research Institute of Tunisia, Agronomy Department, 2040, Ariana, Tunisia

Abstract

During its development cycle, lack of water is one of the factors reducing plant growth and yields, in the world's arid regions. The identification of indices that characterize the most tolerant genotypes to drought is very useful since it allows us to evaluate the tolerance of large varieties collections within a short and early stage. This study aimed to identify the most efficient drought tolerance indicators and evaluate, from the early stage of plant development, the germination parameters that would be correlated with drought tolerance in the field. If such correlations were identified, it would be possible to screen dozens of genotypes in the laboratory and identify the most tolerant ones before moving into the field. To attain this objective, two tests were carried out: The first one was realized in the laboratory to assess some germination parameters (germination rate, root length, root number, etc.) of sixteen North African barley genotypes (Algerians, Tunisians, and Egyptians) at the germination stage, under polyethylene glycol (PEG-6000) induced stress. The second test was carried out in the field to measure the grain yield of the same genotypes, under favorable and limited water conditions. The laboratory test revealed significant differences between root lengths (RL) of different genotypes within each water regime and between different treatments (control and PEG-6000 solution). The obtained result showed the superiority of most Egyptian genotypes, especially under stress conditions induced by PEG-6000. The field trial also showed significant differences in grain yields under both water regimes (stressful and non-stressful regimes) and pointed to the high performance of the majority of Egyptian genotypes. The calculated indices [(STI), (SSI), (YSI), and (TOL)] showed variable correlations depending on the index used and concluded that STI and YSI are the best indicators of drought tolerance compared to the others. Among the germination parameters, only the root length (RL) under PEG stress is positively correlated with grain yield, obtained under drought conditions in the field. Therefore, it would be possible to use this parameter to select, at an early stage, the most drought-tolerant genotypes.

Keywords: Barley; correlation; drought; polyethylene glycol; tolerance index; stress

1. Introduction

Drought is the main factor limiting agricultural productivity in many countries worldwide. It affects all aspects of plant growth and causes a series of changes affecting morphological, physiological, and biochemical plant characteristics related to the expression of drought tolerance genes (Gray and Brady, 2016; Gerszberg and Hnatuszko-Konka,

2017; Seleiman et al., 2021). According to Kuru (2023), plants undergo morphological changes that are critical to responding to water deficiency, such as a decrease in growth rate, an elongation of the root system, and an altered root-to-aerial part ratio.

Underwater scarcity conditions, the most significant root changes were the modification of their architecture, such as root suberization avoiding water loss, and allowing the plant to

* Corresponding author.

E-mail address: nour3alanour@yahoo.com (M. Ben Naceur).

<https://doi.org/10.51753/flsrt.1362571> Author contributions

Received 19 September 2023; Accepted 31 January 2024

Available online 30 April 2024

2718-062X © 2024 This is an open access article published by Dergipark under the [CC BY](https://creativecommons.org/licenses/by/4.0/) license.

survive until the soil humidity becomes suitable again, and the increase in root hairs necessary for the absorption of moisture from the soil (Minocha et al., 2014; Hassan et al., 2023). Basu et al. (2016), stated that the formation of small roots under drought conditions was an adaptive pathway since it improves water absorption by providing a greater absorbent surface. Moreover, the presence of rhizodermal tissue, with thickened outer walls (suberized), or with reduced cortical layers, was also considered an adaptive pathway for drought survival. Other changes, in response to drought, have been reported such as root thickness or root thinner (Kou et al., 2022), and both responses are beneficial for crops subjected to drought. The biochemical changes expressed at the leaf level are related to the osmotic accumulation (proline, glycine betaine, soluble sugars etc.) to maintain the turgidity potential as high as possible and allow the plant to survive (Sakr et al., 2012; Cai and Gao, 2020; Huang et al., 2021). Yooyongwech et al. (2017), working on sweet potatoes also confirmed biochemical changes under drought conditions such as an increase in total soluble sugar in storage root tissues and an increase in proline and sucrose content in leaf tissues to maintain the leaf osmotic potential. In arid and semi-arid regions of North Africa and sub-Saharan Africa, the main livelihood is based on rain-fed agriculture. These regions are characterized by irregular rainfall and frequent and intense droughts, which force farmers to put in place tools to deal with temporal water shortages. In this context, more, than 3/4 of Tunisia's surface area consists of semi-arid, arid, and desert regions. In this country, barley cultivation is rain-fed and covers an area varying from 500 to 600 ha out of 1500 ha of total cereals. The national average barley yield is only 0,08 kg/m². This is mainly due to the recurring lack of precipitation and the inadequate technical package used. Thus, the selection of drought-tolerant barley cultivars in this country is of paramount importance to improve the yields of this crop and exploit potential untapped production areas.

Selecting the most drought-tolerant genotypes is difficult due to the unavailability of rapid and reproducible screening techniques (Hassan et al., 2023). Nevertheless, despite these complications, some studies were realized in different ways. Such as measuring the plant's relative water content, the plant cover temperature (Tembe et al., 2017), the osmoticum accumulation, the membrane integrity (Geetha et al., 2017; Mahdavi et al., 2023), the root system parameters (root length, root number, root diameter, and architecture) (Maiti, 2012; Lalić et al., 2017), and the yield components under stress conditions (EL-Shawy et al., 2017). According to Negisho et al. (2022) and Li et al. (2023), drought tolerance indices provide measures based on yield loss under drought conditions compared to that obtained under favorable conditions. Several authors (Ilker, 2011; Mohammadi et al., 2011; Ayranci et al., 2014; Gitore et al., 2021) defined stress tolerance (TOL) as the difference between the yield obtained under favorable conditions (Y_p) and that obtained under stress conditions (Y_s). For their part, Sánchez-Reinoso et al. (2020) recommended the stress susceptibility index (SSI) for assessing the sensitivity of genotypes in varying environments. Lamba et al. (2023) proposed a yield index (YI) and yield stability index (YSI) as an assessment of genotype stability under water deficit and favorable conditions. Gitore et al. (2021) used the Stress Tolerance Index (STI) to identify the most productive genotypes under favorable and those of water deficit. Other researchers have used other modified indices. Some of them have conceived new methods for monitoring drought-induced vegetation stress

called the Vegetation Drought Response Index (Lamba et al., 2023; Yin and Zhang, 2023). Although none of the drought indices is necessarily better than the others, some indices are better suited for specific purposes than others (Karavitis et al., 2011).

This study focused on assessing the effectiveness of drought tolerance indices for the selection of drought-tolerant barley genotypes at the beginning (germination) and at the end (maturity) stage in the field. We were interested in germination parameters, grain yield, and indices previously cited and tried to identify correlations that may be useful for the identification of drought tolerant genotypes at an early stage.

2. Materials and methods

Sixteen barley genotypes were selected from three North African countries [Tunisia (5 genotypes), Algeria (5 genotypes), and Egypt (6 genotypes)]. This material is as follows: Kairouan (V4), Rihane (V7), Sidi-Bouزيد (V8), Sabra (V9), Tombari (V10) from Tunisia, Techedrett (V15), Saïda (V17), Sidi-Mehdi (V18), Ras-El-mouche (V19), Naïlia (V20) from Algeria and Giza 123 (V23), El Arich (V24), Ksar (V25), Giza 2000 (V26), Giza 125 (V29) and Giza 131 (V30) from Egypt.

2.1. Tests conduct

The first test was carried out in the laboratory where 20 barley seeds of each genotype were germinated in Petri dishes (90mm diameter), containing filter paper and distilled water (Control) or a polyethylene glycol solution (PEG-6000) at a 10% concentration (Stressed). Each treatment (Stressed or not) is repeated 4 times. The second trial was realized in the field with standard agronomic practices of barley crops during two successive growing seasons (2013-2014 and 2014-2015). The 16 barley genotypes were selected as part of the New Partnership for African Development (NEPAD) project, carried out in Algeria, Tunisia, and Egypt at the same time. The soil on which the tests were conducted, and the seedbed preparation actions have been previously described (Ben Naceur et al., 2018). The seed rate was calculated based on 250 seeds/m².

The experiment was carried out using a randomized complete block design (RCBD) with four repetitions for each genotype per block. The area of each elementary plot was 4 m² (2m×2m). The blocks are separated from each other by 2m while the elementary plots and the rows are separated by 0.50m and 0.20 m, respectively. The recorded climatic data through the two experimental growing seasons are shown in Fig. 1. They were obtained from the historical weather site. The comparison of monthly average temperature and precipitation during the two growing seasons (November to May) showed that average temperature values were very near (Fig. 1a), while precipitation in 2014 (349 mm) was much lower than in 2015 (421 mm) (Fig. 1b). If we compare the precipitation of the months during the two growing seasons, we can see a considerable difference in January and February rains with 29 and 18 mm in 2014 compared to 70 and 118 mm in 2015 (Fig. 1b).

2.2. Parameters measured

2.2.1. Germination parameters

Germination was realized in a germination chamber (temperature: 25/18°C and 12h of light to speed growth) in Petri

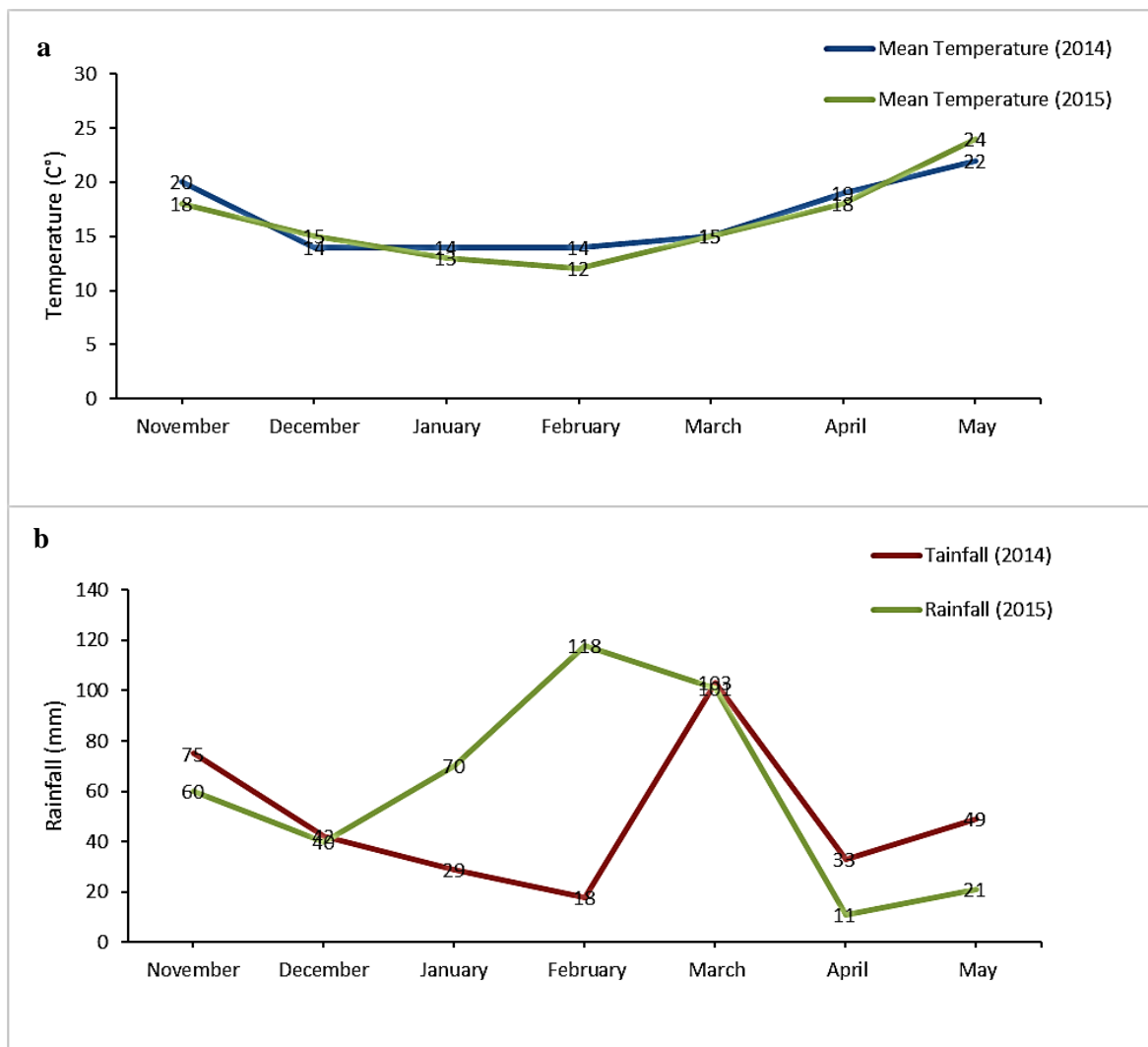


Fig. 1. Comparison of monthly averages of temperature (a) and precipitation (b) during the two growing seasons (2014 and 2015).

dishes containing either distilled water (Control) or a 10% PEG-6000 solution (Stressed). Michel and Kaufmann (1973), established a relationship between the PEG-6000 concentration of a given solution and its osmotic potential:

$$\pi = (-0.0118 \times C) - (0.000118 \times C) + (0.000267 \times CT) + 0.000000839 \times C_2T$$

Where C is the PEG-6000 concentration and T is the temperature.

In this case, the osmotic potential of the solution used is -1.48 bars.

After one week of cultivation in Petri dishes, the parameters measured were:

- The germination rates.
- The root numbers.
- The root length is expressed in cm.
- The Stress Tolerance Index (STI) is based on root length in the PEG-6000 solution.

2.2.2. Grain yield obtained in the field

The total grain yield (stressed or unstressed) is calculated after harvesting the elementary plots and expressing the results in kg/m².

2.2.3. Drought tolerance indices

Several indices that describe drought tolerance defined by (Ayranci et al., 2014; EL-Shawy et al., 2017; Hellal et al., 2019; Sánchez-Reinoso et al., 2020; Li et al., 2023), were used in this study, in the germination test and, in the field trial:

The stress susceptibility index noted SSI:

$$SSI = [1 - (Y_s)/(Y_p)]/SI$$

Stress intensity noted SI (Stress Intensity):

$$SI = [1 - (Y_s)/(Y_p)]$$

The stress tolerance index denoted STI (Stress Tolerance Index):

$$STI = [(Y_p)X(Y_s) / \bar{Y}_p^2]$$

Stress tolerance noted TOL (Tolerance):

$$TOL = (Y_p - Y_s)$$

The yield stability index noted YSI (Yield Stability Index):

$$YSI = Y_s/Y_p$$

Where Y_s and Y_p are the yields of genotypes evaluated under stressful and non-stressful conditions and Y_s and Y_p are

the averages of all genotypes evaluated under stress and favorable conditions.

2.3. Statistical analysis

The experiment was carried out using a randomized complete block design (RCBD) with four repetitions for each genotype per block. The area of each elementary plot was 4 m². The sowing date was realized manually on 1 November for each growing season. The sowing density was 60 grains/linear meter. The first two blocks were conducted in the open field from the sowing date until harvest (Control) and the two-second blocks were also conducted in the open field from the sowing date (November) until the ear swelling and early heading stage (early March). From this date until harvesting, the plants were protected by a plastic film preventing rainfall and without irrigation (Stressed). The data collected during the two growing seasons were statistically analyzed using SAS software. Genotype means were compared using a Fisher's test by least significant difference at (P ≤ 0.05).

3. Results and discussion

3.1. Germination rate, root number, and root length at the germination stage

The germination rate calculated in this study indicates the percentage of germinated grains out of the total number of grains placed in Petri dishes for germination. In this study, PEG-6000 as a stressor did not induce considerable change in the final germination of different barley genotypes. However, it brings a significant delay in germination without completely inhibiting it. This delay is common in all germination tests because the seeds need more time to absorb enough water and initiate germination. Although most seeds have germinated both under non-stressful and under PEG-6000 stressful conditions, the obtained seedlings under stressful conditions are not all viable (poorly developed roots). The same observation was noted for the root number. In fact, the PEG-6000-induced stress did not significantly influence the root number and although a slight reduction was observed under stress conditions, no significant

difference was noticed (Fig. 2). In contrast, some genotypes produced the same root number or sometimes more roots in stress conditions than in non-stress conditions (V8; V23; V25).

Table 1

Root length (RL) variation of 16-barley genotypes under stress (PEG-6000) and non-stressful conditions.

| Genotypes | Non-stress conditions | PEG-6000 stress conditions. |
|-----------|------------------------|-----------------------------|
| | T0 | T10 |
| | Mean root length in cm | Mean root length in cm |
| V4 | 5.97 fgh | 4.08 abcd |
| V7 | 6.58 bc | 5.012 a |
| V8 | 6.16 gh | 4.11 abc |
| V9 | 3.92 h | 2.68 f |
| V10 | 7.99 a | 3.10 def |
| V15 | 5.27 def | 3.49 cdef |
| V17 | 5.00 efgh | 3.76 bcde |
| V18 | 5.98 bcde | 4.50 ab |
| V19 | 4.79 fgh | 3.64 bcdef |
| V20 | 5.14 efg | 3.54 bcdef |
| V23 | 6.32 bcd | 3.53 bcdef |
| V24 | 5.07 efg | 3.10 def |
| V25 | 5.66 cdef | 3.52 bcdef |
| V26 | 6.89 ab | 3.03 ef |
| V29 | 7.94 a | 4.05 abcd |
| V30 | 6.41 bc | 4.14 abc |

*(Means with the same letter are not significantly different from each other)

Therefore, PEG-6000-induced stress did not significantly affect germination rate or root number, but it negatively influenced root length. This is why we focused on root length rather than on root number or on the germination rate itself (Table 1). This result is per those of Kou et al. (2022) who stated that water deficit induces an increase in root hair density, which in turn, increases the contact between the root surface and their environments. It is recognized that, under water-limited conditions, sensitive genotypes were incapable of uptake sufficient water due to their inability to emit deep roots in search of moisture, whereas tolerant genotypes produced extended roots to obtain water from the solution or the lower surface of the soil when they were sown in the field. Therefore, the root

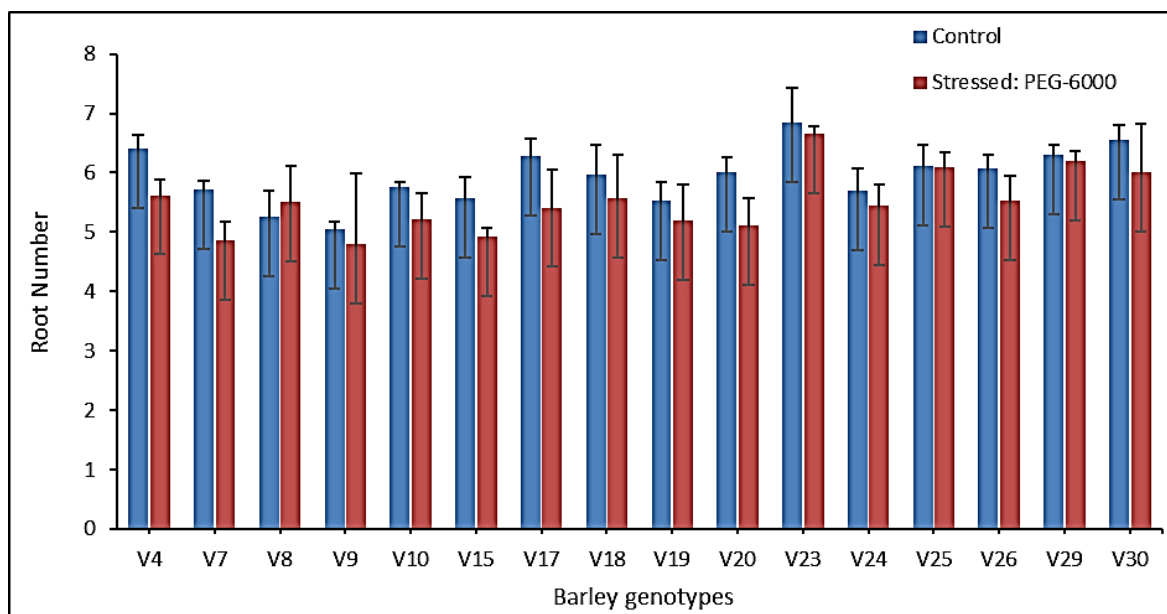


Fig. 2. Barley root number at the germination stage.

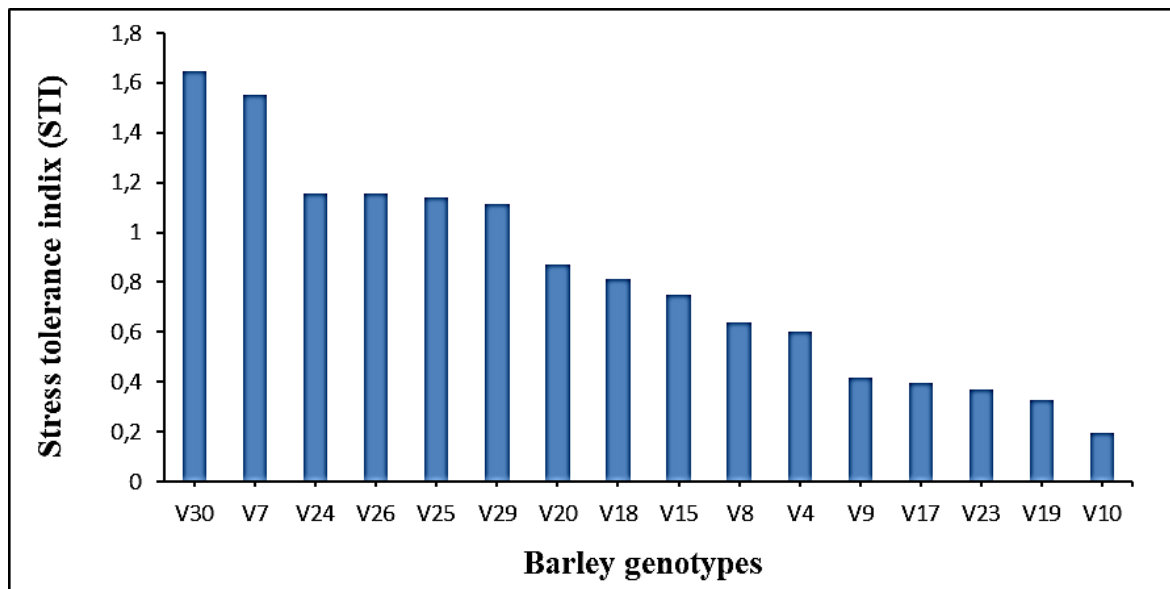


Fig. 3. Stress Tolerance Index of barley genotypes based on root length under PEG-6000 conditions.

length character may be used, among others, as a reliable selection criterion for barley drought resistance. Table 1 revealed variability in the average root length both under the control and under PEG-6000 stress conditions. This parameter, statistically analyzed, had significant differences at the 5% threshold in stressful and non-stressful conditions.

The classification of root length in the Control showed eight different groups. The best performances are observed in the V10, V29, and V26 genotypes, which occupied the first cluster. Their root length varied between 6.89 and 7.99 cm while V4, V8, V17, V19, and V9 occupied the last group and exhibited the shortest root lengths that varied from 3.92 to 6.16 cm. The other genotypes are intermediate. This result, expressing variability between genotypes, complied with those observed by Min et al. (2022) on maize and by Aslam et al. (2023) on cotton. Similarly, under the PEG-6000 conditions, the root length analysis showed significant differences at the 5% threshold and hierarchized the genotypes into six (6) groups where V4, V7, V8, V18, V29, and V30 occupied the first class with 4.05 to 5.012 cm, in length. On the other hand, the remaining genotypes showed the shortest root and therefore occupied the last class with lengths varying between 2.68 and 3.76 cm. Although the stress has reduced the extending root of the majority of the genotypes tested, some of them were able to maintain sufficiently extended roots. The ability of these barley genotypes to maintain growing roots under stress conditions, suggests the upholding of certain gene expressions involved in root elongation such as (Deeper Rooting 1 (DR01) as reported by Uga et al. (2013). These genes would promote the absorption of water and allow a correlative growth of these roots.

Other genes could increase the osmoticum level in the roots of the tolerant genotype exposed to drought and increase the activity of certain antioxidant enzymes (catalase, peroxidase, etc.) to reduce oxidative damage due to environmental stress, as demonstrated by Cai and Gao (2020) and Aslam et al. (2023) in recent studies. Therefore, root extension under stress conditions could inform us about the stress-tolerant genotypes and constitute an appreciable indicator of tolerance to water deficit. The stress tolerance index, based on the root length under favorable or under stress conditions (induced by PEG-6000), illustrated in Fig. 3 showed that V7, V30, and V29 genotypes were the most tolerant ones to stress, on the other hand, V9 was

the most sensitive. Long roots, which were well anchored in the substrate, were a beneficial factor influencing the capacity of the plant to absorb water from the soil's deep layers. Based on the individual root or the whole root system, different parameters such as root length, diameter, or architectural patterns, have been used as potential indicators of stress tolerance in some previous case studies. In this context, Lalić et al. (2017) and Aslam et al. (2023) have used root elongation as an indicator of stress tolerance for barley and cotton, respectively. They suggested that the uptake of water is directly linked to root development and architecture, confirming the choice of this parameter (root length) as a criterion for evaluating plant tolerance to stress under PEG-6000.

3.2. Evaluation of the genotype's tolerance to drought in the field

3.2.1. The harvested grain yield

The grain yield was obtained after collecting the elementary plots and expressing the results in Q/ha. The result obtained showed that the Egyptian genotype V30 produced the best yield in both favorable and drought conditions (Table 2). This genotype produced 48 Q/ha (0.48kg/m²), underwater favorable conditions against the average of all the genotypes which was 35 Q/ha (0.35kg/m²), showing a superiority of about 37%, compared to the average. It also produced 46 Q/ha (0.46kg/m²) under water deficit conditions against the average of all genotypes tested which was 27.28 Q/ha (0.27kg/m²), that to say, an increase of 68.62% compared to the average of all genotypes. Abdel-Moneam et al. (2014) and Hellal et al. (2019) tested the same genotype (V30) in other geographically varied sites and showed its good yield and wide adaptation to different environments.

Statistical analysis (Table 2) classified all the genotypes into eight (8) groups in the control and five (5) groups in the stressed. Whatever, the water regime used, V30 and V7 produced the best yield and therefore occupied the first class while V10 produced the lowest yield. The high grain yield produced by the V30 and V7 genotypes confirms their tolerance to drought as compared to the remaining genotypes. The best performance of these two genotypes observed in both water

regimes was consistent with what Hellal et al. (2019) found. These results were also in agreement with those of Abd El-Raouf et al. (2012) who compared the yield of several barley genotypes under drought conditions of which (V30) was among the most efficient.

Table 2
Indices measured.

| Genotypes | Yp | Ys | TOL | SSI | STI | YSI |
|-----------|-------------|----------|-------|--------|-------|-------|
| V30 | 48.05 a | 43.27 a | 4.79 | 0.429 | 1.646 | 0.900 |
| V7 | 46.11 ab | 42.45 a | 3.66 | 0.342 | 1.550 | 0.921 |
| V24 | 45.74 ab | 31.93 b | 13.80 | 1.300 | 1.156 | 0.698 |
| V26 | 42.59 abc | 34.27 b | 5.74 | 0.841 | 1.155 | 0.805 |
| V25 | 41.50 abcde | 35.27 b | 5.66 | 0.595 | 1.143 | 0.862 |
| V29 | 40.92 abcd | 33.83 b | 7.66 | 0.795 | 1.111 | 0.815 |
| V20 | 38.73 abcde | 28.33 bc | 10.40 | 1.1561 | 0.869 | 0.731 |
| V18 | 37.41 bcdef | 31.67 b | 5.74 | 0.661 | 0.938 | 0.974 |
| V15 | 35.84 bcdef | 26.43 bc | 9.417 | 1.130 | 0.750 | 0.737 |
| V8 | 32.50 cdefg | 21.63 de | 10.87 | 1.440 | 0.557 | 0.675 |
| V4 | 31.66 defg | 23.97 cd | 7.69 | 1.046 | 0.601 | 0.757 |
| V17 | 30.77 efg | 16.16 de | 14.61 | 2.043 | 0.394 | 0.525 |
| V23 | 27.29 fgh | 17.16 de | 10.13 | 1.598 | 0.371 | 0.629 |
| V9 | 27.00 fgh | 19.39 de | 7.62 | 1.215 | 0.414 | 0.718 |
| V19 | 23.10 gh | 18 de | 5.10 | 0.951 | 0.329 | 0.779 |
| V10 | 19.43 h | 12.8 e | 6.63 | 2.044 | 0.197 | 0.659 |

*(Means with the same letter are not significantly different from each other)

3.2.2. Evaluation of grain yield indices under water deficit conditions

The indices describing sensitivity (SSI) and stress tolerance (STI) are illustrated in Table 2, which always showed the superiority of production of V30 and V7 and the low yielding of V10 whatever the water regime used. The high-stress tolerance index (STI) of these two genotypes during the two growing seasons indicated their adaptability to different humidity levels compared to other genotypes whose ranking changed according to the soil moisture conditions. The interaction (genotype x environment) which determined the yield stability (YSI) also revealed the yield superiority of these two genotypes in both cases of water regime. Our result displayed also other high-yielding genotypes (V26, V24, and V25) which could differ in terms of yield stability. This could occur when genotypes are only productive under favorable conditions or when the yield difference, in both water regimes, is small. Consequently, the V30 and V7 genotypes could be used as progenitors in varietal selection programs for drought

resistance. Nevertheless, genotype classification based on TOL or SSI indices exhibited a slightly different trend than that generated by STI (Table 2), confirming the inability of SSI to differentiate drought-tolerant genotypes from those with low yield potential, as Li et al. (2023) have suggested. The highest tolerance index TOL values were obtained in V17, V24, V8, V20, and V23 genotypes (14.61; 13.80; 10.87; 10.40, and 10.13 respectively). Likewise, the highest values of the stress susceptibility index (SSI) were obtained in V10; V17; V23; V8, and V24 genotypes (2.044; 2.043; 1.60, 1.44, and 1.30, respectively) (Table 2). Most of these genotypes showed satisfactory yield under non-stressed conditions but low yield under drought conditions. This implies that choices based on high values of TOL and/or SSI would result in sensitive genotypes with low yields under drought conditions.

However, the lowest values of SSI or TOL (values ≤ 1) could also be practical indices characterizing the most tolerant genotypes, similar to STI or YSI, as proposed by Sánchez-Reinoso et al., (2020) for common bean genotypes subject to water deficit. Nevertheless, when the SSI index was low, it could indicate also that the production potential of the genotype is low and the genotype might not be productive under both water regimes. This observation was confirmed by Li et al. (2023) who used (SSI) as a screening criterion for drought resistance in wheat and revealed the inability of this criterion to distinguish between the most tolerant genotypes and those having low potential yield. Conversely, when STI and YSI indices were higher, the genotype might be productive, under stressful and non-stressful conditions. These results agreed with those of Hellal et al. (2019) on barley and Abdul-Mannan et al. (2023) on maize. Similar results to ours were reported by Mohammadi et al. (2011) indicating that (STI) index was well-appropriate for selecting the most productive RILs (Recombinant Inbred Lines) under two contrasting water regimes.

Moreover, Gitore et al. (2021), working on orange-fleshed sweet potato genotypes, reported that drought tolerance was indicated by genotypes with high Tolerance Index (STI) values. Also, Mahdavi et al. (2023) working on wheat, reported the same conclusion in which tolerant genotypes were characterized by a stress tolerance index and a yield stability index (STI and YSI) both high and indices (TOL and SSI) relatively low. It is therefore clear that the drought tolerance index (STI) is a strong discriminator between potentially water-stress tolerant genotypes and other high-yielding genotypes. However, the (SSI) and (TOL) indices provided usually variable results, which do not allow the selection of the most stress-tolerant genotypes. These two last parameters have already shown their limits in

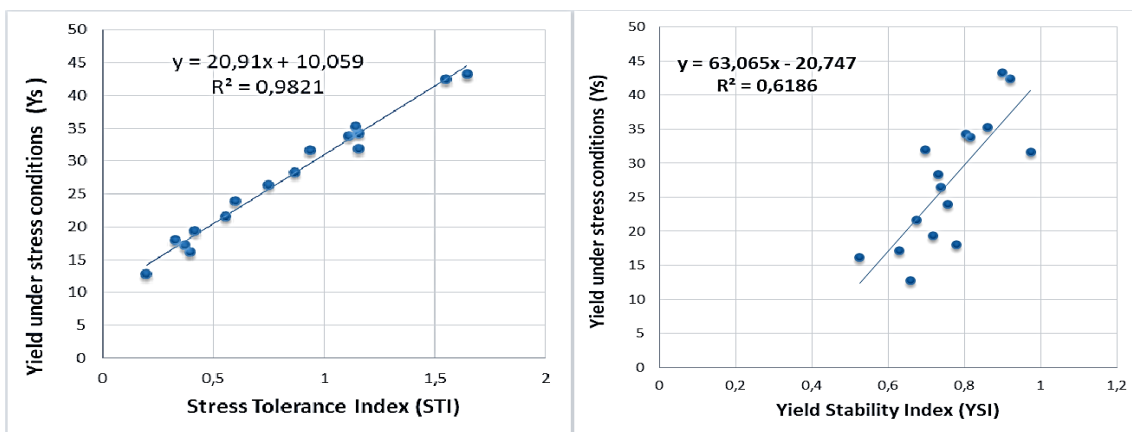


Fig. 4. Correlation between (Ys) on one hand and (STI) and (YSI) on the other.

wheat (Anwar et al., 2011) and in beans (Asadi and Seyedi, 2021).

3.3. Correlations between stress indices and yields under drought conditions (Ys)

Positive correlations between grain yield under stress conditions (Ys) and the stress tolerance Index (STI) on the one hand, and between (Ys) and the yield stability index (YSI), on the other hand, have been established (Fig. 4). High (STI) and (YSI) values indicated that the genotypes are drought tolerant. Consequently, the Egyptian (V30) and Tunisian (V7) genotypes are the most efficient and well-adapted to normal and adverse

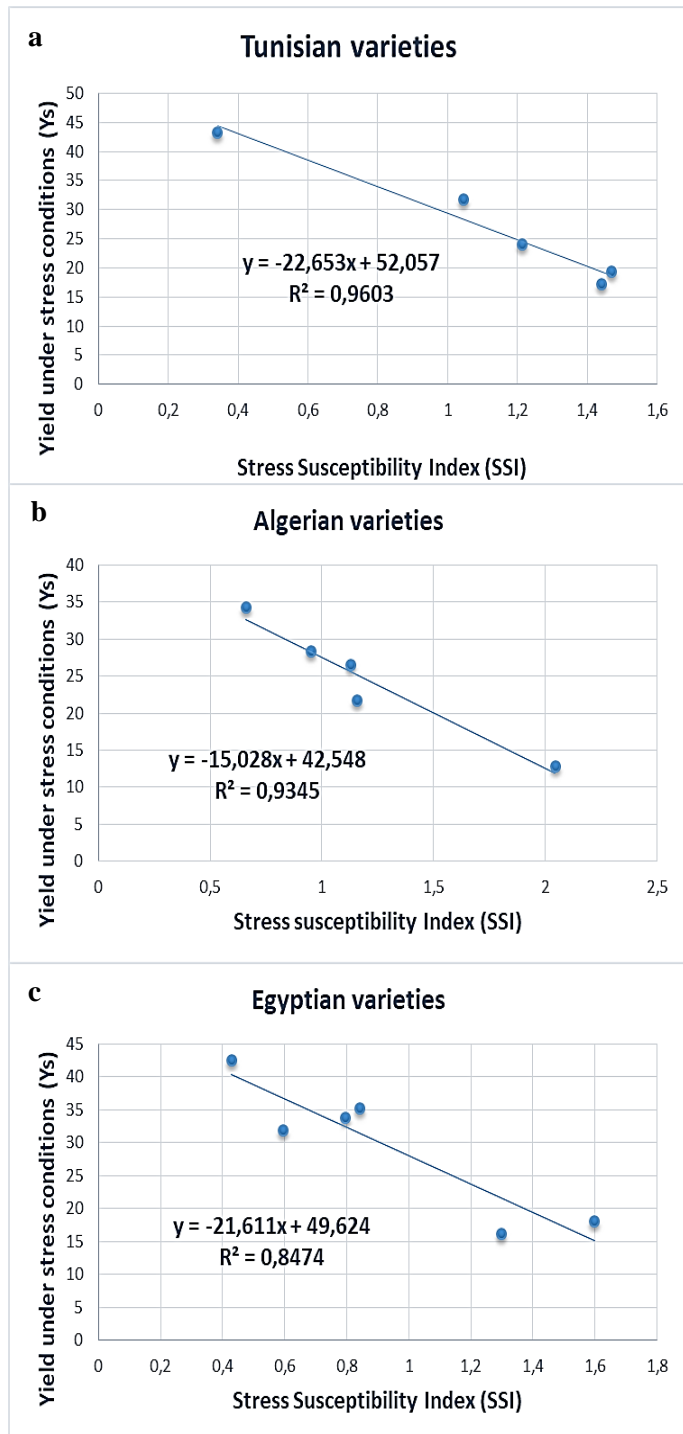


Fig. 5. Correlation between (Ys) and (SSI) indices for Tunisian (a), Algerian (b), Egyptian (c) varieties separately.

conditions. This result was consent with what Nouri et al. (2011) and Mahdavi et al. (2023) have reported on wheat. The obtained results are also similar to what Hellal et al. (2019) have obtained on barley in another geographical region different from ours. These authors showed also a positive and highly significant correlation between the stress tolerance index (STI) and grain yield under water stress_conditions (YS) and stress stability index (YSI). They reported that these indices could discriminate groups of varieties that express superior indices of (STI and/or YSI) which are correlated with high yielding in stress conditions.

Similarly, the recorded data in this study showed that grain yield under stress conditions (YS) had a significantly negative correlation with the (TOL) and with the stress susceptibility index (SSI) for all genotypes (Fig. 5 a-c and Fig. 6.). Poudel et al. (2021) who were working under heat stress confirmed our result and revealed a negative and significant correlation between (SSI) and (Ys). They concluded that selection based on low SSI values would identify the most heat-stress-tolerant genotypes. However, when the SSI value exceeds 1, this index is no longer suitable for selecting the most stress-tolerant genotypes. These results agreed with those of Gitore et al. (2021) obtained on Orange Fleshed Sweet Potato and with that of Hellal et al. (2019) obtained on barley, which suggested that genotypes with the lowest (SSI) displayed drought resistance and those of high value of (SSI) are more susceptible to drought.

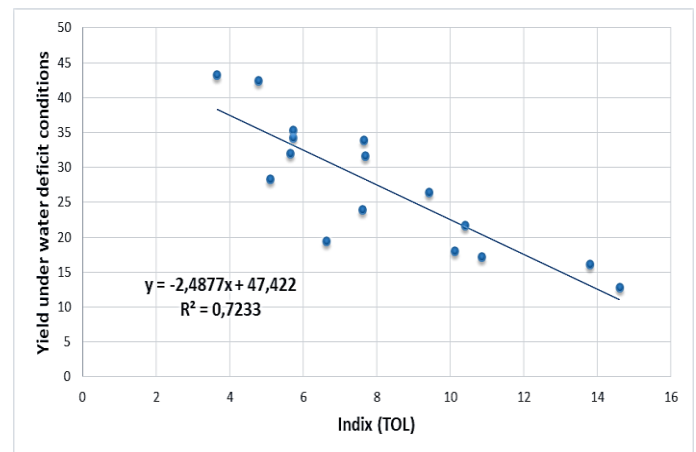


Fig. 6. Correlation between (Ys) and (TOL) index for all genotypes.

3.4. Correlation between yields under water deficit and germination parameters under PEG-6000-induced stress

Many plants are able to develop deep and extensive root systems under water-scarce conditions allowing them to draw water from deeper layers of the soil. This trait is of particular importance for crops, which often experience periods of water deficit. The illustration below (Fig. 7) showed a positive correlation between root length (RL), at the germination stage in PEG-6000, and grain yield (Ys) obtained in the field under drought conditions. The ability of barley genotypes to keep their root system growing despite the constraint imposed by PEG-6000 during the germination phase, informs us about their ability to extend their roots into the soil's deep layers in search of humidity in the event of real drought in the field.

Most of the genotypes whose roots showed an ability to grow despite the stress induced by PEG-6000 at the germination stage (V7; V8; V18; V29; V30) would produce the best yield under drought conditions in the field (V7; V25; V26; V29; V30).

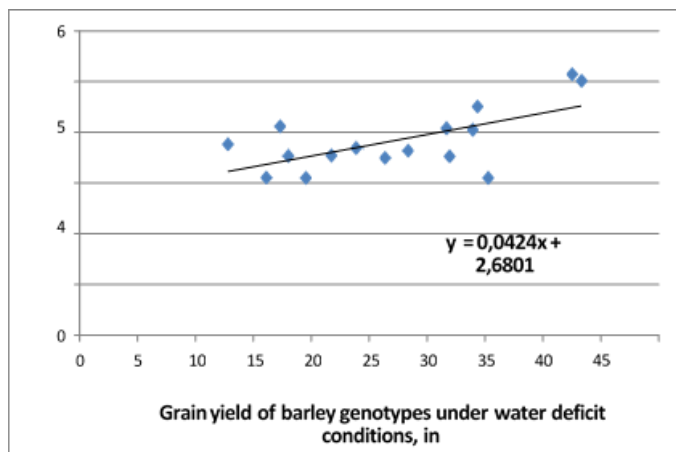


Fig. 7. Correlation between barley yield under drought and seedling root length under PEG-6000 stress conditions.

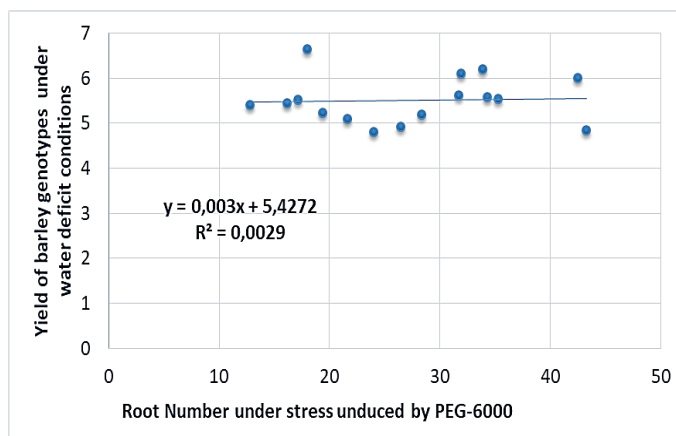


Fig. 8. Relationship between grain yield obtained under drought conditions and the root number (RN) obtained at the germination stage in the presence of PEG-600.

This finding is per those of Mishra et al. (2019) and Kim et al. (2020) for which a deep and prolific root system capable of extracting water from the soil would be an essential trait for adaptation to drought. In addition, it is in harmony with those of Maiti (2012), who showed that the root length and its fineness under water stress conditions could be considered reliable criteria to assess the level of drought tolerance of durum wheat. On the contrary, no correlation was found between grain yields obtained in the field under drought conditions, and the root number emitted at the germination stage, in PEG-6000-induced

References

- Abdel-Moneam, M. A., Sultan, M. S., Eid, A. A., & El-Wakeel, S. E. (2014). Response of Hull-less barley genotypes for high yield potential and stability as affected by different water stress conditions. *Asian Journal of Crop Science*, 6(3), 202-213.
- Abd El-Raouf, M., Kandil, A., El-Sayed, A., & Attya, A. (2012). Evaluation of some barley genotypes under soil moisture stress. *Egyptian Journal of Plant Breeding*, 203(1127), 1-14.
- Abdul-Mannan, M. A., Begum, F., Al Mamun, M. A., & Habib, M. A. (2023). Evaluation of maize (*Zea mays*) genotypes for tolerance to drought using yield based tolerance indices. *Journal of Agriculture and Crops*, 9(3), 329-337.
- Anwar, J., Subhani, G. M., Hussain, M., Ahmad, J., Hussain, M., & Munir, M. (2011). Drought tolerance indices and their correlation with yield in exotic wheat genotypes. *Pakistan Journal of Botany*, 43(3), 1527-1530.
- Asadi, B., & Seyedi, S. M. (2021). Evaluation of drought tolerance indices in red bean lines. *Journal of Crop Breeding*, 13(38), 160-168.
- Aslam, S., Hussain, S. B., Baber, M., Shaheen, S., Aslam, S., Waheed, R.,

stress (Fig. 8). Probably because the dose used was low, enough to induce a substantial reduction compared to the control. Although some authors working on other species have mentioned the reduction of root number (El-Fakhri et al., 2010; Esan et al., 2023) or even an increase in root number under PEG-induced stress (Nupur et al., 2020; Reyes et al., 2023). It is also important to recognize that the stress induced by the PEG does not entirely reproduce the drought conditions in the field, which are very complex and involve the soil nature, the plant species, the variety, and the nutrition conditions. This is why focusing on the effect of PEG-6000 on the root number was not the correct path leading to positive correlations between this parameter (RN) and drought tolerance in the field.

4. Conclusion

This study has allowed us to identify significant positive correlations between Ys and STI on the one hand and between Ys and YSI on the other side. Similarly, significant negative associations between Ys and the indices SSI and TOL showed the effectiveness of (STI and YSI) on the other indices. Among the germination parameters (germination rate, root length, root number, etc.), only root length (RL) was positively and significantly correlated with high yield obtained under drought conditions, in the field. Therefore, it is possible to select the most drought-tolerant genotypes, based on this criterion (RL), at an early stage to assess an important population for its drought tolerance. It would be more interesting, in terms of cost and time saving, to evaluate the drought tolerance of a large number of cultivars, at an early stage, than to evaluate them at a late stage in the field. Moreover, V30 and V7 genotypes were the most productive both under ample and limited water conditions. According to the statistical analysis, these two genotypes were at the top of the ranking and constituted the same cluster. However, V30 showed a slightly higher yield than V7 and presented the highest drought tolerance index; unlike V10 which always exhibited the lowest yield regardless of the water regime used.

Conflict of interest: The authors declare that they have no conflict of interests.

Informed consent: The authors declare that this manuscript did not involve human or animal participants and informed consent was not collected.

- & Azhar, M. T. (2023). Estimation of drought tolerance indices in upland cotton under water deficit conditions. *Agronomy*, 13(4), 984.
- Ayranci, R., Sade, B., & Soylu, S. (2014). The respons of bread wheat genotypes in different drought types i. grain yield, drouhgt tolerance, and grain yield stability. *Turkish Journal of Field Crops*, 19(2), 183-188.
- Basu, S., Ramegowda, V., Kumar, A., & Pereira, A. (2016). Plant adaptation to drought stress. *1000Research*, 5, 1-10.
- Ben Naceur, A., Cheikh-M'Hamed, H., Abdelly, C., & Ben Naceur, M. (2018). Screening of North African barley genotypes for drought tolerance based on yields using tolerance indices under water deficit conditions. *Turkish Journal of Field Crops*, 23(2), 135-145.
- Cai, Z. Q., & Gao, Q. (2020). Comparative physiological and biochemical mechanisms of salt tolerance in five contrasting highland quinoa cultivars. *BMC Plant Biology*, 20(1), 1-15.
- Esan, V. I., Obisesan, I. A., & Ogunbode, T. O. (2023). Root system architecture and physiological characteristics of soybean (*Glycine max*








- L.) seedlings in response to PEG6000-simulated drought stress. *International Journal of Agronomy*, 2023.
- El-Shawy, E. E., El-Sabagh, A., Mansour, M., & Barutcular, C. (2017). A comparative study for drought tolerance and yield stability in different genotypes of barley (*Hordeum vulgare* L.). *Journal of Experimental Biology and Agricultural Sciences*, 5(2), 151-162.
- Geetha, A., Sivasankar, A., & Prayaga, L. (2017). Effect of moisture stress on key physiological parameters in sunflower genotypes. *International Journal of Current Microbiology and Applied Sciences*, 6(5), 147-159.
- Gerszberg, A., & Hnatuszko-Konka, K. (2017). Tomato tolerance to abiotic stress: a review of most often engineered target sequences. *Plant Growth Regulation*, 83, 175-198.
- Gitore, S. A., Danga, B., Henga, S., & Gurmu, F. (2021). Evaluating drought tolerance indices for selection of drought tolerant orange fleshed sweet potato (OFSP) genotypes in Ethiopia. *International Journal of Agricultural Science and Food Technology*, 7(2), 249-254.
- Gray, S. B., & Brady, S. M. (2016). Plant developmental responses to climate change. *Developmental Biology*, 419(1), 64-77.
- Hassan, M. A., Dahu, N., Hongning, T., Qian, Z., Yueming, Y., Yiru, L., & Shimei, W. (2023). Drought stress in rice: morpho-physiological and molecular responses and marker-assisted breeding. *Frontiers in Plant Science*, 14.
- Hellal, F., Abdel-Hady, M., Khatib, I., El-Sayed, S., & Abdelly, C. (2019). Yield characterization of Mediterranean barley under drought stress condition. *AIMS Agriculture & Food*, 4(3), 518-533.
- Huang, H. X., Yang, Q. Q., Cui, P., Lu, G., & Han, G. J. (2021). Changes in morphological and physiological characteristics of *Gymnocarpus przewalskii* roots in response to water stress. *Acta Prataculturae Sinica*, 30(1), 197.
- Ilker, E., Tatar, O., Tonk, F. A., & Tosun, M. (2011). Determination of tolerance level of some wheat genotypes to post-anthesis drought. *Turkish Journal of Field Crops*, 16(1), 59-63.
- Karavitis, C. A., Alexandris, S., Tsesmelis, D. E., & Athanasopoulos, G. (2011). Application of the standardized precipitation index (SPI) in Greece. *Water*, 3(3), 787-805.
- Kim, Y., Chung, Y. S., Lee, E., Tripathi, P., Heo, S., & Kim, K. H. (2020). Root response to drought stress in rice (*Oryza sativa* L.). *International journal of molecular sciences*, 21(4), 1513.
- Kou, X., Han, W., & Kang, J. (2022). Responses of root system architecture to water stress at multiple levels: A meta-analysis of trials under controlled conditions. *Frontiers in Plant Science*, 13, 1085409.
- Kuru, I. S. (2023). The morpho-physiological responses of a tolerant and sensitive wheat (*Triticum aestivum* L.) cultivar to drought stress and exogenous methyl jasmonate. *Frontiers in Life Sciences and Related Technologies*, 4(1), 7-12.
- Lalić, A., Ban, S. G., Perica, S., Novoselović, D., Abičić, I., Kovačević, J., ... & Guberac, V. (2017). The effect of water stress on some traits of winter barley cultivars during early stages of plant growth. *Poljoprivreda*, 23(1), 22-27.
- Lamba, K., Kumar, M., Singh, V., Chaudhary, L., Sharma, R., Yashveer, S., & Dalal, M. S. (2023). Heat stress tolerance indices for identification of the heat tolerant wheat genotypes. *Scientific Reports*, 13(1), 10842.
- Min, L., Wen, D. X., Sun, Q. Q., Wu, C. L., Yan, L. I., & Zhang, C. Q. (2022). Factors influencing seed reserve utilization during seedling establishment in maize inbred lines. *Journal of Integrative Agriculture*, 21(3), 677-684.
- Li, J., Abbas, K., Wang, L., Gong, B., Hou, S., Wang, W., & Gao, H. (2023). Drought resistance index screening and evaluation of lettuce under water deficit conditions on the basis of morphological and physiological differences. *Frontiers in Plant Science*, 14.
- Nouri, A., Etminan, A., Teixeira da Silva, J. A., & Mohammadi, R. (2011). Assessment of yield, yield-related traits and drought tolerance of durum wheat genotypes (*Triticum turgidum* var. *durum* Desf.). *Australian Journal of Crop Science*, 5(1), 8-16.
- Mahdavi, Z., Rashidi, V., Yarnia, M., Aharizad, S., & Roustaii, M. (2023). Evaluation of yield traits and tolerance indices of different wheat genotypes under drought stress conditions. *Cereal Research Communications*, 51(3), 659-669.
- Maiti, R. (2012). Root responses are indicators for salinity and drought stress in crops. *International Journal of Bio-resource and Stress Management*, 3(Sep, 3), 1-3.
- Michel, B. E., & Kaufmann, M. R. (1973). The osmotic potential of polyethylene glycol 6000. *Plant Physiology*, 51(5), 914-916.
- Mishra, S. S., Behera, P. K., & Panda, D. (2019). Genotypic variability for drought tolerance-related morpho-physiological traits among indigenous rice landraces of Jeypore tract of Odisha, India. *Journal of Crop Improvement*, 33(2), 254-278.
- Minocha, R., Majumdar, R., & Minocha, S. C. (2014). Polyamines and abiotic stress in plants: a complex relationship. *Frontiers in Plant Science*, 5, 175.
- Mohammadi, M., Karimizadeh, R., & Abdipour, M. (2011). Evaluation of drought tolerance in bread wheat genotypes under dryland and supplemental irrigation conditions. *Australian Journal of Crop Science*, 5(4), 487-493.
- Negisho, K., Shibru, S., Matros, A., Pillen, K., Ordon, F., & Wehner, G. (2022). Association mapping of drought tolerance indices in Ethiopian durum wheat (*Triticum turgidum* ssp. *durum*). *Frontiers in Plant Science*, 13, 838088.
- Nupur, J. A., Hannan, A., Islam, A. U., Sagor, G. H. M., & Robin, A. H. K. (2020). Root development and anti-oxidative response of rice genotypes under polyethylene glycol induced osmotic stress. *Plant Breeding and Biotechnology*, 8(2), 151-162.
- Poudel, P. B., Poudel, M. R., & Puri, R. R. (2021). Evaluation of heat stress tolerance in spring wheat (*Triticum aestivum* L.) genotypes using stress tolerance indices in western region of Nepal. *Journal of Agriculture and Food Research*, 5, 100179.
- Reyes, J. A. O., Casas, D. E., Gandia, J. L., Parducho, M. J. L., Renovalles, E. M., Quilloy, E. P., & Delfin, E. F. (2023). Polyethylene glycol-induced drought stress screening of selected Philippine high-yielding sugarcane varieties. *Journal of Agriculture and Food Research*, 14, 100676.
- Sakr, M. T., El-Sarkassy, N. M., & Fuller, M. P. (2012). Osmoregulators proline and glycine betaine counteract salinity stress in canola. *Agronomy for Sustainable Development*, 32, 747-754.
- Sánchez-Reinoso, A. D., Ligarreto-Moreno, G. A., & Restrepo-Díaz, H. (2020). Evaluation of drought indices to identify tolerant genotypes in common bean bush (*Phaseolus vulgaris* L.). *Journal of Integrative Agriculture*, 19(1), 99-107.
- Seleiman, M. F., Al-Suhaibani, N., Ali, N., Akmal, M., Alotaibi, M., Refay, Y., & Battaglia, M. L. (2021). Drought stress impacts on plants and different approaches to alleviate its adverse effects. *Plants*, 10(2), 259.
- Tembe, K. O., Chemining'wa, G. N., Ambuko, J., & Owino, W. (2017). Effect of water stress on yield and physiological traits among selected African tomato (*Solanum lycopersicum*) landraces. *International Network for Natural Sciences*, 10(1):78-85.
- Uga, Y., Sugimoto, K., Ogawa, S., Rane, J., Ishitani, M., Hara, N., & Yano, M. (2013). Control of root system architecture by DEEPER ROOTING 1 increases rice yield under drought conditions. *Nature Genetics*, 45(9), 1097-1102.
- Yin, G., & Zhang, H. (2023). A new integrated index for drought stress monitoring based on decomposed vegetation response factors. *Journal of Hydrology*, 618, 129252.
- Yooyongwech, S., Samphumphung, T., Tisaram, R., Theerawitaya, C., & Suriyan, C. U. (2017). Physiological, morphological changes and storage root yield of sweetpotato [*Ipomoea batatas* (L.) Lam.] under peg-induced water stress. *Notulae Botanicae Horti Agrobotanici Cluj-Napoca*, 45(1), 164-171.

Cite as: Ben Naceur, M., & Cheikh-Mhamed, H. (2024). The most relevant drought-tolerant indices for selecting barley drought-tolerant genotypes. *Front Life Sci RT*, 5(1), 15-23.



Research article

Investigation of the effect of superabsorbent polymer application on soil moisture and plant growth

Senem Avaz Seven^{*1,2} , Yesim Menceloglu^{2,3} , Kemal Unlu⁴ , Kadriye Kahraman^{3,5} ,
Ogeday Rodop^{2,3} , Ipek Bilge³ , Mustafa Atilla Yazici¹ , Yusuf Ziya Menceloglu^{3,5} 

¹ Bahcesehir University, Faculty of Engineering and Natural Sciences, Department of Mechatronic Engineering, 34349, Istanbul Türkiye

² SOY Agriculture Technologies Inc, Teknopark Boulevard 1/4C, 34906, Istanbul, Türkiye

³ Sabanci University, Faculty of Engineering and Natural Sciences, 34956, Istanbul, Türkiye

⁴ Marmara University Faculty of Technology, Textile Engineering Department, 34722, Istanbul, Türkiye

⁵ Sabanci University Nanotechnology Research and Application Center, 34956, Istanbul, Türkiye

Abstract

As climate change continues to affect the environment, drought management has become more critical in agri-food production. Farmers are now looking for alternative drought management methods that are easy to apply. In this sense, superabsorbent polymers (SAPs) were proposed as an alternative soil conditioning and drought management tool within this study. To test the efficiency of a developed SAP in terms of soil conditioning and plant growth promotion with different soil types and extreme drought conditions, long-term soil and greenhouse experiments were carried out in at least 4 replicates. The plant growth was monitored by 4 different growth indicators using wheat as a model plant. Plant growth indicators demonstrated that shoot dry matter, spike length, and grain yield were enhanced up to 24%, and 11.6% using different amounts of SAP at varying drought conditions. The study set forth and exemplary of superabsorbent polymer use in agriculture and useful in dose adjustment and understanding the drought-dose relationship in these types of polymers.

Keywords: Drought stress; irrigation; superabsorbent polymer; sustainable agriculture

1. Introduction

Agriculture uses 70% of all the water used globally, and this ratio exceeds 90% in underdeveloped countries (Mateo-Sagasta et al., 2017). Achieving high yields in agriculture requires sufficient promotion of plant growth and an effective fight against pests at the same time, which can be attained by a delicate interplay of water, fertilizers, and pesticides (Sharma et al., 2024). Water is certainly the most important factor in this equation (Dalezios et al., 2017; Monteleone et al., 2019), but it does not necessarily mean it has to be applied in such high quantities to achieve acceptable yields. These main agricultural

inputs should be delivered to plants in optimum quantities, and excessive or restricted application of one of them can affect the activity of others (Magen, 2008), which is especially the case with water. If water is delivered in very large quantities in a short period, for instance during heavy rainfall, fertilizers and pesticides dissolved in soil leach at an accelerated rate and rapidly reach lower levels of the soil, rendering them inaccessible by the plants (Moradi et al., 2024). Conversely, if there is a long dry spell, fertilizers and pesticides applied in solid form cannot dissolve in the soil, and thus cannot be taken up by the plants' roots (Blancon et al., 2024). Therefore, the sustained delivery of water is crucial for crop health (Morison et al., 2008),

* Corresponding author.

E-mail address: senem.seven@bau.edu.tr (S. Avaz Seven).

<https://doi.org/10.51753/flsrt.1348591> Author contributions

Received 06 September 2023; Accepted 08 February 2024

Available online 30 April 2024

2718-062X © 2024 This is an open access article published by Dergipark under the [CC BY](https://creativecommons.org/licenses/by/4.0/) license.

not only because it constantly provides plants with water and eliminates drought stress, but also because it enables necessary nutrients and pesticides to be delivered to them in a more controlled fashion for longer times and limits their leaching (Tanaskovik et al., 2019) and loss to the environment (Feng et al., 2020).

Today, one of the main issues related to agricultural practices is that most of them use a lot of water in inefficient ways (Woyessa, 2024). For example, flood irrigation is one of the oldest methods, which is still widely used. This method causes waterlogging and erosion (Yadav et al., 2013), with adverse effects on many crops and soil (Bett et al., 2017; Cox et al., 2018), along with inefficient water use. Modern, more efficient irrigation methods are termed micro-irrigation systems (Rolbiecki and Rolbiecki, 2004), which deliver water slowly and directly to where it is most needed - the roots of the plants. These systems can be categorized into sprinkler, drip, spray, subsurface, and bubbler irrigation. Each system has its advantages and drawbacks and can be used for different crop types and in different fields. For instance, sprinkler and spray irrigation is being used in large farms, whereas drip irrigation systems can be implemented in smaller farms and greenhouses, and bubbler irrigation is mostly used for watering fruit trees (Mabuza and Ndoro, 2023).

To achieve adequate plant growth with minimum resources, water should be applied where it is needed, regularly and in small quantities. This can be accomplished with micro-irrigation systems. However, in farms where these systems are not implemented, either due to economic or technical feasibility and especially for lands where dry farming practices are employed, superabsorbent polymers (SAP) can be used to regulate water delivery to plants (Satriani et al., 2018). SAP is applied in granular form, together with the seeds, under the soil. Since SAPs' mechanisms of work depend on osmotic pressure difference (Ganji et al., 2010), upon irrigation or rainfalls, SAPs swell, and hold the water in their structure until their surroundings are drier than themselves. This allows SAPs to release the water to plants when they need it the most (Elshafie and Camele, 2021). Also, during heavy rainfalls, since SAPs will compete with plant roots in terms of water absorption and keep some of the water in their structure, they will alleviate the negative effects of too much water (Bhagat et al., 2016). This way, SAPs will transform into a water reservoir for plants. The use of SAPs in agriculture allows farmers to irrigate their farms less frequently with less water. Also, their use lowers yield losses in lands where dry farming is applied since it delivers water more efficiently to plants and allows for plant root areas to stay wet for long periods.

SAPs are lightly crosslinked polymers that are synthesized with natural, synthetic, or a combination of both sources. Since SAPs have a 3D hydrophilic polymer network with a low crosslinking density, they can absorb a significant amount of water while maintaining their physical structure without any intact (Singh et al., 2021).

Natural SAPs are generally made with saccharide (Qureshi et al., 2020), chitosan (Sanchez-Salvador et al., 2021), and cellulose (Zinge and Kandasubramanian, 2020) while synthetic SAP sources are generally based on ionic monomers (Mignon et al., 2019). The unique swelling and water-retaining properties of SAPs are due to the comprising hydrophilic groups such as carboxyl, amine, hydroxyl, amide, and sulfonic groups (Qureshi et al., 2020). SAPs have already been using in hygiene products

(Bachra et al., 2020), biomaterials (Rahimi et al., 2020), medicine, and wastewater treatment (Maji and Maiti, 2021). Nevertheless, the use of SAPs in agriculture is a topic, rising in importance day by day, due to the increase in drought and loss of arable lands (Rizwan et al., 2021).

Nanocomposite materials can demonstrate unusual property combinations for various applications (Ahmed et al., 2023; Ariturk et al., 2024). The nanocomposite SAPs used in agriculture include natural polymers combined with inorganic fillers (Sethi et al., 2023; Wypij et al., 2023). For instance, a copolymer of starch-polyvinyl alcohol combined with zeolite derivative clinoptilolite demonstrated higher water absorption capacity than the pure hydrogel, both at neutral pH and in a saline solution (Olad et al., 2018). The SAP nanocomposite structures may also include chemically modified inorganic fillers (Fu et al., 2022).

In a study on SAP nanocomposite preparation, ball-milled and chemically modified natural char nanofiller was incorporated into starch-g-poly (acrylic acid-co-acrylamide) copolymer and compared to neat hydrogel copolymer (Motamedi et al., 2020). Among them, chemically modified filler containing SAPs demonstrated two-fold water absorbency and three-fold water retention due to the coexistence of both chemical and physical crosslinking between chemically modified filler and the SAP structures.

Depending on the morphology and surface properties, inorganic fillers may also be used as the active agent or the carrier materials for agrochemicals (Seven et al., 2019; Perera et al., 2023). A Nano-titanium dioxide-containing polyacrylamide-based SAP demonstrated enhanced thermal and biological traits, plant growth regulation, and antibacterial activity arising from the chemical structure and function of the nanofiller (Shirsath et al., 2020). The current study describes the preparation and performance evaluation of a nanocomposite SAP in terms of its water retention capacity and its effect on plant growth under drought stress. The water retention capacities of prepared SAP nanocomposites were tested using different soil samples, while the dose-response relationship was demonstrated via greenhouse trials on a set of 64 pots. The effects of a set of SAP nanocomposites in varying doses on plant height, spike height, biomass accumulation, grain weight, and grain yield were investigated via long-term greenhouse trials. Results demonstrate that the SAP nanocomposites enhance water retention capacities of all soil types, particularly of sandy soil samples. In addition, the grain yields and biomass accumulations were observed to enhance by 3-14% and 8-19%, depending on the SAP doses applied.

2. Materials and methods

Monomers acrylamide (AM, $\geq 99\%$ HPLC) and 2-acrylamido-2-methylpropane-1-sulfonic acid (AMPS, $\geq 99\%$) were purchased from Sigma Aldrich. Acrylic acid (AA, analytical grade) was obtained from Alfa Aesar. Monomers were used as received, without any purification. Vinyltrimethoxysilane (VMTS, 98%) and ammonium persulfate (APS, $\geq 99\%$) were purchased from Sigma Aldrich. Sodium hydroxide solution 10 mol/L and ethanol (EtOH, absolute-99.9%) were obtained from Merck and used without further purification. Halloysite nanotubes (HNT) were kindly supplied by ESAN Inc. Distilled water was used for the preparation of all solutions.

2.1. Synthesis of superabsorbent nanocomposite polymer (SAP)

Synthesis of the superabsorbent nanocomposite SAP (WO2021167577) was performed using a previously developed method (Menceloglu et al., 2022), carried out via free-radical polymerization in distilled water. Nanocomposite random copolymer was synthesized by acrylic acid (AA), acrylamide (AM), and 2-acrylamido-2-methylpropane-1-sulfonic acid (AMPS) monomers in the presence of ammonium persulfate (APS) as a free radical initiator and VTMS as a crosslinking agent.

Initially, an amount of AM and AMPS were dissolved in distilled water and AcOH was added to the monomer solution. The pH of monomer solution was adjusted to 7 with 12 M sodium hydroxide before the reaction began. HNT, 1% of total monomer amount, was added to the neutralized monomer solution. After HNT was well dispersed in mixture, monomer solution was transferred to a three necked flask. The reactor was purged with nitrogen for 15 minutes to obtain an inert environment. As an *in-situ* crosslinking agent (Jaber et al., 2012), VTMS was added to the reaction mixture and continued to purge with nitrogen. After dissolving an amount of APS in water was added to the reaction environment. The reflux and heating were started. Nitrogen flow was closed after removing oxygen and air in the environment. The polymerization was carried out at 78°C in an oil bath for 2 hours. The reaction was maintained for 2 hours to complete the reaction and to increase the polymerization efficiency.

At the end of the reaction, the polymer solution was precipitated in ethanol to obtain powder super absorbent polymer. The precipitated polymer was dried at 70°C for 20 hours to remove solvent residues.

2.2. Wheat planting and harvesting

Wheat cultivation trials were carried out in a greenhouse under natural daylight conditions at Sabanci University (Khampuang et al., 2023). Three drought conditions were selected for the experiment, including extreme water shortage (40% of the field capacity), moderate water shortage (60% of the field capacity), and sufficient soil moisture (80% of the field capacity).

Plastic pots were filled with a fertilized medium loamy soil amended with three concentrations (0.0, 0.1, 1, and 2 g/kg) of SAP set including a negative control, and the experiments on each group were carried out with four repetitions. Wheat cultivars were placed at a Venlo-type greenhouse at Sabanci University, Istanbul. During the cultivation, temperature was kept constant ($25 \pm 2^\circ\text{C}$ during daytime and $18 \pm 2^\circ\text{C}$ at night). The cultivars were sown in an order that is 4 m with length and 10 cm inter-row spacing and 10 cm pot spacing distances. Wheat seeds of cultivar "Tekfen 1016" were planted into the pots filled with fertilized soil by the following basal treatment: 100 mg of P in the form of KH_2PO_4 , 25 mg of S in the form of K_2SO_4 , 2.5 mg of Fe in the form of Fe-EDTA, 2 mg of Zn in the form of $\text{ZnSO}_4 \cdot 7\text{H}_2\text{O}$, and 200 mg of N in the form of $\text{Ca}(\text{NO}_3)_2 \cdot 4\text{H}_2\text{O}$. Tap water was added to reach the target moisture content (40, 60, or 80% of the field capacity) for adjusting soil moisture. All samples were irrigated daily for the first three weeks to provide the plant growth without water stress in the first stage. Irrigation was carried out by weighing each pot, calculating the amount of water lost, and bringing it back to 80% field capacity. At the end

of the third week, the irrigation frequency was reduced to three days (equivalent to 1/3 of the normal watering) to examine water release, and the amount of irrigation was reduced to 40, 60, or 80% of field capacity, respectively.

Wheat were harvested after 120 days by cutting plants at the soil surface. Whole plants were placed in a paper bag for each pot and dried to analyze dry biomass. Before harvesting, the grains were collected to calculate grain yield.

2.3. Determination of morphometric characters

Shoot height measurements were performed on the 6th week of the experiment. The shoot heights were recorded from the ground level to the leaf base of the highest fully expanded leaves. Shoot dry weights were recorded by weight measurements of the individual wheat samples (3 samples from each replicate pot) collected from pots in the 6th week of the greenhouse experiment. Prior to weight measurements, wheat samples were removed from pots, washed with d-water, and dried at 70°C. For spike length measurements, the spikes were collected at the full maturation stage of the harvest. 5 spikes were collected from each replicate pot, cut from the spike ends, and their lengths were measured and averaged. Grain weights were determined at the end of the harvest, from the cumulative weights of each replicate pot of the corresponding SAP dose.

2.4. Elemental analysis

For elemental analysis, grain samples were ground to a fine powder in an agate vibrating cup mill (Pulverisette 9; Fritsch GmbH; Germany), and each sample was digested using a closed-vessel microwave system (MarsExpress; CEM Corp., Matthews, NC, USA) with 2 ml of 30% H_2O_2 and 5 ml of 65% HNO_3 . Digested samples were diluted to 20 mL with ultra-deionized water and filtered by quantitative filter papers. Elemental analysis was performed with inductively coupled plasma optical emission spectrometry (ICP-OES; Vista-Pro Axial; Varian Pty Ltd, Mulgrave, Australia) to determine grain concentrations as described (Acar et al., 2023), and whether the SAP has a negative effect on nutrient uptake or not.

3. Results and discussion

3.1. Effect of SAPs on plant growth and grain production

There are several parameters to determine plant growth, including the change in its height, dry weight, and grain production. Hence, the shoot dry weight, shoot height, spike length, and total grain weight of wheat plants planted in soil were investigated concerning SAP dose.

The first indicator investigated to demonstrate the effect of SAP on plant growth is the shoot height, obtained by the average heights of the plants grown in all replicate pots. Here, no significant difference was observed in shoot height at any drought conditions or doses compared to the control plants ($p > 0.05$). However, an increasing trend was observed with increased SAP dose within 80% irrigation regime suggesting that in the shoot height differences would be more pronounced when higher doses of SAP are applied (Fig. 1, 2).

The second parameter investigated is the shoot dry matter of productivity. As demonstrated in Fig. 3, shoot dry matter production linearly increases with increased doses of SAP at every drought regime. This increase was linear with respect to

SAP dose. 18.2% ($p=0.0256$) and 24.0% ($p=0.0344$) increase were observed in the plants treated with 0.1 g and 1 g SAP in low drought conditions (3 days; 80% irrigation), respectively. This shows that SAP application can increase shoot biomass production by up to 24% depending on the dose in low drought conditions. In the application of 2 g SAP, the effect cannot be seen completely due to the experimental errors, but it was observed that up to a 25% increase would be expected due to the increased trend line. When the irrigation was reduced to 60%, we observed an average increase of 12.5%, 16.8%, and 11.9% with respect to increased SAP dose (0.1, 1, and 2 g, respectively) against controls. Even when the irrigation was reduced further to 40%, SAP still promoted shoot dry matter enhanced by 8.9%, 8.8%, and 8.7% (0.1, 1, and 2 g, respectively) against control.

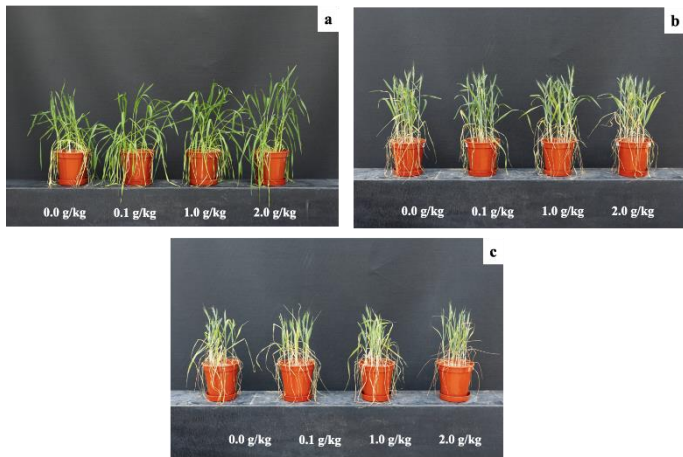


Fig. 1. Snapshots of the selected pots from greenhouse trials datasets. 80% (a), 60% (b), and 40% (c) of the field capacities, with an irrigation frequency of three days. Snapshots were gathered on the 30th day of the experiment.

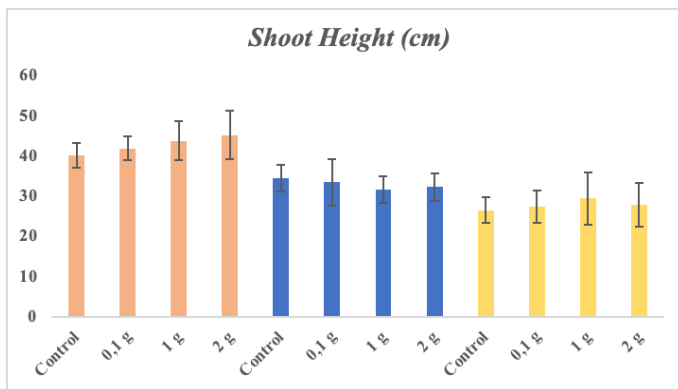


Fig. 2. Shoot height of plants grown under different SAP concentrations and irrigation with 80% (yellow), 60% (blue) and 40% (orange) of the field capacities.

The spike length and spikelet number were not statistically different between the cultivars SAP doses within the 80% irrigation regime (Fig. 4). However, a significant increase (11.56%) was observed in the spike length of 2 g SAP treated plants in moderate drought conditions (irrigation up to 60% of the soil capacity) ($p=0.0021$). The increase indicated that SAP is advantageous at higher doses within the moderate drought regime.

The total grain weight was calculated from the average of the grain weights obtained from each pot within the dose sets. As demonstrated in Fig. 5, an increase was observed at certain doses of SAP, and it was dose-dependent. While a 3.3% increase

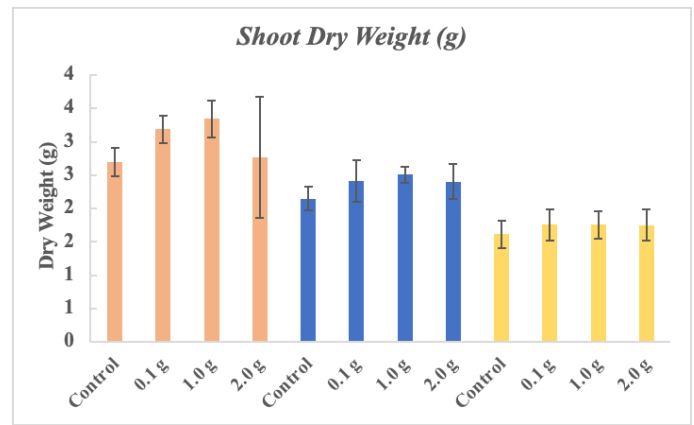


Fig. 3. Shoot biomass production of plants grown under different SAP concentrations and irrigation with 80% (yellow), 60% (blue), and 40% (orange) of the field capacities.

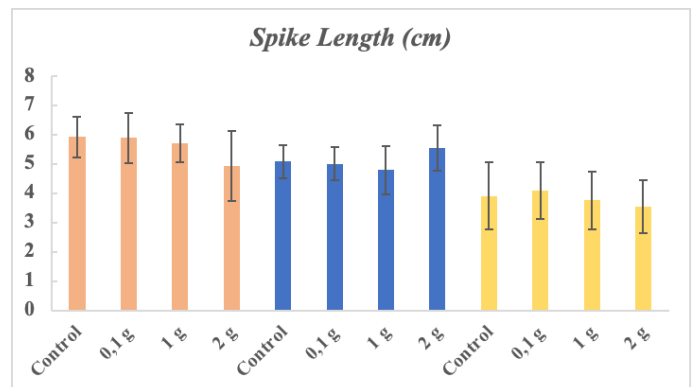


Fig. 4. Spike length of plants grown under different SAP concentrations and irrigation with 80% (yellow), 60% (blue) and 40% (orange) of the field capacities.

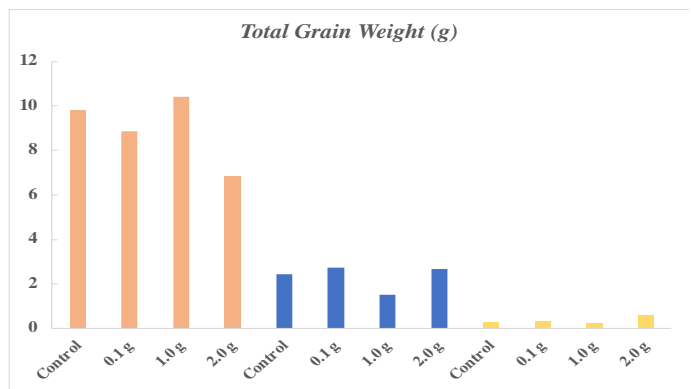


Fig. 5. Total grain weight of plants grown under different SAP concentrations and irrigation capacities with 80% (yellow), 60% (blue), and 40% (orange) of the field capacities.

was observed in 1 g SAP treated samples in low drought conditions, 11.2% and 12.3% increases were observed in 0.1 g and 2 g SAP treated plants in moderate drought conditions, respectively. Moreover, 11.4% and 11.3% increases were observed in plants treated with 0.1 g and 2 g SAP in extreme drought conditions, respectively. However, the total grain weight was found very low in the whole set of extreme drought conditions. Thus, the results could not be reliable. The free variation of total grain weight indicated that the concentration of SAP application should be adjusted according to drought conditions of the soil. When the low and moderate drought conditions were compared, the dose of SAP application should

Table 1

The nutrient uptake study performed by ICP-OES analyses of grains collected at the end of the experiment.

| Sample | Field Capacity | K | P | S | Mg | (mg kg ⁻¹) | | | | | | | | | |
|-----------|----------------|-------|-------|-------|-------|------------------------|-------|-------|-------|------|-------|-------|-------|------|------|
| | | | | | | Ca | Fe | Zn | Mn | Cu | Na | Mo | B | Ni | Al |
| Control | 80% | 0.44± | 0.44± | 0.20± | 0.17± | 497± | 48± 3 | 43± 4 | 52± 5 | 7± 0 | 13± 0 | 0.68± | 0.82± | 4± 0 | 2± 0 |
| | | 0.01 | 0.01 | 0.01 | 0.01 | 12 | | | | | | 0.04 | 0.10 | | |
| 0.1 g SAP | 80% | 0.43± | 0.40± | 0.17± | 0.15± | 458± | 39± 2 | 35± 6 | 44± 2 | 6± 0 | 13± 0 | 0.67± | 0.74± | 3± 0 | 2± 0 |
| | | 0.00 | 0.00 | 0.01 | 0.00 | 39 | | | | | | 0.02 | 0.05 | | |
| 1g SAP | 80% | 0.43± | 0.41± | 0.19± | 0.15± | 502± | 42± 4 | 35± 6 | 45± 4 | 6± 0 | 14± 1 | 0.61± | 0.73± | 3± 0 | 2± 0 |
| | | 0.01 | 0.01 | 0.01 | 0.01 | 13 | | | | | | 0.03 | 0.05 | | |
| 2g SAP | 80% | 0.43± | 0.42± | 0.20± | 0.16± | 529± | 41± 4 | 35± 7 | 48± 7 | 7± 0 | 14± 1 | 0.64± | 0.69± | 3± 1 | 2± 0 |
| | | 0.01 | 0.02 | 0.01 | 0.01 | 49 | | | | | | 0.07 | 0.07 | | |
| Control | 60% | 0.48± | 0.47± | 0.22± | 0.18± | 472± | 58± 2 | 66± 6 | 65± 1 | 8± 0 | 12± 0 | 0.89± | 1.18± | 6± 0 | 2± 0 |
| | | 0.01 | 0.00 | 0.00 | 0.00 | 14 | | | | | | 0.04 | 0.08 | | |
| 0.1 g SAP | 60% | 0.48± | 0.46± | 0.21± | 0.18± | 516± | 51± 4 | 60± 6 | 61± 3 | 7± 0 | 13± 1 | 0.85± | 1.25± | 5± 0 | 1± 0 |
| | | 0.00 | 0.01 | 0.01 | 0.00 | 9 | | | | | | 0.02 | 0.06 | | |
| 1g SAP | 60% | 0.51± | 0.48± | 0.22± | 0.18± | 513± | 57± 4 | 73± 7 | 63± 2 | 8± 0 | 14± 0 | 0.99± | 1.52± | 5± 0 | 1± 0 |
| | | 0.02 | 0.00 | 0.01 | 0.00 | 10 | | | | | | 0.08 | 0.04 | | |
| 2g SAP | 60% | 0.47± | 0.46± | 0.22± | 0.18± | 508± | 50± 4 | 57± 7 | 60± 3 | 8± 0 | 14± 0 | 1.00± | 1.24± | 5± 0 | 1± 0 |
| | | 0.00 | 0.01 | 0.01 | 0.00 | 8 | | | | | | 0.04 | 0.09 | | |
| Control | 40% | 0.50± | 0.46± | 0.23± | 0.18± | 511± | 54± 3 | 73± 7 | 63± 1 | 8± 0 | 9± 1 | 1.00 | 0.38± | 7± 0 | 2± 0 |
| | | 0.03 | 0.01 | 0.01 | 0.00 | 25 | | | | | | | 0.20 | | |
| 0.1 g SAP | 40% | 0.51± | 0.46± | 0.23± | 0.18± | 499± | 55± 7 | 70± | 64± 2 | 8± 0 | 9± 1 | 0.99± | 0.36± | 6± 0 | 1± 0 |
| | | 0.02 | 0.01 | 0.00 | 0.00 | 6 | | 14 | | | | 0.09 | 0.21 | | |
| 1g SAP | 40% | 0.54± | 0.46± | 0.22± | 0.18± | 581± | 53± 7 | 75± | 61± 4 | 8± 0 | 14± 0 | 0.87± | 0.92± | 5± 1 | 4± 1 |
| | | 0.03 | 0.00 | 0.01 | 0.00 | 66 | | 11 | | | | 0.17 | 0.26 | | |
| 2g SAP | 40% | 0.50± | 0.38± | 0.22± | 0.16± | 501± | 55± 1 | 21± 3 | 60± 0 | 7± 0 | 25± 5 | 0.41± | 1.02± | 7± 0 | 3± 1 |
| | | 0.01 | 0.00 | 0.01 | 0.00 | 28 | | | | | | 0.02 | 0.05 | | |

be reduced from 1 g to 0.1 g to increase the grain yield in case of enhanced drought.

3.2. Nutrient uptake & bioaccumulation

The nutrient uptake and residue analysis of SAP applied wheat samples were performed by ICP-OES analyses. Elemental analysis was performed on grinded grain samples obtained from greenhouse cultivation studies. Shoot Na content was slightly increased with SAP under all drought conditions, but generally, SAP application did not make a statistically significant change in the uptake of nutrient elements, nor did it induce accumulation of heavy metals and/or non-nutrient and toxic elements (Table 1) (Taylor et al., 2003). ICP-OES measurement levels for several nutrients are in line with the literature, particularly for Zn (Cakmak et al., 2010), Fe (Dimpka et al., 2020), and for Na, K (Pasałowski and Migaszewski, 2006).

4. Conclusions

The current study describes the implementation of a sub-soil water reservoir polymer into wheat cultivation, demonstrating the efficiency of SAP in drought conditions and different soil types. To carry out soil and greenhouse trials, SAP was first synthesized using a previously developed method (Menceloglu et al., 2022).

SAP was tested in greenhouse cultivation of wheat, to demonstrate the effectiveness in extreme drought conditions. To create drought stress throughout the whole dataset (including controls) the irrigation frequency was reduced to 1/3. In addition to this, irrigation amounts were further reduced to 80%, 60% and 40% of the calculated field capacity. 4 different growth indicators were monitored under the extreme drought stresses applied. The first indicator was the shoot weight, where no significant difference was observed between the control and the

dataset in increasing drought levels. However, a linear trend was observed between the SAP dose and the shoot weight, suggesting that higher doses outside the dataset may promote shoot height elongation. The second growth indicator, spike length increased by 11.6% only when 2 g of SAP was applied in a moderate drought regime. The third growth indicator was the shoot dry matter, where there was a significant increase at every drought regime and every SAP dose applied. The average of 24%, 14%, and 8.8% increase indicates that SAP is very efficient in shoot dry matter enhancement. The final growth indicator, the total grain weight was perhaps the most dose-sensitive parameter investigated. Depending on the dose/drought conditions, a 3.3-12.3% increase was recorded in total grain weight.

Due to the long-term water supply capacity, SAP reacquaints soil types that are either arid and/or non-arable regions such as sandy soils. As it can retain water for extended periods (up to 40 days depending on the soil type), SAP is suitable for irregular rainfall regimes. In addition to that, no negative effect was observed in nutrient uptake of the plant. Investigating the plant growth indicators, dose adjustment of SAP is very critical to ensure the maximum benefit, and when assured, it is observed that SAP promotes plant growth.

Acknowledgments: The authors would like to thank the Ministry of Agriculture and Forestry, General Directorate of Plant Protection Central Research Institute, Türkiye (ZMMAE) for their contribution to this study providing soil samples. This work is supported by The Scientific and Technological Research Council of Türkiye (TUBITAK) Project ID: 2190116.

Conflict of interest: The authors declare that they have no conflict of interests.

Informed consent: The authors declare that this manuscript did

not involve human or animal participants and informed consent was not collected.

References

- Acar, O., Izydorczyk, M. S., McMillan, T., Yazici, M. A., Imamoglu, A., Cakmak, I., & Koksel, H. (2023). A research on milling fractions of biofortified and nonbiofortified hull-less oats in terms of minerals, arabinoxylans, and other chemical properties. *Cereal Chemistry*, 100(5), 1192-1202.
- Ahmed, A. M., Mekonnen, M. L., & Mekonnen, K. N. (2023). Review on nanocomposite materials from cellulose, chitosan, alginate, and lignin for removal and recovery of nutrients from wastewater. *Carbohydrate Polymer Technologies and Applications*, 100386.
- Ariturk, G., Bilge, K., Seven, S. A., & Menciloglu, Y. Z. (2024). Morphological adaptation of expanded vermiculite in polylactic acid and polypropylene matrices for superior thermoplastic composites. *Polymer Composites*, 45(6), 5043-5050.
- Bachra, Y., Grouli, A., Damiri, F., Bennamara, A., & Berrada, M. (2020). A new approach for assessing the absorption of disposable baby diapers and superabsorbent polymers: A comparative study. *Results in Materials*, 8, 100156.
- Bett, B., Said, M. Y., Sang, R., Bukachi, S., Wanyoike, S., Kifugo, S. C., & Grace, D. (2017). Effects of flood irrigation on the risk of selected zoonotic pathogens in an arid and semi-arid area in the Eastern Kenya. *PLoS One*, 12(5), e0172626.
- Bhagat, M. S., Ghare, A. D., & Ralegaonkar, R. V. (2016). Application of super absorbent polymer in flood management and agricultural water management. *Journal of Research in Engineering and Applied Sciences*, 1(1), 30-36.
- Blancou, J., Buet, C., Dubreuil, P., Tixier, M. H., Baret, F., & Praud, S. (2024). Maize green leaf area index dynamics: genetic basis of a new secondary trait for grain yield in optimal and drought conditions. *Theoretical and Applied Genetics*, 137(3), 68.
- Cakmak, I., Kalayci, M., Kaya, Y., Torun, A. A., Aydin, N., Wang, Y., & Horst, W. J. (2010). Biofortification and localization of zinc in wheat grain. *Journal of Agricultural and Food Chemistry*, 58(16), 9092-9102.
- Cox, C., Jin, L., Ganjegunte, G., Borrok, D., Loughheed, V., & Ma, L. (2018). Soil quality changes due to flood irrigation in agricultural fields along the Rio Grande in Western Texas. *Applied Geochemistry*, 90, 87-100.
- Dalezios, N. R., Dercas, N., Spyropoulos, N. V., & Psomiadis, E. (2017). Water availability and requirements for precision agriculture in vulnerable agroecosystems. *European Water*, 59, 387-394.
- Dimkpa, C. O., Andrews, J., Sanabria, J., Bindraban, P. S., Singh, U., Elmer, W. H., & White, J. C. (2020). Interactive effects of drought, organic fertilizer, and zinc oxide nanoscale and bulk particles on wheat performance and grain nutrient accumulation. *Science of the Total Environment*, 722, 137808.
- Elshafie, H. S., & Camele, I. (2021). Applications of absorbent polymers for sustainable plant protection and crop yield. *Sustainability*, 13(6), 3253.
- Feng, J., Hussain, H. A., Hussain, S., Shi, C., Cholidah, L., Men, S., & Wang, L. (2020). Optimum water and fertilizer management for better growth and resource use efficiency of rapeseed in rainy and drought seasons. *Sustainability*, 12(2), 703.
- Fu, E., Zhang, S., Luan, Y., Zhang, Y., Saghir, S., & Xiao, Z. (2022). Novel superabsorbent polymer composites based on α -cellulose and modified zeolite: Synthesis, characterization, water absorbency and water retention capacity. *Cellulose*, 29(3), 1727-1737.
- Ganji, F., Vasheghani, F. S., & Vasheghani, F. E. (2010). Theoretical description of hydrogel swelling: A review. *Iranian Polymer Journal*, 19(5), 2010, 375-398.
- Jaber, F. J. A. A. (2012). New routes for synthesis of environmentally friendly superabsorbent polymers, Doctoral Dissertation, (pp. 1-110). An-Najah National University, Nablus, Palestine.
- Khampuang, K., Chaiwong, N., Yazici, A., Demirer, B., Cakmak, I., & Prom-U-Thai, C. (2023). Effect of sulfur fertilization on productivity and grain zinc yield of rice grown under low and adequate soil zinc applications. *Rice Science*, 30(6), 632-640.
- Mabuza, M., & Ndoro, J. T. (2023). Borich's needs model analysis of smallholder farmers' competence in irrigation water management: case study of Nkomazi local municipality, Mpumalanga province in South Africa. *Sustainability*, 15(6), 4935.
- Magen, H. (2008). Balanced crop nutrition: fertilizing for crop and food quality. *Turkish Journal of Agriculture and Forestry*, 32(3), 183-193.
- Maji, B., & Maiti, S. (2021). Chemical modification of xanthan gum through graft copolymerization: Tailored properties and potential applications in drug delivery and wastewater treatment. *Carbohydrate Polymers*, 251, 117095.
- Mateo-Sagasta, J., Zadeh, S. M., Turrall, H., & Burke, J. (2017). *Water pollution from agriculture: a global review. Executive summary* (pp. 1-35). FAO Colombo, Sri Lanka: International Water Management Institute (IWMI).
- Menciloglu, Y., Menciloglu, Y. Z., & Seven, S. A. (2022). Triblock superabsorbent polymer nanocomposites with enhanced water retention capacities and rheological characteristics. *ACS Omega*, 7(24), 20486-20494.
- Mignon, A., De Belie, N., Dubruel, P., & Van Vlierberghe, S. (2019). Superabsorbent polymers: A review on the characteristics and applications of synthetic, polysaccharide-based, semi-synthetic and 'smart' derivatives. *European Polymer Journal*, 117, 165-178.
- Monteleone, S., De Moraes, E. A., & Maia, R. F. (2019). Analysis of the variables that affect the intention to adopt Precision Agriculture for smart water management in Agriculture 4.0 context. *2019 Global IoT Summit (GloTS)*, 1-6.
- Moradi, S., Babapoor, A., Ghanbarlou, S., Kalashgarani, M. Y., Salahshoori, I., & Seyfaee, A. (2024). Toward a new generation of fertilizers with the approach of controlled-release fertilizers: A review. *Journal of Coatings Technology and Research*, 21(1), 31-54.
- Morison, J. I. L., Baker, N. R., Mullineaux, P. M., & Davies, W. J. (2008). Improving water use in crop production. *Philosophical Transactions of the Royal Society B: Biological Sciences*, 363(1491), 639-658.
- Motamedi, E., Motesharezedeh, B., Shirinfekr, A., & Samar, S. M. (2020). Synthesis and swelling behavior of environmentally friendly starch-based superabsorbent hydrogels reinforced with natural char nano/micro particles. *Journal of Environmental Chemical Engineering*, 8(1), 103583.
- Olad, A., Doustdar, F., & Gharekhani, H. (2018). Starch-based semi-IPN hydrogel nanocomposite integrated with clinoptilolite: Preparation and swelling kinetic study. *Carbohydrate Polymers*, 200, 516-528.
- Pasławski, P., & Migaszewski, Z. M. (2006). The quality of element determinations in plant materials by instrumental methods. *Polish Journal of Environmental Studies*, 15(2a), 154-164.
- Perera, M., Jayarathna, L., Yakandawala, D. M. D., & Seneweera, S. (2023). Nanoclay composites as agrochemical carriers. In: Vithanage M., Lazzara G., Rajapaksha A. U. (eds) *Clay Composites: Environmental Applications* (pp. 543-557). Singapore, Springer Nature Singapore.
- Qureshi, M. A., Nishat, N., Jadoun, S., & Ansari, M. Z. (2020). Polysaccharide based superabsorbent hydrogels and their methods of synthesis: A review. *Carbohydrate Polymer Technologies and Applications*, 1, 100014.
- Rahimi, M., Noruzi, E. B., Sheykhsaran, E., Ebadi, B., Karimimezhad, Z., Molaparast, M., & Kafil, H. S. (2020). Carbohydrate polymer-based silver nanocomposites: Recent progress in the antimicrobial wound dressings. *Carbohydrate Polymers*, 231, 115696.
- Rizwan, M., Gilani, S. R., Durani, A. I., & Naseem, S. (2021). Materials diversity of hydrogel: Synthesis, polymerization process and soil conditioning properties in agricultural field. *Journal of Advanced Research*, 33, 15-40.
- Rolbiecki, R., & Rolbiecki, S. (2004, September). Effects of micro-irrigation systems on lettuce and radish production. In *III Balkan Symposium on Vegetables and Potatoes*, 729 (pp. 331-335).
- Satriani, A., Catalano, M., & Scalcione, E. (2018). The role of superabsorbent hydrogel in bean crop cultivation under deficit irrigation conditions: A case-study in Southern Italy. *Agricultural Water Management*, 195, 114-119.
- Sethi, S., Singh, A., Medha, Thakur, S., Kaith, B. S., & Khullar, S. (2023). Natural polymer-based nanocomposite hydrogels as environmental remediation devices. In: Shanker, U., Hussain, C. M., Rani, M. (eds) *Handbook of Green and Sustainable Nanotechnology: Fundamentals, Developments and Applications* (pp. 407-441). Cham: Springer International Publishing.

- Seven, S. A., Tastan, O. F., Tas, C. E., Unal, H., Ince, I. A., & Menciloglu, Y. Z. (2019). Insecticide-releasing LLDPE films as greenhouse cover materials. *Materials Today Communications*, 19, 170-176.
- Sharma, A., Prakash, A., Bhambota, S., & Kumar, S. (2024). Investigations of precision agriculture technologies with application to developing countries. *Environment, Development and Sustainability*, 1-37.
- Shirsath, N. B., Roy, C. B., & Meshram, J. S. (2020). TiO₂/starch-based biodegradable copolymer nanocomposite as a plant growth regulator. *Green Materials*, 9(2), 69-77.
- Singh, N., Agarwal, S., Jain, A., & Khan, S. (2021). 3-Dimensional cross linked hydrophilic polymeric network "hydrogels": An agriculture boom. *Agricultural Water Management*, 253, 106939.
- Sanchez-Salvador, J. L., Balea, A., Monte, M. C., Negro, C., & Blanco, A. (2021). Chitosan grafted/cross-linked with biodegradable polymers: A review. *International Journal of Biological Macromolecules*, 178, 325-343.
- Tanaskovik, V., Cukaliev, O., Romić, D., Ondrasek, G., Savić, R., Markoski, M., & Nechkovski, S. (2019). Water use efficiency and pepper yield under different irrigation and fertilization regime. *Contributions, Section of Natural, Mathematical and Biotechnical Sciences*, 40(1), 53-62.
- Taylor, V. F., Longerich, H. P., & Greenough, J. D. (2003). Multielement analysis of Canadian wines by inductively coupled plasma mass spectrometry (ICP-MS) and multivariate statistics. *Journal of Agricultural and Food Chemistry*, 51(4), 856-860.
- Woyessa, Y. E. (2024). Sustainable Management of Water Resources in a Semi-arid River Basin Under Climate Change: A Case Study in South Africa. In: Li, Y., Chaudhuri, H., Corrêa Rotunno Filho, O., Guseva, N., Bux, F. (eds) *BRICS Countries: Sustainable Water Resource Management and Pollution Control* (pp. 183-209) Springer, Singapore.
- Wypij, M., Trzcińska-Wencel, J., Golińska, P., Avila-Quezada, G. D., Ingle, A. P., & Rai, M. (2023). The strategic applications of natural polymer nanocomposites in food packaging and agriculture: Chances, challenges, and consumers' perception. *Frontiers in Chemistry*, 10, 1106230.
- Yadav, S., Singh, B., Humphreys, E., & Kukal, S. S. (2013). Effective management of scarce water resources in North-West India. In: Gurbir S. B., Navreet K. B. (eds) *Agricultural Sustainability* (pp. 103-125). Academic Press.
- Zinge, C., & Kandasubramanian, B. (2020). Nanocellulose based biodegradable polymers. *European Polymer Journal*, 133, 109758.

Cite as: Avaz Seven, S., Menciloglu, Y., Unlu, K., Kahraman, K., Rodop, O., Bilge, I., Yazici, M. A., & Menciloglu, Y. Z. (2024). Investigation of the effect of superabsorbent polymer application on soil moisture and plant growth. *Front Life Sci RT*, 5(1), 24-30.



Research article

Effects of cold stress on protein metabolism of certain walnut cultivars

Sergul Ergin^{*1} , Firat Altintas² ¹ *Eskisehir Osmangazi University, Faculty of Agriculture, Department of Agricultural Biotechnology, 26160, Eskisehir, Türkiye*² *Republic of Türkiye Ministry of Agriculture and Forestry, Soke Directorate of Agricultural Production Enterprise, Agricultural Extension and In-Service Training Centre, 9200, Aydin, Türkiye*

Abstract

To investigate the effects of heat shock proteins (HSPs) on walnut (*Juglans regia* L.) plants under low-temperature stress, first of all, low-temperature tolerances of ten walnut cultivars (Chandler, Fernor, Franquette, Pedro, Bilecik, Kaman-I, Kaman-II, Kaman-III, Sebin, and Yalova I) were determined. One-year-old shoot samples were taken from the plants in two different periods, cold-acclimated (CA) and non-acclimated (NA), and were exposed to +5°C, -5°C, -15°C and -25°C for 12 h. Cold injury was determined by ion leakage analysis in the thawed bark tissues. According to the results of this analysis, two cultivars were determined as cold-sensitive (Chandler) and cold-tolerant (Fernor) in terms of low-temperature tolerance. To examine the effects of HSPs on cold tolerance in walnut plants, the protein profiles, the amount of total protein, and the HSPs of these two cultivars were determined. As a result of the immunoblot analysis, it was determined that 44 kDa HSP23 and 59 kDa HSP60 are responsible for low-temperature tolerance in walnut plants.

Keywords: Cold acclimatization; heat shock proteins; HSP23; HSP60; *Juglans regia*; low temperature stress

1. Introduction

Cold stress is one of the important factors affecting plant growth and the geographical distribution of plants in the world. Plants can acclimate to cold temperatures by being previously exposed to low, non-freezing temperatures. This exposure activates adaptation mechanisms that play a crucial role in increasing cold tolerance (Kerbler and Wigge, 2023). During the process of cold acclimation, plants undergo physiological changes such as increased sugar accumulation, altered lipid composition, activation of genes responsible for stress proteins, and reinforcement of their antioxidative mechanisms (Dou et al., 2024). Acclimation begins in the autumn with cessation of growth and development in plants, while freezing damage of plants is lower in this period, in the spring and the summer, freezing injury can be severe as plants are deacclimate (Riikonen et al., 2023). Survival throughout the freeze-thaw cycle depends on maintaining the structural and functional characteristics of

the plasma membrane, which serves as a vital barrier between the cytoplasm and the extracellular environment and is thought to be the primary site of freezing damage (Takahashi et al., 2021). Although there are many methods for determining freeze damage, the most widely used is the electrolyte leakage conductivity method (Rezaei and Rohani, 2023).

Cell survival under stress conditions depends on the preservation of protein structures and functions (Hu et al., 2022). Heat shock proteins (HSPs), which are associated with heat shock, are widely found in plant and animal cells. But they are now known to be responsible for a wide variety of stresses such as cold, UV light, wound healing, tissue remodelling, or biotic stresses (Abdullah et al., 2022). In plants, HSPs are divided into five classes based on their molecular weight: HSP100, HSP90, HSP70, HSP60, and small HSPs (sHSPs). Most HSPs act as chaperones and are essential for the correct three-dimensional folding of newly produced proteins in the cell. They also play a critical role in repairing damaged proteins caused by stress

* Corresponding author.

E-mail address: ergins@ogu.edu.tr (S. Ergin).

<https://doi.org/10.51753/flsrt.1375108> Author contributions

Received 24 October 2023; Accepted 11 February 2024

Available online 30 April 2024

2718-062X © 2024 This is an open access article published by Dergipark under the [CC BY](https://creativecommons.org/licenses/by/4.0/) license.

(Almalki et al., 2021). For this reason, many chaperones are considered HSPs due to their nature to aggregate when denatured by heat stress (Yurina, 2023). The accumulation of HSPs under heat stress and the correlation between HSP accumulation and increased thermotolerance have been well described in previous studies (Ergin et al., 2016; McLoughlin et al., 2016; Yang et al., 2020). Cold stress affects enzymes, and cellular membranes, alters physiology and metabolism, and sometimes causes water starvation and dehydration (Zinta et al., 2022). Cold stress can also cause protein dysfunction and denaturation. In plant cells, the synthesis of HSPs plays a crucial role in protein folding, assembly, degradation, and translocation. These proteins are essential for preventing cellular damage, maintaining cellular homeostasis, and developing tolerance to cold stress (Batool et al., 2022). However, studies on their role in cold stress are quite scarce (Ré et al., 2017; Bourguine and Guihur, 2021).

Cold stress is an important risk in walnut cultivation, which has a high economic value in the world. Especially, late spring frosts and early autumn frosts pose a great risk for crop losses in woody plants (Drepper et al., 2022; Tadić et al., 2023). Cold acclimation caused an increase in cold tolerance of woody plants under winter conditions. However, in the non-acclimated (NA) period, when the plants are not accustomed to the cold, cold damage is more and this causes economic product losses to be high. Although there are studies on the cold tolerance of walnut cultivars in winter and autumn, studies on the responses of walnut cultivars in the NA period, which is a sensitive period for their culture, are limited (Poirier et al., 2004; Aletà et al., 2013; Charrier et al., 2018a,b). Furthermore, comparative research conducted during the cold-acclimated (CA) and NA periods is crucial to understanding the cold tolerance of cultivars. In this regard, selecting frost-tolerant cultivars and understanding the cold tolerance mechanism can greatly improve frost tolerance for walnuts. In the present study, frost tolerance was compared on 10 walnut cultivars (Chandler, Fernor, Franquette, Pedro, Bilecik, Kaman I, Kaman-II, Kaman-III, Sebin, and Yalova I) under CA and NA periods. According to the injury results, two cultivars were determined as cold-sensitive (Chandler) and cold-tolerant (Fernor) in terms of frost tolerance. Although there are many studies on the mechanism of frost tolerance in plants, the effectiveness of HSPs in cold tolerance has not been fully elucidated. In this study, the effects of HSPs on frost tolerance in walnut plants were examined by using frost-tolerant and frost-sensitive walnut cultivars.

2. Materials and methods

2.1. Plant material and low-temperature applications

One-year-old shoot samples were collected randomly from 4-5 trees in 8 years old plants in Kutahya- Türkiye (in Altintas region, latitude 39° 3' 41" N, longitude 30° 6' 35" E) in different periods CA (in January) and NA (in July). The average temperature in January was 0.3°C (-3.3°C to 4.6°C) and the average temperature in July was 20.7°C (13.0°C to 28.0°C).

The shoot samples were prepared for low-temperature tests in the way that Turhan and Ergin (2012) suggested. For this purpose, the shoots wrapped in moist paper and aluminium foil were placed into a manually controlled freezer. Also, a sample of plant tissue that was not exposed to low temperatures was used as a control.

Prepared samples were exposed to +5°C, -5°C, -15°C and

-25°C for 12 hours, and the temperature was reduced gradually to 5°C/h. The samples were removed from the freezer at the end of the 12 hours and left at 4°C for a gentle overnight thawing. Ion leakage analysis was performed using the bark samples that were removed from the shoots. For further analysis, the remaining bark sample portions were stored at -80°C.

2.2. Determination of freezing injury

According to Turhan and Ergin (2012), electrolyte leakage analysis was used to detect freezing injury on shoots. The electrical conductivity of each sample was measured using a conductivity meter (Mettler Toledo, SevenEasy S30, Columbus Ohio, USA). The proportion of injury at each temperature was determined using the ion leakage data and the following formula: $\text{Injury}\% = \frac{[L(t)\% - L(c)\%]}{100 - L(c)\%} \times 100$, where L(t) represents the treatment's ion leakage percentage and L(c) the control's ion leakage percentage (Arora et al. 1992).

2.3. Protein analysis

One gram of bark tissue was homogenized in borate buffer (pH 9.0; 1 mM PMSF, 50 mM sodium tetraborate, 50 mM ascorbic acid, and 1% β-mercaptoethanol) at 4°C to extract all of the soluble proteins (Arora et al., 1992). The homogenates were centrifuged for 1.5 hours at 4°C at 26000 × g. Using the Bradford method, the TSP content in preserved supernatants was determined (Arora and Wisniewski, 1994). Trichloroacetic acid solution (10%) was used to precipitate the proteins (Lim et al., 1999). Pellets were dried and rinsed three times with cold acetone before adding 100 μL of loading buffer. An equivalent amount of sample (30 μg) was placed into each well, and the proteins were separated using SDS-PAGE. The gels were stained with Coomassie dye (Arora et al., 1992). Antibodies of HSP23 [Anti-Heat Shock Protein 23 produced in rabbit affinity isolated antibody (Sigma)] and HSP60 [Monoclonal Anti-Heat Shock Protein 60 antibody produced in mouse (monoclonal LK2, ascites fluid (Sigma))] were diluted 1:1500 and used for immunoblot analyses. Blots on the membrane were detected by the alkaline phosphatase assay using the ProtoBlot Western Blot AP Kit (Promega). Public Domain NIH Image program was used to compare the intensities of the bands (NIH Image, 2024).

2.4. Statistical analysis

Each trial was repeated three times. The obtained data were determined by Duncan's test at $p \leq 0.05$. Statistical analyses were performed with SPSS for Windows software.

3. Results

3.1. Freezing injury

Effects of low-temperature applications on the cell membrane injury of walnut cultivars in cold-acclimated (CA, in January) and non-acclimated (NA, in July) periods were shown in Fig. 1. In general, it has been found that the injury in the NA period is more than in CA period. While the injury did not reach 50% in any cultivar in the CA period at any low-temperature application, it was about 50% at all temperature applications (except for Fernor at 5°C) in the NA period. Significant differences were detected between periods, cultivars, temperatures, and interactions (Table 1).

Table 1

According to the analysis of variance (ANOVA), the factors of period (P), cultivar (Cv.), and temperature (T), as well as their interactions, on injury and total soluble proteins (TSP). Numbers show F values at the 0.05 level.

| Dependent variable | Independent variable | | | | | | |
|--------------------|----------------------|---------|---------|---------|---------|--------|-------------|
| | P | Cv. | T | P × Cv. | P × T | Cv.×T | P × Cv. × T |
| Injury | 54025.68* | 57.14* | 886.39* | 42.71* | 50.61* | 14.34* | 14.46* |
| TSP | 967.25* | 109.28* | 192.63* | 11.43* | 134.78* | 30.92* | 13.51* |

* Significant at $p < 0.05$.

The lowest average freezing injury in the NA period was observed in Fernor at 5°C (43.17%) whereas the highest one was in Chandler, at -25°C (96.33%). Besides, the lowest average freezing injury in the CA period occurred in Fernor at 5°C (7.07%) whereas the highest one was in Bilecik at -25°C (33.69%). Based on the responses of the plants in the NA period, a sensitive cultivar (Chandler) and a tolerant cultivar (Fernor) to low temperatures were determined according to the injury results.

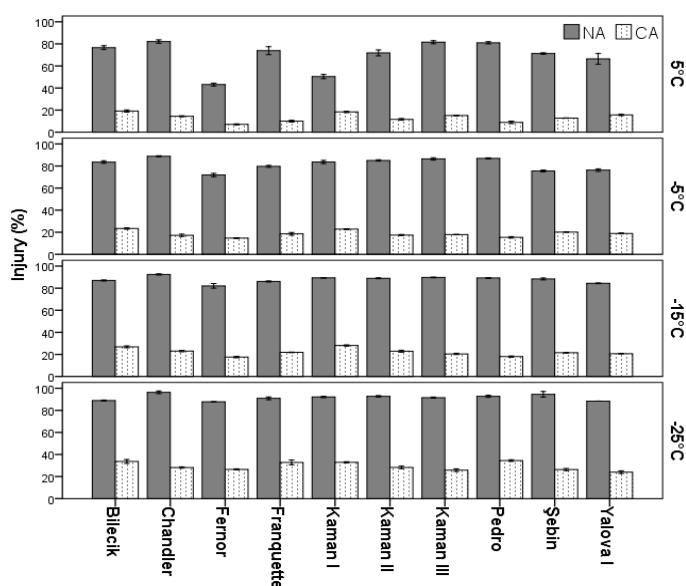


Fig. 1. Variations in injury rates among walnut cultivars exposed to cold temperatures during the NA and CA periods. The error bars indicate \pm SE of three replications.

3.2. Protein analysis

Protein and immunoblotting analysis were performed in the Chandler and Fernor, which are cold sensitive and cold tolerant plants, respectively. Total soluble protein contents of varieties were higher in the CA period than in the NA period (Fig. 2). In the NA period, TSP content of Fernor was increased in response to the low temperature applications especially at -15°C (6.2 mg /gFW) and -25°C (6.0 mg /gFW) but Chandler’s TSP content remained constant. In the CA period, TSP contents of varieties were increased at -25°C and it was determined as 8.33 mg /gFW in Chandler and 9.63 mg /gFW in Fernor. Significant differences were detected between periods, temperatures and interactions (Table 1).

Total protein profiles of Chandler and Fernor cultivars due to low-temperature applications in NA and CA periods were shown in Fig. 3 and Fig. 4, respectively. In both cultivars, protein bands with sizes of 66 kDa, 59 kDa, and 44 kDa were determined; the densities of these bands changed in response to low-temperature treatments. It was determined that the intensity of the 66 kDa protein band increased especially at -15°C and -25°C with low temperatures in both cultivars in the NA period

(Fig. 3), the increase in intensity was observed more clearly in Fernor. A similar situation was also detected for the 59 kDa protein band. Low-temperature treatments caused the 44 kDa protein band’s intensity to rise in Fernor and decrease in Chandler.

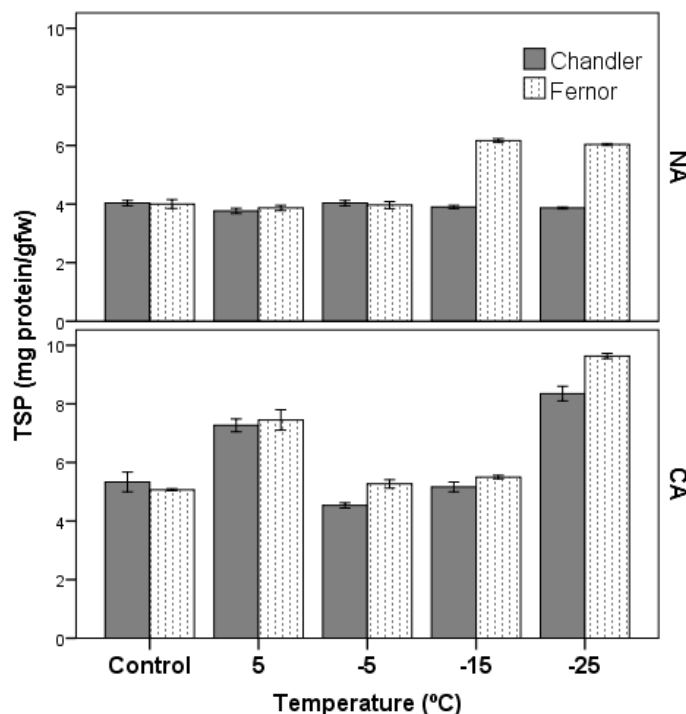


Fig. 2. Effect of low temperature applications on total soluble protein (TSP) contents in walnut cultivars at NA and CA periods. The error bars indicate \pm SE of three replications.

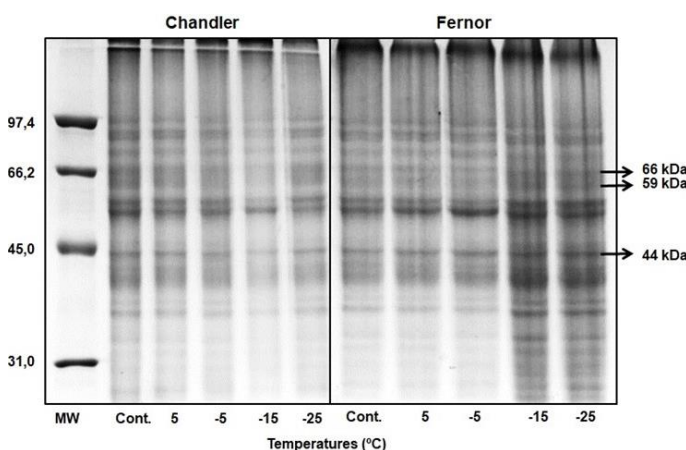


Fig. 3. SDS-PAGE protein profiles of walnut cultivars during the NA period based on low temperature applications. Each well was loaded with 30 μ g of protein. The molecular weight (Mw) of the marker used is displayed on the left in units of kDa. The arrows on the right represent the locations of proteins that varied during low temperature stress.

While the intensity of the 66 kDa protein band was indeterminate in Chandler, it was increased with low

temperatures in Fernor at CA period (Fig. 4). It was observed that the 59 kDa protein band increased at 5°C in Chandler but the other temperatures did not have a significant effect, whereas in Fernor it increased at -15°C and -25°C. While the intensity of the protein band, which was determined as 44 kDa, decreased in Chandler compared to the control due to low-temperature applications, it was determined that it increased at -15°C and -25°C in Fernor.

The immunoblotting results for HSP23 showed that there was a 44 kDa protein band, with varying band intensities based on temperatures and cultivars in the NA and CA periods (Fig. 5 and Fig. 6). Intensity of HSP23 was higher in the CA period than in NA period in both cultivars. Besides, it was determined that the intensity of HSP23 in Fernor was higher than in Chandler in both periods.

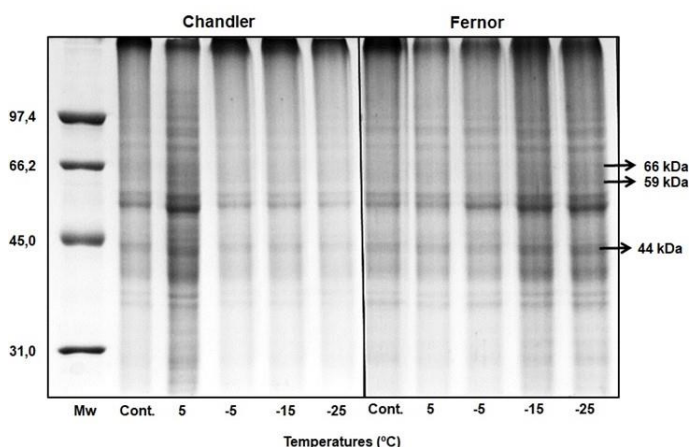


Fig. 4. SDS-PAGE protein profiles of walnut cultivars during the CA period based on low temperature applications. Each well was loaded with 30 µg of protein. The molecular weight (Mw) of the marker used is displayed on the left in units of kDa. The arrows on the right represent the locations of proteins that varied during low temperature stress.

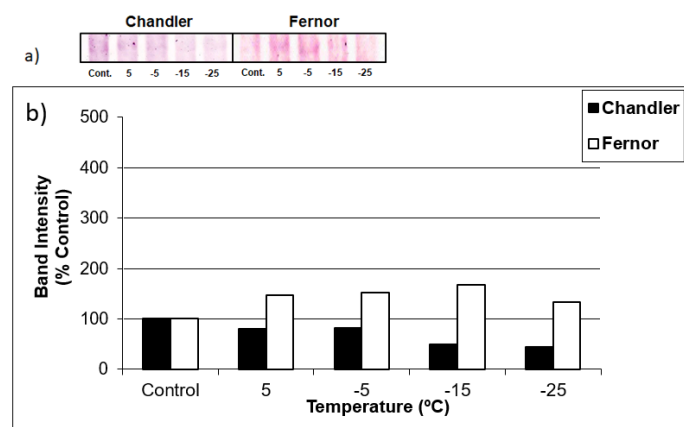


Fig. 5. Appearance of 44 kDa HSP23 protein (a) and band intensities (b) of cultivars due to low temperature applications in NA period.

During the NA period, the intensity of HSP23 in “Chandler” was decreased depending on the low-temperature application compared to the control (Fig. 5). However, synthesis of HSP23 was increased depending on the low-temperature applications in Fernor and it was reached the highest level at -15°C (168%), and then it was decreased at -25°C (133%).

In the CA period, HSP23 has reached the highest level at 5°C (162%) in Chandler compared to the control, thereafter it decreased depending on the low temperature (Fig. 6). In Fernor,

the synthesis of HSP23 was increased depending on the low-temperature application and it was reached the highest level at -25°C (447%).

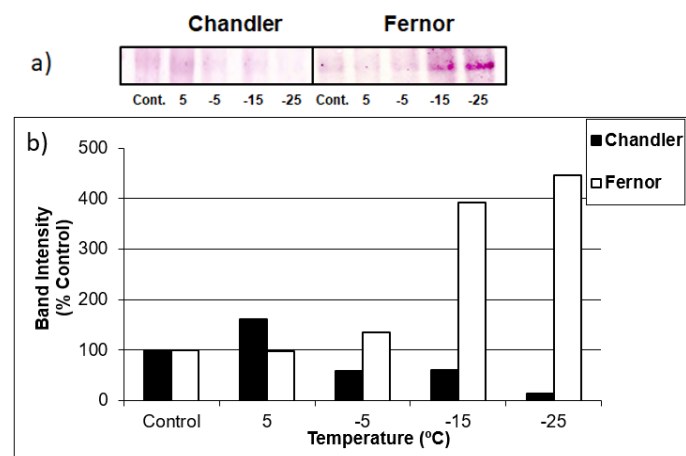


Fig. 6. Appearance of 44 kDa HSP23 protein (a) and band intensities (b) of cultivars due to low temperature applications in CA period.

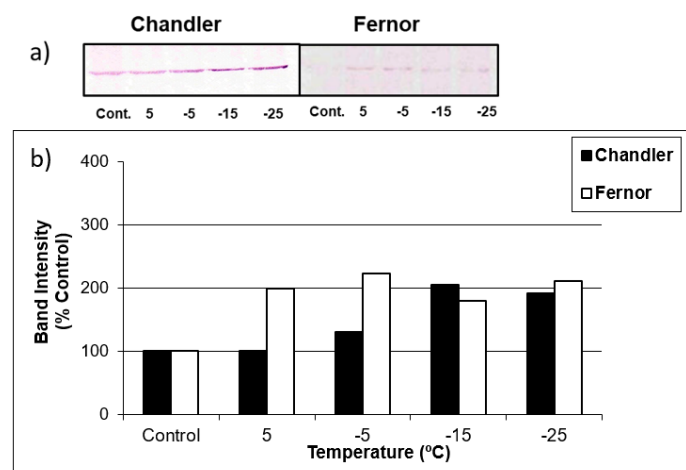


Fig. 7. Appearance of 59 kDa HSP60 protein (a) and band intensities (b) of cultivars due to low temperature applications in NA period.

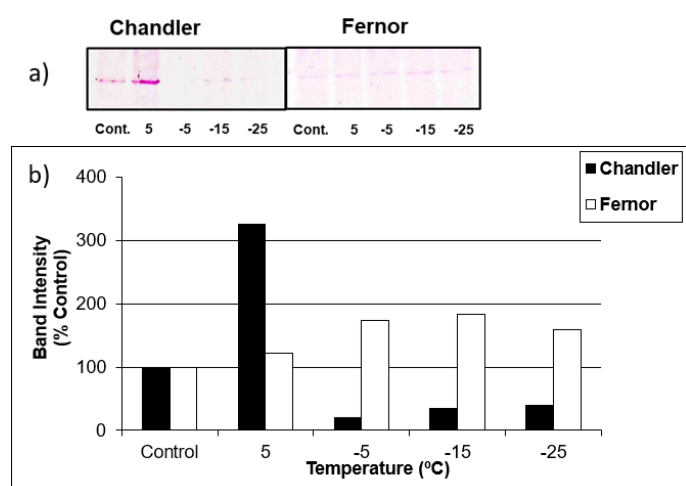


Fig. 8. Appearance of 59 kDa HSP60 protein (a) and band intensities (b) of cultivars due to low temperature applications in CA period.

The immunoblotting investigation results for HSP60 suggested that 59 kDa protein band with various band intensities depending on the cultivars and low temperatures with NA and CA periods (Fig. 7 and Fig. 8). As shown in Fig. 7, during the

NA period, the synthesis of the HSP60 was increased to -15°C (205%) and then it was decreased at -25°C (191%) in Chandler. The intensity of HSP60 in Fernor was increased until -5°C (223%), then it was decreased at -15°C (180%), after it was increased again -25°C (211%). In the CA period, an increase was measured for HSP60 at 5°C (325%) in Chandler, it was found at quite low levels at the other low-temperature applications as compared with the control (Fig. 8). In Fernor the HSP60 was increased until -15°C (184%), then it was decreased at -25°C (154%). The intensity of HSP60 was calculated according to the control of varieties. Generally, the synthesis of HSP60 was more intense in Fernor than in Chandler at all low temperatures in both periods.

4. Discussion

The plasma membrane has a highly dynamic structure to preserve the integrity and identity of closed structures (Casares et al., 2019). Compositional alterations in the plasma membrane, one of the primary sites of freezing injury, are required to achieve cold acclimatization (Miki et al., 2019). The reactions of walnut cultivars to cold stress may vary depending on the season and the region where they are grown. Actually, Aleta et al. (2013) found that, in their research in northeast Spain, the Fernor variety was more tolerant than Chandler in the fall, in contrast, Chandler was more tolerant in the winter. Poirier et al. (2004) according to their research conducted in south-central France, they stated that the Fernor variety was more tolerant than Chandler among seven varieties in the autumn, winter and spring seasons, which is similar to the present study. Since plants are not accustomed to cold during the NA period, it is important to know their reactions to cold stress in this period in order to explain their cold tolerance. Therefore, in this study, two cultivars were determined as cold-sensitive (Chandler) and cold-tolerant (Fernor) in terms of low-temperature tolerance in the NA period.

Cold acclimation boosted the cold tolerance of all walnut cultivars. Low temperatures that happen during the NA period, when plants are not used to the cold, severely harm plants and result in losses of valuable products. For this reason, similar to this study, freezing damage in the field is generally much greater in non-acclimated seasons than the damage that occurs during the winter (Turhan and Ergin, 2012). Especially, late spring frosts and early autumn frosts pose a great risk for crop losses (Heberling and Muzika, 2023). Therefore, among the ten cultivars used in this study, the Chandler with the most damage in the NA period was determined to be cold sensitive and the Fernor, which showed the least damage, was determined to be cold tolerant.

Through a complicated adaption process called “cold acclimation”, plants adapt to withstand freezing temperatures. During the cold acclimation, ultrastructural, compositional, and biochemical changes occur in plant cells (Vafadar et al., 2024). However, the significance of these changes in acquiring frost tolerance is still unclear. To understand frost tolerance, which is a result of cold acclimation, the molecular basis of cold acclimation in plants should be elucidated. In addition to these adaptations, at the onset of stress, normal protein production is reduced and the production of heat shock proteins (HSPs) is increased in plant cells (ul Haq et al., 2019). As previously reported, it was shown that while the synthesis of some other proteins decreased, the synthesis of stress-related proteins increased in the current study. In the present study, it was

determined that 66 kDa, 59 kDa, and 44 kDa protein bands were effective in adaptation to cold in both cultivars. Nevertheless, the increment of these bands is more prominent in Fernor, due to the better cold adaptation of this cultivar.

HSPs prevent stress-induced misfolding and play a role in preventing denatured and aggregated proteins under stress conditions, they are also responsible for maintaining cell homeostasis under normal conditions, transporting newly produced proteins between the organelles of cells and folding (Shahbaz, 2024). HSPs are produced not only under heat stress but also under other stress situations (ul Haq et al., 2019). In Arabidopsis, pea, poplar, and rice, several HSPs were up-regulated in response to cold stress (Bae et al., 2003; Renaut et al., 2004; Cui et al., 2005; Taylor et al., 2005). Like other HSPs, sHSPs work as molecular chaperones and supply protection by binding to non-native forms of proteins and inhibiting the aggregation (Dou et al., 2024). Cold-induced accumulation of sHSPs has been reported in some plant species (Zhang et al., 2020). In this study, the synthesis of HSP23, which belongs to sHSP family, was in the NA period lower than in the CA period. The fact that, the synthesis of HSP23 was significantly increased at the CA period especially in Fernor, which was cold tolerant, suggests that HSP23 is quite effective in gaining cold tolerance in walnut plants.

Correlatively, the synthesis of the HSP60 was higher in Fernor than in Chandler in both periods. The stable increase in HSP60 due to low temperatures in Fernor during the CA period, can be explained by the effect of HSP60 on the cold tolerance of this cultivar. In the CA period, maximum HSP60 synthesis was measured at 5°C in Chandler, it was found at quite low levels at the other low-temperature applications. In this case, it could be this cultivar is tolerant down to 5°C , but not tolerant to lower temperatures. As noted in previous studies (Nagaraju et al., 2021, Tian et al., 2021), it was determined that HSPs act as molecular chaperones that prevent cold-induced protein denaturation and promote the refolding of partially denatured proteins, and therefore, they are closely related to cold tolerance in the walnut plant. In general, the synthesis of HSPs is more intense in Fernor than in Chandler at all low temperatures of the NA and CA periods, due to the better cold tolerance of this cultivar than the other one.

Global warming and climate change brought about by the world's rapidly growing industrialization and urbanization have severe consequences for plant growth, development, yield, and quality, and occasionally even threaten plant existence (Janni et al., 2024). In order to avoid nutritional problems in the future, it is necessary to investigate, identify, and confirm certain traits related to stress tolerance in plants, and develop transgenic plants by revealing and manipulating stress-related genes (Sharma et al., 2023). Related to this, HSPs have a broad function in stress tolerance. Further research is required to fully comprehend the overall function of HSPs in connection to plant cold adaptation. Various scientific studies on the roles of HSP families against various biotic and abiotic stresses in different cultivated plants will be helpful in terms of developing stress-tolerant varieties.

5. Conclusion

The Chandler and Fernor cultivars were identified to be sensitive and tolerant, respectively, among the ten walnut cultivars examined during the NA and CA periods. The differences between these two cultivars in terms of cold

tolerance were investigated in terms of HSPs. The results were emphasized that cold acclimatization is effective in gaining cold tolerance in walnut plants. It was determined for the first time that HSP23 and HSP60 were effective in cold tolerance in walnut plants. According to these findings, to understand HSP's functions in woody plants under cold stress, it is recommended that additional analyses should be performed.

Acknowledgements: Grants from the Scientific Research

References

- Abdullah, S. N. A., Azzeme, A. M., & Yousefi, K. (2022). Fine-Tuning cold stress response through regulated cellular abundance and mechanistic actions of transcription factors. *Frontiers in Plant Science*, 13, 850216.
- Aletà, N., Vilanova, A., Tomàs, E., & Guàrdia, M. (2013). Frost resistance in seven commercial walnut cultivars. *VII International Walnut Symposium*, Shanxi, China. 389-393.
- Almalki, A. F. Y., Arabdin, M., & Khan, A. (2021). The role of heat shock proteins in cellular homeostasis and cell survival. *Cureus*, 13(9), 1-7.
- Arora, R., & Wisniewski, M. E. (1994). Cold acclimation in genetically related (sibling) deciduous and evergreen peach (*Prunus persica* [L.] Batsch) (II. A 60-kilodalton bark protein in cold-acclimated tissues of peach is heat stable and related to the dehydrin family of proteins). *Plant Physiology*, 105(1), 95-101.
- Arora, R., Wisniewski, M. E., & Scorza, R. (1992). Cold acclimation in genetically related (sibling) deciduous and evergreen peach (*Prunus persica* [L.] Batsch) I. Seasonal changes in cold hardiness and polypeptides of bark and xylem tissues. *Plant Physiology*, 99(4), 1562-1568.
- Bae, M. S., Cho, E. J., Choi, E. Y., & Park, O. K. (2003). Analysis of the Arabidopsis nuclear proteome and its response to cold stress. *The Plant Journal*, 36(5), 652-663.
- Batool, F., Agossa, B. A., Sandhu, Z. Y., Sarwar, M. B., Hassan, S., & Rashid, B. (2022). Heat shock proteins (HSP70) gene: Plant transcriptomic oven in the hot desert. In: Kimatu J. N. (eds) *Advances in Plant Defense Mechanisms* (pp. 1-370). IntechOpen.
- Bourgine, B., & Guihur, A. (2021). Heat shock signaling in land plants: From plasma membrane sensing to the transcription of small heat shock proteins. *Frontiers in Plant Science*, 12, 710801.
- Casares, D., Escribá, P. V., & Rosselló, C. A. (2019). Membrane lipid composition: effect on membrane and organelle structure, function and compartmentalization and therapeutic avenues. *International Journal of Molecular Sciences*, 20(9), 2167-2197.
- Charrier, G., Chuine, I., Bonhomme, M., & Améglio, T. (2018a). Assessing frost damages using dynamic models in walnut trees: exposure rather than vulnerability controls frost risks. *Plant, Cell & Environment*, 41(5), 1008-1021.
- Charrier, G., Lacoite, A., & Améglio, T. (2018b). Dynamic modeling of carbon metabolism during the dormant period accurately predicts the changes in frost hardiness in walnut trees *Juglans regia* L. *Frontiers in Plant Science*, 9, 410551.
- Cui, S., Huang, F., Wang, J., Ma, X., Cheng, Y., & Liu, J. (2005). A proteomic analysis of cold stress responses in rice seedlings. *Proteomics*, 5(12), 3162-3172.
- Dou, N., Li, L., Fang, Y., Fan, S., & Wu, C. (2024). Comparative physiological and transcriptome analyses of tolerant and susceptible cultivars reveal the molecular mechanism of cold tolerance in *Anthurium andraeanum*. *International Journal of Molecular Sciences*, 25(1), 250.
- Drepper, B., Bamps, B., Gobin, A., & Van Orshoven, J. (2022). Strategies for managing spring frost risks in orchards: effectiveness and conditionality—a systematic review. *Environmental Evidence*, 11(1), 1-24.
- Ergin, S., Gülen, H., Kesici, M., Turhan, E., Ipek, A., & Köksal, N. (2016). Effects of high temperature stress on enzymatic and nonenzymatic antioxidants and proteins in strawberry plants. *Turkish Journal of Agriculture and Forestry*, 40(6), 908-917.
- Heberling, J. M., & Muzika, R. M. (2023). Not all temperate deciduous trees are leafless in winter: The curious case of marcescence. *Ecosphere*, 14(3), e4410, 1-6.
- Projects Commission of Eskisehir Osmangazi University (2016/23A101) supported the current research.
- Conflict of interest:** The authors declare that they have no conflict of interests.
- Informed consent:** The authors declare that this manuscript did not involve human or animal participants and informed consent was not collected.
- Hu, C., Yang, J., Qi, Z., Wu, H., Wang, B., Zou, F., ... & Liu, Q. (2022). Heat shock proteins: Biological functions, pathological roles, and therapeutic opportunities. *MedComm*, 3(3), e161.
- Janni, M., Maestri, E., Gulli, M., Marmioli, M., & Marmioli, N. (2024). Plant responses to climate change, how global warming may impact on food security: a critical review. *Frontiers in Plant Science*, 14, 1297569-1297582.
- Kerbler, S. M., & Wigge, P. A. (2023). Temperature sensing in plants. *Annual Review of Plant Biology*, 74, 341-366.
- Lim, C. C., Krebs, S. L., & Arora, R. (1999). A 25-kDa dehydrin associated with genotype-and age-dependent leaf freezing-tolerance in *Rhododendron*: a genetic marker for cold hardiness? *Theoretical and Applied Genetics*, 99, 912-920.
- McLoughlin, F., Basha, E., Fowler, M. E., Kim, M., Bordowitz, J., Katiyar-Agarwal, S., & Vierling, E. (2016). Class I and II small heat shock proteins together with HSP101 protect protein translation factors during heat stress. *Plant Physiology*, 172(2), 1221-1236.
- Miki, Y., Takahashi, D., Kawamura, Y., & Uemura, M. (2019). Temporal proteomics of Arabidopsis plasma membrane during cold- and deacclimation. *Journal of Proteomics*, 197(15), 71-81.
- Nagaraju, M., Kumar, A., Jalaja, N., Rao, D. M., & Kishor, P. B. (2021). Functional exploration of chaperonin (HSP60/10) family genes and their abiotic stress-induced expression patterns in Sorghum bicolor. *Current Genomics*, 22(2), 137-152.
- NIH Image, (2024). Official Website of NIH Image Home Page, <https://imagej.net/nih-image/>, Last Accessed on March 20, 2024.
- Poirier, M., Bodet, C., Ploquin, S., Saint-Joanis, B., Lacoite, A., & Améglio, T. (2004). Walnut cultivar performance of cold resistance in south central France. *V International Walnut Symposium*, Sorrento, Italy. 281-285.
- Ré, M. D., Gonzalez, C., Escobar, M. R., Sossi, M. L., Valle, E. M., & Boggio, S. B. (2017). Small heat shock proteins and the postharvest chilling tolerance of tomato fruit. *Physiologia Plantarum*, 159(2), 148-160.
- Renaut, J., Lutts, S., Hoffmann, L., & Hausman, J. F. (2004). Responses of poplar to chilling temperatures: proteomic and physiological aspects. *Plant Biology*, 7(01), 81-90.
- Rezaei, M., & Rohani, A. (2023). Estimating Freezing Injury on Olive Trees: A Comparative Study of Computing Models Based on Electrolyte Leakage and Tetrazolium Tests. *Agriculture*, 13(6), 1137.
- Riikonen, J., Ruhanen, H., & Luoranen, J. (2023). Impact of warm spells during late fall and winter on frost hardiness of short-day treated Norway spruce seedlings. *Forest Ecology and Management*, 542, 121105.
- Shahbaz, M. (2024). Heat and Wheat: Adaptation strategies with respect to heat shock proteins and antioxidant potential; an era of climate change. *International Journal of Biological Macromolecules*, 256, 128379.
- Sharma, P., Pandey, A., Malviya, R., Dey, S., Karmakar, S., & Gayen, D. (2023). Genome editing for improving nutritional quality, post-harvest shelf life and stress tolerance of fruits, vegetables, and ornamentals. *Frontiers in Genome Editing*, 5, 1094965- 1094984.
- Tadić, V., Gligorević, K., Mileusnić, Z., Miodragović, R., Hajmiller, M., & Radočaj, D. (2023). Agricultural engineering technologies in the control of frost damage in permanent plantations. *AgriEngineering*, 5(4), 2079-2111.
- Takahashi, D., Willick, I. R., Kasuga, J., & Livingston III, D. P. (2021). Responses of the plant cell wall to sub-zero temperatures: a brief update. *Plant and Cell Physiology*, 62(12), 1858-1866.

- Taylor, N. L., Heazlewood, J. L., Day, D. A., & Millar, A. H. (2005). Differential impact of environmental stresses on the pea mitochondrial proteome. *Molecular & Cellular Proteomics*, 4(8), 1122-1133.
- Tian, F., Hu, X. L., Yao, T., Yang, X., Chen, J. G., Lu, M. Z., & Zhang, J. (2021). Recent advances in the roles of HSFs and HSPs in heat stress response in woody plants. *Frontiers in Plant Science*, 12, 704905-704912.
- Turhan, E., & Ergin, S. (2012). Soluble sugars and sucrose-metabolizing enzymes related to cold acclimation of sweet cherry cultivars grafted on different rootstocks. *The Scientific World Journal*, 2012, 1-8.
- ul Haq, S., Khan, A., Ali, M., Khattak, A. M., Gai, W. X., Zhang, H. X., ... & Gong, Z. H. (2019). Heat shock proteins: dynamic biomolecules to counter plant biotic and abiotic stresses. *International Journal of Molecular Sciences*, 20(21), 5321-5352.
- Vafadar, M., Rezaei, M., & Khadivi, A. (2024). Frost hardiness of 10 olive cultivars after natural and controlled freezing. *Scientia Horticulturae*, 325, 112687-112696.
- Yang, R., Yu, G., Li, H., Li, X., & Mu, C. (2020). Overexpression of small heat shock protein LimHSP16.45 in *Arabidopsis hsp17.6II* mutant enhances tolerance to abiotic stresses. *Russian Journal of Plant Physiology*, 67, 231-241.
- Yurina, N. P. (2023). Heat shock proteins in plant protection from oxidative stress. *Molecular Biology*, 57(6), 951-964.
- Zhang, N., Zhao, H., Shi, J., Wu, Y., & Jiang, J. (2020). Functional characterization of class I SIHSP17.7 gene responsible for tomato cold-stress tolerance. *Plant Science*, 298, 110568-110580.
- Zinta, G., Singh, R. K., & Kumar, R. (2022). Cold adaptation strategies in plants—An emerging role of epigenetics and antifreeze proteins to engineer cold resilient plants. *Frontiers in Genetics*, 13, 909007.

Cite as: Ergin, S., & Altintas, F. (2024). Effects of cold stress on protein metabolism of certain walnut cultivars. *Front Life Sci RT*, 5(1), 31-37.



Research article

In silico analysis of sirtuin-type histone deacetylase genes in sugar beet (*Beta vulgaris* L.)

Seher Yolcu^{*1} ¹ Sabanci University, Faculty of Engineering and Natural Sciences, 34956, Istanbul, Türkiye

Abstract

Histone deacetylase (HDAC) enzymes catalyze the removal of an acetyl group from the lysine residues of histone N-terminal tails, and they repress gene transcription through condensation of chromatin. In plants, the sirtuins/silent information regulator 2 (SIR2) proteins which are NAD⁺-dependent deacetylases, have been identified in distinct plant species such as *Arabidopsis*, rice, tomato, soybean, maize, etc., but little is known about their functions in plants. They are mainly investigated in *Arabidopsis* and rice and found to be involved in H3K9 acetylation, metabolic pathways, repression of genes associated with stress response, and energy metabolism. A total of eight *RPD3/HDA1* family HDAC genes have been recently identified in the sugar beet (*Beta vulgaris* L.) genome. However, *B. vulgaris* SIR2-type HDACs have not yet been identified and characterized. In this work, an *in silico* analysis of SIR2 family members was performed in sugar beet. Three SIR2 family HDACs were identified from the sugar beet genome, named BvSRT1, BvSRT2, and BvSRT3. The beet *SIR2* gene family is found to be located on chromosomes 4, and 9. The phylogenetic tree building with *B. vulgaris*, *Arabidopsis*, tomato, soybean, *Vitis vinifera*, pepper, rice, maize, and *Sorghum bicolor* showed that 3 sugar beet SRTs were divided into two classes: Class II (BvSRT2) and IV (BvSRT1 and BvSRT3). SIR2 family proteins consisted of SIR2 domain (PF02146). The conserved motifs ranged from 6 to 50 amino acids, while the intron-exon numbers of genes ranged from 10 to 14. *BvSRT1* and *BvSRT3* exhibited similar motif distributions and exon/intron structures. Moreover, nuclear, and cytoplasmic localization of BvSRT1 and BvSRT3 has been predicted. BvSRT2 protein was located on the mitochondrion. Analysis of *cis*-elements revealed the involvement of *BvSRT* genes in hormone regulation, light response, abiotic stress response, and meristem expression. This study may shed light on the potential role of SIR2-type HDACs in beets.

Keywords: *Beta vulgaris*; histone deacetylase (HDAC); *in silico* analysis; sirtuins; SIR2; sugar beet

1. Introduction

Epigenetic modifications including histone acetylation, methylation, phosphorylation, DNA methylation, and RNA interference (RNAi) in eukaryotes regulate numerous cellular processes through gene activation or repression (Salgotra and Gupta, 2019). Deacetylation of the N^ε-acyl-lysine residues converts neutral acetylated lysine residues to positively charged lysine residues, resulting in a strong interaction with the DNA, and inactivation of gene transcription (Zhao et al., 2018; Perrella et al., 2024). This process is catalyzed by two types of

deacetylases: Zn²⁺-containing deacetylases (Zhao et al., 2018), and sirtuins/silent information regulator 2 (SIR2) (Chen et al., 2015; Zhao et al., 2018). The sirtuins/SIR2 are β-NAD⁺-dependent deacetylase enzymes for histone or non-histone proteins that was discovered in yeast for the first time (Imai et al., 2000). Sirtuin family members have been found in different organisms such as fungi, mammals, human parasites, and plants (Greiss and Gartner, 2009). Yeast and mouse SIR2 proteins catalyze deacetylation of lysine 9 and 14 at histone H3, and H4 lysine 16. Seven sirtuins (SIRT1-7) in mammals have NAD⁺-binding catalytic domain and differ in subcellular localization.

* Corresponding author.

E-mail address: seher808@gmail.com (S. Yolcu).

<https://doi.org/10.51753/flsrt.1412729> Author contributions

Received 31 December 2023; Accepted 20 February 2024

Available online 30 April 2024

2718-062X © 2024 This is an open access article published by Dergipark under the [CC BY](https://creativecommons.org/licenses/by/4.0/) license.

Their functions are associated with metabolism, senescence, antioxidant protection, apoptosis, tumor suppression, and regulation of cell cycle (Houtkooper et al., 2012; Carafa et al., 2016; Ziętara et al., 2023). Mammal SIRT1, SIRT6, and SIRT7 exist in the nucleus, while SIRT2 is located in the cytoplasm and nucleus. SIRT3, SIRT4, and SIRT5 are present in mitochondria (Carafa et al., 2016). The SIRT4 controls glutamine metabolism and therefore inhibits cell proliferation (Jeong et al., 2013). Similarly, in a very recent work, *Arabidopsis* sirtuins were found to function in cell proliferation by a decline in NAD-glutamate dehydrogenase (GDH) activity (Bruscalupi et al., 2023). Although the functions of animal sirtuins are known, which are involved in energy metabolism, lifetime regulation, apoptosis, proliferation, DNA repair, and stress tolerance, little is known about the roles of plant sirtuins (Houtkooper et al., 2012; Bruscalupi et al., 2023). In plants, they have been mostly studied in *Arabidopsis* and rice (*Oryza sativa*) (König et al., 2014; Zhang et al., 2017; Zheng, 2020). Up to date, SIR2 proteins have been identified in distinct plant species including *Arabidopsis* (Pandey et al., 2002), *O. sativa* (Huang et al., 2007; Zhang et al., 2016; Zhang et al., 2017), *Solanum lycopersicum* (Zhao et al., 2014), *Glycine max* (Yang et al., 2018), *Litchi chinensis* (Peng et al., 2017), *Zea mays* (Zhang et al., 2020), *Triticum aestivum* (Shu et al., 2021), *Capsicum annuum* (Cai et al., 2022), *Vitis vinifera* (Busconi et al., 2009; Aquea et al., 2010), *Fagopyrum tataricum* (Yan et al., 2023), *Sorghum bicolor* (Du et al., 2022), and *Camellia sinensis* (tea plant) (Yuan et al., 2020). Most of these plant sirtuins have been recently identified, and their functions are not well-studied. Phylogenetic analysis revealed that the mammalian sirtuin proteins are divided into four classes (class I-IV), and they have additional functions along with Lys acetylation. For instance, mammalian class III sirtuin, SIRT5 has Lys succinylase and demalonylase activities (Du et al., 2011). *Arabidopsis* genome includes only class IV and class II sirtuins, Silent Information Regulator1 homolog SRT1 (At5g55760) and SRT2 (At5g09230), respectively (Pandey et al., 2002). SRT2 in *Arabidopsis* is a mitochondrial protein (König et al., 2014). Similar to mammals, the subcellular localization of SIR2s in plants was found in the nucleus, mitochondria, chloroplast, and cytosol (Pandey et al., 2002; Martínez-Redondo and Vaquero, 2013; Zheng, 2020). *Arabidopsis* SRT1 (AtSRT1) was reported to interact with cMyc-Binding Protein 1 (AtMBP-1), a truncated version of the cytosolic glycolytic enolase gene *LOS2/ENO2*. Moreover, plant sirtuins use non-histone proteins as substrates, such as AtMBP-1, and OsGAPDH1, suggesting that SIR2 proteins play a key role in different cellular processes at various organs, tissues, and developmental stages. The *AtSRT1* declined the levels of H3K9 acetylation in the *LOS2/ENO2* and *STZ/ZAT10* that both encode stress regulators (Peng et al., 2017). Yeast SIR2 homolog, *Arabidopsis* SRT2 (AtSRT2) which is localized at the inner mitochondrial membrane, is associated with some proteins related to energy metabolism and metabolite transport including the ATP/ADP carriers and ATP synthase, suggesting the involvement of SRT2 protein in mitochondrial energy metabolism. The *srt2* mutants exhibited alterations in the amounts of sugar, amino acid, and ADP (König et al., 2014). Furthermore, AtSRT2 was found to regulate basal defense in response to a bacterial pathogen, *Pseudomonas syringae* pv. *tomato* DC3000 (Chunzheng et al., 2010). In *Arabidopsis*, *srt2* knock-out lines showed increments in the expression of *salicylic acid-related* (*PAD4*, *EDS5*, *SID2*), and *pathogenesis-related 1* (*PR1*) genes in contrast to *AtSRT2* overexpressor lines. In *O.*

sativa, OsSRT1 is not only involved in the deacetylation of histone H3 lysine 9 (H3K9) but also inhibits transcription of *glyceraldehyde-3-phosphatedehydrogenase* (*GAPDH*), indicating that the OsSRT1 decreases glycolysis (Zhang et al., 2017). In a recent study, in an ornamental woody plant (*Prunus mume*), 2 SIR2 family members (*PmSRT1*, and *PmSRT2*) were found among 13 *PmHDAC* genes, and they significantly responded to cold stress after 12 hours, and their expression levels varied according to geographical environmental factors or cold-resistance levels in individuals (Meng et al., 2022).

Sugar beet (*Beta vulgaris* L.), a member of the Amaranthaceae family, is a diploid (2n=18) crop grown in temperate and subtropical climates (Dohm et al., 2014). It is used for the production of different materials, such as sugar, bioethanol, animal feed, health-promoting foods, and raw materials for health (Hoffmann, 2010; Yu et al., 2020; Yolcu et al., 2022). Sugar beet is an economically important crop species that is tolerant to salt and drought (Wedeking et al., 2016; Fotouhi et al., 2017). Therefore, sugar beet growth in lands unsuitable for agriculture is possible if plant breeders develop highly stress-tolerant sugar beet varieties (Zhang et al., 2021). However, sugar production and beet development are adversely affected by climate change (Zhang et al., 2021). Identification of *B-box* (*BBX*) genes, *BRASSINAZOLE-RESISTANT* (*BZR*) family genes, and *high-affinity K⁺-transporter* (*HAKs*) genes in sugar beet has been performed at the genome level through *in silico* methods (Wang et al., 2019; Yang et al., 2022; Song et al., 2023). Eight RPD3/HDA1 family members of histone deacetylase-encoding genes (*HDACs*) and seven histone acetyltransferase-encoding genes (*HATs*) in *B. vulgaris* have been recently identified and characterized through bioinformatics tools and databases (Yu et al., 2023; Yolcu et al., 2024). However, there are no reports on the *sirtuin-type HDAC* gene family in sugar beet. Importantly, there are few research articles related to the effects of epigenetic modifications on gene expression in *B. vulgaris* under stress applications (Yolcu et al., 2016; Skorupa et al., 2021). Thus, epigenetic regulation of biological processes and the roles of histone modifiers remain elusive in sugar beet.

This study performed an *in silico* analysis of *B. vulgaris* SIR2 family members by using bioinformatics tools and databases and examined their physicochemical properties, gene structure, distribution of motifs, prediction of subcellular localization, phylogenetic analysis, promoter *cis*-acting regulatory elements, and protein 3D structure.

2. Materials and methods

2.1. Identification of SIR2 subfamily members in *B. vulgaris*

A total of 2 SIR2 protein sequences from *Arabidopsis* and 2 sequences from rice were retrieved from the TAIR (Reiser et al., 2024), and Ensembl Plants (Bolser et al., 2017; Ensembl, 2017) databases, and then used to search SIR2s with the BLASTP tool using the sugar beet genome (*Beta vulgaris* ssp. *vulgaris* EL10.2_2, Phytozome genome ID: 782, NCBI taxonomy ID: 3555) in Phytozome version 13 (Goodstein et al., 2012). All homologous protein sequences of the BvSRT candidates are accepted if they have the sequence identity with *Arabidopsis* and rice SRT proteins of more than 50% and $e < 10^{-10}$. SIR2 domain (PF02146) of *B. vulgaris* candidate proteins were confirmed by SMART (Letunic et al., 2012; Letunic and Bork, 2020) and NCBI CDD (Wang et al., 2022) databases.

Physicochemical properties of three BvSRT proteins such as isoelectric point (pI), theoretical molecular weight (MW), and GRAVY (grand average of hydropathy) were predicted online (Gasteiger et al., 2005).

2.2. Prediction of BvSRT subcellular localization

Subcellular localization predictions of beet SRT proteins were carried out using two online predictors including CELLO server (Yu et al., 2006), and WoLFPSORT (Nakai and Horton, 1999).

2.3. Conserved protein motifs and phylogenetic analysis

The motifs of the BvSRT proteins were analyzed by MEME Version 5.5.2 (meme-suite.org/tools/meme) (Bailey and Elkan, 1994), with the maximum number of motifs set to 10. To understand the evolutionary relationship of BvSRTs with other SRTs, a total of 21 SRT protein sequences in a variety of plant species such as *A. thaliana* (*At*), *O. sativa* (*Os*), *S. lycopersicum* (*Sl*), *G. max* (*Gm*), *Z. mays*, *C. annuum* (*Ca*), *V. vinifera*, and *S. bicolor* (*Sb*) (Table 1) were obtained from National Center for Biotechnology Information (NCBI) and Ensembl Plants to perform a phylogenetic analysis. A phylogenetic tree was constructed by MEGA11 using the maximum likelihood method, with 1000 bootstrap replicates (Tamura et al., 2021).

2.4. 3D structures of HAT proteins in B. vulgaris

Three-dimensional structure models have been constructed using the Protein Homology/Analogy Recognition Engine V 2.0 (Phyre2) server (Kelley et al., 2015). The amino acid sequences were used to visualize predicted 3D structures of BvSRT proteins using intensive mood.

2.5. Chromosomal locations, and gene structure

The physical locations of the *BvSRT* genes along each chromosome have been retrieved from the sugar beet genome (Phytozome 13) and the chromosomal distribution graph was drawn by Mapgene2chrom 2.1 (MG2C v2.1) online tool (Jiangtao et al., 2015; Chao et al., 2021).

Gene Structure Display Server (GSDS) (Hu et al., 2015) was used to analyze the exon-intron structures of the *BvSRTs*.

2.6. Genomic synteny analysis

Genomic synteny was comparatively done to examine the relationship between sugar beet, rice, tomato, and *Arabidopsis* using the Circoletto program (Circos) (Krzywinski et al., 2009). Score/max ratio was used coloring with blue \leq 0.25, green \leq 0.50, orange \leq 0.75, red $>$ 0.75. Three SIR2 proteins from *B. vulgaris* and six SRTs from *Arabidopsis*, tomato, and rice in FASTA format were used as query and database files, respectively.

2.7. Analysis of cis-acting regulatory elements and heatmap construction

The sequences 1500 bp upstream of the transcription start site (TSS) were extracted from the sugar beet genome using by Phytozome database. The numbers and types of *cis*-elements were predicted by PlantCARE software (Lescot et al., 2002).

TBtools was used to construct heatmap depending on functional classification of *cis*-elements (Chen et al., 2020).

3. Results

3.1. Identification of SIR2 genes in B. vulgaris

The protein sequences of *A. thaliana* and *O. sativa* SRTs were obtained from TAIR, and Phytozome, and then these queries were used to search SRT proteins in *B. vulgaris* genome through BLASTP in Phytozome 13. A total of 3 SRTs have been identified in *B. vulgaris* and have been named according to their positions on the 9 chromosomes of the beet. The physicochemical properties of SIR2s such as chromosome location, strand, CDS (bp), amino acid length (aa), molecular weight (MW), isoelectric points (pI), and grand average of hydropathicity (GRAVY) were indicated in Table 1. The BvSRT1, BvSRT2, BvSRT3 protein lengths were 497, 390, and 458 aa, respectively. The predicted MWs were 55.57, 43.31, and 51.46 kDa, while the pI was 9.24, 8.78, and 8.31. The highest MW, CDS, and amino acid lengths were reported in BvSRT1. Previously known sirtuin proteins in different plants such as *Arabidopsis*, *O. sativa*, *S. lycopersicum*, *G. max*, *Z. mays*, *C. annuum*, *T. aestivum*, *V. vinifera*, *S. bicolor*, *C. sinensis*, *F. tataricum* and *L. chinensis* were presented in Table 2.

3.2. Subcellular localization

Bioinformatics tools have been extensively used to predict subcellular localization of proteins. Present study includes only *in silico* approach. Two online predictors (cello-life, and WoLFPSORT) were used to predict subcellular localization of BvSRTs, which are presented in Table 3. WoLFPSORT is a subcellular location predictor based on known sorting signal motifs and amino acid contents (Nakai and Horton, 1999). Except for BvSRT2, two SRT proteins were assumed to be localized in nucleus or cytoplasm according to cello-life tool. Consistent with the *Arabidopsis* SRT2 protein, BvSRT2 was predicted to be present in the mitochondrion (Pandey et al., 2002). Consistent with cello-life results, WoLFPSORT also showed the cytoplasmic and nuclear localization of BvSRT3 (Table 3). The subcellular localizations of BvSRT1 and BvSRT2 were found in the peroxisome and mitochondrion with high frequencies, respectively (Table 3).

3.3. Phylogenetic relationships and determination of conserved motifs in SRT proteins

The phylogenetic relationships between BvSRTs and other SRTs from various plant species, such as *A. thaliana* (*At*), *O. sativa* (*Os*), *S. bicolor* (*Sb*), *V. vinifera*, *S. lycopersicum* (*Sl*), *G. max* (*Gm*), *Z. mays*, *C. annuum* (*Ca*) were shown in Fig. 1. According to the phylogenetic analysis, 3 SRT proteins in *B. vulgaris* were divided into two classes: Class II (BvSRT2) and IV (BvSRT1 and BvSRT3). The BvSRT1 protein was closely related to AtSRT1, and clustered together with SRT6901 (*V. vinifera* SRT1), GmSRT3, and GmSRT4. Another class IV member, BvSRT3 was present at the same group with OsSRT1, GRMZM2G058573 (*Z. mays* SRT), and SbSRT1. BvSRT2 was grouped in Class II, and clustered with GmSRT1, GmSRT2, SRT6902 (*V. vinifera* SRT2), AtSRT2, CaSRT2, and SISRT2.

MEME analysis which was carried out to study the diversity of SIR2 protein structures, identified 10 motifs in

Table 1

The physicochemical properties of *SIR2*-type *HDAC* genes and *SIR2* proteins in *Beta vulgaris*.

| Phytozome Sequence ID | Gene name | Chromosome location | Strand | CDS (bp) | Length (aa) | MW (kDa) | pI | GRAVY |
|-----------------------|---------------|-------------------------|---------|----------|-------------|----------|------|--------|
| Bevul.4G007100 | <i>BvSRT1</i> | Chr4: 802701-812273 | Reverse | 1491 | 497 | 55.57 | 9.24 | -0.220 |
| Bevul.4G180100 | <i>BvSRT2</i> | Chr4: 56999487-57004409 | Reverse | 1170 | 390 | 43.31 | 8.78 | -0.272 |
| Bevul.9G035800 | <i>BvSRT3</i> | Chr9: 6905704-6919466 | Forward | 1374 | 458 | 51.46 | 8.31 | -0.149 |

Table 2

Previously identified sirtuin proteins in different plants, such as *A. thaliana*, *O. sativa*, *S. lycopersicum*, *G. max*, *Z. mays*, *C. annuum*, *T. aestivum*, *V. vinifera*, *S. bicolor*, *C. sinensis*, *F. tataricum* and *L. chinensis*.

| Plant species | SIR2 proteins | Reference(s) |
|------------------------|--|---|
| <i>A. thaliana</i> | SRT1, SRT2 | (Pandey et al., 2002) (Huang et al., 2007; |
| <i>O. sativa</i> | SRT1, SRT2 | Zhang et al., 2016; Zhang et al., 2017) |
| <i>S. lycopersicum</i> | SRT1, SRT2 | (Zhao et al., 2014) |
| <i>G. max</i> | SRT1, SRT2, SRT3, SRT4 | (Yang et al., 2018) |
| <i>Z. mays</i> | GRMZM2G058573, GRMZM5G807054 | (Zhang et al., 2020) |
| <i>C. annuum</i> | CaSRT1, CaSRT2 | (Cai et al., 2022) |
| <i>T. aestivum</i> | TaSRT1A, TaSRT1B, TaSRT1D, TaSRT2A, TaSRT2D, TaSRT2U | (Shu et al., 2021) |
| <i>V. vinifera</i> | SRT6901, SRT6902 | (Aquea et al., 2010) |
| <i>S. bicolor</i> | SbSRT1, SbSRT2 | (Du et al., 2022) |
| <i>C. sinensis</i> | CsSRT1, CsSRT2, CsSRT3, CsSRT4 | (Yuan et al., 2020) |
| <i>F. tataricum</i> | FtSRT1, FtSRT2 | (Yan et al., 2023) |
| <i>L. chinensis</i> | LcSRT1, LcSRT2 | (Peng et al., 2017) |

Table 3

Predicted subcellular localization of *B. vulgaris* SRT proteins. Two online prediction tools such as cello-life, and WoLFPSORT were used to investigate the possible subcellular localization of *BvSRTs*.

| Protein | Subcellular localization | |
|---------------|--------------------------|-------------------|
| | cello-life | WoLF PSORT |
| BvSRT1 | Nuclear/cytoplasmic | pero(11), cyto(2) |
| BvSRT2 | Mitochondrial | mito(7), chlo(3) |
| BvSRT3 | Cytoplasmic/nuclear | cyto(7), nucl(2) |

*cyto: cytosol, nucl: nucleus, chlo: chloroplast, mito: mitochondrium, pero: peroxisome

BvSRT proteins (Fig. 2). Amino acid lengths of conserved domains ranged from 6 to 50. Identical motifs including motifs 1-10 (except for motif 9) were found in Class IV proteins, *BvSRT1* and *BvSRT3*, suggesting that these proteins may possess similar functions. Only *BvSRT2* and *BvSRT3* contained motif 9. There are fewer motifs in *BvSRT2* as compared to *BvSRT1* and *BvSRT3* proteins. The *BvSRT2* comprised three motifs: 1, 2 and 9 (Fig. 2). All SRT proteins contained motif 1

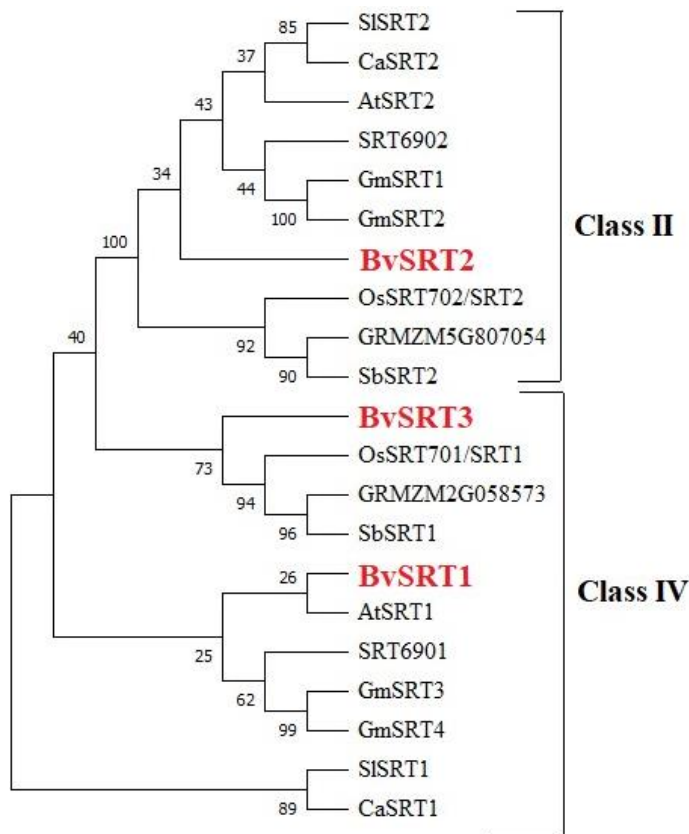


Fig. 1. Phylogenetic tree of *SIR2* proteins in different plant species. Maximum Likelihood method and Poisson correction model were used to generate the phylogenetic tree (1000 bootstrap replicates) based on multiple alignments with ClustalW. The analysis contains 21 amino acid sequences from *B. vulgaris* (*Bv*), *A. thaliana* (*At*), *O. sativa* (*Os*), *S. bicolor* (*Sb*), *G. max*, *V. vinifera*, *C. annuum* (*Ca*), *Z. mays* and *S. lycopersicum* (*Sl*).

and 2, which are sirtuin_cat domains (PS50305). Motif 3 exists in *BvSRT1* and *BvSRT3* is a DHS-like_NAD/FAD-binding domain (IPR029035), which is catalytic domain of sirtuin family.

3.4. Chromosomal distribution, and gene structures

To investigate the chromosomal distribution of the *BvSRT*

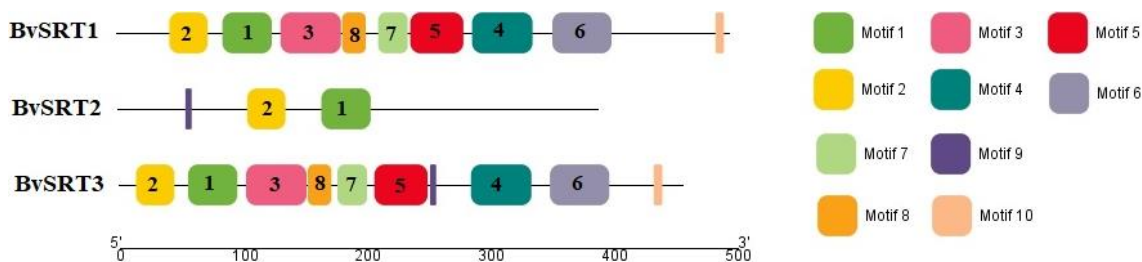


Fig. 2. Motif analysis of the *SIR2*-type *HDAC* proteins in *B. vulgaris*. The MEME online tool and TBtools were used to analyze and construct the domains. Distinct motifs are indicated by different colors and numbers.

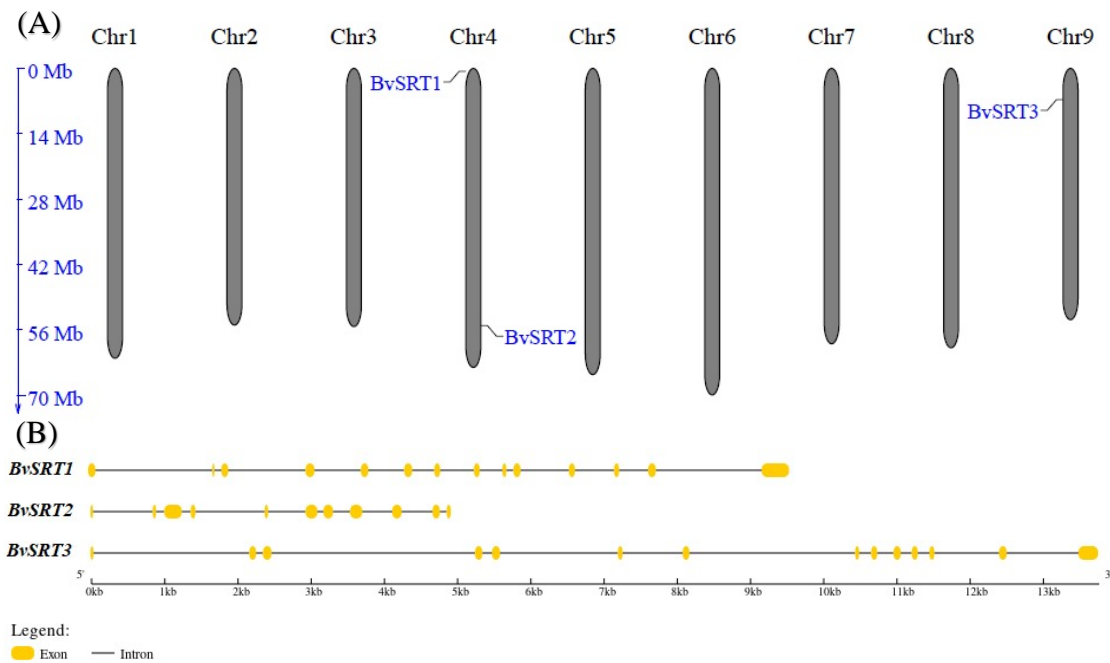


Fig. 3. Chromosomal distribution and structure of *BvSRT* genes. **(A)** Chromosomal positions of three *SRT* genes in sugar beet genome generated in MG2C tool. The number of the chromosomes is displayed at the top of each chromosome. The genome-scale in megabases (Mb) is given on the left. **(B)** Gene structure analyses of the *BvSRTs* performed in the GSDS 2.0 tool. Exons and introns are indicated by yellow boxes, and black lines, respectively. Kb: kilobases.

genes, they are mapped on the chromosomes by using information from the sugar beet genomic database. The sugar beet *SIR2* gene family is found to be dispersed on chromosomes 4, and 9 (Fig. 3A). Two genes belonging to Class IV and Class II, *BvSRT1* and *BvSRT2* located on chromosome 4. No genes were found on chromosomes 1, 2, 3, 5, 6, 7, and 8.

Structures of *BvSRT* genes are indicated in Fig. 3B. The intron-exon numbers ranged from 10 to 14. In *BvSRT2*, there are ten introns, and 11 exons, while *BvSRT1* and *BvSRT3* both have 13 introns and 14 exons. *BvSRT1* and *BvSRT3* exhibited similar exon/intron structures and identical numbers. Taken together, the intron-exon distribution was conserved in Class IV members.

3.5. Genomic synteny results

Circoletto results (Darzentas, 2010) used to investigate the evolutionary relationship between the SRTs of sugar beets and other plant species such as *Arabidopsis*, *Oryza sativa*, *Sorghum bicolor*, *Glycine max*, *Vitis vinifera*, *Capsicum annuum*, *Zea mays*, and *Solanum lycopersicum* were shown in Fig. 4. The red and orange colors exhibit the level of evolutionary conservation among *SIR2* proteins. The tool used “score/max” ratio colouring with orange ≤ 0.75 , and red > 0.75 . It has been found that *BvSRT1* showed synteny with *GmSRT4*, and the sequence similarity was greater than 75%. *BvSRT2* had syntenic relationships with *GmSRT1*, while the *BvSRT3* possessed synteny with *SRT6901* (*Vitis vinifera* SRT). The lowest similarity was demonstrated in *BvSRT3*-*SRT6901* pairs.

3.6. Cis-elements in promoter regions

To predict functional characteristics of *BvSRT* genes, *cis elements* in promoters were analyzed by searching the 1500 bp upstream region of the transcriptional activation site.

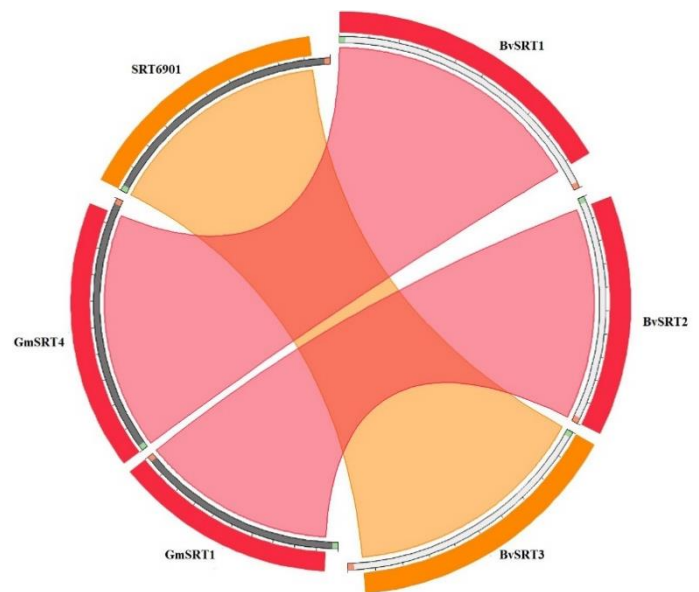


Fig. 4. Representation of genomic synteny in various plant species such as *B. vulgaris*, *A. thaliana*, *S. lycopersicum*, and *O. sativa* identifying the level of conservation at the amino acid sequence level in 2 colors. The red and orange colors exhibit the level and intensity of evolutionary conservation among *SIR2* proteins. The maximum intensity between proteins is shown in orange color.

PlantCARE results showed 36 types of *cis*-acting elements, which were classified into six different groups: common or unknown promoter elements (12), hormone response (7), light response (9), stress response (9), endosperm expression (1) and MYBHv1-binding (1) (Fig. 5A, 5B). There were 276 *cis*-acting elements in total: light (ATC-motif, Box 4, chs-CMA2a, GATA-motif, G-box, GT1-motif, I-box, MRE, TCT-motif), abscisic acid (ABRE, MYC, MYB), gibberellin/methyl jasmonate (MeJA) (GARE-motif, TGACG-motif, CGTCA-motif), salicy-

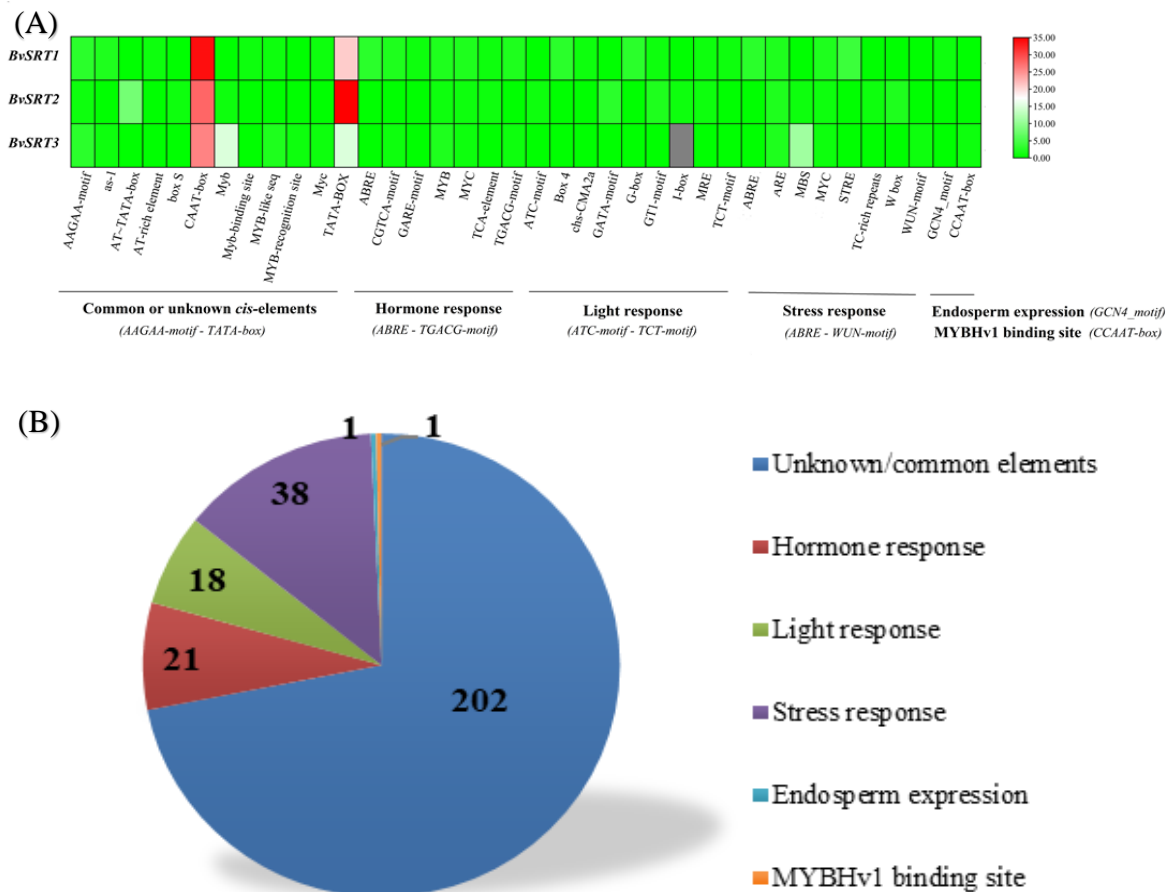


Fig. 5. (A) The heatmap demonstrates all *cis*-acting regulatory elements that are found in the promoter regions of *BvSRT1*, *BvSRT2*, and *BvSRT3* genes. (B) Total numbers and functions of *cis*-acting regulatory elements related to promoter regions, hormone response, light-responsiveness, stress-response, endosperm expression, and MYBHv1 binding, which were predicted by PlantCARE software.

lic acid (TCA-element), drought (ABRE, MYB, MYC, MBS) and stress (TC-rich repeats, STRE) response elements, common or unknown promoter elements (AAGAA-motif, as-1, AT~TATA box, AT-rich element, box S, CAAT-box, Myb, Myb-binding site, MYB-like seq, MYB-recognition site, Myc, TATA-box) (Fig. 5A, 5B). The largest group was common or unknown *cis*-elements with 202 members, and the second largest group was stress response-related elements. All *SIR2* genes in *B. vulgaris* contained three stress response-related elements including ARE, MYC, and MYB. MYC is involved in dehydration and ABA response. However, the abscisic acid response element (ABRE) and stress-response element (STRE) were both found only in the *BvSRT1* promoter. TC rich repeats and W box were both present only in the promoter of the *BvSRT2* gene. Two types of *cis*-elements involved in MeJA response (TGACG-motif, CGTCA-motif) existed in *BvSRT1* and *BvSRT3* genes. Wound responsive element, WUN-motif was assumed to be contained in the *BvSRT3*. Hormone-specific *cis*-elements such as GARE-motif (gibberellin), and TCA-element (salicylic acid) existed in the *BvSRT1* promoter. Light response-specific elements, ATC-motif, GATA-motif, and I-box in *BvSRT2* promoter were recorded. The *cis*-regulatory elements that are involved in the light response (Box-4, G-box, TCT-motif) were found in the promoter region of the *SRT1* in *B. vulgaris*. Furthermore, there was only one *cis* element (GCN4_motif) in *BvSRT1* involved in endosperm expression. MYBHv1 binding site, CCAAT-box was present only in the *BvSRT3* promoter.

3.7. Protein 3D structure

A protein bioinformatics tool, Phyre2 has been widely used to predict and analyze protein structures, functions, and mutations (Kelley et al., 2015). 3D models of *BvSRT1*, *BvSRT2*, *BvSRT3* proteins obtained from Phyre2 server were formed with >90% confidence at 54%, 73%, 52% coverage and 53%, 43%, 48% identity, respectively. The 3D protein structure models are shown in Fig. 6. Images are colored by rainbow N → C terminus. The identity and coverage were found 43%, and 75% for *BvSRT2*, respectively. Alpha-helix is the secondary structure element for *BvSRT1* (15%), *BvSRT2* (26%), and *BvSRT3* (14%). The β -strands are distributed by 22% (*BvSRT1*), 10% (*BvSRT2*), and 20% (*BvSRT3*). Templates

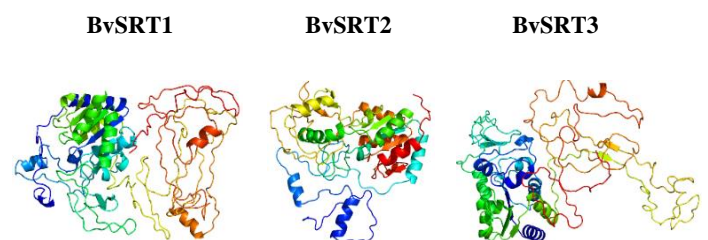


Fig. 6. Predicted 3D structures of *BvSRT1*, *BvSRT2*, and *BvSRT3* proteins. The protein models were built in the Phyre2 web portal by using amino acid sequences.

used to form 3D structural homology of BvSRT1, 2, 3 include NAD⁺-dependent protein deacetylase sirtuin 2 (c3zg6A, c3pkiF, c3k35D), DHS-like NAD/FAD binding domain (d1y5a1, d1j8fa, d2b4ya1), NAD⁺-dependent deacetylase sirtuin 3 (c3glsC), transcriptional regulatory protein sir2 homolog (c3jwpA), NAD-dependent protein deacetylase sirtuin 4 orthologue, etc.

4. Discussion

Gene activity is controlled by epigenetic mechanisms including DNA methylation, histone modifications and RNA interference (RNAi) in eukaryotic cells and these mechanisms are used by plants to survive under different environmental conditions (Yuan et al., 2013; Salgotra and Gupta, 2019). Histones are highly conserved globular proteins whose N-terminal tails are located at the surface of the nucleosome for post-translational modifications (PTMs) that regulate transcription through controlling the accessibility of the transcriptional machinery to certain genomic regions (Kouzarides, 2007). In eukaryotes, histone deacetylase enzymes (HDACs) remove the acetyl group from the tails of the core histones, and lead to transcriptional repression. Epigenetic regulation of biological processes such as development and stress response in sugar beet is unknown. Furthermore, there are few research articles regarding the roles of histone modifications or histone modifiers in sugar beet cultivars (Yolcu et al., 2016; Yu et al., 2023; Yolcu et al., 2024). Among histone modifier proteins, RPD3/HDA1-type HDACs and HATs have been recently identified and characterized in *B. vulgaris* (Yu et al., 2023; Yolcu et al., 2024). Other histone modifiers associated with histone methylation, and phosphorylation have not yet been identified and characterized in sugar beet. This work performed *in silico* analyses of *B. vulgaris* SIR2 genes by using bioinformatics tools or databases and examined their physiochemical properties, subcellular localization, phylogenetic relationships, gene structure, motif distribution, chromosomal distribution, genomic synteny, promoter *cis*-elements, and protein 3D structure models. Plants have fewer SIR2 family proteins than fungi and animals. Here, 3 SIR2 members were identified in *B. vulgaris*, and they were phylogenetically classified into two classes (Class II and IV). The number of sugar beet SIR2 subfamily is not similar to other plant species. For example, *Arabidopsis*, rice, tomato, maize, pepper, grape, *P. mume*, *Sorghum*, Tartary buckwheat and litchi include only two SIR2 proteins (Pandey et al., 2002; Huang et al., 2007; Aquea et al., 2010; Zhao et al., 2014; Peng et al., 2017; Zhang et al., 2020; Cai et al., 2022; Du et al., 2022; Meng et al., 2022; Yan et al., 2023), while the wheat, tea plant, and soybean contain a total of 6, 4 and 4 SIR2 proteins, respectively (Yang et al., 2018; Yuan et al., 2020; Shu et al., 2021). Like SIR2 proteins from *F. tataricum* (Yan et al., 2023), *S. bicolor* (Du et al., 2022), class IV proteins (BvSRT1 and BvSRT3) have more than 400 amino acids in length, respectively. All SIR2 family proteins in sugar beet contained a SIR2 domain, consistent with SIR2 proteins in distinct plant species, such as *Arabidopsis* (Pandey et al., 2002), *O. sativa* (Zhang et al., 2016), *S. lycopersicum* (Zhao et al., 2014), *Z. mays* (Zhang et al., 2020), *F. tataricum* (Yan et al., 2023), *V. vinifera* (Aquea et al., 2010), *L. chinensis* (Peng et al., 2017), *T. aestivum* (Shu et al., 2021), *C. annuum* (Cai et al., 2022) and *C. sinensis* (Yuan et al., 2020). This suggests that sugar beet SIR2-type HDACs may have similar functions to their homologous genes identified in other plant species. The

conserved motifs of the BvSRT proteins were similar, especially for BvSRT1 and BvSRT3, which may be due to the functional similarities. Additionally, SIR2 proteins in *B. vulgaris* showed amino acid similarities with *G. max* and *V. vinifera* SIR2 proteins. No SIR2 proteins from rice indicated synteny with beet proteins. Prediction of protein-3D structures is important to find out the biological functions of proteins. In the present work the homology modeling was used (Kelley et al., 2015), which depends on SIR2s from different organisms. Protein models presented above contained NAD⁺-dependent protein deacetylase sirtuin 2 and DHS-like NAD/FAD-binding domains.

This work predicted nuclear, cytoplasmic, and mitochondrial localizations of BvSRT proteins. Previous studies demonstrated that SIR2-type HDACs were localized in different subcellular compartments, such as the nucleus, cytoplasm, chloroplast, and mitochondria. For instance, AtSRT1 was localized in the cytoplasm/nucleus (Pandey et al., 2002), but the OsSRT1 and SiSRT1 were present in the nucleus (Huang et al., 2007; Zhao et al., 2014). WOLF PSORT prediction tool and experimental results both indicated the nuclear localization of SiSRT1, which may demonstrate the reliability of prediction tools. Consistently with *B. vulgaris* SRT2 protein, OsSRT2, and AtSRT2 were localized in the mitochondrion (König et al., 2014), but SiSRT2 was found in both the nucleus and cytoplasm (Zhao et al., 2014). Interestingly, SbSRT1, SbSRT2, CsSRT2, and CsSRT3 were assumed to be localized in the chloroplast, suggesting that they may have different functions in *Sorghum* and *C. sinensis* (Yuan et al., 2020; Du et al., 2022). In contrast, WOLF PSORT predicted peroxisomal localization of the BvSRT1 protein. RPD3/HDA1-type HDAC proteins in sugar beet showed nuclear and cytoplasmic localization, while the localization of BvHDAC4 near nuclei implied its location in the chloroplast or mitochondrion (Yu et al., 2023). Taken together, it is difficult to interpret SIR2 protein localizations in *B. vulgaris* without wet lab studies. Further experimental studies are needed to verify the results from the prediction data mentioned above.

Transcription profiles are mediated by *cis*-acting regulatory elements that play key roles in the expression of genes involved in environmental stress response, and plant development (Biłas et al., 2016; Marand et al., 2023). Recently identified RPD3/HDA1-type HDACs in *B. vulgaris* contained *cis*-elements related to light, stress, and hormones (Yu et al., 2023), consistent with PlantCARE data of the present study. Three SIR2 genes in *B. vulgaris* have 15 stress-responsive elements including ARE, MYB, and MYC. Furthermore, the most abundant stress-related *cis*-element was recorded for MBS in the BvSRT3 gene. Interestingly, even though the BvSRT1 and BvSRT3 belong to the same class, and have similar motifs and exon/intron structures, no MBS and WUN-motifs were found in the BvSRT1 promoter. Many abiotic stress-inducible genes have *cis*-regulatory elements such as ABRE (Narusaka et al., 2003), which was found only in the promoter of BvSRT1. Wheat TaSRT1D and TaSRT2U promoter regions were also found to have ABRE elements (Shu et al., 2021). In a recent study, ABA treatment remarkably inhibited the transcription of *O. sativa* SRT and *S. bicolor* SRT2 genes, suggesting that ABA could regulate the expression of HDAC genes (Fu et al., 2007; Du et al., 2022). MYB transcription factors along with MBS are required for transcription of drought-induced genes. Parallel with BvSRT results, MBS and WUN-motif also existed in the promoters of RPD3/HDA1-type HDACs in *B. vulgaris* (Yu et al., 2023). Similarly, MYB and MBS elements were present in promoter regions of the *S. bicolor* SRTs (Du et al., 2022). MeJA-

specific *cis*-elements, CGTCA, and TGACG motifs were found in sugar beet *SRT1* and *SRT3* genes. CGTCA-motif also induces defense mechanisms under environmental constraints such as salt, drought, and low temperature stresses (Kaur et al., 2017). Similarly, promoter regions of *P. mume SRT1* and *SRT2* genes contained hormone and stress response-related *cis*-elements (Meng et al., 2022). In *F. tataricum*, *FtSRT1* and *FtSRT2* genes also contained *cis*-elements correlated with light response and MeJA response. It has been reported that a SIR2 homolog in rice, OsSRT1 negatively regulates leaf senescence by inactivating the transcription of JA biosynthesis genes and *PECTIN METHYLESTERASE1 (OsPME1)*. ChIP assays revealed direct binding of OsSRT1 to the promoter of *OsPME1*, and *OsPME1* transcript levels were enhanced in the *SRT1* RNAi plants (Fang et al., 2016). Thus, the effects of hormone treatments on SIR2 proteins and their gene expression patterns should be investigated in *B. vulgaris*. Gene expression data showed the differential expression patterns of *FtSRT* and *V. vinifera SRT6901* genes in distinct tissues such as stems, leaves, roots, fruits, and flowers (Aquea et al., 2010; Yan et al., 2023). *SRT6902* in *V. vinifera* was expressed in an organ-specific manner. Transcript levels of *P. mume SRT2* were higher in flowering buds than in leaves and stems, whereas *PmSRT1* was remarkably expressed in stems (Meng et al., 2022). *RPD3/HDA1-type HDAC* genes were expressed in response to salt, drought and low-temperature stresses (Yu et al., 2023). In *Sorghum* plants, elevated histone acetylation levels were recorded under cold, heat, osmotic, and salt stresses (Du et al., 2022). Moreover, transcript levels of *FtSRT1* and *FtSRT2* genes fluctuated under different light wavelengths, suggesting their involvement in the light response (Yan et al., 2023). In the present study, 9 types of light response-related *cis*-elements were assumed to be present in the *BvSRT1* and *BvSRT2* promoter regions. There were no light response-specific *cis*-elements found in the *BvSRT3* promoter. At least eight types of light-responsive *cis*-elements were determined in each *RPD3/HDA1* gene of sugar beet (Yu et al., 2023). However, the effect of different light conditions on the transcriptional activity of *SRT* genes is unknown in sugar beet. In addition to hormone-, light- and stress-correlated *cis*-elements, the core promoter elements such as TATA box (71), and CAAT box (88) were included in the *BvSIR2* genes that regulate the appropriate initiation of the transcription process by RNA polymerase II (Biłas et al., 2016). A higher number of stress-related *cis*-regulatory elements may correlate with the stress-induced upregulation of *BvSRT* genes. Taken together, monocotyledonous and dicotyledonous plant species both share similar *cis elements*. However, up to date, no

experimental findings have been reported on how and whether the *SIR2* genes of *B. vulgaris* respond to environmental stresses, hormone treatments, and light conditions. Thus, wet-lab studies along with *in silico* analysis should be performed to further characterize the functions of *BvSIR2* genes.

Overall, the findings presented above provide insight into the potential roles of sugar beet *SIR2-type HDAC* genes. *In-silico* analyses could help plant biologists select genes encoding histone deacetylation proteins for further functional characterization.

5. Conclusion

The SILENT INFORMATION REGULATOR2 (SIR2) proteins are NAD⁺-dependent protein deacetylases, found in different organisms such as bacteria, mammals, fungi, and plants. They participate in development, stress response, and energy metabolism in plants. In the present study, an *in silico* analysis of SIR2 family members was done in sugar beet. Three SIR2 family HDAC-encoding genes (*BvSRT1*, *BvSRT2*, and *BvSRT3*) were identified from the sugar beet genome, and they were located on chromosomes 4 and 9. The phylogenetic analysis exhibited that 3 sugar beet SRTs were divided into two classes: Class II (*BvSRT2*) and IV (*BvSRT1* and *BvSRT3*). SIR2 family proteins were confirmed to have an SIR2 domain (PF02146) using by SMART and NCBI CDD databases. Through the MEME tool, the conserved motifs were found to range from 6 to 50 amino acids in length, while the GSDS showed that the intron-exon numbers ranged from 10 to 14. The *BvSRT1* and *BvSRT3* proteins were assumed to be localized in both the nucleus and cytoplasm, while the *BvSRT2* protein was located in the mitochondrion. Promoter analysis showed the potential involvement of *BvSRT* genes in hormone regulation, light response, abiotic stress response, and meristem expression. This study might provide preliminary information for further research on SIR2-type histone deacetylases in sugar beet. However, experimental findings are needed to confirm the data obtained from bioinformatics tools/databases and examine the transcript abundance of SIR2-encoding genes under different stresses, light conditions, and hormone treatments.

Conflict of interest: The author declares that she has no conflict of interests.

Informed consent: The author declares that this manuscript did not involve human or animal participants and informed consent was not collected.

References

- Aquea, F., Timmermann, T., & Arce-Johnson, P. (2010). Analysis of histone acetyltransferase and deacetylase families of *Vitis vinifera*. *Plant Physiology and Biochemistry*, 48, 194-199.
- Bailey, T. L., & Elkan, C. (1994). Fitting a mixture model by expectation maximization to discover motifs in biopolymers. *Second International Conference on Intelligent Systems for Molecular Biology*, California, USA. 28-36.
- Biłas, R., Szafran, K., Hnatuszko-Konka, K., & Kononowicz, A. K. (2016). Cis-regulatory elements used to control gene expression in plants. *Plant Cell, Tissue and Organ Culture (PCTOC)*, 127, 269-287.
- Bolser, D. M., Staines, D. M., Perry, E., & Kersey, P. J. (2017). Ensembl plants: integrating tools for visualizing, mining, and analyzing plant genomic data. *Methods in Molecular Biology*, 1-31.
- Bruscalupi, G., Di Micco, P., Failla, C. M., Pascarella, G., Morea, V., Saliola, M., ... & Mauro, M. L. (2023). *Arabidopsis thaliana* sirtuins control proliferation and glutamate dehydrogenase activity. *Plant Physiology and Biochemistry*, 194, 236-245.
- Busconi, M., Reggi, S., Fogher, C., & Bavaresco, L. (2009). Evidence of a sirtuin gene family in grapevine (*Vitis vinifera* L.). *Plant Physiology and Biochemistry*, 47, 650-652.
- Cai, Y., Xu, M., Liu, J., Zeng, H., Song, J., Sun, B., ... & Zhu, Z. (2022). Genome-wide analysis of histone acetyltransferase and histone deacetylase families and their expression in fruit development and ripening stage of pepper (*Capsicum annuum*). *Frontiers in Plant Science*, 13, 971230.
- Carafa, V., Rotili, D., Forgione, M., Cuomo, F., Serretiello, E., Hailu, G. S., ... & Altucci, L. (2016). Sirtuin functions and modulation: from chemistry to the clinic. *Clinical Epigenetics*, 8, 1-21.
- Chao, J., Li, Z., Sun, Y., Aluko, O. O., Wu, X., Wang, Q., & Liu, G. (2021). MG2C: A user-friendly online tool for drawing genetic maps.

- Molecular Horticulture*, 1, 1-4.
- Chen, B., Zang, W., Wang, J., Huang, Y., He, Y., Yan, L., ... & Zheng, W. (2015). The chemical biology of sirtuins. *Chemical Society Reviews*, 44(15), 5246-5264.
- Chen, C., Chen, H., Zhang, Y., Thomas, H. R., Frank, M. H., He, Y., & Xia, R. (2020). TBtools: an integrative toolkit developed for interactive analyses of big biological data. *Molecular Plant*, 13(8), 1194-1202.
- Chunzheng, W., Feng, G., Jianguo, W., Jianli, D., Chunhong, W., & Yi, L. (2010). Arabidopsis putative deacetylase AtSRT2 regulates basal defense by suppressing PAD4, EDS5 and SID2 expression. *Plant and Cell Physiology*, 51, 1291-1299.
- Darzentas, N. (2010). Circoletto: visualizing sequence similarity with Circos. *Bioinformatics*, 26, 2620-2621.
- Dohm, J. C., Minoche, A. E., Holtgräwe, D., Capella-Gutiérrez, S., Zakrzewski, F., Tafer, H., ... & Himmelbauer, H. (2014). The genome of the recently domesticated crop plant sugar beet (*Beta vulgaris*). *Nature*, 505(7484), 546-549.
- Du, J., Zhou, Y., Su, X., Yu, J. J., Khan, S., Jiang, H., ... & Lin, H. (2011). Sirt5 is a NAD-dependent protein lysine demalonylase and desuccinylase. *Science*, 334(6057), 806-809.
- Du, Q., Fang, Y., Jiang, J., Chen, M., Fu, X., Yang, Z., ... & Xie, X. (2022). Characterization of histone deacetylases and their roles in response to abiotic and PAMPs stresses in *Sorghum bicolor*. *BMC genomics*, 23(1), 28.
- Ensembl, (2017). Ensembl Plants, <https://plants.ensembl.org/>. Last accessed on December 25, 2023.
- Fang, C., Zhang, H., Wan, J., Wu, Y., Li, K., Jin, C., ... & Luo, J. (2016). Control of leaf senescence by an MeOH-jasmonates cascade that is epigenetically regulated by OsSRT1 in rice. *Molecular Plant*, 9(10), 1366-1378.
- Fotouhi, K., Heravan, E. S., Rajabi, A., & Azizinejad, R. (2017). Screening sugar beet genotypes in drought stress condition using tolerance indices. *Agri Forest*, 63, 105-109.
- Fu, W., Wu, K., & Duan, J. (2007). Sequence and expression analysis of histone deacetylases in rice. *Biochemical and Biophysical Research Communications*, 356(4), 843-850.
- Gasteiger, E., Hoogland, C., Gattiker, A., Duvaud, S. E., Wilkins, M. R., Appel, R. D., & Bairoch, A. (2005). *Protein Identification and Analysis Tools on the ExPASy Server* (pp. 571-607). Humana Press.
- Goodstein, D. M., Shu, S., Howson, R., Neupane, R., Hayes, R. D., Fazo, J., ... & Rokhsar, D. S. (2012). Phytozome: a comparative platform for green plant genomics. *Nucleic Acids Research*, 40(D1), D1178-D1186.
- Greiss, S., & Gartner, A. (2009). Sirtuin/Sir2 phylogeny, evolutionary considerations and structural conservation. *Molecules and Cells* 28, 407-415.
- Hoffmann, C. M. (2010). Sucrose accumulation in sugar beet under drought stress. *Journal of Agronomy and Crop Science*, 196(4), 243-252.
- Houtkooper, R. H., Pirinen, E., & Auwerx, J. (2012). Sirtuins as regulators of metabolism and healthspan. *Nature reviews Molecular cell biology*, 13(4), 225-238.
- Hu, B., Jin, J., Guo, A. Y., Zhang, H., Luo, J., & Gao, G. (2015). GSDB 2.0: an upgraded gene feature visualization server. *Bioinformatics*, 31(8), 1296-1297.
- Huang, L., Sun, Q., Qin, F., Li, C., Zhao, Y., & Zhou, D. X. (2007). Down-regulation of a SILENT INFORMATION REGULATOR2-related histone deacetylase gene, OsSRT1, induces DNA fragmentation and cell death in rice. *Plant Physiology*, 144, 1508-1519.
- Imai, S., Armstrong, C. M., Kaerberlein, M., & Guarente, L. (2000). Transcriptional silencing and longevity protein Sir2 is an NAD-dependent histone deacetylase. *Nature* 403, 795-800.
- Jeong, S. M., Xiao, C., Finley, L. W., Lahusen, T., Souza, A. L., Pierce, K., ... & Haigis, M. C. (2013). SIRT4 has tumor-suppressive activity and regulates the cellular metabolic response to DNA damage by inhibiting mitochondrial glutamine metabolism. *Cancer Cell*, 23(4), 450-463.
- Jiangtao, C., Yingzhen, K., Qian, W., Yuhe, S., Daping, G., Jing, L., & Guanshan, L. (2015). Mappgene2chrom, a tool to draw gene physical map based on perl and svg languages. *Yi Chuan*, 37, 91-97.
- Kaur, A., Pati, P. K., Pati, A. M., & Nagpal, A. K. (2017). In-silico analysis of cis-acting regulatory elements of pathogenesis-related proteins of *Arabidopsis thaliana* and *Oryza sativa*. *PLoS One*, 12(9), e0184523.
- Kelley, L. A., Mezulis, S., Yates, C. M., Wass, M. N., & Sternberg, M. J. (2015). The Phyre2 web portal for protein modeling, prediction and analysis. *Nature Protocols*, 10(6), 845-858.
- König, A. C., Hartl, M., Pham, P. A., Laxa, M., Boersema, P. J., Orwat, A., ... & Finkemeier, I. (2014). The *Arabidopsis* class II sirtuin is a lysine deacetylase and interacts with mitochondrial energy metabolism. *Plant Physiology*, 164(3), 1401-1414.
- Kouzarides, T. (2007). Chromatin modifications and their function. *Cell* 128, 693-705.
- Krzywinski, M., Schein, J., Birol, I., Connors, J., Gascoyne, R., Horsman, D., ... & Marra, M. A. (2009). Circos: an information aesthetic for comparative genomics. *Genome Research*, 19(9), 1639-1645.
- Lescot, M., Déhais, P., Thijs, G., Marchal, K., Moreau, Y., Van de Peer, Y., ... & Rombauts, S. (2002). PlantCARE, a database of plant cis-acting regulatory elements and a portal to tools for in silico analysis of promoter sequences. *Nucleic Acids Research*, 30(1), 325-327.
- Letunic, I., and Bork, P. (2020). SMART, <http://smart.emblheidelberg.de/>. Last accessed on December 25, 2023.
- Letunic, I., Doerks, T., & Bork, P. (2012). SMART 7: recent updates to the protein domain annotation resource. *Nucleic Acids Research*, 40, 302-305.
- Marand, A. P., Eveland, A. L., Kaufmann, K., & Springer, N. M. (2023). cis-Regulatory elements in plant development, adaptation, and evolution. *Annual Review of Plant Biology*, 74, 111-137.
- Martinez-Redondo, P., & Vaquero, A. (2013). The diversity of histone versus nonhistone sirtuin substrates. *Genes & Cancer*, 4(3-4), 148-163.
- Meng, J., Wen, Z., Li, M., Cheng, T., Zhang, Q., & Sun, L. (2022). HDACs gene family analysis of eight Rosaceae genomes reveals the genomic marker of cold stress in *Prunus mume*. *International Journal of Molecular Sciences*, 23(11), 5957.
- Nakai, K., & Horton, P. (1999). PSORT: a program for detecting sorting signals in proteins and predicting their subcellular localization. *Trends in Biochemical Sciences*, 24(1), 34-35.
- Narusaka, Y., Nakashima, K., Shinwari, Z. K., Sakuma, Y., Furihata, T., Abe, H., ... & Yamaguchi-Shinozaki, K. (2003). Interaction between two cis-acting elements, ABRE and DRE, in ABA-dependent expression of Arabidopsis rd29A gene in response to dehydration and high-salinity stresses. *The Plant Journal*, 34(2), 137-148.
- Pandey, R., Muëller, A., Napoli, C. A., Selinger, D. A., Pikaard, C. S., Richards, E. J., ... & Jorgensen, R. A. (2002). Analysis of histone acetyltransferase and histone deacetylase families of *Arabidopsis thaliana* suggests functional diversification of chromatin modification among multicellular eukaryotes. *Nucleic Acids Research*, 30(23), 5036-5055.
- Peng, M., Ying, P., Liu, X., Li, C., Xia, R., Li, J., & Zhao, M. (2017). Genome-wide identification of histone modifiers and their expression patterns during fruit abscission in litchi. *Frontiers in Plant Science*, 8, 639.
- Perrella, G., Fasano, C., Donald, N. A., Daddiego, L., Fang, W., Martignago, D., Carr, C., Conti, L., Herzyk, P., & Amtmann, A. (2024). Histone Deacetylase Complex 1 and histone 1 epigenetically moderate stress responsiveness of *Arabidopsis thaliana* seedlings. *New Phytologist*, 241, 166-179.
- Reiser, L., Bakker, E., Subramaniam, S., Chen, X., Sawant, S., Khosa, K., ... & Berardini, T. Z. (2024). The *Arabidopsis* information resource in 2024. *Genetics*, iyae027.
- Salgotra, R. K., & Gupta, M. (2019). Exploring the role of epigenetics in cereal and leguminous crops exposed to abiotic stress. In: Alvarez-Venegas R., De-la-Peña C., Casas-Mollano J. (eds) *Epigenetics in Plants of Agronomic Importance: Fundamentals and Applications: Transcriptional Regulation and Chromatin Remodelling in Plants* (pp. 149-170). Springer, Cham.
- Shu, B., Xie, Y., Zhang, F., Zhang, D., Liu, C., Wu, Q., & Luo, C. (2021). Genome-wide identification of citrus histone acetyltransferase and deacetylase families and their expression in response to arbuscular mycorrhizal fungi and drought. *Journal of Plant Interactions*, 16, 367-376.
- Skorupa, M., Szczepanek, J., Mazur, J., Domagalski, K., Tretyn, A., & Tyburski, J. (2021). Salt stress and salt shock differently affect DNA methylation in salt-responsive genes in sugar beet and its wild, halophytic ancestor. *PLoS One*, 16, e0251675.
- Song, H., Ding, G., Zhao, C., & Li, Y. (2023). Genome-wide identification of b-box gene family and expression analysis suggest its roles in responses to cercospora leaf spot in sugar beet (*Beta Vulgaris* L.). *Genes*, 14(6), 1248.
- Tamura, K., Stecher, G., & Kumar, S. (2021). MEGA11: Molecular evo-








- lutionary genetics analysis version 11. *Molecular Biology and Evolution*, 38, 3022-3027.
- Wang, J., Chitsaz, F., Derbyshire, M. K., Gonzales, N. R., Gwadz, M., Lu, S., Marchler, G. H., ... & Marchler-Bauer, A. (2022). Conserved Domain Database, <https://www.ncbi.nlm.nih.gov/cdd/>, Last accessed on December 25, 2023.
- Wang, W., Sun, Y. Q., Li, G. L., & Zhang, S. Y. (2019). Genome-wide identification, characterization, and expression patterns of the BZR transcription factor family in sugar beet (*Beta vulgaris* L.). *BMC Plant Biology*, 19, 1-12.
- Wedeking, R., Mahlein, A. K., Steiner, U., Oerke, E. C., Goldbach, H. E., & Wimmer, M. A. (2016). Osmotic adjustment of young sugar beets (*Beta vulgaris*) under progressive drought stress and subsequent rewatering assessed by metabolite analysis and infrared thermography. *Functional Plant Biology*, 44, 119-133.
- Yan, H., Chen, H., Liao, Q., Xia, M., Yao, T., Peng, L., Zou, L., Zhao, G., Zhao, J., & Wu, D. T. (2023). Genome-wide identification of histone deacetylases and their roles related with light response in tartary buckwheat (*Fagopyrum tataricum*). *International Journal of Molecular Sciences*, 24, 8090.
- Yang, C., Shen, W., Chen, H., Chu, L., Xu, Y., Zhou, X., ... & Luo, M. (2018). Characterization and subcellular localization of histone deacetylases and their roles in response to abiotic stresses in soybean. *BMC Plant Biology*, 18, 1-13.
- Yang, X., Wu, G., Wei, M., & Wang, B. (2022). Genome-wide identification of BvHAK gene family in sugar beet (*Beta vulgaris*) and their expression analysis under salt treatments. *Sheng Wu Gong Cheng Xue Bao*, 38, 3773-3789.
- Yolcu, S., Alavilli, H., Ganesh, P., Asif, M., Kumar, M., and Song, K. (2022). An insight into the abiotic stress responses of cultivated beets (*Beta vulgaris* L.). *Plants*, 11, 12.
- Yolcu, S., Ozdemir, F., Guler, A., & Bor, M. (2016). Histone acetylation influences the transcriptional activation of POX in *Beta vulgaris* L. and *Beta maritima* L. under salt stress. *Plant Physiology and Biochemistry*, 100, 37-46.
- Yolcu, S., Skorupa, M., Uras, M. E., Mazur, J., & Ozyigit, I. I. (2024). Genome-wide identification, phylogenetic classification of histone acetyltransferase genes, and their expression analysis in sugar beet (*Beta vulgaris* L.) under salt stress. *Planta*, 259(4), 85.
- Yu, B., Chen, M., Grin, I., & Ma, C. (2020). Mechanisms of sugar beet response to biotic and abiotic stresses. *Advances in Experimental Medicine and Biology*, 1241, 167-194.
- Yu, C. S., Chen, Y. C., Lu, C. H., & Hwang, J. K. (2006). Prediction of protein subcellular localization. *Proteins*, 64, 643-651.
- Yu, Q., Guo, Q., Li, B., Tan, X., Wang, L., Li, S., & Pi, Z. (2023). Identification of RPD3/HDA1 family genes in sugar beet and response to abiotic stresses. *Sugar Technology*, 25(4), 834-845.
- Yuan, L., Dai, H., Zheng, S., Huang, R., & Tong, H. (2020). Genome-wide identification of the HDAC family proteins and functional characterization of CsHD2C, a HD2-type histone deacetylase gene in tea plant (*Camellia sinensis* L. O. Kuntze). *Plant Physiology and Biochemistry*, 155, 898-913.
- Yuan, L., Liu, X., Luo, M., Yang, S., & Wu, K. (2013). Involvement of histone modifications in plant abiotic stress responses. *Journal of Integrative Plant Biology*, 55(10), 892-901.
- Zhang, H., Lu, Y., Zhao, Y., & Zhou, D. X. (2016). OsSRT1 is involved in rice seed development through regulation of starch metabolism gene expression. *Plant Science*, 248, 28-36.
- Zhang, H., Zhao, Y., & Zhou, D. X. (2017). Rice NAD⁺-dependent histone deacetylase OsSRT1 represses glycolysis and regulates the moonlighting function of GAPDH as a transcriptional activator of glycolytic genes. *Nucleic Acids Research*, 45, 12241-12255.
- Zhang, K., Yu, L., Pang, X., Cao, H., Si, H., Zang, J., Xing, J., & Dong, J. (2020). In silico analysis of maize HDACs with an emphasis on their response to biotic and abiotic stresses. *PeerJ*, 8, e8539.
- Zhang, P., Liu, L., Wang, X., Wang, Z., Zhang, H., Chen, J., ... & Li, C. (2021). Beneficial effects of exogenous melatonin on overcoming salt stress in sugar beets (*Beta vulgaris* L.). *Plants*, 10(5), 886.
- Zhao, L., Lu, J., Zhang, J., Wu, P. Y., Yang, S., & Wu, K. (2014). Identification and characterization of histone deacetylases in tomato (*Solanum lycopersicum*). *Frontiers in Plant Science*, 5, 760.
- Zhao, S., Zhang, X., & Li, H. (2018). Beyond histone acetylation-writing and erasing histone acylations. *Current Opinion in Structural Biology*, 53, 169-177.
- Zheng, W. (2020). Review: The plant sirtuins. *Plant Science*, 293, 110434.
- Ziętara, P., Dziewięcka, M., & Augustyniak, M. (2023). Why is longevity still a scientific mystery? Sirtuins-past, present and future. *International Journal of Molecular Sciences*, 24, 728.

Cite as: Yolcu, S. (2024). *In silico* analysis of sirtuin-type histone deacetylase genes in sugar beet (*Beta vulgaris* L.). *Front Life Sci RT*, 5(1), 38-47.



Research article

The effect of epetraborole on the transcriptome and proteome profiles of an *Escherichia coli* strain overexpressing *leuS*, Leucyl-tRNA Synthetase

Anara Babayeva¹ , Esra Dibek^{2,3} , Deniz Sunnetci Akkoyunlu⁴ , Naci Cine⁴ , Murat Kasap⁵ , Gurler Akpınar⁵ , Bekir Col^{*3,6} 

¹ Mugla Sitki Kocman University, Institute of Natural Sciences, Department of Biology, 48000, Mugla, Türkiye

² Mugla Sitki Kocman University, Koycegiz Vocational School of Health Services, Pharmacy Services Division, 48000, Mugla, Türkiye

³ Mugla Sitki Kocman University, Biotechnology Research Center, 48000, Mugla, Türkiye

⁴ Kocaeli University, Kocaeli Health Services Vocational School, Medical Services and Techniques, 41380, Kocaeli, Türkiye

⁵ Kocaeli University, Faculty of Medicine, Basic Medical Sciences, 41380, Kocaeli, Türkiye

⁶ Mugla Sitki Kocman University, Faculty of Science, Department of Biology, 48000, Mugla, Türkiye

Abstract

Epetraborole (EP) is a boron-containing antibiotic known for its effectiveness against gram-negative enteric bacteria and *Mycobacterium* species. It is designed to bind and inhibit the LeuS enzyme (Leucyl-tRNA Synthetase), which is encoded by the essential gene *leuS* in *Escherichia coli*. EP inhibits protein translation, impeding bacterial growth. However, when *leuS* is overexpressed in a recombinant plasmid, the amount of EP required for growth inhibition needs to be increased. This study explored the impact of EP on the transcriptome and proteome of *E. coli* overexpressing *leuS*, aiming to reveal additional gene and pathway insights beyond LeuS, shedding light on the biochemical players orchestrating the bacterium's molecular response. 2D-PAGE Proteomics analysis identified four differentially regulated proteins influenced by EP in the *leuS* overexpression strain. Notably, LeuA and DeoA emerged as identified proteins. EP may affect LeuA in the cells overexpressing LeuS, which could result in truncated LeuA protein variants. Transcriptomics analyses, based on microarray data, revealed 23 up-regulated and 9 down-regulated genes responding to EP in the overexpression strain ($p < 0.05$, fold change; FC > 2). Based on the statistical analyses, the first five up- and down-regulated genes showing the highest fold differences in their mRNA levels are *yiaW*, *mglB*, *narH*, *ybiO*, *flgB* and *yhdY*, *deoR*, *recX*, *yobB*, *potF*, respectively. Analyses using the Omics Dashboard pathway and String indicate that the EP effect on the *leuS* overexpressing strain mainly induces alterations in the expression of genes related to the cell exterior, regulation, and response to stimuli. It is suggested that EP and higher levels of LeuS may interfere with the translational and transcriptional regulation of the expression of the *leuA* gene, which encodes the first enzyme, 2-isopropylmalate synthase, in L-leucine biosynthesis. This study offers new insights into the effects of EP on the bacterium, specifically when the level of the aminoacyl-tRNA synthetase LeuS is increased.

Keywords: Epetraborole; *Escherichia coli*; *LeuS*; Leucyl-tRNA Synthetase; proteomics; transcriptomics

1. Introduction

The global antibiotic crisis is a growing concern due to the

rapid development of resistance by pathogenic bacteria to existing antibiotics, which has surpassed the discovery and introduction of new antibiotics to the market. Therefore, it is

* Corresponding author.

E-mail address: bcol@mu.edu.tr (B. Col).

<https://doi.org/10.51753/flsrt.1416938> Author contributions

Received 09 January 2024; Accepted 01 March 2024

Available online 30 April 2024

2718-062X © 2024 This is an open access article published by Dergipark under the [CC BY](https://creativecommons.org/licenses/by/4.0/) license.

crucial to prioritize scientific research that not only identifies novel antibiotics but also comprehensively understands their impact on microorganisms. Recent investigations have revealed boron-containing metabolites with antibiotic properties in specific microorganisms (Monteferrante et al., 2016; Dibek et al., 2020). Examples of such antibiotics include boromycin (Kohno et al., 1996; Arai et al., 2004), aplasmomycin (Nakamura et al., 1977), and tartrolone (Irschik et al., 1995). Additionally, epetraborole (AN3365), a boron-containing molecule, has been synthesized and tested as an antibiotic by the ANACOR company in the United States. Epetraborole (EP) inhibits the leucyl-tRNA synthetase enzyme in the cell (Monteferrante et al., 2016). However, its effects on other molecules and systems within the cell are not yet fully understood.

EP binds specifically to the editing active site of leucyl-tRNA synthetase. The boron atom in the antibiotic binds to the *cis*-diol group of the ribose in the terminal nucleotide of tRNA^{Leu}, preventing the addition of leucine, disrupting the synthesis of the polypeptide chain, and inhibiting the survival of microbial cells (Monteferrante et al., 2016). EP has been reported to have bactericidal and bacteriostatic effects on various bacteria, including *Pseudomonas aeruginosa*, *Escherichia coli*, *Streptococcus pneumoniae*, and *Bacteroides fragilis*. Studies have shown that EP is effective against *E. coli* and *P. aeruginosa* in rat hip infection models (Hernandez et al., 2013).

The studies evaluated the effectiveness of EP (AN3365, GSK2251052, GSK052), a boron-containing protein synthesis inhibitor, against clinical isolates of Enterobacteriaceae and some gram-negative bacilli. Minimum Inhibitory Concentration (MIC) values were determined for selected clinical isolates. The antibiotic was found to be effective against some antibiotic-resistant isolates. AN3365 (EP) inhibited both wild-type and carbapenem-resistant strains of *Pseudomonas aeruginosa* (MIC 50/90, 2/8 µg/ml), as well as *Klebsiella pneumoniae* (MIC50/90, 1/2 µg/ml), *Acinetobacter baumannii* (MIC50/90, 2/8 µg/ml), and *Stenotrophomonas maltophilia* (MIC50/90, 2/4 µg/ml). However, the efficacy of this antibiotic was relatively lower against multidrug-resistant *Acinetobacter baumannii* (MIC50/90, 8/16 µg/ml) and *Burkholderia cepacia* (MIC50/90, 8/32 µg/ml) (Mendes et al., 2013). Furthermore, it has been demonstrated that this antibiotic inhibits Chlamydial growth and induces transcriptional changes (Hatch and Ouellette, 2020).

EP was found to be effective against *Mycobacterium abscessus* in both *in vitro* conditions and a mouse infection model (Ganapathy et al., 2021; Nguyen et al., 2023). EP has also been reported as a novel and effective candidate for *M. abscessus* treatment through *in vitro* screening against rough (R) and smooth (S) variants of *M. abscessus* (Kim et al., 2021). The effectiveness of EP antibiotic against the clinically relevant cystic fibrosis pathogen *M. abscessus* has been demonstrated. Co-treatment with EP and norvaline has been demonstrated to be effective in treating other Mycobacterial infections, including *M. abscessus* and *M. tuberculosis* (Sullivan et al., 2021).

A study was conducted to test the effect of epetraborole on *M. avium* complex (MAC) (Shafiee and Chanda, 2024). The results indicate that the EP antibiotic can be co-administered with some of the current standard care (SoC) antibiotics at clinically relevant concentrations, with a reduced likelihood of side effects from drug-drug interactions (DDI). Phase 2/3 clinical trials are currently underway to evaluate the safety and efficacy of EP in patients with MAC lung disease. Clinical trials

are planned to assess the safety of EP in patients with melioidosis (Shafiee and Chanda, 2024).

Cummings et al. (2023) conducted a study to evaluate the *in vitro* activity and efficacy of epetraborole against *Burkholderia pseudomallei* infections in a mouse model. The results suggest that EP has potential as a treatment for melioidosis. Furthermore, the study identified leucyl-tRNA synthetase as a clinically relevant drug target in *B. pseudomallei*. A recent study by Sivasankar et al. (2023) reported that the EP antibiotic is highly effective against pan-drug resistant *Klebsiella pneumoniae* with low MIC values of 10 µM. These findings emphasize the growing significance of the EP antibiotic in recent years.

Further research is necessary to investigate the impact of EP on bacterial cells. EP is an antibiotic that targets the LeuS enzyme, and one of the mechanisms of antibiotic resistance is target overexpression. In this study, the *E. coli* strain AG1(pCA24N::leuS), in which *leuS* is overexpressed by IPTG, was exposed to sub-lethal concentrations of EP. Transcriptome and proteome analyses were conducted to investigate changes in mRNA and protein levels in the bacterial cell. The article presents and discusses the effects of EP on a strain that overexpresses the target gene by providing information on genes that are differently regulated.

2. Materials and methods

2.1. Bacterial strain and culture conditions

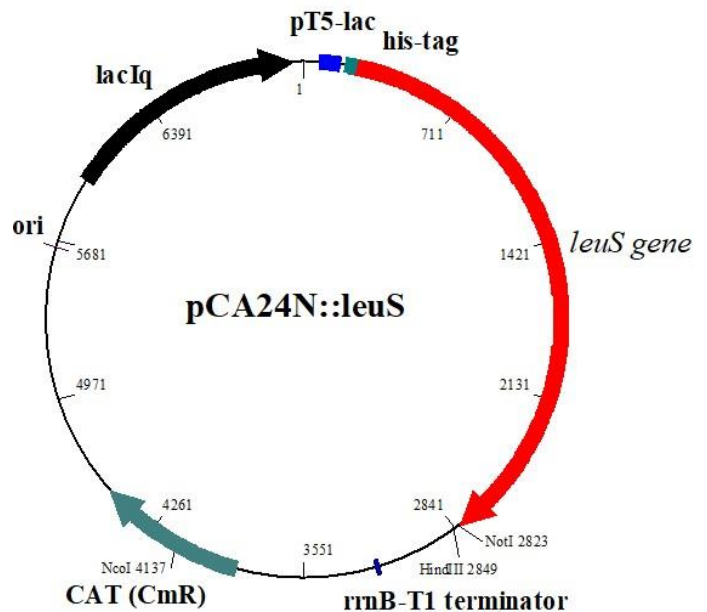


Fig. 1. Map of the plasmid pCA24N::leuS. The recombinant plasmid pCA24N::leuS is present in the strain that overexpresses the *leuS* gene. The gene was cloned into the MCS region and has a his-tag at the N terminus. Transcription is controlled by the T5 promoter, and the *lac* operator was cloned nearby the promoter region. The gene expression is negatively controlled by the Lac repressor, encoded by the *lacIq*, which is also present in the plasmid. IPTG removes the repressor from the operator region, allowing for the expression of the *leuS* gene. Transcription is terminated by the T1 terminator cloned downstream of the *leuS* gene. The plasmid contains a chloramphenicol resistance gene (CAT) and an ori region for replication in *E. coli* (Kitagawa et al., 2005).

The *Escherichia coli* AG1 strain containing the pCA24N::leuS plasmid was utilized. Fig. 1 displays the map of

the plasmid. The experiments were conducted in duplicate. For proteomic analysis, bacterial cells were cultured in 200 ml of Luria Bertani (LB) (Sigma, USA) medium supplemented with chloramphenicol (cm) (Sigma, USA). Growth curve experiments were conducted to determine the optimal concentration and exposure time for the antibiotic. The culture was initiated at an OD₆₀₀ of 0.05 and grown until reaching the logarithmic phase (OD₆₀₀ 0.5). Then, the cells were exposed to the culture medium both with and without the EP antibiotic, at a concentration of 0.25 µg/ml, for a duration of 1 hour. For the microarray experiments, bacterial cells were grown in 7 ml of LB-cm medium, starting from an OD₆₀₀ of 0.05, and cultured until reaching the logarithmic phase (OD₆₀₀ 0.5). The cells were incubated in the culture medium without EP and the culture medium containing 0.25 µg/ml of the EP antibiotic for 15 minutes. Total RNA isolation was then performed from the cells.

2.2. Protein extraction and TCA precipitation

The cells from the bacterial culture were centrifuged at 10,000 rpm for 10 minutes in a refrigerated centrifuge at +4°C. The supernatant was then discarded, and the resulting cell pellets were washed twice with cold Phosphate-Buffered Saline (PBS) (Sigma, USA). Afterward, the cell pellets were centrifuged again at +4°C to remove any remaining culture media, resulting in cell pellets. To disrupt the cells, 2D Rehydration buffer (8M Urea, 2M Thiourea, 2% CHAPS, 50 mM DTT, 0.2% Ampholytes, 0.002% Bromophenol blue) (Sigma, USA) was used. Additionally, the samples were sonicated for five repetitions with a 20-second cycle and then centrifuged at 10,000 rpm for 10 minutes at +4°C. The protein extracts were treated with a solution of 10% trichloroacetic acid (TCA) and 20 mM dithiothreitol (DTT), using at least three times the volume to eliminate salts and other unwanted components. After treatment, the samples were kept at -20°C overnight and then centrifuged at 15,200 rpm in a refrigerated centrifuge at +4°C for 20 minutes. The supernatants were carefully separated from the pellet, which was washed twice with 500 µl of cold acetone. After centrifugation at 15,200 rpm in a refrigerated centrifuge at +4°C for 10 minutes, 200 µl of 2D rehydration buffer was added to the pellet, and the mixture was vortexed at room temperature until fully dissolved. After centrifugation at 15,200 rpm in a refrigerated centrifuge at +4°C for 10 minutes, 200 µl of 2D rehydration buffer was added to the pellet, and the mixture was vortexed at room temperature until fully dissolved. The supernatants were then transferred to sterile Eppendorf tubes. Protein concentrations were measured using the Bradford method (Bradford, 1976).

2.2.1. SDS-PAGE

Protein separation was performed using sodium dodecyl sulfate-polyacrylamide gel electrophoresis (SDS-PAGE). A 12% SDS-PAGE separating gel and a 4% stacking (upper) gel were prepared. Each well was loaded with 20 µg of protein and underwent vertical electrophoresis in a tank containing 1X SDS running buffer (1X 25 mM Tris, 192 mM glycine, 0.1% SDS pH 8.3) at 180 volts and 400 milliamps for approximately 60 minutes. The gels were transferred to a fixation solution containing 50 ml of MeOH, 10 ml of acetic acid, and 40 ml of distilled water. They were then shaken on an orbital shaker for 30 minutes. After fixation, the gels were stained with Coomassie Brilliant Blue R-250 dye (BioRad, USA) for 30 minutes. Once

the staining process was completed, the gels were immersed in distilled water and washed until free from dye.

2.2.2. 2D-PAGE and MALDI-TOF analysis

The protein extract (100 µg protein) was resuspended in 2D rehydration buffer and loaded onto an 11 cm IPG strip with a pH range of 3-10 (ReadyStrip, BioRad, USA). The IPG strips were left to rehydrate overnight without applying any voltage in the Passive Rehydration Program, which took approximately 13 hours at 20°C (BioRad, USA Protean IEF Cell). Increasing voltage values were applied during the focusing process at 20°C. The program for focusing comprised three steps, taking approximately 10-12 hours. The first step involved applying 250 Volts for 20 minutes using a linear ramp. The second step involved applying 4000 Volts for 2 hours using a linear ramp. Finally, a rapid ramp of 40,000 Volts V/H was applied using an IEF cell Protean from BioRad. The strips were focused and then transferred to an equilibration container. They were successively washed for 15 minutes each with Equilibration Buffer I (6 M Urea, 0.375 M Tris-HCl pH 8.8, 2% SDS, 20% Glycerol, 2% (w/v) DTT), Buffer II (6 M Urea, 0.375 M Tris-HCl pH 8.8, 2% SDS, 20% Glycerol, 2.5% (w/v) Iodoacetamide), and 1X SDS buffer.

The second-dimensional vertical SDS-PAGE was conducted using a 12% polyacrylamide gel. IPG strips and 3 µl of unstained protein marker (Fermentas, SM0431) were placed onto the separating gel. Electrophoresis was conducted using 1X SDS buffer (25 mM Tris, 192 mM glycine, 0.1% SDS, pH 8.3) as a running buffer, and gels were run at 400 mA (maximum), approximately 180 volts for about 55 minutes (BioRad, Mini Protean Tetra Cell, USA). The gels were initially placed in a fixation solution consisting of 50% methanol and 10% acetic acid. They were then shaken on an orbital shaker for a period ranging from 6 to 24 hours. For staining, a freshly prepared Colloidal Coomassie dye (KeraFAST, Bloomoose, USA) in a 4:1 ratio (Reagent I: Reagent II) was used for each gel. The gels were gently shaken in an orbital shaker at room temperature for 6-24 hours until protein spots became visible. To fix and enhance spots on gels after removing excess dye, an "intensifying" solution was prepared. To obtain the solution, mix Reagent II and Milli-Q water in a 1:4 ratio and gently shake the gels in an orbital shaker at room temperature. Obtain gel images of protein spots using the Quantity One program (BioRad, USA). Before excising the spots in 2D gels, compare the protein profiles using the PD Quest Advanced program (BioRad, USA). Identify protein spots that show differences in regulation by checking spot densities between matched protein spots. The gel spots that were removed underwent several destaining steps. The proteins within were then digested using 10 ng/µl of trypsin enzyme from Promega. Afterward, MALDI TOF-TOF analysis was performed, and the mass spectra were identified using the Mascot protein identification search engine (Kocaeli University, Proteomics Laboratory).

2.3. Microarray analysis

Following cell growth and antibiotic treatment of the *Escherichia coli* AG1(pCA24N::leuS) strain, total RNA was isolated from the cell pellets using a commercial kit (PureLink RNA Mini Kit, 12183018A). DNaseI treatment was applied to the isolated RNA to remove any DNA contamination (Thermo, Scientific, EN0521). For microarray analysis, RNA at a

concentration of 100 ng/ μ l was used. Microarray analysis was conducted following the protocol of Agilent's "Single-Color Microarray-Based Gene Expression Analysis". According to the protocol, the process involved cRNA synthesis and amplification, followed by cRNA purification. RNA samples were labeled with Cy3 dye. After the labeling process, the amounts of RNA labeled with Cy3 dye were measured using a Nanodrop spectrophotometer (Implen, Germany). Subsequently, the samples underwent the hybridization process, using 600 ng of RNA. Prepared hybridization samples were applied to the 8-array Agilent chip without creating bubbles. The samples were left to hybridize with array slides at 65°C for 17 hours. Following the hybridization process, the samples were washed with wash buffers and prepared for imaging. The arrays were scanned using the Agilent Microarray scanner (Agilent, USA). The image intensity data were recorded and transferred into text files using the Agilent Feature Extraction Software, version A.4.0.45 (Agilent, USA).

2.4. Statistical and bioinformatic analyses

The data was collected using Agilent Feature Extraction Software 8.0 and analyzed with GeneSpring 14.9 Software (Agilent, USA) using the t-test and ANOVA. Datasets with p-values <0.05 were filtered to analyze the extent of change (increase or decrease) compared to the control condition. The microarray results, which contain gene information and fold differences, were analyzed using the EcoCyc (Keseler et al., 2005) and Omics Dashboard (Pathway Tools) programs (Paley et al., 2017) to identify metabolic pathways or cellular processes. Additionally, EcoCyc was used to obtain more information about the genes of interest, and relevant publications were searched for in the literature.

3. Results

3.1. Proteomics analysis of the *leuS* overexpressing strain exposed to EP

The protein profiles of the AG1(pCA24N::*leuS*) strain were examined under two conditions: with and without EP exposure. To assess the quality and integrity of the proteins, a 1D-SDS-PAGE page was performed to visualize the protein bands. After ensuring the quality of the protein extracts, 2D-PAGE was performed.

After the second dimension, proteins were stained, and the protein spots were observed and photographs were taken. Fig. 2A illustrates the images of 2D-PAGE gels showing the protein spots obtained from the cells as a result of exposure to EP antibiotic (0.25 μ g/ml) and the control (no exposure). The images were captured using the Quantity One program and then compared using the PDQuest Advanced program (BioRad). Four protein spots with differential regulation were identified by examining the spot densities of the matched protein spots, as shown in Fig. 2B.

The EP effect on the *E. coli* AG1(pCA24N::*leuS*) strain resulted in the upregulation of two protein spots (spots 4103 and 9105) and the downregulation of two protein spots (spots 7405 and 8303) (Fig. 2B). MALDI TOF-TOF analysis of the selected protein spots identified 2-isopropylmalate synthase (LeuA) and thymidine phosphorylase (DeoA) (Table 1). Three spots were found to be associated with LeuA, indicating the possibility of truncated forms of this protein.

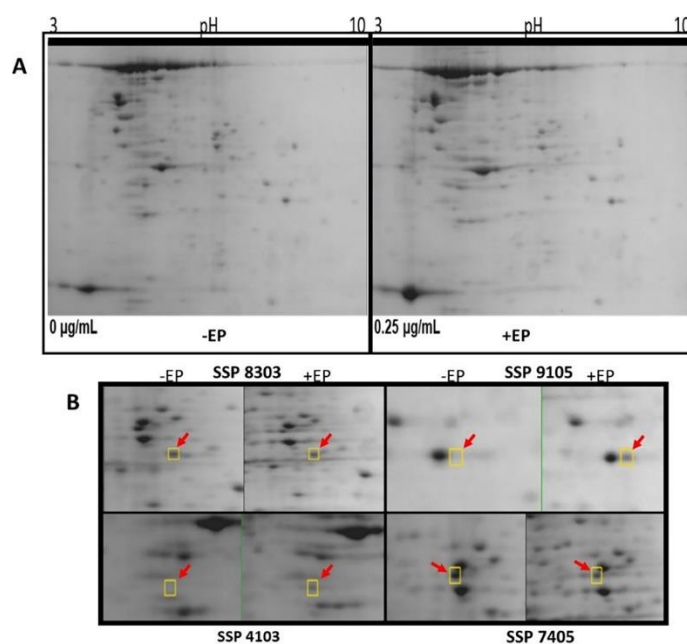


Fig. 2. 2D-PAGE profiles of the AG1(pCA24N::*leuS*) strain under EP treatment, highlighting spots exhibiting regulation. 2A. Protein spots obtained from the strain exposed to EP (right gel) and no treatment control (left gel). pI strip (3-10) was used and EP concentration of 0.25 μ g/ml was applied, 2B. Comparative images of protein spots from the AG1(pCA24N::*leuS*) strain showing regulation differences without EP antibiotic (-EP) and with 0.25 μ g/ml EP (+EP). Spots numbered 4103, 7405, 8303, and 9105 are shown with red arrows.

Table 1

Identification of proteins differentially regulated upon EP effect on the AG1(pCA24N::*leuS*) strain.

| Spot No | Protein ID | Score | Regulation | Gene |
|---------|----------------------------|-------|------------|-------------|
| 7405 | 2-isopropylmalate synthase | 51 | down | <i>leuA</i> |
| 4103 | 2-isopropylmalate synthase | 37 | up | <i>leuA</i> |
| 8303 | Thymidine phosphorylase | 35 | down | <i>deoA</i> |
| 9105 | 2-isopropylmalate synthase | 30 | up | <i>leuA</i> |

3.2. Microarray-based transcriptomic analysis results

Microarray analysis was performed to assess the levels of regulated mRNAs in the bacterial strain under both EP antibiotic (0.25 μ g/ml) and antibiotic-free conditions. The analysis revealed that the mRNA levels of 23 genes increased ($p < 0.05$, fold change; $FC > 2$), while those of 9 genes decreased in response to the EP effect (Tables 2 and 3). Up-regulated genes were *yiaW*, *mgIB*, *narH*, *ybiO*, *flgB*, *lacZ*, *yibH*, *yedN*, *yhbW*, *glpB*, *murB*, *hydN*, *ymfC*, *fadE*, *yidF*, *gltI*, *dkgB*, *frdA*, *yafU*, *yidJ*, *creB*, *yhfZ* and *yfhG* (Table 2). In summary, these genes in *E. coli* encode various proteins with diverse functions, including transport, metabolism, regulation, and biosynthesis. Many of them are involved in essential cellular processes, but specific details about some genes are not available in the literature. These genes were classified based on the cellular processes or metabolic pathways and were seen to be associated with chemotaxis, transport, biosynthesis, and metabolism of galactose, lactose, glycerol, peptidoglycan, fatty acids, hydrogen, and sulfate. Some genes have unknown functions (Tables 4 and 5). Down-regulated genes, on the other hand, were *yhdY*, *deoR*, *recX*, *yobB*, *potF*, *yccE*, *yraJ*, *ycaD*, and *mutH* genes, which are involved in various cellular functions, including DNA repair, regulation of gene expression, cell division, and transport processes.

Table 2

List of up-regulated genes as a result of EP effect on *E. coli* AG1(pCA24N::*leuS*) strain.

| Gene | Definition | Fold change | Regulation |
|-------------|---|-------------|------------|
| <i>viaW</i> | orf, hypothetical protein [b3587] | 5.1 | up |
| <i>mgIB</i> | galactose-binding transport protein; receptor for galactose taxis [b2150] | 4.9 | up |
| <i>narH</i> | nitrate reductase 1, beta subunit [b1225] | 4.2 | up |
| <i>ybiO</i> | putative transport protein [b0808] | 4.2 | up |
| <i>flgB</i> | flagellar biosynthesis, cell-proximal portion of basal-body rod [b1073] | 4.1 | up |
| <i>lacZ</i> | beta-D-galactosidase [b0344] | 4 | up |
| <i>yibH</i> | putative membrane protein [b3597] | 3.9 | up |
| <i>yedN</i> | orf, hypothetical protein [b1934] | 3.8 | up |
| <i>yhbW</i> | putative enzyme [b3160] | 3.3 | up |
| <i>glpB</i> | sn-glycerol-3-phosphate dehydrogenase [b2242] | 3.2 | up |
| <i>murB</i> | acetylenolpyruvoylglucosamine reductase [c_4931] | 3.1 | up |
| <i>hydN</i> | Electron transport protein hydN [c_3269] | 2.9 | up |
| <i>ymfC</i> | orf, hypothetical protein [Z1864] | 2.5 | up |
| <i>fadE</i> | putative acyl-CoA dehydrogenase [b0221] | 2.4 | up |
| | Putative cell cycle protein mesJ [c_0226] | 2.4 | up |
| <i>yidF</i> | putative transcriptional regulator [Z5169] | 2.4 | up |
| | Hypothetical protein [c_3755] | 2.3 | up |
| <i>glH</i> | putative periplasmic binding transport protein [b0655] | 2.3 | up |
| <i>dkgB</i> | putative aldose reductase [b0207] | 2.2 | up |
| <i>frdA</i> | fumarate reductase, anaerobic, flavoprotein subunit [b4154] | 2.2 | up |
| <i>yafU</i> | orf, hypothetical protein [b0218] | 2.2 | up |
| <i>yidJ</i> | putative sulfatase [b3678] | 2.1 | up |
| <i>creB</i> | catabolic regulation response regulator [Z6001] | 2 | up |
| <i>yhfZ</i> | orf, hypothetical protein [b3383] | 2 | up |
| <i>yfhG</i> | putative alpha helix protein [b2555] | 2 | up |

Table 3

List of down-regulated genes as a result of EP effect on *E. coli* AG1(pCA24N::*leuS*) strain.

| Gene | Definition | Fold change | Regulation |
|-------------|--|-------------|------------|
| <i>yhdY</i> | putative transport system permease protein | 2.8 | down |
| <i>deoR</i> | transcriptional repressor for deo operon, tsx, nupG [b0840] | 2.6 | down |
| <i>recX</i> | regulator, OraA protein [Z4001] | 2.5 | down |
| <i>yobB</i> | orf, hypothetical protein [b1843] | 2.5 | down |
| <i>potF</i> | periplasmic putrescine-binding protein; permease protein [b0854] | 2.5 | down |
| | Hypothetical protein ydcX [c_1870] | 2.4 | down |
| <i>yccE</i> | orf, hypothetical protein [b1001] | 2.4 | down |
| | putative outer membrane protein [b3144] | 2.4 | down |
| <i>yraJ</i> | | 2.4 | down |
| <i>ycaD</i> | Hypothetical protein ycaD [c_1037] | 2.2 | down |
| | methyl-directed mismatch repair [b2831] | 2 | down |

4. Discussion

The objective of this study was to examine the effect of epetaborole (EP) on the transcriptome and proteome of the *Escherichia coli* strain that overexpresses the *leuS* gene, which encodes Leucyl-tRNA synthetase. The study provides valuable insights into the molecular response of the bacterium to this boron-containing antibiotic, exploring changes at both the genetic and protein levels. The findings shed light on the broader effects beyond the primary target, LeuS.

Proteomics analysis based on 2D-PAGE and MALDI TOF-TOF revealed four differentially regulated protein spots influenced by EP in the *leuS* overexpression strain. The study identified two regulated proteins, LeuA and DeoA. LeuA catalyzes the initial step in leucine synthesis (Stieglitz and Calvo, 1974). EP and higher levels of LeuS may affect LeuA, potentially leading to truncated LeuA protein variants. LeuA was identified in three locations on the 2D-PAGE gel, with two spots up-regulated and one down-regulated (Table 2). Despite the relatively low identification scores for LeuA (51, 37, and 30), the regulation levels of the spots were visible on the 2D gel (refer to Fig. 2). While considering the possibility of misidentification, it is also possible that the cell may produce varying lengths of LeuA protein due to increased levels of LeuS and EP effect.

LeuA is a crucial enzyme in the biosynthesis of leucine. The activity of LeuA is regulated to ensure that leucine biosynthesis occurs only when necessary. Regulation commonly involves feedback inhibition, where the end product of the pathway, leucine, acts as an allosteric inhibitor of LeuA. This feedback mechanism helps to maintain optimal levels of leucine within the cell. Overexpression of LeuS and EP may indirectly affect the translational and transcriptional regulation of LeuA, resulting in the production of shorter LeuA proteins and subsequent impacts on leucine biosynthesis.

Wessler and Calvo (1981) proposed that the expression of the *leuA* gene is controlled by Ribosome-Mediated Attenuation. This mechanism involves the promotion of transcription termination at the attenuator by charged Leucyl-tRNA (L-leucyl-tRNA^{Leu}). Also, Gemmill et al. (1979) demonstrated that the operon of leucine biosynthesis genes, including *leuA*, is controlled by attenuation in *Salmonella typhimurium*. Therefore, it may be possible that, if there is a sufficient amount of L-leucyl-tRNA^{Leu} in the cell, premature translation of LeuA may occur through the involvement of ribosomes, facilitated by the attenuation of transcription. Due to the absence of a nuclear membrane in bacteria, transcription and translation are coupled. This may result in the synthesis of truncated versions of the LeuA protein, which can be detected by 2D-PAGE.

In the current study, the overexpression of *leuS* by a recombinant plasmid may have led to an increase in the L-leucyl-tRNA^{Leu} level. This increase, combined with the presence of EP, may have disrupted the balance between LeuS enzyme activity and the product L-leucyl-tRNA^{Leu}, leading to the detection of truncated forms of the LeuA protein. Future studies could explore and clarify the relationship between the LeuA attenuation mechanism and EP effect in the presence of higher levels of LeuS. Attenuation may indirectly regulate and maintain amino acid levels in the cell for other aminoacyl-tRNA synthetases and amino acid synthesis operons.

Transcriptomics analysis based on microarray data revealed 23 genes up-regulated and 9 genes down-regulated in response to EP in the *leuS* overexpression strain. The identified genes cover a range of functions, indicating a multifaceted

Table 4
Omics Dashboard Pathway analysis of the up-regulated genes.

| System | Subsystem | Gene ID | Gene | Fold change | Regulation | Function | |
|--|---|-------------------------------|-------------|-------------|--|--|--|
| Biosynthesis | | EG11205 | <i>murB</i> | 3.1 | up | UDP-N-acetylenolpyruvoylglucosamine reductase | |
| | Carbohydrates and Carboxylates Degradation | EG10392 | <i>glpB</i> | 3.2 | up | anaerobic glycerol-3-phosphate dehydrogenase subunit B | |
| | | EG10527 | <i>lacZ</i> | 4.0 | up | β -galactosidase | |
| Degradation | Alcohol Degradation | EG10392 | <i>glpB</i> | 3.2 | up | anaerobic glycerol-3-phosphate dehydrogenase subunit B | |
| | Fatty Acid and Lipid Degradation | G6105 | <i>fadE</i> | 2.4 | up | acyl-CoA dehydrogenase | |
| | Other Degradation | EG11205 | <i>murB</i> | 3.1 | up | UDP-N-acetylenolpyruvoylglucosamine reductase | |
| Energy | Anaerobic Respiration | EG10392 | <i>glpB</i> | 3.2 | up | anaerobic glycerol-3-phosphate dehydrogenase subunit B | |
| | | EG10639 | <i>narH</i> | 4.2 | up | nitrate reductase A subunit β | |
| Central Dogma | Other Energy | EG10392 | <i>glpB</i> | 3.2 | up | anaerobic glycerol-3-phosphate dehydrogenase subunit B | |
| | | G6581 | <i>yjfC</i> | 2.5 | up | 23S rRNA pseudouridine2457 synthase | |
| | | G358 | <i>flgB</i> | 4.1 | up | flagellar basal-body rod protein | |
| | | EG10392 | <i>glpB</i> | 3.2 | up | anaerobic glycerol-3-phosphate dehydrogenase subunit B | |
| | Sigma and Transcription Factor Regulons | EG11552 | <i>hydN</i> | 2.9 | up | putative electron transport protein | |
| | | EG10593 | <i>mglB</i> | 4.9 | up | D-galactose/methyl-galactoside ABC transporter periplasmic binding protein | |
| | Regulation | | EG10639 | <i>narH</i> | 4.2 | up | nitrate reductase A subunit β |
| | | | EG10527 | <i>lacZ</i> | 4.0 | up | β -galactosidase |
| | | | G6581 | <i>yjfC</i> | 2.5 | up | 23S rRNA pseudouridine2457 synthase |
| | | Transcription Factor Regulons | G7654 | <i>yhbW</i> | 3.3 | up | putative luciferase-like monooxygenase |
| G6417 | | | <i>ybiO</i> | 4.2 | up | moderate conductance mechanosensitive channel | |
| EG12291 | | | <i>yiaW</i> | 5.1 | up | DUF3302 domain-containing protein | |
| | | G6105 | <i>fadE</i> | 2.4 | up | acyl-CoA dehydrogenase | |
| | | EG11764 | <i>yibH</i> | 3.9 | up | inner membrane protein | |
| Response to Stimulus | Proteins Involved in Response to DNA Damage | | | | | | |
| | Proteins Involved in Response to Osmotic Stress | G6417 | <i>ybiO</i> | 4.2 | up | moderate conductance mechanosensitive channel | |
| | Other Proteins involved in Stimulus Response | G358 | <i>flgB</i> | 4.1 | up | flagellar basal-body rod protein | |
| Cellular Processes | | EG10593 | <i>mglB</i> | 4.9 | up | D-galactose/methyl-galactoside ABC transporter periplasmic binding protein | |
| | | EG11205 | <i>murB</i> | 3.1 | up | UDP-N-acetylenolpyruvoylglucosamine reductase | |
| Virulence-Related | Proteins Involved in Locomotion | G358 | <i>flgB</i> | 4.1 | up | flagellar basal-body rod protein | |
| | | EG10593 | <i>mglB</i> | 4.9 | up | D-galactose/methyl-galactoside ABC transporter periplasmic binding protein | |
| | Flagellar Proteins | G358 | <i>flgB</i> | 4.1 | up | flagellar basal-body rod protein | |
| | | EG10392 | <i>glpB</i> | 3.2 | up | anaerobic glycerol-3-phosphate dehydrogenase subunit B | |
| | | G6417 | <i>ybiO</i> | 4.2 | up | moderate conductance mechanosensitive channel | |
| | | EG11764 | <i>yibH</i> | 3.9 | up | inner membrane protein | |
| | Plasma Membrane Proteins | EG10593 | <i>mglB</i> | 4.9 | up | D-galactose/methyl-galactoside ABC transporter periplasmic binding protein | |
| | | G6105 | <i>fadE</i> | 2.4 | up | acyl-CoA dehydrogenase | |
| | | EG12291 | <i>yiaW</i> | 5.1 | up | DUF3302 domain-containing protein | |
| | Cell Exterior | Periplasmic Proteins | EG10639 | <i>narH</i> | 4.2 | up | nitrate reductase A subunit β |
| G358 | | | <i>flgB</i> | 4.1 | up | flagellar basal-body rod protein | |
| EG10593 | | <i>mglB</i> | 4.9 | up | D-galactose/methyl-galactoside ABC transporter periplasmic binding protein | | |
| Transport Proteins | | EG10593 | <i>mglB</i> | 4.9 | up | D-galactose/methyl-galactoside ABC transporter periplasmic binding protein | |
| Cell Wall Biogenesis/Organization Proteins | | EG11205 | <i>murB</i> | 3.1 | up | UDP-N-acetylenolpyruvoylglucosamine reductase | |

*The evaluation of cellular systems and subsystems, based on the microarray analysis results of the up-regulated genes in response to Epetraborole in the *E. coli* AG1(pCA24N::*leuS*) strain, was performed using the Omics Dashboard Pathway (Tools) program.

Table 5
Omics Dashboard Pathway analysis of the down-regulated genes.

| System | Subsystem | Gene ID | Gene | Fold change | Regulation | Function |
|-------------------------|---|-------------|-------------|-------------|--|--|
| Central Dogma | RNA Metabolism | EG10223 | <i>deoR</i> | 2.6 | down | DNA-binding transcriptional |
| | DNA Metabolism | EG10624 | <i>mutH</i> | 2.0 | down | DNA mismatch repair protein |
| Regulation | Sigma and Transcription Factor | EG12080 | <i>recX</i> | 2.5 | down | RecA inhibitor |
| | | EG12080 | <i>recX</i> | 2.5 | down | RecA inhibitor |
| | Regulons | EG11629 | <i>potF</i> | 2.5 | down | putrescine ABC transporter periplasmic binding protein |
| | Regulons | EG12836 | <i>yhdY</i> | 2.8 | down | DNA-binding transcription regulator |
| | Signal transmission pathways | EG12196 | <i>yccE</i> | 2.4 | down | uncharacterized protein |
| | Transcription Factor Regulons | EG10223 | <i>deoR</i> | 2.6 | down | DNA-binding transcriptional repressor |
| Response to Stimulus | Proteins Involved in Response to DNA Damage | EG11242 | <i>ycaD</i> | 2.2 | down | putative transporter |
| | | G7015 | <i>yobB</i> | 2.5 | down | putative carbon-nitrogen hydrolase family protein |
| | EG12080 | <i>recX</i> | 2.5 | down | RecA inhibitor | |
| | EG10624 | <i>mutH</i> | 2.0 | down | DNA mismatch repair protein | |
| | G7639 | <i>yraJ</i> | 2.4 | down | putative fimbrial usher protein | |
| | EG11629 | <i>potF</i> | 2.5 | down | putrescine ABC transporter periplasmic binding protein | |
| Cell Exterior | Plasma Membrane Proteins | EG12836 | <i>yhdY</i> | 2.8 | down | putative ABC transporter membrane subunit |
| | | G7015 | <i>yobB</i> | 2.5 | down | putative carbon-nitrogen hydrolase family protein |
| | EG11242 | <i>ycaD</i> | 2.2 | down | putative transporter | |
| | Periplasmic Proteins | EG11629 | <i>potF</i> | 2.5 | down | putrescine ABC transporter periplasmic binding protein |
| | Transport Proteins | EG11629 | <i>potF</i> | 2.5 | down | putrescine ABC transporter periplasmic binding protein |
| Outer Membrane Proteins | G7639 | <i>yraJ</i> | 2.4 | down | putative fimbrial usher protein | |

cellular response. Upon evaluating differentially regulated genes, it is evident that up-regulated genes are associated with biosynthesis, cellular processes, virulence-related degradation, and energy metabolism within the cell, in contrast to down-regulated genes. The study found that genes that were both up-regulated and down-regulated played a role in regulating responses to stimuli, cell exterior, and the central dogma.

Analyses were conducted using Omics Dashboard pathway (EcoCyc) (Paley et al., 2017) and String DB (Snel et al., 2000) to interpret the microarray results. The results suggest that EP has a significant impact on the *leuS* overexpressing strain, particularly in terms of altering the expression of genes associated with the cell exterior, regulation, and response to stimuli. This broader impact on cellular processes suggests a systemic response to EP beyond the direct inhibition of *LeuS*.

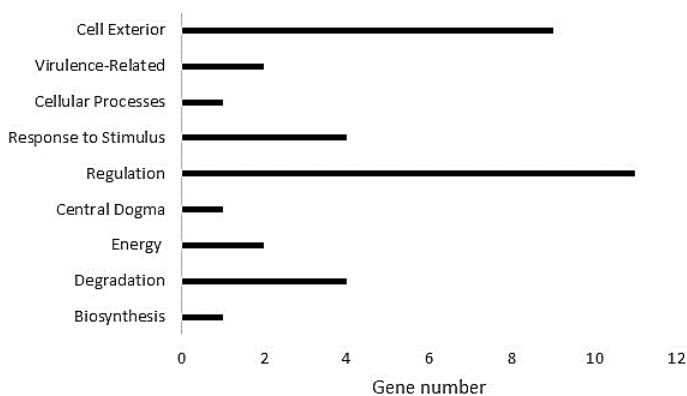


Fig. 3. Enrichment analysis of up-regulated genes. The results related to the cellular functions of the genes showing upregulation in the microarray analysis of the AG1(pCA24N::*leuS*) strain are provided. Several genes match with more than one subsystem. The numbers are derived based on the Omics Dashboard analysis results in the EcoCyc database.

The Omics Dashboard analysis (BioCyc, 2024) is a useful tool for analyzing large datasets, such as transcriptomics results,

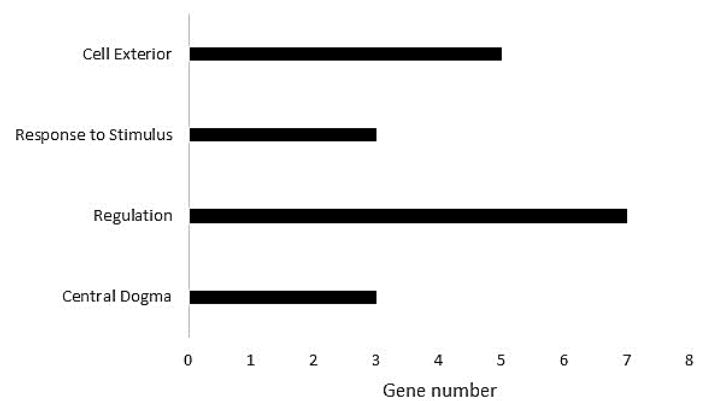


Fig. 4. Enrichment analysis of down-regulated genes. The results related to the cellular functions of the genes showing downregulation in the microarray analysis of the AG1(pCA24N::*leuS*) strain are provided. Several genes match with more than one subsystem. The numbers are derived based on the Omics Dashboard analysis results in the EcoCyc database.

to identify pathways and cell processes related to the topic of interest (Paley et al., 2017). Separate analyses were conducted for up-regulated and down-regulated genes, and the affected pathways and processes are presented in Tables 4 and 5, respectively. Additionally, the up-regulated genes were analyzed using the “Enrichment” tool (NIH, 2024), which revealed that the most affected pathways or cellular processes were regulation (n=11 genes), cell exterior (n=9), response to stimulus (n=4), and degradation (n=4) (Fig. 3). According to the enrichment analysis module of the Omics Dashboard, the down-regulated genes showed a greater impact on regulation, cell exterior, response to stimulus, and central dogma genes compared to others (Fig. 4). The gene information related to these processes and pathways can be utilized for further studies to investigate specific gene involvement and understand the impact of EP on bacteria.

Furthermore, String analysis was also performed (STRING, 2024) on both up-regulated and down-regulated

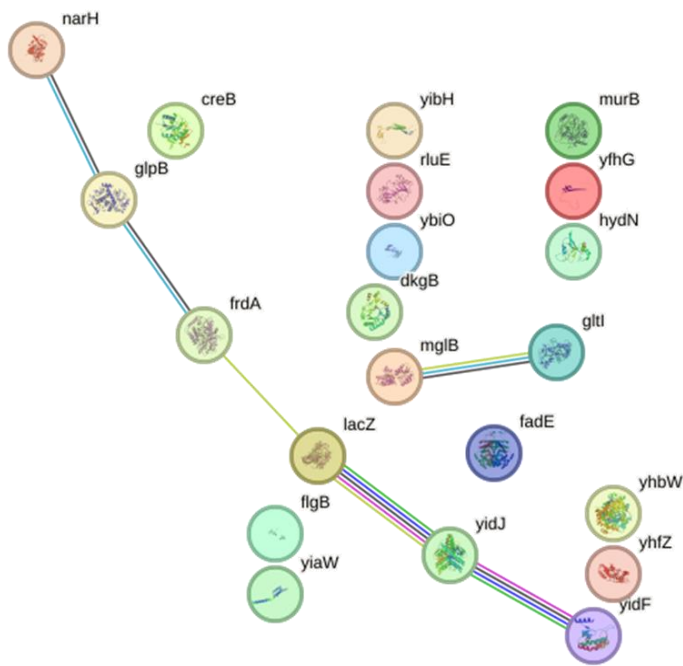


Fig. 5. STRING network analysis of the up-regulated genes. A connection map illustrating the predicted functional relationships among the genes up-regulated in response to epetraborole on the *E. coli* AG1(pCA24N::leuS) strain. The thickness of the lines indicates the degree of interaction based on fusion, co-occurrence, experimental, and co-expression data. The figure was generated using STRING (version 12.0) with a medium confidence score of 0.4 (approximate probability).

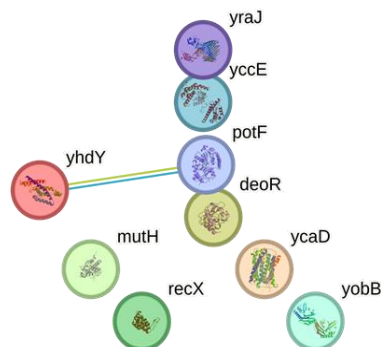


Fig. 6. STRING network analysis of the down-regulated genes. A connection map illustrating the predicted functional relationships among the genes down-regulated in response to epetraborole on the *E. coli* AG1(pCA24N::leuS) strain. The thickness of the lines indicates the degree of interaction based on fusion, co-occurrence, experimental, and co-expression data. The figure was generated using STRING (version 12.0) with a medium confidence score of 0.4 (approximate probability).

genes (Mering et al., 2003). Among the up-regulated genes, *yidF*, *yidJ*, *lacZ*, *frdA*, *glpB*, and *narH* formed a network, while *mglB* and *gltL* formed another network (Fig. 5) (interaction score values: *narH* vs *glpB*- 0.505, *glpB* vs *frdA*- 0.515, *frdA* vs *lacZ*- 0.524, *lacZ* vs *yidJ*- 0.523, *yidJ* vs *yidF*- 0.669, *mglB* vs *gltL*- 0.783). A link was observed between *potF* and *yhdY* for down-regulated genes (Fig. 6) with an interaction score value of 0.654. The network nodes represent proteins, and the edges represent protein-protein associations. These associations should be specific and meaningful, indicating that the proteins contribute jointly to a shared function. However, this does not necessarily imply that they are physically bound to each other (Fig. 5 and Fig. 6). These protein interactions are displayed in three ways. The program displays protein interactions using blue to indicate information from selected databases and purple to indicate

experimentally determined information. The proximity of gene regions is represented by the color green, gene fusion interactions by red, and gene co-occurrence by dark blue. During the interaction, the color yellow indicates text mining, black indicates co-expression and light navy blue indicates protein homology.

The genes *mglB* and *flgB* are involved in chemotaxis and flagellar biosynthesis, respectively, while genes *glpB*, *murB*, and *fadE* are associated with metabolic pathways, including glycerol metabolism, peptidoglycan biosynthesis, and fatty acid metabolism (Scholle et al., 1987; Spoering et al., 2006; Egan et al., 2020; Pavoncello et al., 2022; Sun et al., 2022).

The literature indicates that *yidF* is involved in activating sulfatases in *E. coli* (Benjdia et al., 2007; Alméciga-Díaz et al., 2017). Overexpression of *yidF* enhances resistance to D-serine (Soo et al., 2011). The function of the *yidJ* gene is unknown, but it is a putative Cys-type sulfatase (Schirmer and Kolter, 1998). The *frdA* gene is one of four genes involved in acetyl-CoA consumption (Seong et al., 2020). The *glpB* gene encodes a subunit of anaerobic glycerol-3-phosphate dehydrogenase B, which converts glycerol-3-phosphate to dihydroxyacetone phosphate using fumarate under anaerobic conditions (Cole et al., 1988). Metcalf et al. (1990) found that this gene was induced during phosphate starvation. The literature information suggests that the *gltL* gene is the putative ATP-binding subunit of a glutamate/aspartate ABC transporter complex (Linton and Higgins, 1998). The *potF* gene is a putrescine-specific binding protein, as reported by Pistocchi et al. (1993). The *yhdY* gene, on the other hand, is predicted to be an inner membrane protein with eight transmembrane domains (Daley et al., 2005) and is predicted to be one of the two inner membrane subunits of a putative ABC transporter (Saier et al., 2016). A transcriptomic analysis of an *E. coli* strain in the presence of poly-gamma-glutamic acid (gamma-PGA) revealed an upregulation in the mRNA level of the *yhdY* gene (Jiang et al., 2006).

Harayama et al. (1983) conducted a study on MglB, a periplasmic binding protein of a D-galactose/methyl-galactose ABC transporter. The study found that *mglB*⁺ plasmids synthesized both the precursor and mature forms of the galactose binding protein in the cells. According to Ito et al. (2008), FlgB, one of the four proteins that make up the rod of the flagellar basal body in bacteria, exhibited increased expression in *ΔrpoS* biofilms. However, DNA microarray analysis revealed no difference in expression in wild-type biofilms.

Genes *yiaW*, *yibH*, *yedN*, *yhbW*, *ymfC*, *yafU*, *yhfZ*, and *yfhG* have unknown functions, indicating areas for further investigation. This study has shown that these genes are differentially regulated by the EP antibiotic.

Furthermore, the literature contains additional studies on antibiotics. For example, Xu et al. (2006) conducted a proteomics study to screen the outer membrane proteome of *E. coli* K-12. They identified 11 protein spots representing nine proteins associated with tetracycline resistance and nine protein spots representing eight proteins associated with ampicillin resistance. Another proteomic study was conducted on an *E. coli* strain resistant to piperacillin/tazobactam antibiotics. The study found that 12 proteins were up-regulated and 14 proteins were down-regulated (p<0.05) (dos Santos et al., 2010). Bie et al. (2023) conducted a transcriptomic analysis to investigate the effect of nine different antibiotics on the transcriptome of *E. coli*. The study revealed that mRNA levels of eight genes were up-regulated, while 30 genes were down-regulated. Transcriptomic analysis was performed to examine the impact of ciprofloxacin

antibiotic on the transcriptome of *E. coli* MG1655 strain. The analysis showed differential regulation of mRNA levels of 41 genes (Goswami and Narayana Rao, 2018). In another study, Zhao et al. (2023) conducted a transcriptomic analysis to investigate the effects of gentamicin and ampicillin antibiotics. The study found that gentamicin caused differential expression of 51 genes, while ampicillin caused differential expression of 23 genes.

Inhibition of essential aminoacyl tRNA synthetases in various bacteria can be a potential target for antibiotics. Blocking these enzymes interrupts protein synthesis and prevents cell growth (Hurdle et al., 2005). Further research is necessary to understand the relation between these enzymes and antibiotic susceptibility or tolerance, and to combat antibiotic resistance. After reviewing the literature, it is evident that mutations in certain tRNA synthetase genes can reduce susceptibility to ciprofloxacin and other antibiotics. A study demonstrated that mutations in three different aminoacyl tRNA synthetase genes (*leuS*, *aspS*, and *thrS*) decreased susceptibility to ciprofloxacin. Transcriptome analysis showed that two mutations, independently selected in *leuS* (Asp162Asn and Ser496Pro), specifically up-regulated three loci (*mdtK*, *acrZ*, and *ydhJJK*). Genetic analysis showed that the bacterium's reduced susceptibility was linked to the activity of these loci. Additional antimicrobial sensitivity tests revealed that *leuS* mutations also decreased sensitivity to other antibiotic classes, including chloramphenicol, rifampicin, mecillinam, ampicillin, and trimethoprim (Garoff et al., 2018). Mutations in the *alaS*, *argS*, *ileS*, and *leuS* tRNA synthetase genes have also been linked to *E. coli*'s resistance to the antibiotic novobiocin (Milija et al., 1999). Vinella et al. (1993) reported a mutant of *E. coli* aminoacyl-tRNA synthetase that was resistant to amdinocillin (mecillinam), a beta-lactam antibiotic that binds to penicillin-binding protein 2 (PBP2), preventing cell wall elongation and leading to cell death.

Novikova et al. (2007) conducted a study analyzing a random transposon library using the antibiotic Microcin C (McC), which targets aspartyl-tRNA synthetase, and identified

McC-resistant *E. coli* mutants. The study found that *yej* gene mutations interfere with McC uptake. YejABEF, the inner membrane transporter, was identified as responsible for McC uptake in *E. coli*.

Targeting aminoacyl tRNA synthetases with specific antibiotics, including boron-containing compounds, may lead to effective treatment strategies, especially against *Mycobacterium* species. Engineering structural variations has been shown to be effective in fine-tuning the antibacterial properties of these compounds, opening up new possibilities for combating bacterial infections (Cardenas, 2023). The effects of EP and other boron-containing antibiotics on bacterial cells should be studied across various microorganism species. The results of this study will likely prove useful in this field.

In summary, the results of the current study contribute novel insights into the impact of EP, a boron-containing antibiotic, on *E. coli*, unraveling molecular mechanisms governing cellular responses. This is particularly relevant when the level of an aminoacyl-tRNA synthetase, namely LeuS, is increased. In conclusion, the integrated proteomic and transcriptomic approach provides a comprehensive understanding of the molecular dynamics induced by EP in an *E. coli* strain overexpressing *leuS*. The genes and proteins discussed above offer a foundation for additional research into the broader impacts of EP and its potential in combating antibiotic-resistant bacteria.

Acknowledgments: This study was funded by the Scientific and Technological Research Council of Türkiye (TUBITAK) 1001 Grant No 119Z080. The authors would like to express their gratitude to TUBITAK and Mugla Sitki Kocman University.

Conflict of interest: The authors declare that they have no conflict of interests.

Informed consent: The authors declare that this manuscript did not involve human or animal participants and informed consent was not collected.

References

- Alméciga-Díaz, C. J., Tolosa-Díaz, A. D., Pimentel, L. N., Bonilla, Y. A., Rodríguez-López, A., Espejo-Mojica, A. J., ... & Gonzalez-Santos, J. (2017). Anaerobic sulfatase maturase AslB from *Escherichia coli* activates human recombinant iduronate-2-sulfate sulfatase (IDS) and N-acetylgalactosamine-6-sulfate sulfatase (GALNS). *Gene*, 634, 53-61.
- Arai, M., Koizumi, Y., Sato, H., Kawabe, T., Suganuma, M., Kobayashi, H., ... & Omura, S. (2004). Boromycin abrogates bleomycin-induced G2 checkpoint. *The Journal of Antibiotics*, 57(10), 662-668.
- Benjdia, A., Dehò, G., Rabot, S., & Berteau, O. (2007). First evidences for a third sulfatase maturation system in prokaryotes from *E. coli* aslB and ydeM deletion mutants. *FEBS Letters*, 581(5), 1009-1014.
- Bie, L., Zhang, M., Wang, J., Fang, M., Li, L., Xu, H., & Wang, M. (2023). Comparative analysis of transcriptomic response of *Escherichia coli* K-12 MG1655 to nine representative classes of antibiotics. *Microbiology Spectrum*, 11(2), e00317-23.
- BioCyc, (2024). BioCyc Pathway/Genome Database Collection, <https://biocyc.org/dashboard/dashboard-intro.shtml>, Last accessed on March 30, 2024.
- Bradford, M. M. (1976). A rapid and sensitive method for the quantitation of microgram quantities of protein utilizing the principle of protein-dye binding. *Analytical Biochemistry*, 72(1-2), 248-254.
- Cardenas, C. A. (2023). Review of boron-based compounds: Advancing cancer therapy and beyond. *Clinical Oncology: Case Reports* 6, 8, 2.
- Cole, S. T., Eiglmeier, K., Ahmed, S., Honore, N., Elmes, L., Anderson, W. F., & Weiner, J. H. (1988). Nucleotide sequence and gene-polypeptide relationships of the *glpABC* operon encoding the anaerobic sn-glycerol-3-phosphate dehydrogenase of *Escherichia coli* K-12. *Journal of Bacteriology*, 170(6), 2448-2456.
- Cummings, J. E., Lunde, C. S., Alley, M. R. K., & Slayden, R. A. (2023). Epetraborole, a leucyl-tRNA synthetase inhibitor, demonstrates murine efficacy, enhancing the *in vivo* activity of ceftazidime against *Burkholderia pseudomallei*, the causative agent of melioidosis. *PLOS Neglected Tropical Diseases*, 17(11), e0011795.
- Daley, D. O., Rapp, M., Granseth, E., Melén, K., Drew, D., & Von Heijne, G. (2005). Global topology analysis of the *Escherichia coli* inner membrane proteome. *Science*, 308(5726), 1321-1323.
- Dibek, E., Babayeva, A., Kürkcü, M. S., Çöl, N. A., & Çöl, B. (2020). Bor içeren bazı biyoaktif bileşikler. *Journal of Boron*, 5(1), 29-39.
- dos Santos, K. V., Diniz, C. G., de Castro Veloso, L., de Andrade, H. M., da Silva Giusta, M., da Fonseca Pires, S., ... & de Macêdo Farias, L. (2010). Proteomic analysis of *Escherichia coli* with experimentally induced resistance to piperacillin/tazobactam. *Research in Microbiology*, 161(4), 268-275.
- Egan, A. J., Errington, J., & Vollmer, W. (2020). Regulation of peptidoglycan synthesis and remodeling. *Nature Reviews Microbiology*, 18(8), 446-460.
- Ganapathy, U. S., Gengenbacher, M., & Dick, T. (2021). Epetraborole is active against *Mycobacterium abscessus*. *Antimicrobial Agents and Chemotherapy*, 65(10), 10-1128.
- Garoff, L., Huseby, D. L., Praski Alzirgat, L., & Hughes, D. (2018). Effect of aminoacyl-tRNA synthetase mutations on susceptibility to

- ciprofloxacin in *Escherichia coli*. *Journal of Antimicrobial Chemotherapy*, 73(12), 3285-3292.
- Gemmill, R. M., Wessler, S. R., Keller, E. B., & Calvo, J. M. (1979). leu operon of *Salmonella typhimurium* is controlled by an attenuation mechanism. *Proceedings of the National Academy of Sciences*, 76(10), 4941-4945.
- Goswami, M., & Narayana Rao, A. V. S. S. (2018). Transcriptome profiling reveals interplay of multifaceted stress response in *Escherichia coli* on exposure to glutathione and ciprofloxacin. *Msystems*, 3(1), 10-1128.
- Harayama, S., Bollinger, J., Iino, T., & Hazelbauer, G. L. (1983). Characterization of the mgl operon of *Escherichia coli* by transposon mutagenesis and molecular cloning. *Journal of Bacteriology*, 153(1), 408-415.
- Hatch, N. D., & Ouellette, S. P. (2020). Inhibition of tRNA synthetases induces persistence in Chlamydia. *Infection and Immunity*, 88(4), 10-1128.
- Hernandez, V., Crépin, T., Palencia, A., Cusack, S., Akama, T., Baker, S. J., ... & Plattner, J. J. (2013). Discovery of a novel class of boron-based antibacterials with activity against gram-negative bacteria. *Antimicrobial Agents and Chemotherapy*, 57(3), 1394-1403.
- Hurdle, J. G., O'Neill, A. J., & Chopra, I. (2005). Prospects for aminoacyl-tRNA synthetase inhibitors as new antimicrobial agents. *Antimicrobial Agents and Chemotherapy*, 49(12), 4821-4833.
- Irschik, H., Schummer, D., Gerth, K., Höfle, G., & Reichenbach, H. (1995). The tartrolons, new boron-containing antibiotics from a myxobacterium, *Sorangium cellulosum*. *The Journal of Antibiotics*, 48(1), 26-30.
- Ito, A., May, T., Kawata, K., & Okabe, S. (2008). Significance of rpoS during maturation of *Escherichia coli* biofilms. *Biotechnology and Bioengineering*, 99(6), 1462-1471.
- Jiang, H., Shang, L., Yoon, S. H., Lee, S. Y., & Yu, Z. (2006). Optimal production of poly- γ -glutamic acid by metabolically engineered *Escherichia coli*. *Biotechnology Letters*, 28, 1241-1246.
- Keseler, I. M., Collado-Vides, J., Gama-Castro, S., Ingraham, J., Paley, S., Paulsen, I. T., ... & Karp, P. D. (2005). EcoCyc: a comprehensive database resource for *Escherichia coli*. *Nucleic Acids Research*, 33(suppl_1), D334-D337.
- Kim, T., Hanh, B. T. B., Heo, B., Quang, N., Park, Y., Shin, J., ... & Jang, J. (2021). A screening of the mmv pandemic response box reveals epetraborole as a new potent inhibitor against mycobacterium abscessus. *International Journal of Molecular Sciences*, 22(11), 5936.
- Kitagawa, M., Ara, T., Arifuzzaman, M., Ioka-Nakamichi, T., Inamoto, E., Toyonaga, H., & Mori, H. (2005). Complete set of ORF clones of *Escherichia coli* ASKA library (A Complete Set of *E. coli* K-12 ORF Archive): Unique resources for biological research. *DNA Research*, 12(5), 291-299.
- Kohno, J., Kawahata, T., Otake, T., Morimoto, M., Mori, H., Ueba, N., ... & Kawashima, K. (1996). Boromycin, an anti-HIV antibiotic. *Bioscience, Biotechnology and Biochemistry*, 60(6), 1036-1037.
- Linton, K. J., & Higgins, C. F. (1998). The *Escherichia coli* ATP-binding cassette (ABC) proteins. *Molecular Microbiology*, 28(1), 5-13.
- Mendes, R. E., Alley, M. R. K., Sader, H. S., Biedenbach, D. J., & Jones, R. N. (2013). Potency and spectrum of activity of AN3365, a novel boron-containing protein synthesis inhibitor, tested against clinical isolates of Enterobacteriaceae and nonfermentative Gram-negative bacilli. *Antimicrobial Agents and Chemotherapy*, 57(6), 2849-2857.
- Mering, C. V., Huynen, M., Jaeggi, D., Schmidt, S., Bork, P., & Snel, B. (2003). STRING: a database of predicted functional associations between proteins. *Nucleic Acids Research*, 31(1), 258-261.
- Metcalf, W. W., Steed, P. M., & Wanner, B. L. (1990). Identification of phosphate starvation-inducible genes in *Escherichia coli* K-12 by DNA sequence analysis of psi::lacZ (Mu d1) transcriptional fusions. *Journal of Bacteriology*, 172(6), 3191-3200.
- Milija, J., Lilic, M., Janjusevic, R., Jovanovic, G., & Savic, D. J. (1999). tRNA synthetase mutants of *Escherichia coli* K-12 are resistant to the gyrase inhibitor novobiocin. *Journal of Bacteriology*, 181(9), 2979-2983.
- Monteferrante, C. G., Jirgensons, A., Varik, V., Hauryliuk, V., Goessens, W. H. F., & Hays, J. P. (2016). Evaluation of the characteristics of leucyl-tRNA synthetase (LeuRS) inhibitor AN3365 in combination with different antibiotic classes. *European Journal of Clinical Microbiology & Infectious Diseases*, 35, 1857-1864.
- Nakamura, H., Iitaka, Y., Kitahara, T., Okazaki, T., & Okami, Y. (1977). Structure of aplasmomycin. *The Journal of Antibiotics*, 30(9), 714-719.
- Nguyen, T. Q., Heo, B. E., Hanh, B. T. B., Jeon, S., Park, Y., Choudhary, A., ... & Jang, J. (2023). DS86760016, a Leucyl-tRNA Synthetase Inhibitor, Is Active against *Mycobacterium abscessus*. *Antimicrobial Agents and Chemotherapy*, 67(6), e01567-22.
- NIH, (2024). Official Website of National Institutes of Health, <https://david.ncifcrf.gov/tools.jsp>, Last accessed on March 30, 2024
- Novikova, M., Metlitskaya, A., Datsenko, K., Kazakov, T., Kazakov, A., Wanner, B., & Severinov, K. (2007). The *Escherichia coli* Yej transporter is required for the uptake of translation inhibitor microcin C. *Journal of Bacteriology*, 189(22), 8361-8365.
- Paley, S., Parker, K., Spaulding, A., Tomb, J. F., O'Maille, P., & Karp, P. D. (2017). The Omics Dashboard for interactive exploration of gene-expression data. *Nucleic Acids Research*, 45(21), 12113-12124.
- Pavoncello, V., Barras, F., & Bouveret, E. (2022). Degradation of exogenous fatty acids in *Escherichia coli*. *Biomolecules*, 12(8), 1019.
- Pistocchi, R., Kashiwagi, K., Miyamoto, S., Nukui, E., Sadakata, Y., Kobayashi, H., & Igarashi, K. (1993). Characteristics of the operon for a putrescine transport system that maps at 19 minutes on the *Escherichia coli* chromosome. *Journal of Biological Chemistry*, 268(1), 146-152.
- Saier Jr, M. H., Reddy, V. S., Tsu, B. V., Ahmed, M. S., Li, C., & Moreno-Hagelsieb, G. (2016). The transporter classification database (TCDB): recent advances. *Nucleic Acids Research*, 44(D1), D372-D379.
- Schirmer, A., & Kolter, R. (1998). Computational analysis of bacterial sulfatases and their modifying enzymes. *Chemistry & Biology*, 5(8), R181-R186.
- Scholle, A., Vreemann, J., Blank, V., Nold, A., Boos, W., & Manson, M. D. (1987). Sequence of the mglB gene from *Escherichia coli* K12: comparison of wild-type and mutant galactose chemoreceptors. *Molecular and General Genetics MGG*, 208, 247-253.
- Seong, W., Han, G. H., Lim, H. S., Baek, J. I., Kim, S. J., Kim, D., ... & Lee, D. H. (2020). Adaptive laboratory evolution of *Escherichia coli* lacking cellular by product formation for enhanced acetate utilization through compensatory ATP consumption. *Metabolic Engineering*, 62, 249-259.
- Shafiee, A., & Chanda, S. (2024). *In vitro* evaluation of drug-drug interaction potential of epetraborole, a novel bacterial leucyl-trna synthetase inhibitor. *Pharmaceuticals*, 17(1), 120.
- Sivasankar, S., Premnath, M. A., Boppe, A., Grobusch, M. P., & Jeyaraj, S. (2023). Screening of MMV pandemic response and pathogen box compounds against pan-drug-resistant *Klebsiella pneumoniae* to identify potent inhibitory compounds. *New Microbes and New Infections*, 55, 101193.
- Soo, V. W., Hanson-Manful, P., & Patrick, W. M. (2011). Artificial gene amplification reveals an abundance of promiscuous resistance determinants in *Escherichia coli*. *Proceedings of the National Academy of Sciences*, 108(4), 1484-1489.
- Sporing, A. L., Vulic, M., & Lewis, K. (2006). GlpD and PlsB participate in persister cell formation in *Escherichia coli*. *Journal of Bacteriology*, 188(14), 5136-5144.
- Stieglitz, B. I., & Calvo, J. M. (1974). Distribution of the isopropylmalate pathway to leucine among diverse bacteria. *Journal of Bacteriology*, 118(3), 935-941.
- STRING, (2024). Official Website of String, <https://string-db.org/>, Last accessed on March 30, 2024.
- Snel, B., Lehmann, G., Bork, P., & Huynen, M. A. (2000). STRING: a web-server to retrieve and display the repeatedly occurring neighbourhood of a gene. *Nucleic Acids Research*, 28(18), 3442-3444.
- Sullivan, J. R., Lupien, A., Kalthoff, E., Hamela, C., Taylor, L., Munro, K. A., .. & Behr, M. A. (2021). Efficacy of epetraborole against *Mycobacterium abscessus* is increased with norvaline. *PLoS Pathogens*, 17(10), e1009965.
- Sun, H., Wang, M., Liu, Y., Wu, P., Yao, T., Yang, W., ... & Yang, B. (2022). Regulation of flagellar motility and biosynthesis in enterohemorrhagic *Escherichia coli* O157: H7. *Gut Microbes*, 14(1), 2110822.
- Vinella, D., Joseleau-Petit, D., Thévenet, D., Bouloc, P., & D'Ari, R. (1993). Penicillin-binding protein 2 inactivation in *Escherichia coli* results in cell division inhibition, which is relieved by FtsZ overexpression. *Journal of Bacteriology*, 175(20), 6704-6710.
- Wessler, S. R., & Calvo, J. M. (1981). Control of leu operon expression in *Escherichia coli* by a transcription attenuation mechanism. *Journal of Molecular Biology*, 149(4), 579-597.
- Xu, C., Lin, X., Ren, H., Zhang, Y., Wang, S., & Peng, X. (2006). Analysis

of outer membrane proteome of *Escherichia coli* related to resistance to ampicillin and tetracycline. *Proteomics*, 6(2), 462-473.
Zhao, Q., Wu, Y., Li, B., He, L., Sun, J., Pang, X., ... & Li, X. (2023). OmpA





is involved in the early response of *Escherichia coli* to antibiotics as a Hub outer membrane protein. *Applied Biochemistry and Microbiology*, 59(5), 608-621.

Cite as: Babayeva, A., Dibek, E., Sunnetci Akkoyunlu, D., Cine, N., Kasap, M., Akpınar, G., & Col, B. (2024). The effect of epetraborole on the transcriptome and proteome profiles of an *Escherichia coli* strain overexpressing *leuS*, Leucyl-tRNA Synthetase. *Front Life Sci RT*, 5(1), 48-58.



Research article

Impact of the COVID-19 pandemic on pharmacy students: A comprehensive survey

Ahmet Canbaz¹ , Harika Oyku Dinc^{*1} , Aysenur Kilic² , Bekir Kocazeybek³ ,
Gulactı Topcu⁴ 

¹ Bezmialem Vakıf University, Faculty of Pharmacy, Department of Pharmaceutical Microbiology, 34093, Istanbul, Türkiye

² Bezmialem Vakıf University, Faculty of Pharmacy, Department of Pharmaceutical Technology, 34093, Istanbul, Türkiye

³ Istanbul University, Cerrahpaşa Medical Faculty, Department of Medical Microbiology, 34098, Istanbul, Türkiye

⁴ Bezmialem Vakıf University, Faculty of Pharmacy, Department of Pharmacognosy, 34093, Istanbul Türkiye

Abstract

The COVID-19 pandemic has caused numerous changes in all aspects of human life and behavior, especially in the education system. Because of these reasons, our study aimed to evaluate the approaches and attitudes of pharmacy faculty students to the COVID-19 pandemic as a survey study. This study is an analytical cross-sectional study. It was conducted with the online questionnaire technique. The questionnaire form consists of 5 different sections, and the participants were asked questions aiming to determine the level of knowledge, behavioral patterns, and approaches to online education of pharmacy faculty students against the COVID-19 pandemic, along with socio-demographic questions. 151 pharmacy students, 99 (65.6%) female and 52 (34.4%) male, participated in our study. When the participants with COVID-19 infection were asked about their post-infection approach, 31 (50%) of the participants stated that "no change in the ways of protection", 20 (32.3%) felt the need for more protection, and 11 (17.7%) also announced that he had loosened the protection measures. It has been shown that there is an increase in students' anxiety during the pandemic. In addition, it was determined that a high rate of vaccination and vaccines were relied upon. Our data show that the COVID-19 pandemic has brought about some changes in the attitudes and behaviors of pharmacy students. Time will tell the long-term results of this study, in which we showed how these changes caused by the pandemic affect pharmacy students in the short term.

Keywords: COVID-19; pandemic effect; pharmacy students; survey

1. Introduction

It was understood that the source of the epidemic, which started in December 2019 with pneumonia of unknown etiology and associated with the seafood and wet animal market in Wuhan, China, is a new type of coronavirus. The disease caused by the virus, called severe acute respiratory syndrome coronavirus-2 (SARS-CoV-2) by the International Committee on Taxonomy of Viruses, has been defined as "coronavirus disease-2019" (COVID-19) by the World Health Organization

(WHO) (Jiang et al., 2020). With the rapid spread of SARS-CoV-2 to many countries of the world and the increase in deaths due to COVID-19 cases, WHO declared the COVID-19 epidemic as a pandemic on 12th March 2020 (WHO, 2020a). The COVID-19 pandemic, caused by the SARS-CoV-2, maintains high morbidity and mortality worldwide (Chen et al., 2024). As of February 4, 2024, worldwide; 774,593,066 confirmed cases of SARS-CoV-2 infection were reported, resulting in 7,028,881 deaths (WHO, 2024). As stated in the guidelines of WHO, Centers for Disease Control and Prevention

* Corresponding author.

E-mail address: harikaoykudinc@gmail.com (H. O. Dinc).

<https://doi.org/10.51753/flsrt.1378523> Author contributions

Received 19 October 2023; Accepted 19 March 2024

Available online 30 April 2024

2718-062X © 2024 This is an open access article published by Dergipark under the [CC BY](https://creativecommons.org/licenses/by/4.0/) license.

(CDC), and T.C. Ministry of Health, the most effective protection method is the mask, social distancing, and hand hygiene (WHO, 2020b; CDC, 2022; Turkish Republic Ministry of the Health, 2022; Erkencioglu et al., 2023). However, it is seen that compliance with the prevention methods in society has decreased in the time approaching two years and with the confidence given by the vaccination. However, the COVID-19 pandemic has caused numerous changes in all aspects of human life and behavior, especially in the education system. In a study conducted at Hokkaido University, when three education types (face-to-face, online and mixed) were investigated on medical school students during COVID-19, the online/mixed education method produced better academic results compared to face-to-face education (Goudarzi et al., 2024). In another study investigating the effects of the COVID-19 pandemic on the mental health of nursing students, the negative effects of the pandemic in terms of mental health were mentioned (Jardon and Choi, 2024). In this context, our study aimed to evaluate the approaches and attitudes of Bezmialem Vakıf University Faculty of Pharmacy students to the COVID-19 pandemic as a survey study. In addition to demographic data, the survey includes questions about the sources and level of students' access to information about the COVID-19 pandemic, their anxiety and stress status, their approach to COVID-19 vaccines, and their thoughts on education during the pandemic period, and it is aimed to answer all the questions of pharmacy students.

2. Materials and methods

This study is an analytical type of cross-sectional study conducted with the questionnaire application technique on the online platform. Our study was carried out between 03 March-30 April 2022 at Bezmialem Vakıf University (BVU), Faculty of Pharmacy. It is designed to cover all grade students. Since our study is based on volunteerism, the volunteers who participated in the survey were included in the study. During the application phase of the questionnaire, it was ensured that the text regarding the purpose of the study and confidentiality principles was included before the volunteers answered the questions. The identity information of the volunteers and the questions that would reveal their identities were not included in the questionnaires. Care was taken not to direct the patients to respond positively or negatively to the statements in the data collection forms.

Along with the demographic data of the students (age, gender, class, COVID-19 history), their attitudes and behaviors related to the pandemic process, their attitudes and behaviours regarding the vaccine, and their views on education during the pandemic period were evaluated. During the evaluation, the students were asked to mark the appropriate option among the options "strongly disagree", "disagree", "undecided", "agree", and "strongly agree".

Statistical analysis was done with IBM SPSS 20.0 (IBM Corp., Armonk, NY, USA) package program and Microsoft Excel version 2013. In the analysis of the collected data, frequency (n), percentage (%), and mean values were determined. This study was approved by the Ministry of Health's COVID-19 Scientific Research Evaluation Commission on 25/12/2021. Ethics committee approval of the study was obtained with the decision dated 02.03.2022 and numbered 53294 by T.C. BVU, Non-Interventional Research Ethics Committee. The informed consent form was obtained during the study.

3. Results

A total of 151 pharmacy students, 99 (65.6%) female, and 52 (34.4%) male, were included in our study. The demographic data of the participants and their distribution by period are shown in Table 1. When the participants with COVID-19 infection were asked about their post-infection approach, 29 (51.7%) of the participants stated that there was no change in the ways of protection, 18 (32.2%) felt the need for more protection, 9 (16.1%) announced that he had loosened the protection measures. When participants want to get the most up-to-date information about the COVID-19 pandemic, the most frequently referenced source is the T.C. Ministry of Health (n:119, 78.8%) (Fig.).

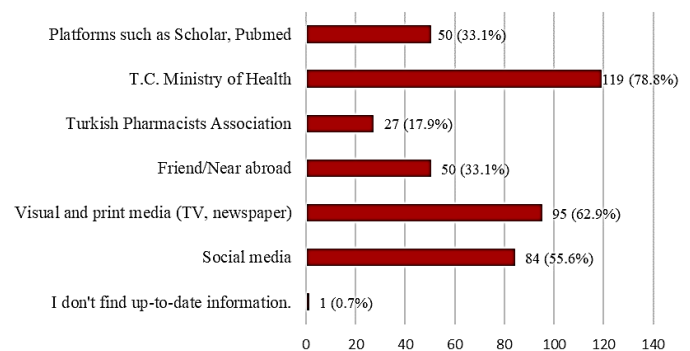


Fig. Where do you find up-to-date information about COVID-19? (151 Answers).

Table 1

Demographic data and COVID-19 history of volunteers participating in the study.

| Demographic Data | n (%) |
|---|------------|
| Gender | |
| Female | 99 (65.6%) |
| Male | 52 (34.4%) |
| Age (mean ± SD) | 21 |
| Class | |
| Term I | 49 (32.5%) |
| Term II | 18 (11.5%) |
| Term III | 13 (8.6%) |
| Term IV | 29 (19.2%) |
| Term V | 42 (27.5%) |
| COVID-19 History and Severity (n:56) | |
| Mild | 29 (51.7%) |
| Moderate | 24 (42.9%) |
| Severe | 3 (5.4%) |
| Family history of COVID-19 (n:83) | |
| Mother | 27 (32.1%) |
| Father | 20 (23.8%) |
| Sibling | 21 (25%) |
| Other | 15 (22.1%) |

3.1. Attitudes and behaviors related to the pandemic

43 (28.5%) of the participants stated that the virus originated from the laboratory, 82 (54.2%) stated that the new variants formed as a result of the SARS-CoV-2 mutation worried them, 80 (53%) stated that they were concerned about contracting COVID-19, 122 (80.8%) stated that they were afraid of losing their relatives during the pandemic process, 115 (76.1%) stated that the pandemic process caused their stress levels to increase, 43 (28.4%) stated that they had difficulty in

Table 2

Questions and answers in the section on attitudes and behaviors related to the pandemic process.

| | Strongly Disagree | Disagree | Undecided | Agree | Strongly Agree |
|--|-------------------|------------|------------|------------|----------------|
| I think the SARS-CoV-2 virus originated in the laboratory. | 15(9.9%) | 44 (29.1%) | 49 (32.5%) | 33 (21.9%) | 10 (6.6%) |
| The new variants resulting from the SARS-CoV-2 mutation worry me. | 7 (4.6%) | 23 (15.2%) | 39 (25.8%) | 72 (47.7%) | 10 (6.6%) |
| I am worried about contracting COVID-19. | 16 (10.6%) | 24 (15.9%) | 31 (20.5%) | 71 (47%) | 9 (6%) |
| I am afraid of losing my relatives during the pandemic process. | 6 (4%) | 11 (7.3%) | 12 (7.9%) | 85 (56.3%) | 37 (24.5%) |
| The pandemic process has caused the stress level to increase. | 6 (4%) | 12 (7.9%) | 18 (11.9%) | 47 (31.1%) | 68 (45%) |
| I'm having trouble keeping up with current data on the pandemic. | 12 (7.9%) | 52 (34.4%) | 44 (29.1%) | 36 (23.8%) | 7 (4.6%) |
| I do not follow the prominent new information about the pandemic. | 16 (10.6%) | 70 (46.4%) | 36 (23.8%) | 24 (15.9%) | 5 (3.3%) |
| Even if the COVID-19 pandemic ends, I think we will experience similar pandemic processes in the coming years. | 2 (1.3%) | 10 (6.6%) | 35 (23.2%) | 80 (53%) | 24 (15.9%) |

Table 3

Questions and answers in the section on attitudes and behaviors related to the COVID-19 vaccine.

| | Strongly Disagree | Disagree | Undecided | Agree | Strongly Agree |
|---|-------------------|------------|------------|------------|----------------|
| I felt safe after getting vaccinated. | 5 (3.3%) | 24 (15.9%) | 33 (21.9%) | 68 (45%) | 21 (13.9%) |
| After getting vaccinated, I was able to move safely in eating and drinking places, indoor areas, and public transportation. | 16 (10.6%) | 34 (22.5%) | 35 (23.2%) | 56 (37.1%) | 10 (6.6%) |
| After getting vaccinated, I continue to pay attention to my hand hygiene. | 2 (1.3%) | 11 (7.3%) | 17 (11.3%) | 72 (47.7%) | 49 (32.5%) |
| After getting vaccinated, I also continue to pay attention to the use of masks. | 3 (2%) | 23 (15.2%) | 16 (10.6%) | 61 (40.4%) | 48 (31.8%) |
| After getting vaccinated, I also pay attention to social distance. | 4 (2.6%) | 31 (20.5%) | 22 (14.6%) | 55 (36.4%) | 39 (25.8%) |
| After getting vaccinated, my social life normalized. | 20 (13.2%) | 48 (31.8%) | 47 (31.1%) | 28 (18.5%) | 8 (5.3%) |
| I think vaccines save lives in the fight against the pandemic. | 4 (2.6%) | 5 (3.3%) | 25 (16.6%) | 80 (53%) | 37 (24.5%) |
| I can have the reminder dose vaccine at the time intervals recommended by the ministry. | 7 (4.6%) | 9 (6%) | 42 (27.8%) | 67 (44.4%) | 26 (17.2%) |
| I trust COVID-19 vaccines. | 5 (3.3%) | 10 (6.6%) | 43 (28.5%) | 74 (49%) | 19 (12.5%) |
| I encourage people around me to get vaccinated. | 3 (2%) | 15 (9.9%) | 52 (34.4%) | 55 (36.4%) | 26 (17.2%) |

Table 4

Questions and answers in the education status section during the pandemic process.

| | Strongly Disagree | Disagree | Undecided | Agree | Strongly Agree |
|---|-------------------|------------|------------|------------|----------------|
| I think it was the right decision to close universities at the beginning of the pandemic. | 8 (5.3%) | 17 (11.3%) | 17 (11.3%) | 37 (25.2%) | 71 (47%) |
| I think that the process of opening universities in the pandemic took longer than I expected. | 68 (45%) | 17 (11.3%) | 16 (10.6%) | 68 (45%) | 45 (29.8%) |
| I think the pandemic has negatively affected my university life. | 4 (2.6%) | 10 (6.6%) | 15 (9.9%) | 52 (34.4%) | 70 (46.4%) |
| I think that academicians easily adapt to the online education process. | 16 (10.6%) | 43 (28.5%) | 58 (38.4%) | 27 (17.9%) | 7 (4.6%) |
| I think that students adapt easily to the online education process. | 31 (20.5%) | 54 (35.8%) | 37 (24.5%) | 23 (15.2%) | 6 (4%) |
| I think that online education is more efficient in theoretical courses. | 40 (26.5%) | 44 (29.1%) | 40 (26.5%) | 18 (11.9%) | 9 (6%) |
| I think that theoretical lessons should be given as online education after the pandemic. | 45 (29.8%) | 42 (27.8%) | 40 (26.5%) | 16 (10.6%) | 8 (5.3%) |
| I find it risky to continue face-to-face education during the pandemic process. | 24 (15.9%) | 51 (33.8%) | 44 (29.1%) | 25 (16.6%) | 7 (4.6%) |
| During the pandemic process, I pay great attention to personal protection precautions (mask, distance, hygiene) in face-to-face education conditions. | 3 (2%) | 3 (2%) | 16 (10.6%) | 97 (64.2%) | 32 (21.2%) |

following the current data about the pandemic, 29 (19.2%) stated that they did not follow the prominent new information about the pandemic, 104 (68.9%) stated that they think that similar pandemic processes will occur in the coming years even if the COVID-19 pandemic ends, 63 (41.7%) of the participants stated that the use of masks should continue until the number of active cases is reset all over the world, while 58 (38.4%) stated that the use of masks should continue only in closed areas. Opinions about this subsection are presented in Table 2.

3.2. Vaccination-related attitudes and behaviors

It was determined that 146 (96.7%) of the participants were vaccinated against COVID-19, and the remaining 5 participants were not vaccinated because they had just had the infection. 89 (58.9%) of the participants stated that they felt safe after being vaccinated, 66 (43.7%) stated that they could move safely in eating and drinking places, indoor areas, and public transportation after vaccination, 121 (80.2%) stated that they pay

attention to hand hygiene even after vaccination, 109 (72.2%) stated that they continue to use masks even after vaccination, 94 (62.2%) stated that they pay attention to social distance as well after vaccination, 36 (23.8%) stated that their social life normalized after vaccination, 117 (77.5%) stated that the vaccines were life-saving, 93 (61.6%) stated that they could receive a reminder dose at the time intervals recommended by the ministry and that they trusted the COVID-19 vaccines, 81 (53.6%) stated that they encouraged vaccination of the people around them. Opinions about this subsection are presented in Table 3.

3.3. Education status during the pandemic process

109 (72.2%) of the participants stated that it was the right decision to close the universities at the beginning of the pandemic, 113 (74.8%) stated that the opening of universities took longer than they expected, 122 (80.8%) stated that the pandemic had a negative impact on their university life, 34 (22.5%) stated that academicians easily adapt to the online education process, 29 (19.2%) stated that students easily adapt to the online education process, 27 (17.9%) stated that online education is more efficient in theoretical courses, 24 (15.9%) stated that the theoretical courses should be given as online training after the pandemic, 32 (21.2%) stated that they found it risky to continue face-to-face education during the pandemic process, 129 (85.4%) of the participants stated that they paid great attention to personal protection measures (mask, distance, hygiene) in face-to-face training conditions during the pandemic process (Table 4).

4. Discussion

The COVID-19 pandemic has brought serious educational and social repercussions, including the closure of university campuses and the transition to online learning at universities. University students had to forego the social advantages of the “university experience” (i.e. social gatherings, group work, and face-to-face lectures and meetings) as well as face-to-face education. This study presents the perspectives of pharmacy students regarding the pandemic and education during a period when the devastating effects of the COVID-19 epidemic were felt, and face-to-face education was cancelled.

According to UNESCO data, schools were partially or completely closed in 45 countries until 11 March 2020, after the World Health Organization decided on an epidemic on March 11, between March 12 and April 10, there was a period in which school closures on a national scale peaked all over the world (UNICEF, 2022). After the first case was reported in Turkey on March 11, 2020, face-to-face education was interrupted for approximately 1.5 years. When the results in the first part of our study are evaluated, it is seen that the students have a high level of anxiety. Similarly, in a study conducted at the University of Vermont in the USA, it was shown that there are permanent negative effects on the behavioral and emotional functions of students during the pandemic process (Copeland et al., 2021). At the same time, it has been shown that the findings they obtained are compatible with studies conducted among students who experienced natural disasters (Gutierrez et al., 2005; Davis et al., 2010; Carter et al., 2014; Copeland et al., 2021). In a study conducted among nursing students, it was stated that many unusual new developments experienced during the pandemic process increased the stress level of students (Aslan and Pekince,

2021). During the time of the COVID-19 pandemic in the UK, especially with restrictions, students reported that they felt their mental health was affected “quite a lot” or “really a lot”, with 70% of respondents reporting that they were concerned about contracting the virus. However, participants also reported that their family members were worried about contracting the virus (Evans et al., 2021). In a study reported by Peru, nursing and pharmacy students reportedly affected the mental health of the COVID-19 epidemic (Horton et al., 2024). When our data on attitudes and behaviors related to the pandemic are evaluated, it is seen that students from different countries and different departments have the same anxiety and concern.

Since there is no effective treatment in combating SARS-CoV-2 infection, vaccines based on many different techniques have been developed recently for prevention. Among them, vaccines based on mRNA technology were used for the first time in the COVID-19 pandemic, and it brought along various discussions. In our study, it is seen that 96.7% of our students preferred to be vaccinated, and 53% of them contributed to public health by stating that they encouraged their relatives to be vaccinated. In a study conducted among students in China, it was reported that 87.4% accepted the COVID-19 vaccine and 10.1% of the participants had a change in their attitudes after vaccination (Li et al., 2022). In our study, it is seen that our vaccination rate is higher than those reported by students in some other countries such as Japan (69.8%), Egypt (34.9%), and Jordan (28.8%), however, it is seen that our vaccination rate is close to Saudi Arabia (83.6%) and Italy (86.1%) (Barello et al., 2020; Bari et al., 2021; Bou Hamdan et al., 2021; Saied et al., 2021; Sallam et al., 2021; Khalafalla et al., 2022; Tsutsumi et al., 2022). Regardless of the student population, the vaccine acceptance rate appears to vary around the world. We think that this difference may be due to cultural backgrounds, teaching habits, government policies, social environments, and other potential factors.

During the pandemic period, online education was started at our university on March 19, 2020, and before the pandemic, students had never experienced online education. Although the students of our faculty supported the universities to take a break from face-to-face education during the pandemic process, they stated that both academicians and they had difficulties in adapting to this process. However, despite the increasing digitalization in the current period, it is remarkable that students still prefer traditional education. In some studies, it has been reported that the online education experience is not suitable for most medical students due to limitations related to technology, and the traditional face-to-face teaching method is preferred for various reasons (Sindiani et al., 2020; Samannodi et al., 2022). Considering that intensive laboratory practices are also included in pharmacy education, it is understandable that faculty students prefer face-to-face education.

5. Conclusion

Due to factors such as the increase in the world population, increased human mobility, and climate change, new pandemics are expected to occur in the following processes. In this context, the experiences and data obtained in the COVID-19 pandemic that started in 2019 are quite significant. The results of our study are important in terms of addressing the education preferences, stress levels, preferred sources of information, and approaches to vaccines of the pharmacist candidates, who will be at the forefront of the struggle against pandemics, during the COVID-

19 pandemic. We think that careful monitoring of the stress levels and demands of pharmacy faculty students, who are the public health soldiers of the future, is of critical significance in terms of protecting both their own and the public's health.

Acknowledgments: The authors would like to thank all participants for their contributions to the paper.

Conflict of interest: The authors declare that they have no

References

- Aslan, H., & Pekince, H. (2021). Nursing students' views on the COVID-19 pandemic and their perceived stress levels. *Perspectives in Psychiatric Care*, 57(2), 695.
- Barello, S., Nania, T., Dellafiore, F., Graffigna, G., & Caruso, R. (2020). 'Vaccine hesitancy' among university students in Italy during the COVID-19 pandemic. *European Journal of Epidemiology*, 35(8), 781.
- Bari, M. S., Hossain, M. J., Ahmmmed, F., Sarker, M. M. R., Khandokar, L., Chaithy, A. P., ... & Mohamed, I. N. (2021). Knowledge, perception, and willingness towards immunization among Bangladeshi population during COVID-19 vaccine rolling period. *Vaccines*, 9(12), 1449.
- Bou Hamdan, M., Singh, S., Polavarapu, M., Jordan, T. R., & Melhem, N. M. (2021). COVID-19 vaccine hesitancy among university students in Lebanon. *Epidemiology and Infection*, 149, e242.
- Carter, F., Bell, C., Ali, A., McKenzie, J., & Wilkinson, T. (2014). The impact of major earthquakes on the psychological functioning of medical students: a Christchurch, New Zealand study. *The New Zealand Medical Journal*, 127(1398), 54-66.
- CDC. (2022). Infection Control Guidance for Healthcare Professionals about Coronavirus (COVID-19), https://www.cdc.gov/coronavirus/2019-ncov/index.html?CDC_AA_refVal=https%3A%2F%2Fwww.cdc.gov%2Fcoronavirus%2F2019-ncov%2Fhcp%2Finfection-control.html, Last Accessed on August 7, 2023.
- Chen, Y. H., Lee, C. Y., Cheng, H. Y., Chen, C. M., Cheuh, Y. N., Lee, C. L., & Kuo, H. W. (2024). Risk factors and mortality of SARS-CoV-2 reinfection during the Omicron era in Taiwan: A nationwide population-based cohort study. *Journal of Microbiology, Immunology and Infection*, 57(1), 30-37.
- Copeland, W. E., McGinnis, E., Bai, Y., Adams, Z., Nardone, H., Devadanam, V., Rettew, J., & Hudziak, J. J. (2021). Impact of COVID-19 pandemic on college student mental health and wellness. *Journal of the American Academy of Child and Adolescent Psychiatry*, 60(1), 134-141.e2.
- Davis, T. E., Grills-Tauchel, A. E., & Ollendick, T. H. (2010). The psychological impact from Hurricane Katrina: effects of displacement and trauma exposure on university students. *Behavior Therapy*, 41(3), 340-349.
- Erkencioglu, B. N., Zuhail, M., Tokel, D., & Ozyigit, I. I. (2023). Worldwide cotton production and trade during COVID-19 pandemic: An empirical analysis for a three-year observation. *Notulae Botanicae Horti Agrobotanici Cluj-Napoca*, 51(4), 13341-13341.
- Evans, S., Alkan, E., Bhangoo, J. K., Tenenbaum, H., & Ng-Knight, T. (2021). Effects of the COVID-19 lockdown on mental health, wellbeing, sleep, and alcohol use in a UK student sample. *Psychiatry Research*, 298.
- Goudarzi, H., Onozawa, M., & Takahashi, M. (2024). Impact of the Covid-19 pandemic and ensuing online teaching on pre-clinical medical education. *BMC Medical Education*, 24(1), 66.
- Gutierrez, D., Hollister, D., & Beninati, A. (2005). Hurricane madness: Teaching, learning and the importance of flexibility in the wake of disaster. *Journal of College Teaching & Learning (TLC)*, 2(2), 49.
- Horton, A. G., Chalco, E. F., Cuellar, M., Paredes, G. I. M., & Cuellar, N. (2024). Impact of COVID-19 on depression, anxiety, stress, coping, and grief in pre-health professional students in Lima, Peru. *Hispanic Health Care International: The Official Journal of The National Association of Hispanic Nurses*, 22(1), 46-55.
- Jardon, C., & Choi, K. R. (2024). COVID-19 Experiences and mental health conflict of interests.
- Informed consent:** This study was approved by the Ministry of Health's COVID-19 Scientific Research Evaluation Commission on 25/12/2021. Ethics committee approval of the study was obtained with the decision dated 02.03.2022 and numbered 53294 by T.C. Bezmialem Vakif University (BVU), Non-Interventional Research Ethics Committee.
- among graduate and undergraduate nursing students in Los Angeles. *Journal of the American Psychiatric Nurses Association*, 30(1), 86-94.
- Jiang, S., Shi, Z., Shu, Y., Song, J., Gao, G. F., Tan, W., & Guo, D. (2020). A distinct name is needed for the new coronavirus. *The Lancet*, 395(10228), 949.
- Khalafalla, H. E., Tumabeng, M. Z., Halawi, M. H. A., Masmali, E. M. A., Tashari, T. B. M., Arishi, F. H. A., ... & Mahfouz, M. S. (2022). COVID-19 vaccine hesitancy prevalence and predictors among the students of Jazan University, Saudi Arabia using the health belief model: a Cross-Sectional Study. *Vaccines*, 10(2), 289.
- Li, S., Gao, Z., Zhong, M., Yu, Z., Li, J., & Bi, H. (2022). Chinese University Students' awareness and acceptance of the COVID-19 vaccine: A cross-sectional study. *Risk Management and Healthcare Policy*, 15, 845-864.
- Saied, S. M., Saied, E. M., Kabbash, I. A., & Abdo, S. A. E. F. (2021). Vaccine hesitancy: Beliefs and barriers associated with COVID-19 vaccination among Egyptian medical students. *Journal of Medical Virology*, 93(7), 4280.
- Sallam, M., Dababseh, D., Eid, H., Hasan, H., Taim, D., Al-Mahzoum, K., ... & Mahafzah, A. (2021). Low COVID-19 vaccine acceptance is correlated with conspiracy beliefs among university students in Jordan. *International Journal of Environmental Research and Public Health*, 18(5), 2407.
- Samannodi, M., Bulkhi, A., Alwafi, H., Bukhari, R., Salawati, E., Hafiz, B., ... & Almatrafi, M. A. (2022). Impact of Covid-19 pandemic on medical education: a cross-sectional study in the western region of Saudi Arabia. *Advances in Medical Education and Practice*, 13, 741-754.
- Sindiani, A. M., Obeidat, N., Alshdaifat, E., Elsalem, L., Alwani, M. M., Rawashdeh, H., ... & Tawalbeh, L. I. (2020). Distance education during the COVID-19 outbreak: A cross-sectional study among medical students in North of Jordan. *Annals of Medicine and Surgery*, 59, 186-194.
- Tsutsumi, S., Maeda, N., Tashiro, T., Arima, S., Mizuta, R., Fukui, K., ... & Urabe, Y. (2022). Willingness to receive the COVID-19 vaccination and the psychological state of Japanese University Students: a Cross-Sectional Study. *International Journal of Environmental Research and Public Health*, 19(3), 1654.
- Turkish Republic Ministry of the Health, (2022). COVID-19 Salgin Yonetimi ve Calisma Rehberi, <https://covid19.saglik.gov.tr/TR-66393/covid-19-salgin-yonetimi-ve-calisma-rehberi.html>, Last Accessed on August 7, 2023.
- UNICEF, (2022). Situation Analysis - COVID-19 and Education | UNICEF South Asia, <https://www.unicef.org/rosa/situation-analysis-covid-19-and-education>, Last Accessed on August 7, 2023.
- WHO, (2020a). Coronavirus Disease 2019 (COVID-19) Situation Report 51, https://www.who.int/docs/default-source/coronaviruse/situation-reports/20200311-sitrep-51-covid-19.pdf?sfvrsn=1ba62e57_10, Last Accessed on March 11, 2024.
- WHO, (2020b). WHO Director-General's opening remarks at the Mission briefing on COVID-19 - 12 March 2020, <https://www.who.int/director-general/speeches/detail/who-director-general-s-opening-remarks-at-the-mission-briefing-on-covid-19---12-march-2020>, Last Accessed on August 7, 2023.
- WHO, (2024). Coronavirus Disease (COVID-19) Situation Reports. <https://data.who.int/dashboards/covid19/cases?n=c>, Last Accessed on February 4, 2024.

Cite as: Dinc, H. O., Canbaz, A., Kilic, A., Kocazeybek, B., & Topcu, G. (2024). Impact of the COVID-19 pandemic on pharmacy students: A comprehensive survey. *Front Life Sci RT*, 5(1), 59-64.



Research article

Effects of keratin6/16 heterodimer on diabetic wound healing treatment with topical metformin

Fatma Kubra Tombulturk*¹ ¹ *Istinye University, Vocational School of Health Services, Department of Medical Laboratory Techniques, 34010, Istanbul, Türkiye*

Abstract

Diabetes is an important public health problem, and it is well known that healing processes are impaired in diabetic wounds as one of its complications. Keratins are structural proteins found in skin cells and play a vital role in wound healing and skin integrity. While there is increasing interest in the anti-inflammatory properties of metformin, a drug commonly used for diabetes, its potential effect on wound healing and keratins is not yet fully understood. In this context, it was aimed to evaluate how metformin administration affects keratin 6 and keratin 16 expression at both mRNA and protein levels. In this study conducted on diabetic rats, the effects of topically applied metformin on keratins in wound healing were investigated. Then, protein and mRNA expression levels of keratin 6 and keratin 16 in treated wounds were compared with untreated wounds using reverse transcription polymerase chain reaction and immunohistochemistry methods. The results of the study are likely to detail changes in the expression levels of keratin 6 and keratin 16 after metformin administration. This information will shed light on how metformin affects the molecular mechanisms involved in wound healing, particularly concerning these important structural proteins. Understanding these changes may provide insight into potential therapeutic approaches to improve diabetic wound healing. By elucidating the effect of metformin on keratin expression, the study may contribute to the development of targeted therapies aimed at improving the healing process in diabetic wounds.

Keywords: *Diabetes mellitus; diabetic wound model; keratin; metformin; K6/16*

1. Introduction

Keratins that compose the major intermediate filament cytoskeleton of the epidermis are classified as type I (K9-K40) or type II (K1-K8, K70). Keratins of both types are generated by activated keratinocytes and are always co-expressed as a heterodimer between a type I and a type II keratin (Franke et al., 1981; Moll et al., 1982; Hatzfeld and Weber, 1990; Oshima, 2002; Schweizer et al., 2006; Herrman et al., 2009; Jacob et al., 2018). Keratins, which are important for organized keratinocyte proliferation and epithelial integrity, are said to be engaged in intracellular signaling pathways such as stress protection, apoptosis, and wound healing (Pan et al., 2013; Mayet et al., 2014).

Wound healing occurs in four overlapping stages: coagulation and haemostasis, inflammation, proliferation, and tissue remodelling. Keratinocytes have two roles in wound healing: they fill the wound site by proliferation and migration, and they build the epidermal layer through maturation and differentiation (Velnar et al., 2009; Mayet et al., 2014; Pastar et al., 2014). During the proliferation phase, epidermal keratinocytes re-epithelialize the wound, which is an important stage in wound healing. Promoting keratinocyte proliferation is therefore an important step in enhancing the skin wound healing process. Keratinocytes at the wound front travel across the underlying granulation tissue during re-epithelialization, finally meeting keratinocytes moving from the other edge to heal the defect (Bellavia et al., 2014). Migrating keratinocytes generate

* Corresponding author.

E-mail address: kubra_tmbtrk@hotmail.com (F. K. Tombulturk).

<https://doi.org/10.51753/flsrt.1399275> Author contributions

Received 02 December 2023; Accepted 19 March 2024

Available online 30 April 2024

2718-062X © 2024 This is an open access article published by Dergipark under the [CC BY](https://creativecommons.org/licenses/by/4.0/) license.

more K6, K16, and K17 keratins, which are hypothesized to increase migrating cells' viscoelastic properties and are regulated by growth factors found in the wound environment. Because various keratins play diverse functions in the wound-healing process, their expression changes depending on the stage of wound healing (Freedberg et al., 2001; Wong and Coulombe, 2003; Shawandi et al., 2017). Keratinocytes move from wound borders, multiply, and release cytokines to trigger tissue response in acute wounds. However, decreased wound healing, such as that seen in diabetes mellitus (DM), can result in chronic wounds in which keratinocytes fail to migrate, leaving this stage of wound repair incomplete (Krzyszczak et al., 2018).

DM impairs immune response capability, including immune cell function reduction, and is a serious public health issue (Khanra et al., 2015). Hyperglycaemia impairs re-epithelialization processes such as protein synthesis, migration, and proliferation of keratinocytes and fibroblasts (Park et al., 2011; Andrade et al., 2017; Lima et al., 2017; Kim et al., 2018). The expression of key keratinocyte proteins involved in re-epithelialization, including cytoskeletal keratin proteins (K2, K6, and K10), which are critical for keratinocyte differentiation, is disrupted in diabetic foot ulcer patients (Blakytyn and Jude, 2009).

Derived from galegin, a natural product derived from the *Galega officinalis* plant used in herbal medicine, metformin is not designed to target a specific pathway or disease mechanism. However, although it was subsequently accepted as the first-choice drug in the treatment of Type II DM worldwide, its molecular mechanisms of action are still debated (Howlett and Bailey, 2007; Graham et al., 2011). Studies on wound healing and diabetic wounds involve many complex factors, such as various growth factors, cell signalling, inflammatory process, and tissue regeneration. The specific role of K6/16 in these processes is not fully understood and information in the existing literature is limited. Furthermore, studies on the effects of metformin on K6 and K16 specifically in the context of wound healing are lacking. The treatment and healing process of diabetic wounds is often a result of multiple factors, and the effects of drugs are complex, so more scientific studies are needed to have a clear understanding of the effects of metformin on these keratin proteins. In this context, metformin was applied,

the most commonly used antidiabetic agent today, topically on the wounds by creating a diabetic wound model and aimed to investigate its effects on wound healing on K6 and K16.

2. Materials and methods

2.1. Animal study

For this study, an application was made to Bezmialem Vakif University Animal Experiments Local Ethics Committee, and it was approved with the decision numbered 2020/15. In the study, it was used 24 adult male Wistar Hannover albino rats (300 g \pm 20 g, LD; 12:12). During the trial, all rats were housed in separate cages. These rats were separated into two groups: diabetic and non-diabetic rats, and then divided each group into four groups: metformin-treated and saline-applied groups, with six rats randomly assigned to each. At the beginning of the study, all animals' blood glucose levels and body weights were measured. A single intraperitoneal dose of 60 mg/kg Streptozotocin (STZ) was injected to induce diabetes, while the non-diabetic groups were injected with saline only. The glucose levels were examined in blood samples collected from the rats' tail veins at least 72 hours later. Rats with values greater than 250 mg/dL were termed diabetic, whereas rats with values less than this cut off were excluded from the experiment.

The metformin solution was prepared freshly every day at a concentration of 3 mM. It was filtered before each application and then applied it to the wound. Before each operation, rats were anesthetized with penthal sodium. The dorsal region of each anaesthetized rat was shaved and made ready for the operation by providing aseptic conditions. In the dorsal region of each animal in the experimental groups, 3 circular full-thickness excisional wound models were created with a 12 mm diameter sterile punch. Based on the midline in the dorsal region of the animal, the location of the wounds was determined by placing the first wound on the upper left, the second wound on the upper right and the third wound in the middle and below both wounds opened on the top. This first procedure was accepted as day 0 and the experimental period was started. According to the stages of wound healing physiology, other biopsy days were planned as day 3 for the inflammation stage, day 7 for the proliferation

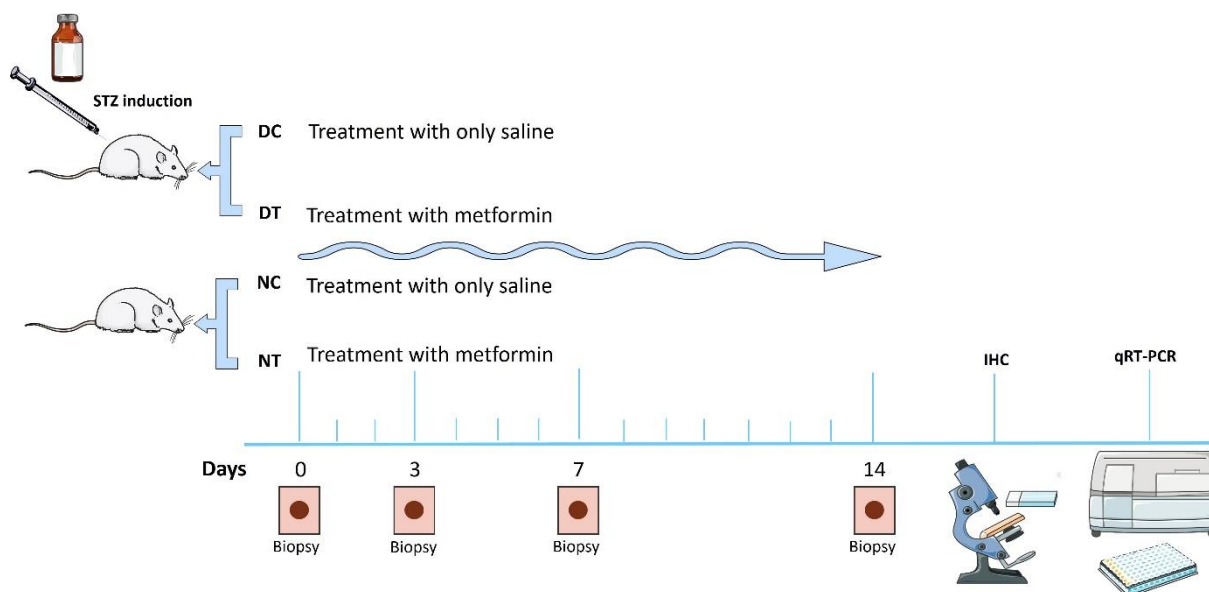


Fig. 1. The animal study is diagrammed on the figure.

stage, and day 14 for the remodelisation stage. The upper left scar tissue was removed on the 3rd day, the upper right scar tissue on the 7th day and the scar tissue in the lower and middle line of the two wounds on the 14th day under anaesthesia and under sterile conditions. On day 14, after taking the last wound biopsy, the experiment was terminated without any treatment and sacrificed all rats under high-dose anaesthesia. Every day, sterile saline was administered to the control wounds and a newly made 3 mM metformin solution to the treatment wounds. By absorbing sterile surgical sponges, both applications were supplied. the wound area was covered with a single layer of gauze to prevent any infection or physical manipulation and continued to apply the treatment at the same time every day for 14 days. The animal study is diagrammed in Fig. 1.

2.2. Quantitative reverse transcription polymerase chain reaction (qRT-PCR)

At the end of the 0th, 3rd, 7th and 14th days, wound biopsy tissues of the rats in the treated group and the control group were surgically removed under anaesthesia. Wound biopsy tissues taken using nuclease-free microtubes and zirconium beads were lysed in lysis solution by a homogenizer. The purity and quantity of total RNA extracted with a ready-to-use kit were then determined in NanoDrop Microvolume Spectrophotometer. The change in the quantity of *KRT6A* and *KRT16* mRNA was quantified using the SYBR green reverse transcription real-time polymerase chain reaction method (Table 1). The *G6PD* gene was used as a reference gene to precisely determine the mRNA levels. To check for contamination, the reaction was always run with a negative control. The system calculated the relative mRNA expression levels of *KRT6A* and *KRT16* and compared them to *G6PD*.

Table 1

Primers of genes *KRT6A*, *KRT16* and *G6PD* for performing qRT-PCR.

| Gene Name (Symbol) | Primer Sequence (5'→3') |
|---|-------------------------|
| Keratin 6A (<i>KRT6A</i>) | F: ATGTGTGGGAACCATCTG |
| | R: TCCTCAGGAAGAGGAAATG |
| Keratin 16 (<i>KRT16</i>) | F: GCAGAGCCAGGAGTACAACA |
| | R: GAATAGGACTGCCAGAGGA |
| Glucose 6-phosphate dehydrogenase (<i>G6PD</i>) | F: ACATCCGCAAACAGAGTGAG |
| | R: GCTGTTGAGGTGCTGTAGG |

2.3. Immunohistochemistry (IHC)

Following each operation, the tissues were fixed in a 10% neutral formalin fixative before utilizing standard light microscopy follow-up techniques to embed the tissues in paraffin. 4-5 mm-thick paraffin sections were taken using a microtome and placed on positively charged slides for immunohistochemistry. The tissue sections that had undergone standard procedures for deparaffinization, rehydration, and removal of antigenic masking shortly prior to immunostaining were then subjected to immunohistochemical staining. Using the pre-made kit (Rabbit specific HRP/DAB Detection IHC Detection Kit-Abcam), the immunohistochemical staining was carried out using rabbit polyclonal anti-cytokeratin 6 and anti-cytokeratin 16 primary antibodies to identify tissue antigens. Light microscopy was used to do semi-quantitative immunoreaction measurements in 10 randomly chosen locations at a 40X magnification. It was evaluated semi-quantitatively by accepting -, +, ++, and +++ according to the severity of

immunoreactivity (Niu et al., 2014).

2.4. Statistical evaluation

The Graphpad Prism 8.0.2 package program was used to analyse the data acquired after the study. Differences between groups were assessed using the ANOVA test, and pairwise comparisons were done using the Tukey test for significant results. On day 0, the t-test was used to compare the non-diabetic and diabetic groups in pairs. As descriptive statistics, the mean standard error value was provided. $P < 0.05$ was regarded as statistically significant.

3. Results

3.1. Demonstration of *KRT6A* expression by qRT-PCR

Pairwise comparisons were done using the t-test for each parameter and the effects of diabetes were presented as a result of analyses made on tissue samples collected from the normal groups (N0) and STZ-induced diabetic groups (D0) on the day of the initial wound (day 0). The qRT-PCR method was used to examine *KRT6A* mRNA expression levels in diabetic and non-diabetic control and treatment groups. The diabetic group had a statistically significant rise in *KRT6A* mRNA levels when compared to the non-diabetic group, according to the data ($p=0.0058$).

According to these data (Fig. 2A), when compared to the first day of treatment, there was a considerable rise on the 14th day in the non-diabetic control (NC) group. ($p=0.0199$). In the non-diabetic treatment (NT) group, wound healing improved significantly on all three treatment days as compared to the first day (respectively; $p=0.0406$, $p=0.031$, $p=0.0163$). On treatment days, there was no significant difference in the diabetic control (DC) group compared to day 0. In the diabetic treatment (DT) group, however, there was a considerable increase on the seventh day as compared to the initial day ($p=0.0392$).

3.2. Demonstration of *KRT16* expression by qRT-PCR

Pairwise comparisons were done using the t-test for each parameter and the effects of diabetes were presented as a result of analyses made on tissue samples collected from the normal groups and STZ-induced diabetic groups on the day of the initial wound (day 0). According to the resulting data, it was determined that there was a statistically significant increase in *KRT16* mRNA level in the diabetic group compared to the healthy group ($p=0.0392$).

Considering these findings (Fig. 2B), the NT group showed a substantial increase on the seventh day of wound healing compared to day 0 ($p=0.0027$). There was no significant difference in the NC, DC, and DT groups on treatment days compared to the first day.

3.3. Evaluation of keratin 6 expression by IHC

Pairwise comparisons were done using the t-test for each parameter and the effects of diabetes were presented as a result of analyses made on tissue samples collected from the normal groups and STZ-induced diabetic groups on the day of the initial wound (day 0). The IHC method was used to examine the levels of K6 protein expression in all groups. According to the results, a statistically significant increase in immunopositivity was

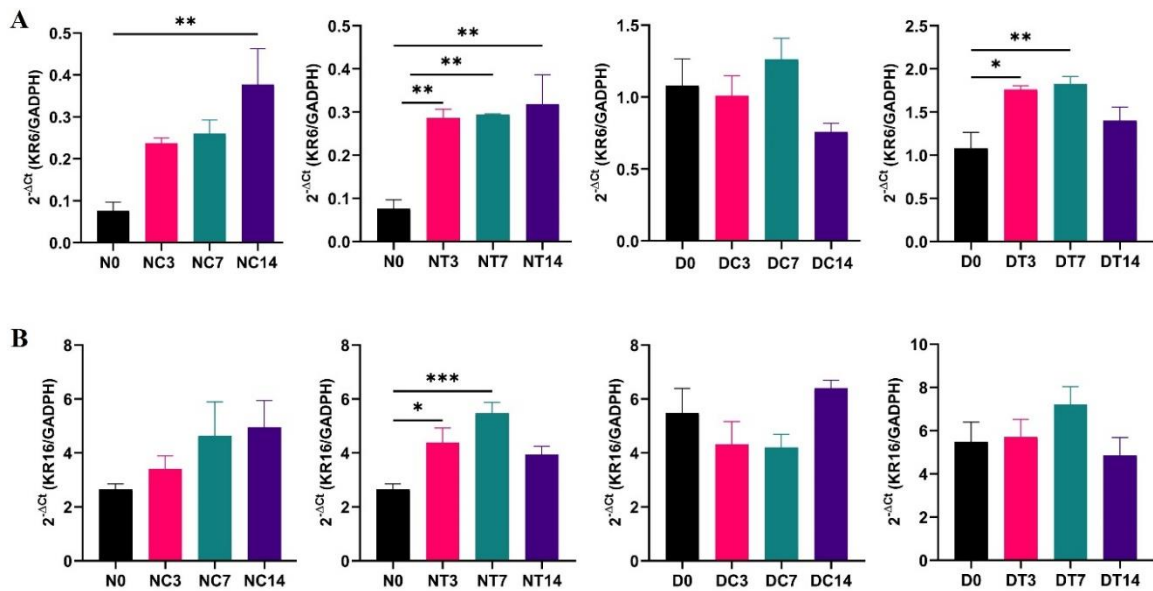


Fig. 2. KERATIN6A (A) and KERATIN16 (B) relative mRNA levels were measured using RT-qPCR for every group. All data were compared to the baseline of day 0. * $p < 0.05$, ** $p < 0.01$, *** $p < 0.001$. On the first day after wound opening, the groups were non-diabetic (N0), diabetic (D0); The groups are as follows: non-diabetic treatment (NT), non-diabetic control (NC), diabetic control (DC), and diabetic treatment (DT).

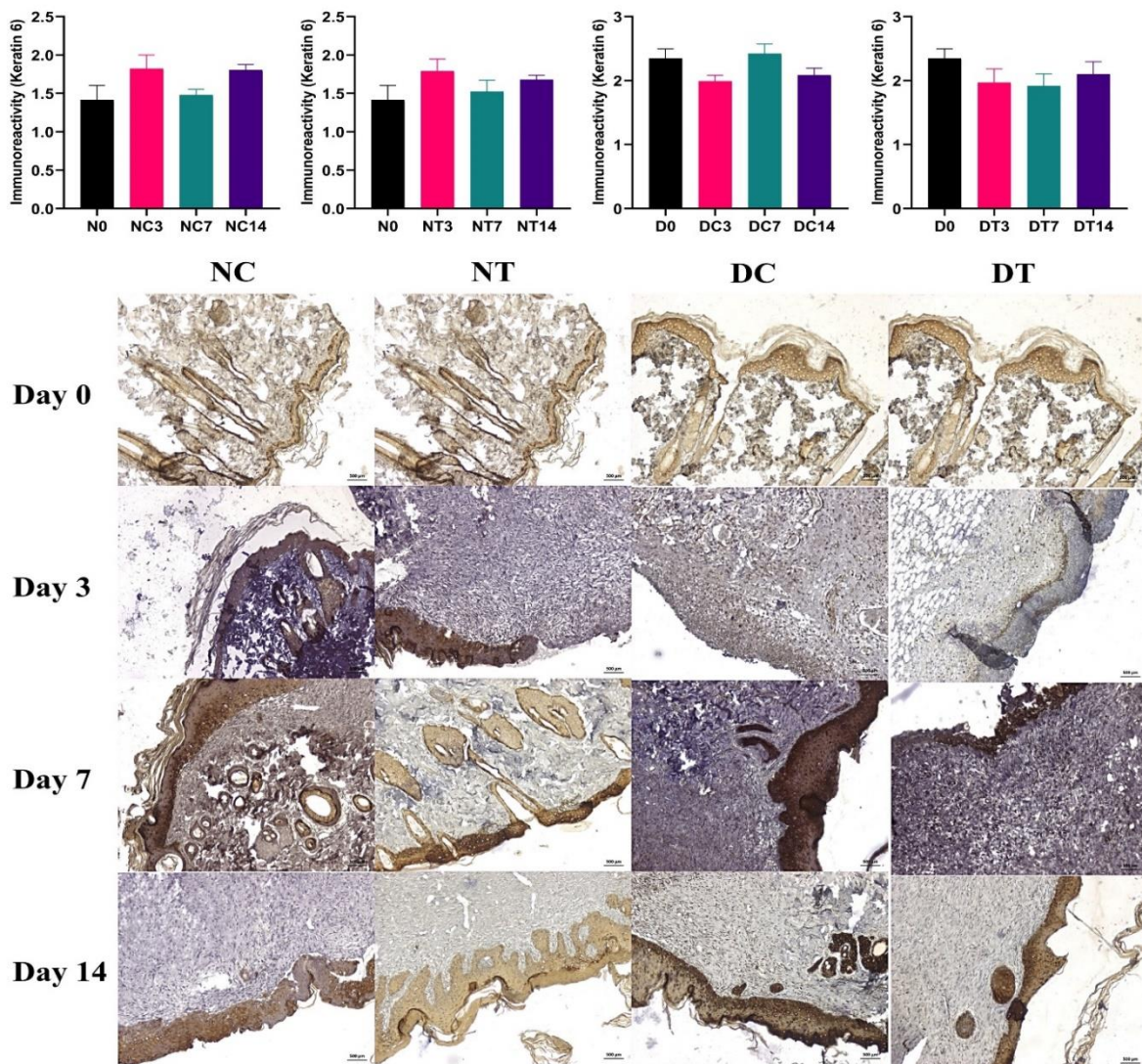


Fig. 3. Graphical representation of Keratin 6 immunoreactivity and microscopic images of wound tissue preparations after IHC staining in all control and treatment groups. Type II IF Keratin 6 was labelled in brown in the wound tissue preparations, and nuclei were labelled in blue with Mayer's haematoxylin.

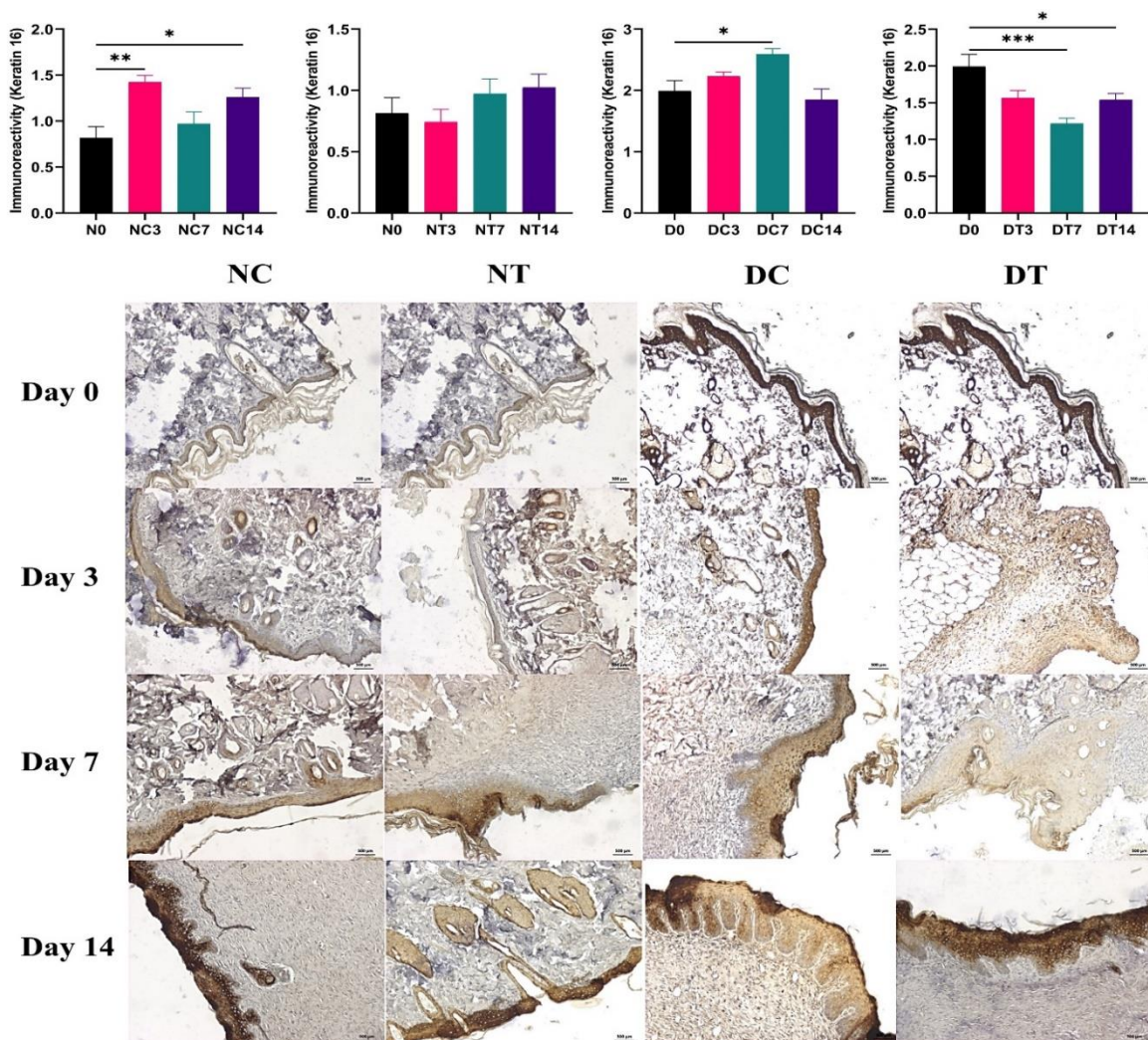


Fig. 4. Graphical representation of Keratin 16 immunoreactivity and microscopic images of wound tissue preparations after IHC staining for every group. Type I IF Keratin 16 was labelled in brown in the wound tissue preparations, and nuclei were labelled in blue with Mayer's haematoxylin. * $p < 0.05$, ** $p < 0.01$, *** $p < 0.001$.

detected in the diabetic group compared to the normal group in the assessment of K6 immunohistochemical staining ($p = 0.0044$). According to these findings (Fig. 3); When intragroup comparison was made according to days in all four groups, no significant difference was seen compared to day 0.

3.4. Evaluation of keratin 16 expression by IHC

Pairwise comparisons were done using the t-test for each parameter and the effects of diabetes were presented as a result of analyses made on tissue samples collected from the normal groups and STZ-induced diabetic groups on the day of the initial wound (day 0). The IHC method was used to examine the levels of K16 protein expression in diabetic and non-diabetic control and treatment groups. According to the findings, a statistically significant increase in immunopositivity was identified in the diabetic group compared to the normal group in the assessment of K16 immunohistochemical staining ($p = 0.0004$).

According to these data (Fig. 4), a substantial increase was seen in the NC group on the third and fourteenth days as compared to the initial day. (respectively; $p = 0.0051$, $p = 0.0451$). Analysing intragroup comparisons based on days compared to the first day showed that there was no significant difference in the NT group. While the DC group had a substantial increase on the seventh treatment day compared to the first day, the DT

group saw a significant decline on the seventh day (respectively; $p = 0.0253$, $p = 0.0021$).

4. Discussion

The function of the skin epidermis, which protects our bodies from environmental pathogens and attacks by forming a physical and immunological barrier, is highly dependent on the presence and integrity of the keratin network, the epidermis' dominant cell type. In keratinocytes, keratins are the most prominent cytoskeletal proteins (Schweizer et al., 2006; Raja et al., 2007; Jacob et al., 2018). When the skin is physically injured, resident keratinocytes, fibroblasts, and other inflammatory immune cells contribute to a cellular and molecular wound-healing process that includes carefully regulated stages of haemostasis, inflammation, proliferation, and remodelling. Keratinocytes are rapidly activated in response to damage and create a range of "alarmins" to guard against a danger signal. Wound proximal keratinocytes momentarily delay terminal differentiation during wound healing to prepare for active migration and proliferation (Martin, 1997; Wikramanayake et al., 2014). Keratinocytes migrate and multiply from wound edges in acute wounds, but in delayed wound healing, such as DM, the inability of keratinocytes to migrate may contribute to the establishment of chronic wounds and delay wound recovery

(Krzyszczczyk et al., 2018). Keratinocytes on the borders of chronic wounds vary from those on the edges of intact epidermis or acute wounds. In contrast to normal skin, which only has mitotically active keratinocytes at the basal layer, keratinocytes in chronic wounds divide along the suprabasal layers (Stojadinovic et al., 2005).

Under homeostatic conditions, suprabasal keratinocytes in the intact epidermis express differentiation-specific keratins K1 and K10, whereas the interfollicular epidermis does not normally express K6, 16, or K17, even though these keratins are considered barrier alarmins that are rapidly induced in keratinocytes upon wounding. Suprabasal keratinocytes, on the other hand, quickly downregulate K1/K10 expression after damage. Transient wound-specific keratins Type II IFs K6a/K6b isoforms are rapidly and significantly elevated in stressed keratinocytes in the suprabasal layers of the epidermis within hours after injury (Usui et al., 2005; Patel et al., 2006; Savatin et al., 2014; Gravino et al., 2017). This induction occurs mostly in the postmitotic compartment of the wound edge epidermis, making it easier to stimulate proliferation rather than differentiation (Paladini et al., 1996; McGowan and Coulombe, 1998; Takahashi et al., 1998; Hobbs et al., 2012). K6, 16, and 17 expression is maintained during epithelial remodelling until barrier function is restored, demonstrating that keratins play critical physiological roles during healing.

Furthermore, K16/17-K6 expression in keratinocytes suggests a highly active and proliferative phase in pathological conditions (Sun et al., 1983; Mansbridge and Knapp, 1987; Takahashi et al., 1998; Koch and Roop, 2004; Zhang, 2018). These keratin couples form a flexible scale that allows keratinocytes to tolerate physical stress and govern a range of activities, including apoptosis protection and immunological homeostasis management. Thus, activation of these genes signifies keratinocyte hyper-proliferation in response to injury or inflammation, and they have been widely used as wound-activated keratinocyte indicators in both human and mouse skin (Paladini et al., 1996; Wong and Coulombe, 2003). Following this knowledge, metformin was used as a topical therapy on the model of a full-thickness excisional wound that it was generated in STZ-induced diabetic and non-diabetic rats. K6 and K16 mRNA and protein expression levels were evaluated in wound biopsy samples collected on days 0, 3, 7, and 14. When hyperglycaemia, a clinical indication in DM that is considered to be an inflammatory condition, was compared to the non-diabetic group, K6/16 levels were found to be considerably higher in wound biopsy samples obtained on day 0. This finding suggests that these two forms of keratin, also known as alarmin, might be used as a biomarker in diabetic wounds.

The induction of K16 by interfollicular keratinocytes is a critical response to epidermal injury. K16 promotes the rearrangement of cytoplasmic keratin filaments at a wound site. Moreover, it is stated that the induction and increased amount of K16 protein helps the keratinocyte activation process and therefore has a positive effect on epithelialization (Paladini et al., 1996). However, contrary to these data, a study conducted with transgenic mice showed that high K16 protein levels had the opposite effect, thus high K16 protein levels partially impaired keratinocyte migration, and K16 overexpression delayed the closure of full-thickness skin wounds *in vivo* (Wawersik et al., 2001). The result of the same study group's study in mouse keratinocytes revealed that forced expression of K16 caused a decrease in cell adhesion while not changing cell proliferation (Wawersik and Coulombe, 2000). Whey protein

therapy was used for full-thickness excisional wounds generated in STZ-induced diabetic rats in a study shared similarities with this study. As a result of the therapy, K16 reactivity was found to be low and intense in diabetic-injured and diabetic-injured treated animals on the fourth day, whereas it was moderate in both normal-injured untreated and normal-injured treated groups. On the eighth day, they have reported that the normal injured group has low reactivity, the treated normal injured group has nil reactivity, the diabetes injured group has medium reactivity, and the treated diabetic injured group has low reactivity (Ahmed et al., 2015). Data from the same study, on the other hand, also report that experimentally tested diabetic wounds are unable to properly regulate the healing phases when K16 expression is delayed to day 8. This study showed that after topical metformin treatment was applied to the wounds, the K16 protein level in the non-diabetic (healthy) and diabetic groups was lower than in the controls. The rise on the third day in the untreated non-diabetic group and the seventh day in the diabetic group was linked to a delay in wound healing. These findings can be explained by the fact that K16 activation was turned on earlier in the therapy. Alternatively, metformin may be able to manage the appropriate time of K16 activation by regulating it, particularly in diabetic wounds. Especially in the diabetic treatment group, the decrease compared to day 0 and the fact that the protein level is parallel to normal wound healing on day 3 suggest that these proteins are expressed at earlier stages and initiate the molecular cascade for wound healing at an earlier stage.

K16 gene expression results on the 7th day were higher in the treated groups compared to the controls, at the protein level. However, considering the gene expression level results within the group, it is concluded that based on the standard wound healing process, metformin induces gene expression until the 7th day, but this level decreases on the 14th day, and there is an irregular expression in untreated diabetic wounds, which negatively affects wound healing. In this regard, a clinical investigation on adult participants used coarse-grit microdermabrasion, discovered that 6 and 24 hours after the treatment, there was an 11-fold increase in K16 gene expression. While K16 was not originally detected, it was discovered in the suprabasal layers of the epidermis 24 and 48 hours after treatment, and samples with increased K16 expression also had the largest increase in type I collagen expression (Karimipour et al., 2009). When looking at the profile of K6, which forms a heterodimer with K16, previous studies also show that complex results are obtained. K6a does not play a substantial function in keratinocyte proliferation or migration, although it may play a role in keratinocyte activation following damage, according to a study in knockout mice (Wojcik et al., 2000). Another study employing an *ex vivo* skin explant culture model to highlight the significance of K6 loss during wound healing discovered that despite normal *KRT6A* mRNA levels in the *KRT6A/KRT6B* null skin segment, there was a lower concentration of K16, resulting in K16 forming K6/16 heteropolymers. They discovered that K6 is essential for keratinocyte stability and that these proteins are required to improve keratinocyte wound epithelialization potential (Wong and Coulombe, 2003).

Moreover, the role of keratins is very critical not only in skin defects caused by diabetes but also in skin damage induced by many different factors (Baek et al., 2024; Blumer, 2024; Majid, 2024). For instance, in clinical studies on Pachyonychia congenita syndrome, which is an autosomal dominant disease and has a prevalence of one in a million

worldwide, they showed that there is a mutation in keratin 6/16 proteins and that the disease exhibits a serious condition in its course (Cheng et al., 2023; Chu et al., 2023). Recent studies also demonstrate the significant role of keratin 6/16 in wound healing (Ghatak et al., 2023; Groh and Magin, 2023; Cohen et al., 2024; Michalak-Micka et al., 2024). One of these studies showed that the extract of *Tarantula cubensis*, a spider species, increased cytokeratin, and collagen in both epithelial and connective tissue in rats with buccal mucosa lesions and had a significant healing effect (Simsek and Ozmen, 2024). Studies show not only the change in the amount of keratin in the wound as a result of the applied treatment, but also the angiogenic, proliferative, and antimicrobial effects of keratin-based treatment approaches (Ramey-Ward et al., 2023; Sun et al., 2023; Tavakoli et al., 2023; Sellappan et al., 2024; Sun et al., 2024; Winkfield et al., 2024).

These findings demonstrate that there is no significant difference in protein quantity across groups when comparing K6, however, the diabetic group exhibited an increase compared to the non-diabetic group on the 7th day. While the gene expression levels in the diabetic control group were irregular, it was found that metformin administration induced gene expression relative to day 0 in both the non-diabetic and treatment groups. These findings show that the K6/16 keratin pair is necessary to maintain the flexibility required to endure the rigors of a wound site at the expense of a delay in epithelialization, and they highlight the keratins' involvement in collective cell migration.

5. Conclusion

DM is a chronic metabolic condition that can interfere with

References

- Ahmed, R. R., Mahmoud, A., Ahmed, O. M., Metwalli, A., & Ebaid, H. (2015). Up-regulation of Hsp72 and keratin16 mediates wound healing in streptozotocin diabetic rats. *Biological Research*, 48, 54.
- Andrade, T. A. M., Masson-Meyers, D. S., Caetano, G. F., Terra, V. A., Ovidio, P. P., Jordão-Júnior, A. A., & Frade, M. A. C. (2017). Skin changes in streptozotocin-induced diabetic rats. *Biochemical and Biophysical Research Communications*, 490(4), 1154-1161.
- Baek, E. J., Jung, D. Y., Seung, N. R., Jang, Y. J., Park, E. J., & Kim, K. H. (2024). Immunohistochemical differentiation of keratins and involucrin between palmar psoriasis, chronic hand eczema and hyperkeratotic hand eczema. *Contact Dermatitis*, 90(4).
- Bellavia, G., Fasanaro, P., Melchionna, R., Capogrossi, M. C., & Napolitano, M. (2014). Transcriptional control of skin reepithelialization. *Journal of Dermatological Science*, 73(1), 3-9.
- Blakytmy, R., & Jude, E. B. (2009). Altered molecular mechanisms of diabetic foot ulcers. *The International Journal of Lower Extremity Wounds*, 8(2), 95-104.
- Blumer, S., Khan, P., Artysh, N., Plappert, L., Savic, S., Knudsen, L., ... & Hostettler, K. E. (2024). The use of cultured human alveolar basal cells to mimic honeycomb formation in idiopathic pulmonary fibrosis. *Respiratory Research*, 25(1), 26.
- Cheng, J. R., Mao, H., Hui, H. Z., Li, S., Wan, Y. F., & Shi, B. J. (2024). A recurrent missense mutation in the KRT16 gene causing pachyonychia congenita in a patient. *International Journal of Dermatology*, 63(2), e47-e49.
- Chu, H. T., Dinh Duong, T. A., Le, D. H., Le, T. V., Nguyen, B. B., Dang, C. V., & Vu, Q. V. (2023). Phenotype and genotype features of Vietnamese children with pachyonychia congenita. *Pediatrics and Neonatology*, 64(4), 405-410.
- Cohen, E., Johnson, C. N., Wasikowski, R., Billi, A. C., Tsoi, L. C., Kahlenberg, J. M., ... & Coulombe, P. A. (2024). Significance of stress keratin expression in normal and diseased epithelia. *iScience*, 27(2), 108805.
- Franke, W. W., Schiller, D. L., Moll, R., Winter, S., Schmid, E., Engelbrecht, I., ... & Platzer, B. (1981). Diversity of cytokeratins. Differentiation specific expression of cytokeratin polypeptides in epithelial cells and tissues. *Journal of Molecular Biology*, 153(4), 933-959.
- Freedberg, I. M., Tomic-Canic, M., Komine, M., & Blumenberg, M. (2001). Keratins and the keratinocyte activation cycle. *The Journal of Investigative Dermatology*, 116(5), 633-640.
- Ghatak, S., Hemann, C., Boslett, J., Singh, K., Sharma, A., El Masry, M. S., ... & Sen, C. K. (2023). Bacterial pyocyanin inducible keratin 6A accelerates closure of epithelial defect under conditions of mitochondrial dysfunction. *Journal of Investigative Dermatology*, 143(10), 2052-2064.
- Graham, G. G., Punt, J., Arora, M., Day, R. O., Doogue, M. P., Duong, J. K., ... & Williams, K. M. (2011). Clinical pharmacokinetics of metformin. *Clinical Pharmacokinetics*, 50(2), 81-98.
- Gravino, M., Locci, F., Tundo, S., Cervone, F., Savatin, D. V., & De Lorenzo, G. (2017). Immune responses induced by oligogalacturonides are differentially affected by AvrPto and loss of BAK1/BKK1 and PEP1/PEPR2. *Molecular Plant Pathology*, 18(4), 582-595.
- Groh, N., & Magin, T. M. (2023). Pseudomonas-derived pyocyanin links oxidative stress and keratin 6 expression to wound healing. *The Journal of Investigative Dermatology*, 143(10), 1865-1867.
- Hatzfeld, M., & Weber, K. (1990). The coiled coil of *in vitro* assembled keratin filaments is a heterodimer of type I and II keratins: use of site-specific mutagenesis and recombinant protein expression. *The Journal of Cell Biology*, 110(4), 1199-1210.
- Herrmann, H., Strelkov, S. V., Burkhard, P., & Aebi, U. (2009). Intermediate filaments: primary determinants of cell architecture and plasticity. *The Journal of Clinical Investigation*, 119(7), 1772-1783.
- Hobbs, R. P., Lessard, J. C., & Coulombe, P. A. (2012). Keratin intermediate filament proteins - novel regulators of inflammation and immunity in skin. *Journal of Cell Science*, 125(Pt 22), 5257-5258.

- Howlett, H. C. S., & Bailey, C. J. (2007). Galegine and antidiabetic plants. In: Bailey C. J., Campbell I. W., Chan J. C. N., Davidson J. A., Howlett H. C. S., Ritz P. (eds) *Metformin - The Gold Standard: A Scientific Handbook* (pp. 3-9). Wiley, Chichester.
- Jacob, J. T., Coulombe, P. A., Kwan, R., & Omary, M. B. (2018). Types I and II keratin intermediate filaments. *Cold Spring Harbor Perspectives in Biology*, 10(4), a018275.
- Karimipour, D. J., Rittié, L., Hammerberg, C., Min, V. K., Voorhees, J. J., Orringer, J. S., ... & Fisher, G. J. (2009). Molecular analysis of aggressive microdermabrasion in photoaged skin. *Archives of Dermatology*, 145(10), 1114-1122.
- Khanra, R., Dewanjee, S., K Dua, T., Sahu, R., Gangopadhyay, M., De Feo, V., & Zia-Ul-Haq, M. (2015). *Abroma augusta* L. (Malvaceae) leaf extract attenuates diabetes induced nephropathy and cardiomyopathy via inhibition of oxidative stress and inflammatory response. *Journal of Translational Medicine*, 13, 6.
- Kim, J. H., Yoon, N. Y., Kim, D. H., Jung, M., Jun, M., Park, H. Y., ... & Choi, E. H. (2018). Impaired permeability and antimicrobial barriers in type 2 diabetes skin are linked to increased serum levels of advanced glycation end-product. *Experimental Dermatology*, 27(8), 815-823.
- Koch, P. J., & Roop, D. R. (2004). The role of keratins in epidermal development and homeostasis--going beyond the obvious. *The Journal of Investigative Dermatology*, 123(5), x-xi.
- Krzyszczak, P., Schloss, R., Palmer, A., & Berthiaume, F. (2018). The role of macrophages in acute and chronic wound healing and interventions to promote pro-wound healing phenotypes. *Frontiers in Physiology*, 9, 419.
- Lima, A. L., Illing, T., Schliemann, S., & Elsner, P. (2017). Cutaneous manifestations of diabetes mellitus: A review. *American Journal of Clinical Dermatology*, 18(4), 541-553.
- Majid, O. W. (2024). Preliminary evidence of impaired oral wound healing in e-cigarette users: a call for perioperative vaping cessation. *Evidence-Based Dentistry*, 1-2.
- Mansbridge, J. N., & Knapp, A. M. (1987). Changes in keratinocyte maturation during wound healing. *The Journal of Investigative Dermatology*, 89(3), 253-263.
- Martin P. (1997). Wound healing--aiming for perfect skin regeneration. *Science*, 276(5309), 75-81.
- Mayet, N., Choonara, Y. E., Kumar, P., Tomar, L. K., Tyagi, C., Du Toit, L. C., & Pillay, V. (2014). A comprehensive review of advanced biopolymeric wound healing systems. *Journal of Pharmaceutical Sciences*, 103(8), 2211-2230.
- McGowan, K. M., & Coulombe, P. A. (1998). Onset of keratin 17 expression coincides with the definition of major epithelial lineages during skin development. *The Journal of Cell Biology*, 143(2), 469-486.
- Michalak-Micka, K., Tenini, C., Böttcher-Haberzeth, S., Mazzone, L., Pontiggia, L., Klar, A. S., ... & Biedermann, T. (2024). The expression pattern of cytokeratin 6a in epithelial cells of different origin in dermo-epidermal skin substitutes in vivo. *Biotechnology Journal*, 19(1), 2300246.
- Moll, R., Franke, W. W., Schiller, D. L., Geiger, B., & Krepler, R. (1982). The catalog of human cytokeratins: patterns of expression in normal epithelia, tumors and cultured cells. *Cell*, 31(1), 11-24.
- Niu, Y., Li, F., Tang, B., Shi, Y., Hao, Y., & Yu, P. (2014). Clinicopathological correlation and prognostic significance of sonic hedgehog protein overexpression in human gastric cancer. *International Journal of Clinical and Experimental Pathology*, 7(8), 5144-5153.
- Oshima R. G. (2002). Apoptosis and keratin intermediate filaments. *Cell Death and Differentiation*, 9(5), 486-492.
- Paladini, R. D., Takahashi, K., Bravo, N. S., & Coulombe, P. A. (1996). Onset of re-epithelialization after skin injury correlates with a reorganization of keratin filaments in wound edge keratinocytes: defining a potential role for keratin 16. *The Journal of Cell Biology*, 132(3), 381-397.
- Pan, X., Hobbs, R. P., & Coulombe, P. A. (2013). The expanding significance of keratin intermediate filaments in normal and diseased epithelia. *Current Opinion in Cell Biology*, 25(1), 47-56.
- Park, H. Y., Kim, J. H., Jung, M., Chung, C. H., Hasham, R., Park, C. S., & Choi, E. H. (2011). A long-standing hyperglycaemic condition impairs skin barrier by accelerating skin ageing process. *Experimental Dermatology*, 20(12), 969-974.
- Pastar, I., Stojadinovic, O., Yin, N. C., Ramirez, H., Nusbaum, A. G., Sawaya, A., ... & Tomic-Canic, M. (2014). Epithelialization in wound healing: A comprehensive review. *Advances in Wound Care*, 3(7), 445-464.
- Patel, G. K., Wilson, C. H., Harding, K. G., Finlay, A. Y., & Bowden, P. E. (2006). Numerous keratinocyte subtypes involved in wound re-epithelialization. *The Journal of Investigative Dermatology*, 126(2), 497-502.
- Raja, Sivamani, K., Garcia, M. S., & Isseroff, R. R. (2007). Wound re-epithelialization: modulating keratinocyte migration in wound healing. *Frontiers in Bioscience: A Journal and Virtual Library*, 12, 2849-2868.
- Ramey-Ward, A. N., Walthall, H. P., Smith, S., & Barrows, T. H. (2023). Human keratin matrices promote wound healing by modulating skin cell expression of cytokines and growth factors. *Wound Repair and Regeneration*, 1-11.
- Savatin, D. V., Bisceglia, N. G., Marti, L., Fabbri, C., Cervone, F., & De Lorenzo, G. (2014). The Arabidopsis nucleus-and phragmoplast-localized kinase1-related protein kinases are required for elicitor-induced oxidative burst and immunity. *Plant Physiology*, 165(3), 1188-1202.
- Schweizer, J., Bowden, P. E., Coulombe, P. A., Langbein, L., Lane, E. B., Magin, T. M., ... & Wright, M. W. (2006). New consensus nomenclature for mammalian keratins. *The Journal of Cell Biology*, 174(2), 169-174.
- Shavandi, A., Silva, T. H., Bekhit, A. A., & Bekhit, A. E. A. (2017). Keratin: dissolution, extraction and biomedical application. *Biomaterials Science*, 5(9), 1699-1735.
- Sellappan, L. K., & Manoharan, S. (2024). Fabrication of bioinspired keratin/sodium alginate based biopolymeric mat loaded with herbal drug and green synthesized zinc oxide nanoparticles as a dual drug antimicrobial wound dressing. *International Journal of Biological Macromolecules*, 259(Pt 1), 129162.
- Simsek, A., & Ozmen, O. (2024). Histopathological and immunohistochemical effects of tarantula cubensis extract on mucosal healing in rats. *Journal of Veterinary Dentistry*, 41(1), 17-25.
- Stojadinovic, O., Brem, H., Vouthounis, C., Lee, B., Fallon, J., Stallcup, M., ... & Tomic-Canic, M. (2005). Molecular pathogenesis of chronic wounds: the role of beta-catenin and c-myc in the inhibition of epithelialization and wound healing. *The American Journal of Pathology*, 167(1), 59-69.
- Sun, C., Huang, Y., Wang, L., Deng, J., Qing, R., Ge, X., ... & Hao, S. (2024). Engineered keratin/bFGF hydrogel to promote diabetic wound healing in rats. *International Journal of Biological Macromolecules*, 261(Pt 1), 129725.
- Sun, C., Liu, W., Wang, L., Meng, R., Deng, J., Qing, R., ... & Hao, S. (2023). Photopolymerized keratin-PGLA hydrogels for antibiotic resistance reversal and enhancement of infectious wound healing. *Materials Today Bio*, 23, 100807.
- Sun, T. T., Eichner, R., Nelson, W. G., Vidrich, A., & Woodcock-Mitchell, J. (1983). Keratin expression during normal epidermal differentiation. *Current Problems in Dermatology*, 11, 277-291.
- Takahashi, K., Yan, B., Yamanishi, K., Imamura, S., & Coulombe, P. A. (1998). The two functional keratin 6 genes of mouse are differentially regulated and evolved independently from their human orthologs. *Genomics*, 53(2), 170-183.
- Tavakoli, M., Mirhaj, M., Varshosaz, J., Al-Musawi, M. H., Almajidi, Y. Q., Danesh Pajooh, A. M., ... & Esfahani, S. N. (2023). Keratin- and VEGF-incorporated honey-based sponge-nanofiber dressing: An ideal construct for wound healing. *ACS Applied Materials & Interfaces*, 15(48), 55276-55286.
- Usui, M. L., Underwood, R. A., Mansbridge, J. N., Muffley, L. A., Carter, W. G., & Olerud, J. E. (2005). Morphological evidence for the role of suprabasal keratinocytes in wound reepithelialization. *Wound Repair and Regeneration*, 13(5), 468-479.
- Velnar, T., Bailey, T., & Smrkolj, V. (2009). The wound healing process: an overview of the cellular and molecular mechanisms. *The Journal of International Medical Research*, 37(5), 1528-1542.
- Wawersik, M. J., Mazzalupo, S., Nguyen, D., & Coulombe, P. A. (2001). Increased levels of keratin 16 alter epithelialization potential of mouse skin keratinocytes in vivo and ex vivo. *Molecular Biology of The Cell*, 12(11), 3439-3450.
- Wawersik, M., & Coulombe, P. A. (2000). Forced expression of keratin 16 alters the adhesion, differentiation, and migration of mouse skin keratinocytes. *Molecular Biology of The Cell*, 11(10), 3315-3327.
- Wikramanayake, T. C., Stojadinovic, O., & Tomic-Canic, M. (2014). Epidermal differentiation in barrier maintenance and wound healing.

- Advances in Wound Care*, 3(3), 272-280.
- Winkfield, K. M., Hughes, R. T., Brown, D. R., Clohessy, R. M., Holder, R. C., ... & Burnett, L. R. (2024). Randomized pilot study of a keratin-based topical cream for radiation dermatitis in breast cancer patients. *Technology in Cancer Research & Treatment*, 23, 15330338231222137.
- Wojcik, S. M., Bundman, D. S., & Roop, D. R. (2000). Delayed wound healing in keratin 6a knockout mice. *Molecular and Cellular Biology*, 20(14), 5248-5255.
- Wong, P., & Coulombe, P. A. (2003). Loss of keratin 6 (K6) proteins reveals a function for intermediate filaments during wound repair. *The Journal of Cell Biology*, 163(2), 327-337.
- Zhang, L. J. (2018). Keratins in skin epidermal development and diseases. In: Blumenberg, M., Surguchov, A. (eds) *Keratin* (pp. 1-17). Intech Open London, UK.

Cite as: Tombulturk, F. K. (2024). Effects of keratin6/16 heterodimer on diabetic wound healing treatment with topical metformin. *Front Life Sci RT*, 5(1), 65-73.



Research article

Identification of potential hub genes as biomarkers for breast, ovarian, and endometrial cancers

Sema Atasever^{*1} 

¹ Nevsehir Hacı Bektas Veli University, Faculty of Engineering-Architecture, Department of Computer Engineering, 50300, Nevsehir, Türkiye

Abstract

Breast cancer (BC) and gynecological cancers have emerged as significant threats to women's health and are known to be among the primary causes of cancer-related fatalities in women. Innovative treatments and early detection may significantly cut mortality rates for these diseases. In this study, potential hub genes were thoroughly evaluated in the contexts of BC, ovarian cancer (OC), and endometrial cancer (EC). Initially, a total of 374 overlapping differentially expressed genes (DEGs) were identified within the microarray datasets. The STRING database and Cytoscape software analyzed protein-protein interaction (PPI) network structure, whereas FunRich found hub genes. The five hub genes that were ultimately discovered are *PTEN*, *SMAD2*, *FASN*, *CYCS*, and *KRAS*. As a result, these genes may serve as potential biomarkers for the aforementioned diseases. Importantly, this study offers valuable insights into all three diseases based on recent molecular advancements. However, further investigation is required to precisely measure these biomarkers' effectiveness.

Keywords: Breast cancer; DEGs; endometrial cancer; enriched pathway; hub gene; ovarian cancer; potential biomarker

1. Introduction

Today, breast cancer (BC) and gynecological cancers have become a major threat to women's health (Zhang et al., 2019). In addition to the aging population, the incidence increases due to risk factors such as smoking, excess weight, and physical inactivity (Arakal et al., 2021). According to statistics in 2020, more than 2 million new cases of breast cancer were seen in women (BCS, 2023). Statistics show that BC is the most common cancer seen worldwide. However, gynecological cancers are among the deadliest cancers in the world (Yadav et al., 2020). Again, statistics in 2020 show that EC is the 6th most common cancer in women (ECS, 2023). With more than 313,000 new cases in 2020, OC is the 8th most common cancer in women and the 18th most common cancer overall (OCS, 2023). The incidence of these cancers, which seriously threaten women's health, continues to increase worldwide despite

medical advances (Zhang et al., 2022).

Both OC and EC occur as part of Lynch syndrome or hereditary nonpolyposis colorectal cancer (Gayther et al., 2010). With the increase in obesity, mortality rates caused by EC are increasing in developed countries (Li et al., 2020). Studies have shown that *BRCA1*- and *BRCA2* gene mutations are important hereditary risk factors for the development of breast and ovarian cancer (Petrucci et al., 2022). Microarray and sequencing technologies are commonly used today to identify biomarkers (Xue et al., 2021), but the hub genes shared by BC and EC have not yet been fully clarified (Rahman et al., 2019). Despite numerous researches into the molecular mechanisms of cancer, the processes of gynecological cancers are still not well understood. Therefore, the search for new biomarkers for early detection is very important (Zhang et al., 2019).

Next-generation sequencing technologies offer remarkable sequencing speed and lower costs (Lee et al., 2013; Toss et al.,

* Corresponding author.

E-mail address: sema@nevsehir.edu.tr (S. Atasever).

<https://doi.org/10.51753/flsrt.1405816> Author contributions

Received 16 December 2023; Accepted 02 April 2024

Available online 30 April 2024

2718-062X © 2024 This is an open access article published by Dergipark under the [CC BY](https://creativecommons.org/licenses/by/4.0/) license.

2015). Despite these developments, the survival rate of OC is low. Therefore, it is of great importance to detect OC at an early stage (Yadav et al., 2020).

This study aims to use bioinformatics tools to analyze microarray data, identify new biomarkers, and explore the molecular mechanisms of BC, OC, and EC. It is collected microarray datasets of BC, OC, and EC from Gene Expression Omnibus (GEO). Searching for a possible biological link between BC, OC, and EC disease, sequencing data from patients with specified diseases from GEO databases was used.

2. Materials and methods

The microarray datasets GEO42568, GEO27651, and GEO17025 were downloaded from GEO database. These three datasets were analysed and normalized using the GEO2R tool to find common DEGs. PPI network structure was performed using STRING (Szklarczyk et al., 2010) database and Cytoscape (Shannon et al., 2003) software, respectively. A brief workflow is indicated in Fig. 1.

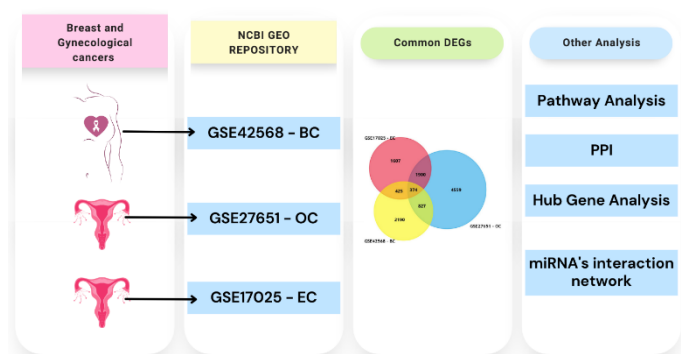


Fig. 1. Overall workflow of methodology. Microarray data was obtained from the GEO database. The number of samples in the study was 273, of which 238 were cancerous and 35 were normal tissue. The largest samples in the database belong to the breast tissues.

2.1. Data acquisition

In this study, three cancer-related gene expression profiles with GEO accession numbers GSE42568 (GSE42568, 2023), GSE27651 (GSE27651, 2023), and GSE17025 (GSE17025, 2023) were extracted from the GEO database, and DEGs were obtained using GEO2R. There is total of 121 patient samples in dataset GSE42568, 49 patient samples in dataset GSE27651, and 103 patient samples in dataset GSE17025 (see Table 1).

2.2. Data processing

All patient records were selected as test and control using the GEO2R tool, which was used to compare two or more sets of samples to identify DEGs under experimental conditions (see Fig. 2). Results are obtained as a table of genes ordered in order of importance. After processing each examined dataset with the

GEO2R tool, thousands of DEGs were obtained.

2.3. Selection of DEGs

DEG lists downloaded using the GeoR tool, as shown in Fig. 3, were filtered according to p-value and log₂ fold-change (Log₂FC) values, and genes belonging to the related disease were obtained (Sarkar et al., 2021). The Benjamini–Hochberg approach was used to adjust the p-values (Benjamini et al., 1995).

2.4. Method for identification of DEGs

A systematic approach using the FunRich tool (version 3.1.3) (Fonseka et al., 2021) was used to identify DEGs in this study. Initially, gene expression data were extracted from three different datasets from GEO database. The main criteria for selecting these datasets were their relevance to the research topic and the quality of the data.

For each dataset, gene expression data were normalized for comparability. Then, statistical methods were used to find genes with significant expression differences between test and control groups, using criteria of a log₂ fold change ≥ 0.5 and an adjusted p-value of < 0.05 to identify DEGs.

The Venn diagram function in FunRich was then used to visually represent and identify common genes across the three datasets. This step was crucial for locating hub genes that consistently showed different expressions across multiple datasets. The Venn diagram (see Fig. 4) shows the overlap of DEGs and helps isolate the most important candidates for further analysis.

In summary, the identification of DEGs involved several steps: normalizing the data, analyzing it statistically to find differences in expression, and using graphs to identify common genes in different datasets. This comprehensive strategy guaranteed that DEGs were statistically significant.

2.5. Network analysis of DEGs

Network analysis of DEGs was necessary for the study to better understand the complex gene interactions. All shared DEGs from the FunRich tool were brought into STRING during this step. This allowed for a comprehensive exploration of the dynamic interactions and functional relationships that shape the molecular landscape of BC, OC, and EC.

3. Results

3.1. Identification of DEGs

After the data was downloaded, a significance threshold was defined with a p-value < 0.05 and a log₂FC (fold change) ≥ 0.5 . Adhering to these criteria, a total of 5676 genes out of 54675 in BC (GSE42568), 10219 genes out of 54675 in OC (GSE27651), and 5824 genes out of 54675 in EC (GSE17025)

Table 1
Datasets obtained from GEO.

| Disease | Accession number of the dataset | #of patients | Diseased samples / Test species | Healthy samples / Control species |
|--------------------|---------------------------------|--------------|---------------------------------|-----------------------------------|
| Breast Cancer | GSE42568 | 121 | 104 | 17 |
| Ovarian Cancer | GSE27651 | 49 | 43 | 6 |
| Endometrial Cancer | GSE17025 | 103 | 91 | 12 |
| Total: | | 273 | 238 | 35 |

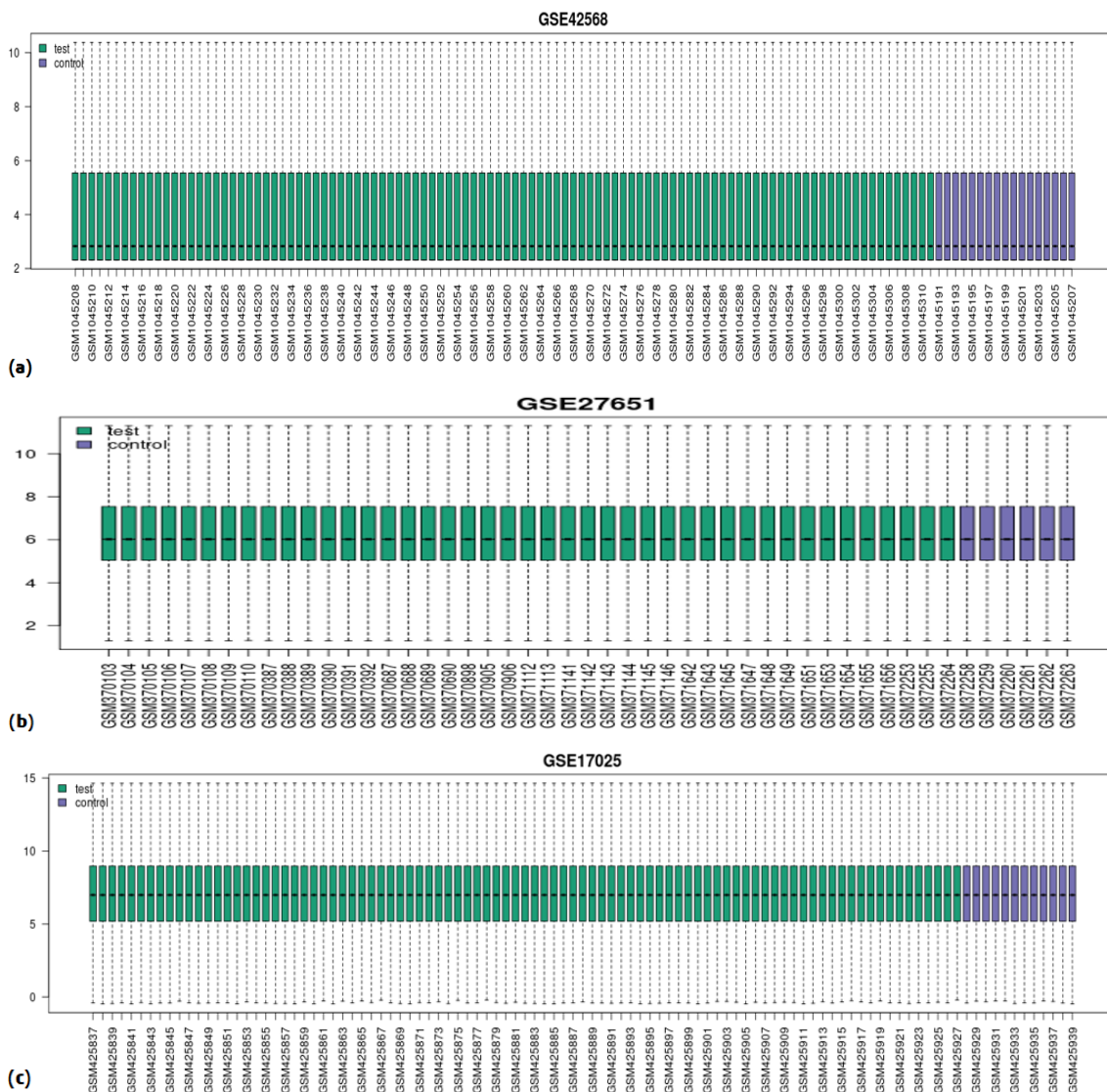


Fig. 2. Box plots of gene expression values (a) BC (GSE42568), (b) OC (GSE27651), (c) EC (GSE17025).

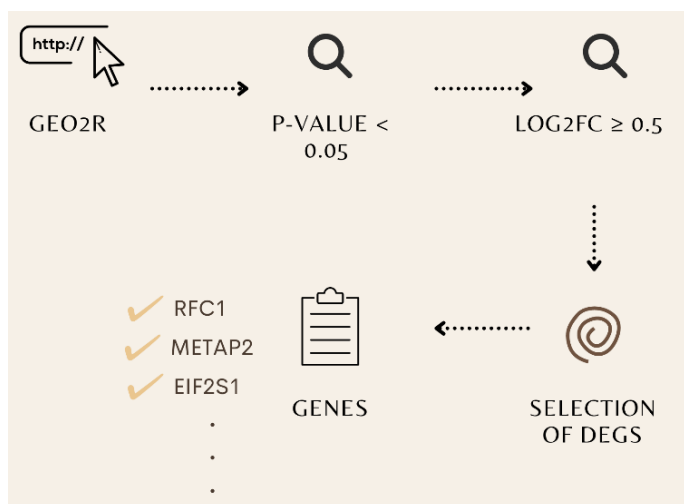


Fig. 3. Basic steps of selection of DEGs.

were selected for further analysis. This rigorous filtering process resulted in the identification of 3816 DEGs in BC, 7660 DEGs in OC, and 4306 DEGs in EC, providing a more refined subset for subsequent investigation.

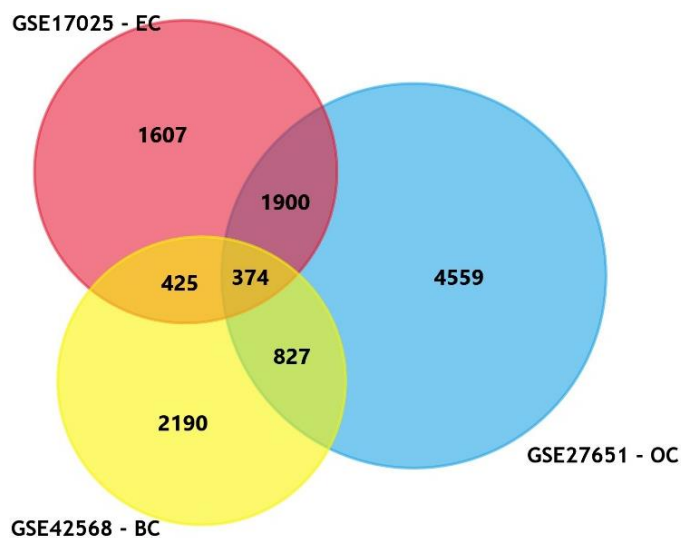


Fig. 4. The Venn diagram shows 374 common hub genes.

3.2. Common DEGs analysis

Venn diagram analysis yielded 374 genes reflecting dataset

intersections.

3.3. Common DEGs network

3.3.1. Construction of PPIs network

Protein-Protein Interaction (PPI) networks helped uncover hub genes for various illnesses. All 374 common DEGs related to these disorders were imported into the STRING, constructing a comprehensive network with 355 nodes and 964 edges. The resulting PPI network exhibited an average node degree of 5.43 and a clustering coefficient of 0.328, visually represented in Fig. 5 and Fig. 6. This network analysis provides a holistic view of the interconnected relationships among the differentially expressed genes, offering valuable insights into the molecular dynamics underlying breast cancer, ovarian cancer, and endometrial cancer.

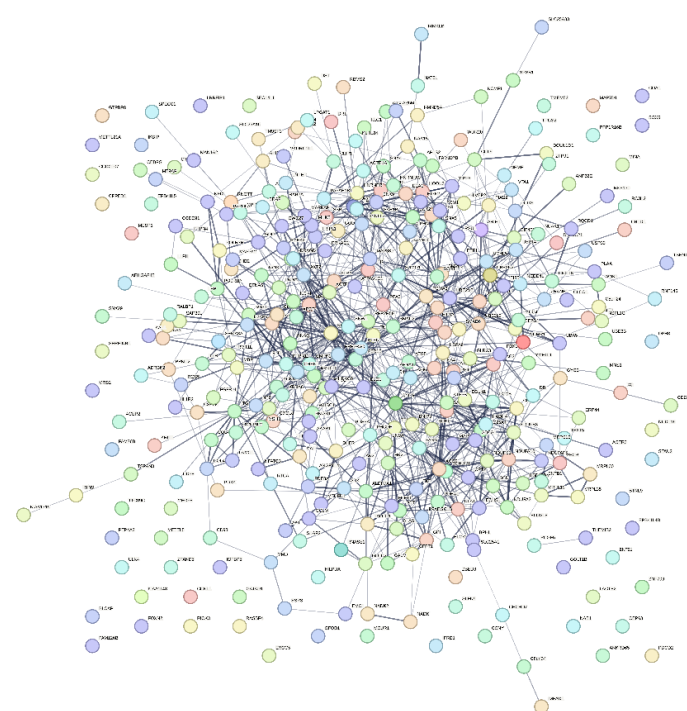


Fig. 5. PPIs network produced by STRING.

3.3.2. Hub gene analysis

In this study, the identification of hub genes was achieved by combining advanced bioinformatics tools and network analysis techniques. Initially, the STRING database (Szklarczyk et al., 2010) was used to construct a PPI network based on DEGs associated with BC, OC, and EC. This network forms the basis for identifying key genes that play central roles in these cancers.

Cytoscape software (Shannon et al., 2003), a powerful tool, was then used to develop the analysis and visualize molecular interaction networks. The Cyto-Hubba plugin was used in Cytoscape, a module specifically designed to identify hub genes in a network. Cyto-Hubba ranks genes within the network based on various topological algorithms such as degree centrality, closeness centrality, and betweenness centrality (Zhou et al., 2021). These algorithms calculate the importance of each gene in the network based on their connections and positions. In this study, degree filters were used. The top 20 genes with the highest scores in these degree centrality measurements were selected as

centrality genes. These genes are shown in Fig. 7, which shows their positions and interactions within the network. By integrating these computational tools, the precision of hub gene selection has been increased and focused information has been provided on key players within the PPI network.

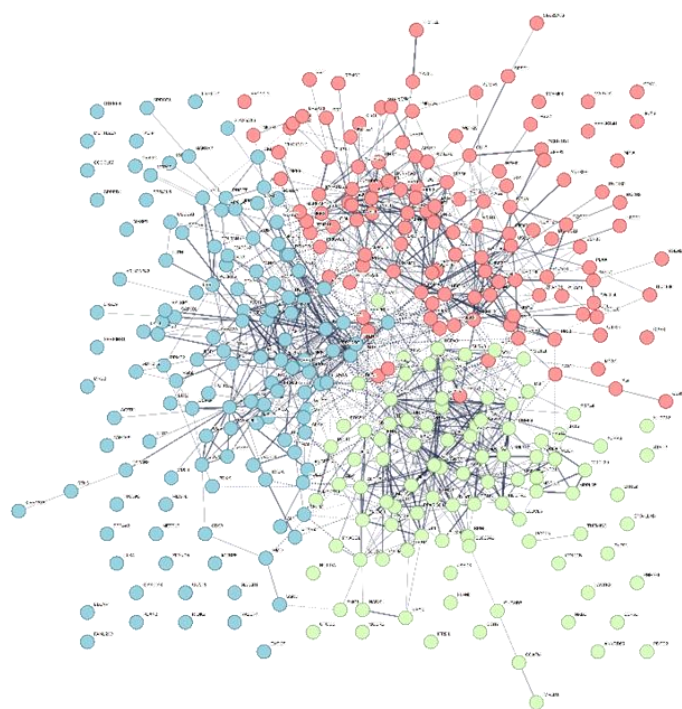


Fig. 6. K-means clustering applied in PPIs network.

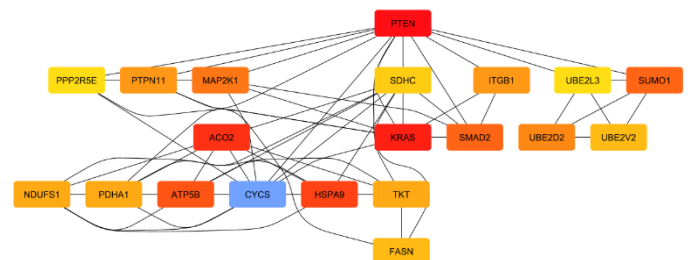


Fig. 7. Hub genes were identified using the plug-in cytoHubba in Cytoscape software.

Table 2

List of common Hub genes using degree centrality ranking methods.

| No. | Gene Name | No. | Gene Name |
|-----|-----------|-----|-----------|
| 1 | "CYCS" | 11 | "PTPN11" |
| 2 | "PTEN" | 12 | "ITGB1" |
| 3 | "KRAS" | 13 | "TKT" |
| 4 | "ACO2" | 14 | "PDHA1" |
| 5 | "HSPA9" | 15 | "NDUFS1" |
| 6 | "ATP5B" | 16 | "FASN" |
| 7 | "SMAD2" | 17 | "UBE2V2" |
| 8 | "SUMO1" | 18 | "SDHC" |
| 9 | "MAP2K1" | 19 | "PPP2R5E" |
| 10 | "UBE2D2" | 20 | "UBE2L3" |

Table 2 serves as a comprehensive overview, summarizing the list of common hub genes based on degree centrality ranking methods. Notably, *CYCS* emerges as the hub gene with the highest degree of interaction, underscoring its potential significance, while *UBE2L3* stands out as the least connected node among the top 20 hub genes.

3.3.3. miRNA's interaction network

Upon identification, the top 20 hub genes were subsequently integrated into the miRNet 2.0 software (Chang et al., 2022), allowing for a comprehensive exploration of their intricate interactions with miRNAs, as visually depicted in Fig. 8. This multi-layered analysis not only sheds light on the hub genes but also unravels potential regulatory relationships between these genes and miRNAs, offering a more holistic understanding of their roles in the molecular landscape of breast cancer, ovarian cancer, and endometrial cancer.

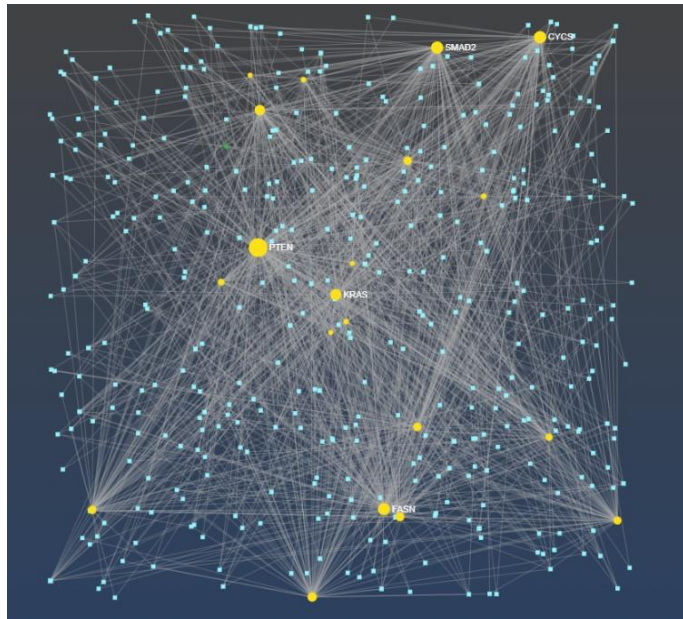


Fig. 8. Interaction between miRNA and 20 common genes of BC, OC and, EC obtained via miRNet 2.0. The five large nodes indicate the hub genes.

Table 3
miRNet 2.0 screening results.

| Hub genes | Degree | Betweenness |
|--------------|--------|-------------|
| <i>PTEN</i> | 160 | 23099.09 |
| <i>SMAD2</i> | 107 | 12475.8 |
| <i>FASN</i> | 106 | 12336.65 |
| <i>CYCS</i> | 104 | 12544.66 |
| <i>KRAS</i> | 99 | 10806.33 |

Table 4
A list of common biomarker candidates.

| Hub genes | Roles of the Biomolecules | Reference |
|--------------|----------------------------------|---|
| <i>PTEN</i> | Phosphatase and tensin homolog | (Chou et al., 2014; Smith et al., 2016) |
| <i>SMAD2</i> | Cancer-related genes | (Martinez-Ledesma et al., 2015) |
| <i>FASN</i> | Fatty acid synthase | (Fernández et al., 2020) |
| <i>CYCS</i> | Cytochrome c, somatic | (Emmanuel et al., 2011) |
| <i>KRAS</i> | Regulation of cell proliferation | (Emmanuel et al., 2011) |

Table 3 shows a list of central genes with their connections (degree) and importance (betweenness) in the network. Nodes with higher node degree act as hubs in a network (miRNet, 2024). *PTEN*, with the highest degree of 160, is the most connected gene in this network, followed by *SMAD2*, *FASN*, *CYCS*, and *KRAS*. A higher betweenness centrality score can indicate a gene's strategic role in the communication within the

network. *PTEN* has the highest betweenness centrality at 23099.09, indicating it may play a significant role in the flow of information in the network.

3.3.4. Survival analysis

A method using both statistical significance and biological importance selected 5 hub genes for survival analysis (Table 4). These genes, central in the PPI network, are vital for cancer-related cellular processes. Their high interaction and central role in the network highlight their potential regulatory importance in cancer pathways. This study analyzed overall and disease-free survival (DFS) data for 1,668 patients with BC, OC, and EC using the GEPIA online service.

Fig. 9A shows a Kaplan-Meier curve for the OS of patients grouped by their high or low *PTEN*, *SMAD2*, *FASN*, *KRAS*, and *CYCS* gene expression levels. Fig. 9B does the same for DFS. In both figures, the blue line shows patients with low expression, and the red line shows those with high expression. Both groups start with a DFS probability of 1.0 (or 100%), which decreases over time as events (recurrence of disease) occur.

In summary, Kaplan-Meier survival curves showed that higher expression levels of the *PTEN*, *SMAD2*, *FASN*, and *KRAS* genes were associated with longer OS, whereas higher expression of *CYCS* was associated with lower OS. Therefore, the *PTEN*, *SMAD2*, *FASN*, and *KRAS* genes could be considered a positive prognostic biomarker for patients with BC and gynecological cancers.

In summary, Kaplan-Meier survival curves showed that higher expression levels of the *PTEN*, *SMAD2*, *FASN*, and *KRAS* genes were associated with a longer period of DFS. Therefore, the expression levels of these genes (*PTEN*, *SMAD2*, *FASN*, and *KRAS*) may serve as a prognostic biomarker for BC and gynecological cancers.

3.4. Pathways analysis

Gene Ontology (GO) and Kyoto Encyclopedia of Genes and Genomes (KEGG) pathway enrichment analyses were conducted using the "Enrichr" online platform (Enrichr, 2024) to decipher crucial biological processes. This was accomplished for the top 20 hub genes, thereby illuminating significant insights.

The 374 overlapping DEGs were analyzed for GO enrichment, revealing the top 10 enriched terms in biological processes, cellular components, and molecular functions in Fig. 10A, including significant enrichment in "negative regulation of organ growth" and "cell-cell adhesion mediated by integrin". KEGG analysis showed significant enrichment in pathways like the "citrate cycle" and "central carbon metabolism in cancer" (Fig. 10B).

Fig. 10(a) provides a list of biological processes from GO, a major bioinformatics initiative that aims to unify the representation of gene and gene product features across all species. Each listed process is accompanied by a unique identifier (e.g., GO:0046621 for "negative regulation of organ growth"), allowing easy reference and cross-database comparisons.

Highlighted processes include various regulatory functions such as "negative regulation of organ growth", "cell-cell adhesion mediated by integrin", and "neuroinflammatory response". There are also specific pathways like "ribosome phosphate metabolic process", "regulation of inward rectifier

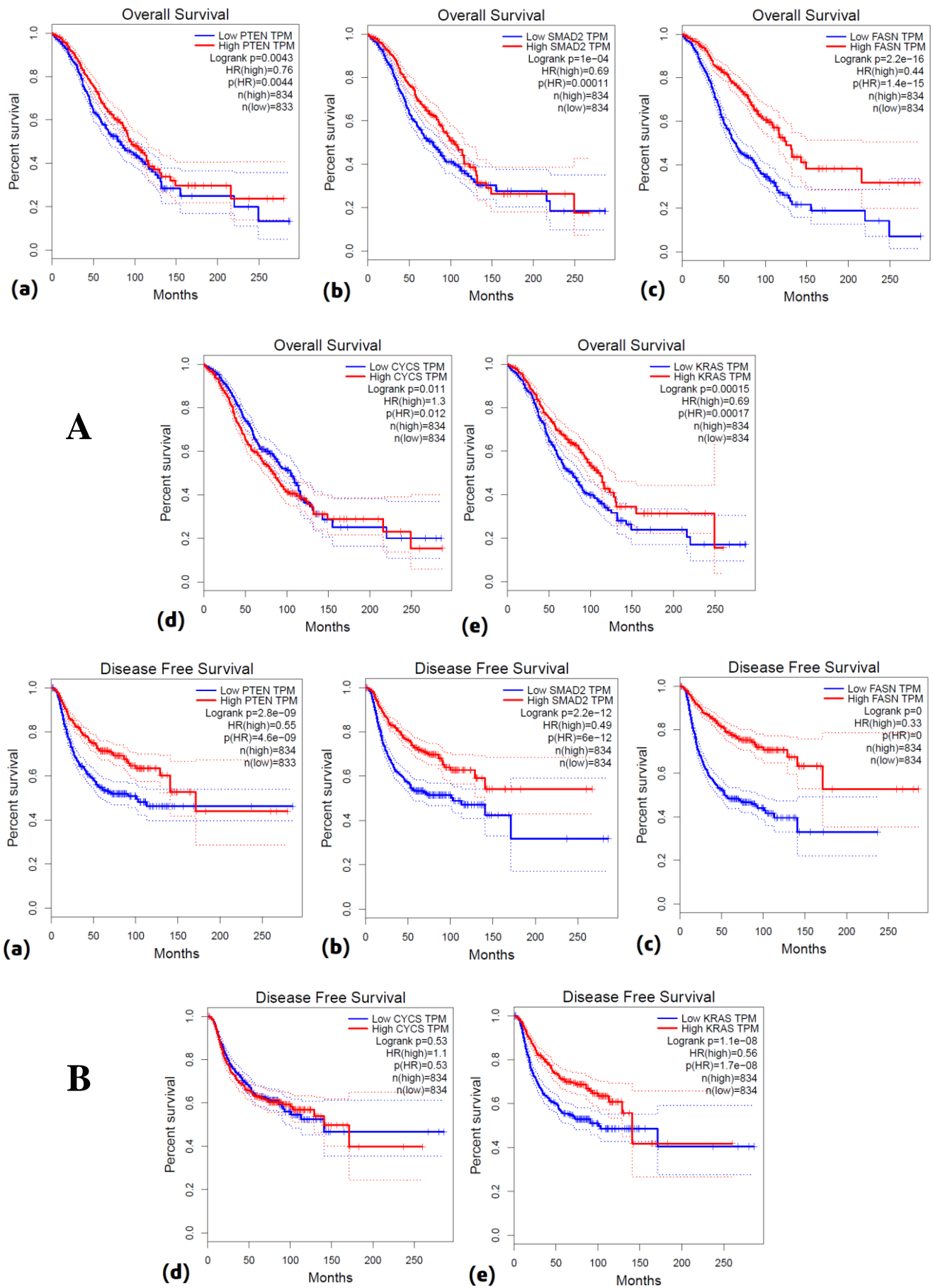
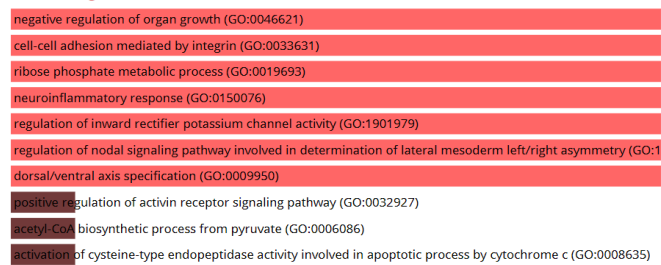


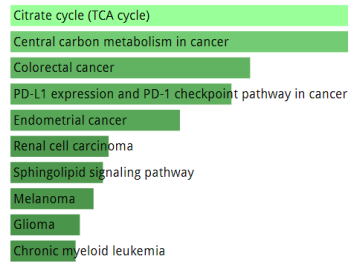
Fig. 9. Overall survival (OS) analysis of the candidate hub genes. (A) OS analysis. (a) *PTEN*, (b) *SMAD2*, (c) *FASN*, (d) *CYCS*, and (e) *KRAS*. (B) DFS analysis. (a) *PTEN*, (b) *SMAD2*, (c) *FASN*, (d) *CYCS*, and (e) *KRAS*. The threshold Log-rank $p < 0.05$ was considered as statistically significant.

GO Biological Process



(a)

KEGG



(b)

Fig. 10. Bioinformatics analysis of DEGs in the progression of BC, OC and EC cancers. Functional enrichment analysis of the overlapping DEGs. The GO enrichment analysis of DEGs in the categories of (a) biological process, (b) The KEGG pathway enrichment analysis of the overlapping DEGs. The top 10 enriched KEGG pathways were shown.

potassium channel activity". The functional enrichment analysis indicated that the overlapping DEGs were mainly associated with "negative regulation of organ growth" and "cell-cell adhesion mediated by integrin", "ribose phosphate metabolic process", and so on.

The analysis used in Fig. 10(b) is used to identify important biological pathways enriched in a set of DEGs. The bar chart shows the top 10 enriched KEGG pathways among the overlapping DEGs analyzed in this study. From the list, we can see that it includes metabolic pathways such as the "Citrate cycle (TCA cycle)" and "Central carbon metabolism in cancer", as well as pathways directly related to various cancers like "Colorectal cancer", "Endometrial cancer", "Renal cell carcinoma", "Melanoma", "Glioma", and "Chronic myeloid leukemia". The "PD-L1 expression and PD-1 checkpoint pathway in cancer" indicates a focus on immunological pathways that are targeted in cancer immunotherapy. In cancer treatment, tumor microenvironment is sensitive to treatment with immune checkpoint such as the PD-1/PD-L1 pathway because of radiotherapy (Du et al., 2020). The "Sphingolipid signaling pathway" is involved in signaling mechanisms that can affect cell growth, survival, differentiation, and apoptosis, which are processes relevant to cancer biology. Members of the sphingolipid family are widely involved in cancer cell growth, migration, invasion, and other biological processes (Sun et al., 2022).

4. Discussion

Numerous studies have been conducted in recent years to identify genetic markers for cancer (Banno et al., 2012; Toss et al., 2015; Walsh et al., 2016; Zhang et al., 2022). The US National Cancer Institute (NCI) defines a biomarker as "a biological molecule found in the blood, other body fluids, or tissues that is a sign of a normal or abnormal process, or a condition or disease" (Banno et al., 2012). New biomarkers are revealed by next-generation sequencing. This will allow clinicians to present in the most informative way recommendations for administering new treatments modifying existing treatments and adjusting dosage (Walsh et al., 2016). The generation of high-throughput technologies has improved our understanding of complex biological features such as tumors (Wang et al., 2022). Despite surgical and chemotherapy treatment applications in various cancer types such as EC, mortality rates are still increasing in recent years. Therefore, it is necessary to better understand the mechanisms that cause cancer (Li et al., 2020). In this study, by downloading three cancer datasets, 374 common DEGs were screened out. From

their study of colorectal cancer patients treated with cetuximab, Li et al. (2010) concluded that *KRAS* mutation and *PTEN* protein expression were significantly associated with patient response rate and survival time.

The study by Zhang et al. (2024) identified 13 ferroptosis-related genes in Crohn's disease (CD) using bioinformatics analysis of two Gene Expression Omnibus datasets and further validated three of these genes (*IL-6*, *PTGS2*, and *DUOX2*) as key regulators of ferroptosis in CD through qPCR analysis of clinical samples. These findings suggest new biomarkers and therapeutic targets for CD, offering fresh insights into its pathogenesis and potential treatment strategies.

In recent years, efforts have been made to identify new biomarkers for gynecological cancer. For example, upregulation of *TRIM44* predicts poor prognosis in OC. Previous studies have found *SMYD2* to be an oncogene in several types of cancer. *MMP8* has been reported to be associated with BC. *HSDL2* acts as an oncogene in OC (Zhang et al., 2019). *PTEN* gene encodes a tumor suppressor phosphatase that has been found to be frequently mutated in patients with OC and EC (Smith et al., 2016).

In this study, a Venn diagram obtained using the FunRich tool was analyzed to identify hub genes. By determining 20 hub genes by the degree centrality method, in the analysis of common hub genes, "negative regulation of organ growth" and "cell-cell adhesion mediated by integrin", "ribose phosphate metabolic process", etc. It has been determined that there are genes associated with five unreported genes in BC, OC, and EC. The results may help us understand the development of BC, OC, and EC and guide further experiments.

In Fig. 8, the five large nodes (*PTEN*, *SMAD2*, *FASN*, *CYCS*, and *KRAS*) represent hub genes that are likely central in the network due to their high degree of connections, indicating they may play key roles in the regulatory processes across the three types of cancer. The study by Davies et al. (2014) showed that mutations in *PTEN* and *KRAS* alone predispose mice to a spectrum of serrated lesions reflective of the serrated pathway of colorectal cancer progression in humans. The study by Qian et al. (2022) stated that *SMAD2* was related to colorectal cancer, *KRAS* was related to ovarian cancer, and *KRAS* and *PTEN* were related to endometrial cancer. In another study (Stebbing et al., 2014), the alterations observed in phosphatases and the resulting malignancies were associated with the *PTEN* gene in cervical, ovarian, and breast cancers.

In the literature, studies have been carried out examining various gene expressions to evaluate their ability as prognostic markers. Yndestad et al. (2017) conducted a study indicating that high *PTEN* gene expression is a negative prognostic marker

in human primary breast cancers with preserved p53 function. Another study showed that loss of *PTEN* expression was associated with worse survival (Ferraldeschi et al., 2015). Although Liu et al. (2020) found that *SMAD2*, *p-SMAD2*, and *SMAD4* are not independent predictors by multivariate analysis, *SMAD4* positivity correlates with longer OS and progression-free survival. They also found that combined *p-SMAD2* and *SMAD4* expression can serve as an independent prognostic factor, suggesting that testing for these proteins in breast ductal carcinoma biopsies could offer extra prognostic insights. Ramanathan et al. (2017) showed that although *VEGFA* alone did not correlate with survival, high *ANG2* and high *VEGFA* co-expression correlated with decreased OS for breast cancer.

Inferences made with Kaplan-Meier curves are generally not sufficient to fully understand the prognostic value of a gene. Kaplan-Meier analysis evaluates OS or DFS by grouping patients based on a given gene expression level and produces survival curves for each group. This analysis is useful for visualizing the impact of a gene's high or low expression on patient survival, but this relationship is not definitive and does not account for other influencing factors. Multivariate analysis is necessary to support Kaplan-Meier results because it considers other important variables such as age, gender, type of treatment, stage, and other potential confounding factors. In their study, Scaglia et al. (2013) in addition to the Kaplan-Meier method, also used the Cox proportional hazards regression model to evaluate the effect of potential confounding factors and adjust their effects in the comparison between genders. Methods such as the Cox proportional hazards model (Liu et al., 2020) are used in multivariate analysis to determine whether the effect of a gene on survival is independent of all other variables. Therefore, complementing Kaplan-Meier analysis with

multivariate analysis is crucial to confirm whether a gene is an independent prognostic marker, which is one of the limitations of this study.

5. Conclusion

In this study, it was aimed to analyze microarray samples by using bioinformatics tools to identify new biomarkers. Searching for a possible biological link between BC, OC, and EC disease, sequencing data from patients with specified diseases from GEO databases was used. 374 DEGs were common, and five of them came to the fore. These include the *PTEN*, *SMAD2*, *FASN*, *CYCS*, and *KRAS* genes. The functional enrichment analysis indicated that the overlapping DEGs were mainly associated with “negative regulation of organ growth” and “cell-cell adhesion mediated by integrin”, “ribose phosphate metabolic process”, and so on. Higher *PTEN*, *SMAD2*, *FASN*, and *KRAS* gene expressions correlate with increased overall and disease-free survival, unlike *CYCS*, which shows reduced overall survival with no significant impact on disease-free survival. However, further work is required to quantify the potency of these biomarkers. Understanding the role of the key genes identified in this study in signal transduction could help in creating targeted drugs for cancer treatment, either alone or combined with other therapies.

Conflict of interest: The author declares that she has no conflict of interests.

Informed consent: The author declares that this manuscript did not involve human or animal participants and informed consent was not collected.

References

- Arakal, N. G., Sharma, V., Kumar, A., Kavaya, B., Devadath, N. G., Kumar, S. B., ... & Murahari, M. (2021). Ligand-based design approach of potential Bcl-2 inhibitors for cancer chemotherapy. *Computer Methods and Programs in Biomedicine*, 209, 106347.
- Banno, K., Kisu, I., Yanokura, M., Tsuji, K., Masuda, K., Ueki, A., ... & Aoki, D. (2012). Biomarkers in endometrial cancer: Possible clinical applications. *Oncology letters*, 3(6), 1175-1180.
- Benjamini, Y., & Hochberg, Y. (1995). Controlling the false discovery rate: a practical and powerful approach to multiple testing. *Journal of the Royal Statistical Society: Series B (Methodological)*, 57(1), 289-300.
- BCS, (2023). Breast Cancer Statistics, <https://www.wcrf.org/cancer-trends/breast-cancer-statistics/>, Last Accessed on December 16, 2023.
- Chang, L., & Xia, J. (2022). MicroRNA regulatory network analysis using miRNet 2.0. In: Song Q., Tao Z. (eds) *Transcription Factor Regulatory Networks* (pp. 185-204). Springer, Humana, New York.
- Chou, W. C., Cheng, A. L., Brotto, M., & Chuang, C. Y. (2014). Visual gene-network analysis reveals the cancer gene co-expression in human endometrial cancer. *BMC Genomics*, 15(1), 1-12.
- Davies, E. J., Marsh Durban, V., Meniel, V., Williams, G. T., & Clarke, A. R. (2014). PTEN loss and KRAS activation leads to the formation of serrated adenomas and metastatic carcinoma in the mouse intestine. *The Journal of Pathology*, 233(1), 27-38.
- Du, Z., Yan, D., Li, Z., Gu, J., Tian, Y., Cao, J., & Tang, Z. (2020). Genes involved in the PD-L1 pathway might associate with radiosensitivity of patients with gastric cancer. *Journal of Oncology*, 2020.
- Emmanuel, C., Gava, N., Kennedy, C., Balleine, R. L., Sharma, R., Wain, G., ... & deFazio, A. (2011). Comparison of expression profiles in ovarian epithelium in vivo and ovarian cancer identifies novel candidate genes involved in disease pathogenesis. *PLoS One*, 6(3), e17617.
- ECS, (2023). Endometrial Cancer Statistics, <https://www.wcrf.org/cancer-trends/endometrial-cancer-statistics/>, Last Accessed on December 16, 2023.
- Enrichr, (2024). Enrichr Database, <https://maayanlab.cloud/Enrichr/>, Last Accessed on December 16, 2023.
- Fernández, L. P., de Cedron, M., & de Molina, A. (2020). Alterations of lipid metabolism in cancer: Implications in prognosis and treatment. *Frontiers in Oncology*, 10, 577420.
- Ferraldeschi, R., Rodrigues, D. N., Riisnaes, R., Miranda, S., Figueiredo, I., Rescigno, P., ... & de Bono, J. (2015). PTEN protein loss and clinical outcome from castration-resistant prostate cancer treated with abiraterone acetate. *European Urology*, 67(4), 795-802.
- Fonseka, P., Pathan, M., Chitti, S. V., Kang, T., & Mathivanan, S. (2021). FunRich enables enrichment analysis of OMICs datasets. *Journal of Molecular Biology*, 433(11), 166747.
- Gayther, S. A., & Pharoah, P. D. P. (2010). The inherited genetics of ovarian and endometrial cancer. *Current Opinion in Genetics & Development*, 20(3), 231-238.
- GSE17025, (2023). National Center for Biotechnology Information, <https://www.ncbi.nlm.nih.gov/geo/query/acc.cgi?acc=GSE17025>, Last Accessed on December 16, 2023.
- GSE27651, (2023). National Center for Biotechnology Information, <https://www.ncbi.nlm.nih.gov/geo/query/acc.cgi?acc=GSE27651>, Last Accessed on December 16, 2023.
- GSE42568, (2023). National Center for Biotechnology Information, <https://www.ncbi.nlm.nih.gov/geo/query/acc.cgi?acc=GSE42568>, Last Accessed on December 16, 2023.
- Li, F. H., Shen, L., Li, Z. H., Luo, H. Y., Qiu, M. Z., Zhang, H. Z., ... & Xu, R. H. (2010). Impact of KRAS mutation and PTEN expression on cetuximab-treated colorectal cancer. *World Journal of Gastroenterology: WJG*, 16(46), 5881.
- Li, Y., & Li, L. (2020). Bioinformatic screening for candidate biomarkers and their prognostic values in endometrial cancer. *BMC Genetics*, 21(1), 1-13.

- Liu, N., Qi, D., Jiang, J., Zhang, J., & Yu, C. (2020). Expression pattern of p-Smad2/Smad4 as a predictor of survival in invasive breast ductal carcinoma. *Oncology Letters*, 19(3), 1789-1798.
- Martinez-Ledesma, E., Verhaak, R. G. W., & Treviño, V. (2015). Identification of a multi-cancer gene expression biomarker for cancer clinical outcomes using a network-based algorithm. *Scientific Reports*, 5(1), 11966.
- miRNet, (2024). miRNet Tutorial Starting with a List, https://www.mirnet.ca/miRNet/resources/data/tutorials/Start_with_list.pdf, Last Accessed on January 24, 2024.
- OCS, (2023). Ovarian Cancer Statistics, <https://www.wcrf.org/cancer-trends/ovarian-cancer-statistics/>, Last Accessed on December 16, 2023.
- Petrucelli, N., Daly, M. B., & Pal, T. (2022). *BRCA1-and BRCA2-associated hereditary breast and ovarian cancer*. GeneReviews.
- Qian, F., Kong, W., & Wang, S. (2022). Exploring autophagy-related prognostic genes of Alzheimer's disease based on pathway crosstalk analysis. *Bosnian Journal of Basic Medical Sciences*, 22(5), 751.
- Rahman, M. F., Rahman, M. R., Islam, T., Zaman, T., Shuvo, M. A. H., Hossain, M. T., ... & Moni, M. A. (2019). A bioinformatics approach to decode core genes and molecular pathways shared by breast cancer and endometrial cancer. *Informatics in Medicine Unlocked*, 17, 100274.
- Ramanathan, R., Olex, A. L., Dozmorov, M., Bear, H. D., Fernandez, L. J., & Takabe, K. (2017). Angiopoietin pathway gene expression associated with poor breast cancer survival. *Breast Cancer Research and Treatment*, 162, 191-198.
- Sarkar, D., Chakraborty, S., Bhowmick, S., & Maiti, T. (2021). *In-silico* analysis: common biomarkers of NDs. *BioRxiv*, 2021-2029.
- Scaglia, N. C., Chatkin, J. M., Pinto, J. A., Tsukazan, M. T. R., Wagner, M. B., & Saldanha, A. F. (2013). Role of gender in the survival of surgical patients with nonsmall cell lung cancer. *Annals of Thoracic Medicine*, 8(3), 142.
- Shannon, P., Markiel, A., Ozier, O., Baliga, N. S., Wang, J. T., Ramage, D., ... & Ideker, T. (2003). Cytoscape: a software environment for integrated models of biomolecular interaction networks. *Genome Research*, 13(11), 2498-2504.
- Smith, I. N., & Briggs, J. M. (2016). Structural mutation analysis of PTEN and its genotype-phenotype correlations in endometriosis and cancer. *Proteins: Structure, Function, and Bioinformatics*, 84(11), 1625-1643.
- Stebbing, J., Lit, L. C., Zhang, H., Darrington, R. S., Melaiu, O., Rudraraju, B., & Giamas, G. (2014). The regulatory roles of phosphatases in cancer. *Oncogene*, 33(8), 939-953.
- Sun, Y., Xu, Y., Che, X., & Wu, G. (2022). Development of a novel sphingolipid signaling pathway-related risk assessment model to predict prognosis in kidney renal clear cell carcinoma. *Frontiers in Cell and Developmental Biology*, 10, 881490.
- Szklarczyk, D., Franceschini, A., Kuhn, M., Simonovic, M., Roth, A., Minguez, P., ... & Mering, C. V. (2010). The STRING database in 2011: functional interaction networks of proteins, globally integrated and scored. *Nucleic Acids Research*, 39(suppl_1), D561-D568.
- Toss, A., Tomasello, C., Razzaboni, E., Contu, G., Grandi, G., Cagnacci, A., ... & Cortesi, L. (2015). Hereditary ovarian cancer: not only BRCA 1 and 2 genes. *BioMed Research International*, 2015.
- Walsh, M. F., Nathanson, K. L., Couch, F. J., & Offit, K. (2016). Genomic biomarkers for breast cancer risk. *Novel Biomarkers in the Continuum of Breast Cancer*, 1-32.
- Wang, Y., Wang, J., Hu, Y., Shangguan, J., Song, Q., Xu, J., ... & Zhang, Y. (2022). Identification of key biomarkers for STAD using filter feature selection approaches. *Scientific Reports*, 12(1), 19854.
- Xue, H., Sun, Z., Wu, W., Du, D., & Liao, S. (2021). Identification of hub genes as potential prognostic biomarkers in cervical cancer using comprehensive bioinformatics analysis and validation studies. *Cancer Management and Research*, 117-131.
- Yadav, G., Vashisht, M., Yadav, V., & Shyam, R. (2020). Molecular biomarkers for early detection and prevention of ovarian cancer—A gateway for good prognosis: A narrative review. *International Journal of Preventive Medicine*, 11.
- Yndestad, S., Austreid, E., Knappskog, S., Chrisanthar, R., Lilleng, P. K., Lønning, P. E., & Eikesdal, H. P. (2017). High PTEN gene expression is a negative prognostic marker in human primary breast cancers with preserved p53 function. *Breast Cancer Research and Treatment*, 163, 177-190.
- Zhang, S., Jiang, H., Gao, B., Yang, W., & Wang, G. (2022). Identification of diagnostic markers for breast cancer based on differential gene expression and pathway network. *Frontiers in Cell and Developmental Biology*, 9, 811585.
- Zhang, W., Li, Z., Li, H., & Zhang, D. (2024). Identification of differentially expressed genes associated with ferroptosis in Crohn's disease. *Experimental and Therapeutic Medicine*, 27(2), 1-12.
- Zhang, X., & Wang, Y. (2019). Identification of hub genes and key pathways associated with the progression of gynecological cancer. *Oncology Letters*, 18(6), 6516-6524.
- Zhou, C., Guo, H., & Cao, S. (2021). Gene Network Analysis of Alzheimer's Disease Based on Network and Statistical Methods. *Entropy*, 23(10), 1365.

Cite as: Atasever, S. (2024). Identification of potential hub genes as biomarkers for breast, ovarian, and endometrial cancers. *Front Life Sci RT*, 5(1), 74-82.